Journal of Advanced Transportation

Advances in Traffic Safety Methodologies and Technologies

Lead Guest Editor: Chunjiao Dong
Guest Editors: Chunfu Shao, Helai Huang, Xiaoming Chen, and Tony Sze

Advances in Traffic Safety Methodologies and Technologies

Journal of Advanced Transportation

Advances in Traffic Safety Methodologies and Technologies

Lead Guest Editor: Chunjiao Dong
Guest Editors: Chunfu Shao, Helai Huang, Xiaoming Chen, and Tony Sze

Editorial Board

Contents

Advances in Traffic Safety Methodologies and Technologies
Chunjiao Dong, Chunfu Shao, Helai Huang, Xiaoming Chen, and N. N Sze
Editorial (2 pages), Article ID 4129582, Volume 2018 (2018)

Microscopic Simulation-Based High Occupancy Vehicle Lane Safety and Operation Assessment: A Case Study
Chao Li, Mohammad Karimi, and Ciprian Alecsandru
Research Article (12 pages), Article ID 5262514, Volume 2018 (2018)

Investigating the Differences of Single-Vehicle and Multivehicle Accident Probability Using Mixed Logit Model
Bowen Dong, Xiaoxiang Ma, Feng Chen, and Suren Chen
Research Article (9 pages), Article ID 2702360, Volume 2018 (2018)

Modeling Lane-Changing Behavior in Freeway Off-Ramp Areas from the Shanghai Naturalistic Driving Study
Lanfang Zhang, Cheng Chen, Jiayan Zhang, Shouen Fang, Jinming You, and Jingqiu Guo
Research Article (10 pages), Article ID 8645709, Volume 2018 (2018)

Effects of Human-Centered Factors on Crash Injury Severities
Emmanuel Kofi Adanu and Steven Jones
Research Article (11 pages), Article ID 1208170, Volume 2017 (2018)

A Novel Surrogate Safety Indicator Based on Constant Initial Acceleration and Reaction Time Assumption
Adrian Fazekas, Friederike Hennecke, Eszter Kalló, and Markus Oeser
Research Article (9 pages), Article ID 8376572, Volume 2017 (2018)

A Novel Approach for Operating Speed Continuous Predication Based on Alignment Space Comprehensive Index
Ying Yan, Gengping Li, Jinjun Tang, and Zhongyin Guo
Research Article (14 pages), Article ID 9862949, Volume 2017 (2018)

Analyzing Traffic Crash Severity in Work Zones under Different Light Conditions
Xinxin Wei, Xiang Shu, Baoshan Huang, Edward L. Taylor, and Huaxin Chen
Research Article (10 pages), Article ID 5783696, Volume 2017 (2018)

Developing a Clustering-Based Empirical Bayes Analysis Method for Hotspot Identification
Yajie Zou, Xinzhi Zhong, John Ash, Ziqiang Zeng, Yinhai Wang, Yanxi Hao, and Yichuan Peng
Research Article (9 pages), Article ID 5230248, Volume 2017 (2018)

Turnout Fault Diagnosis through Dynamic Time Warping and Signal Normalization
Shize Huang, Fan Zhang, Rongjie Yu, Wei Chen, Fei Hu, and Decun Dong
Research Article (8 pages), Article ID 3192967, Volume 2017 (2018)

Influences of Waiting Time on Driver Behaviors While Implementing In-Vehicle Traffic Light for Priority-Controlled Unsignalized Intersections
Bo Yang, Rencheng Zheng, Tsutomu Kaizuka, and Kimihiko Nakano
Research Article (12 pages), Article ID 7871561, Volume 2017 (2018)

Road Surface State Recognition Based on SVM Optimization and Image Segmentation Processing
Jiandong Zhao, Hongqiang Wu, and Liangliang Chen
Research Article (21 pages), Article ID 6458495, Volume 2017 (2018)

Hindawi
Journal of Advanced Transportation
Volume 2018, Article ID 4129582, 2 pages
https://doi.org/10.1155/2018/4129582

Editorial

Advances in Traffic Safety Methodologies and Technologies

Chunjiao Dong,[1,2] **Chunfu Shao**,[2] **Helai Huang**,[3] **Xiaoming Chen**,[4] **and N. N Sze**[5]

[1]*Center for Transportation Research, Tickle College of Engineering, University of Tennessee, 600 Henley Street, Knoxville, TN 37996, USA*
[2]*MOE Key Laboratory for Urban Transportation Complex Systems Theory and Technology, School of Traffic & Transportation, Beijing Jiaotong University, Beijing 100044, China*
[3]*School of Traffic and Transportation Engineering, Central South University, 22 Shao Nan Road, Changsha, Hunan 410075, China*
[4]*Traffic Engineers, Inc., 801 Congress Avenue, Houston, TX 77002, USA*
[5]*Department of Civil and Environmental Engineering, The Hong Kong Polytechnic University, Hung Hom, Kowloon, Hong Kong*

Correspondence should be addressed to Chunjiao Dong; cdong5@utk.edu

Received 2 April 2018; Accepted 3 April 2018; Published 6 June 2018

Traffic safety represents a significant challenge for current, transitional, and future transportation systems, where the advanced communication and automation systems within vehicles and in the road infrastructure might interfere with the driving behavior of individual vehicles and raise concerns regarding the implications on safety. Developing better traffic safety methodologies, strategies, and policies is of practical importance to reduce traffic crashes and improve transportation system operations and might lead to a mitigation of congestion, together with a reduction of traffic-related air pollution. Enabled by emerging vehicle, sensing, and control technologies, Smart City research initiatives, big data analytics, and recent advances in driving experiments, traffic safety research will greatly enhance our scientific understanding of the new interactions and phenomena between conventional, connected, and automated vehicles. In addition, the innovative data sources and increasing computing capabilities provide a great potential to extend the application of advanced methodologies in traffic safety research. Advances in traffic safety modeling, simulation, and management will play a critical role in addressing the competitiveness, sustainability, and mobility issues of current, transitional, and future transportation systems. This special issue is focused on the crucial aspects of current, transitional, and future traffic safety issues, with particular emphasis on the implications of advanced vehicle communication and automation technologies. Scientific research that develops and refines methodologies and technologies using new sources of data, such as data from naturalistic driving, connected vehicles, social media, and smart phones, is also incorporated. In total, 36 papers were submitted to this special issue, 11 of which were accepted for publication. As the guest editors of this special issue, we would like to summarize the 11 accepted papers below.

One study is chosen under the topic of safety implications and evaluation of advanced driving assistance systems. In "Influences of Waiting Time on Driver Behaviors While Implementing In-Vehicle Traffic Light for Priority-Controlled Unsignalized Intersections" by B. Yang et al., the authors investigated the effects of the waiting time on driver behaviors to improve the in-vehicle traffic light for the priority-controlled unsignalized intersections. Gap acceptance theory that considers the waiting time was employed in the implementation of the in-vehicle traffic light to assist minor-road drivers in passing through the intersections by selecting appropriate major-road gaps. The results show that the maximum acceleration strokes of minor-road vehicles were significantly reduced, which indicate a lower possibility of aggressive driving when the in-vehicle traffic light was applied with the consideration of waiting time. In addition, an improved steering stability was observed from the driver behaviors at the intersections, as the maximum lateral acceleration of minor-road vehicles significantly decreased.

Three studies examined the impacts of influencing factors on traffic crashes. In "Analyzing Traffic Crash Severity in Work Zones under Different Light Conditions" by X.

Wei et al., the authors examined the contributing factors to crash severity in highway work zones under different light conditions. The results show that an increase in the number of lanes increases the crash severity level in work zones during the daytime while decreasing the severity at nighttime. Drugs and alcohol are found to increase the severity level significantly under the dark-not-lighted conditions while it has a limited influence under daylight and dark-lighted conditions. In "Effects of Human-Centered Factors on Crash Injury Severities" by E. K. Adanu and S. Jones, the authors analyzed the effects of human-centered crash contributing factors on crash outcomes using the latent class (LC) logit model and random parameters logit (RPL) model. The results show that serious injury crashes were more likely to involve unemployed drivers, no seatbelt use, elderly drivers, fatigued driving, and drivers without a valid license. Comparison of model fit statistics shows that the LC logit model outperformed the RPL model, as an alternative to the traditional multinomial logit (MNL) model. In "Investigating the Differences of Single-Vehicle and Multivehicle Accident Probability Using Mixed Logit Model" by B. Dong et al., the authors investigated the different contributing factors on single-vehicle (SV) and multivehicle (MV) crashes. A mixed logit model is employed using disaggregated data with the response variable categorized as no crashes, SV crashes, and MV crashes. The results indicate that the speed gap, length of segment, and wet road surfaces have significant effects on both SV and MV crashes. Hourly traffic volume, inside shoulder width, and wet road surface are found to produce statistically significant random parameters.

Two papers addressed the topic of data-driven traffic safety monitoring, assessment, and improvement. In "Microscopic Simulation-Based High Occupancy Vehicle Lane Safety and Operation Assessment: A Case Study" by C. Li et al., the authors proposed two general alternative designs to enhance the operation and safety of High Occupancy Vehicle (HOV) lanes at junctions with bus terminals or parking lots. The microscopic simulation, video-based vehicle tracking technique, and Surrogate Safety Assessment Model (SSAM) are employed to assess the safety and operational efficiency of an HOV road segment near a bus terminal. The results show that the proposed alternative geometry design efficiently ameliorates the traffic conflict issues. In addition, the alternative control design scheme significantly reduces the public transit delay. In "Modeling Lane-Changing Behavior in Freeway Off-Ramp Areas from the Shanghai Naturalistic Driving Study" by L. Zhang et al., the authors investigated lane-changing characteristics in freeway off-ramp areas using Shanghai Naturalistic Driving Study (SH-NDS) data. A logit model was developed to analyze the choice of target lanes and estimate the parameters. The results suggested that the lane-changing behavior of exiting vehicles is the consequence of the balance between route plan (mandatory incentive) and expectation to improve driving conditions (discretionary incentive).

From the perspective of methodological advancement in traffic safety modeling, two studies investigated the advanced methodologies for crash frequency and severity analyses. In "Developing a Clustering-Based Empirical Bayes Analysis Method for Hotspot Identification" by Y. Zou et al., the authors proposed three clustering-based Empirical Bayer (EB) methods for hotspot identification. The considered clustering methods include the GFMNB-g model, K-means clustering, and hierarchical clustering with complete linkage. The results indicated that all three clustering-based EB analysis methods are preferred over the conventional statistical methods. Additionally, it seems that the accuracy of hotspot identification can be enhanced by appropriately classifying roadway segments according to the heterogeneity of the crash data (i.e., clustering the data before developing SPFs for use in EB estimates). In "A Novel Surrogate Safety Indicator Based on Constant Initial Acceleration and Reaction Time Assumption" by A. Fazekas et al., the authors presented the derivation of a novel surrogate safety indicator based on a constant initial acceleration and reaction time assumption. The evaluation is based on video-based microscopic traffic data collection. The results showed that the new indicator is more sensitive in detecting critical situations than the other indicators and can describe the conflict situations more realistically.

The remaining three articles focus on the topic of innovative traffic safety data collection, analysis, and molding using advanced technologies. In "A Novel Approach for Operating Speed Continuous Predication Based on Alignment Space Comprehensive Index" by Y. Yan et al., the authors proposed a novel method to estimate the operating speed for multilane highways in China from the aspect of the three-dimensional alignment combination. The results indicate that the proposed models have a superior performance. In "Road Surface State Recognition Based on SVM Optimization and Image Segmentation Processing" by J. Zhao et al., the authors proposed a method of video image processing technology for road surface state recognition. The results show that the method based on SVM and video image segmentation is feasible. The accuracy of particle swarm optimization algorithm is more than 90%, which effectively solves the problem of road surface state recognition under the condition of hybrid or different video scenes. In "Turnout Fault Diagnosis through Dynamic Time Warping and Signal Normalization" by S. Huang et al., the authors developed an intelligent diagnosis method for railway turnout through Dynamic Time Warping. The results indicate that the analyzed five turnout fault types can be diagnosed automatically with 100% accuracy.

Chunjiao Dong
Chunfu Shao
Helai Huang
Xiaoming Chen
N. N. Sze

Hindawi
Journal of Advanced Transportation
Volume 2018, Article ID 5262514, 12 pages
https://doi.org/10.1155/2018/5262514

Research Article

Microscopic Simulation-Based High Occupancy Vehicle Lane Safety and Operation Assessment: A Case Study

Chao Li, Mohammad Karimi, and Ciprian Alecsandru

Department of Building, Civil and Environmental Engineering, Concordia University, Montréal, QC, Canada H3G 2W1

Correspondence should be addressed to Chao Li; chaoli0351@gmail.com

Received 2 June 2017; Revised 18 January 2018; Accepted 4 March 2018; Published 5 April 2018

Academic Editor: Alain Lambert

This study proposes two general alternative designs to enhance the operation and safety of High Occupancy Vehicle (HOV) lanes at junctions with bus terminals or parking lots. A series of analysis tools, including microscopic simulation, video-based vehicle tracking technique, and Surrogate Safety Assessment Model (SSAM), are applied to model and test the safety and operational efficiency of an HOV road segment near a bus terminal in Québec as a case study. A metaheuristic optimization algorithm (i.e., Whale Optimization Algorithm) is employed to calibrate the microscopic model while deviation from the observed headway distribution is considered as a cost function. The results indicate that this type of HOV configurations exhibits significant safety problems (high number of crossing conflicts) and operational issues (high value of total delay) due to the terminal-bound buses that frequently need to travel across the main road. It is shown that the proposed alternative geometry design efficiently ameliorates the traffic conflicts issues. In addition, the alternative control design scheme significantly reduces the public transit delay. It is expected that this methodology can be applied to other reserved lane configurations similar to the investigated case study.

1. Introduction

The HOV lane represents a restricted usage traffic lane reserved for vehicles carrying a predetermined number of occupants. The implementation of an HOV lane system targets mobility improvement of both current and future roadway networks. Considering over forty years of deployment of HOV lanes, it has been proven that reserved lanes contribute to mitigating traffic congestion in urban areas and reduce the person-hour delay effectively [1, 2]. However, many problems related to various implementations of HOV lanes have been identified. These problems can be roughly classified into two categories, the reduction of capacity (for the non-HOV users) and potential traffic safety issues, respectively. The former category may include increased congestion on the adjacent General Purpose (GP) lanes and/or reduction of vehicle speeds due to the merging maneuvers of High Occupancy Vehicles into the GP lanes. The latter category is mainly related to the lane changes at prohibited locations, especially in the proximity of junctions with other road facilities, such as bus terminals or parking lots [3].

Currently, efforts are continually being made to explore the new ways to improve the operation and safety of HOV facilities. However, there is no universally accepted method to evaluate the effectiveness of safety of certain HOV facilities [4]. Some studies focused on the HOV safety evaluation based on the statistical analysis of accidents data during long periods [5]. Several studies examined the safety of HOV facilities with respect to different types of geometric design based on the collision and driving behavior (i.e., lane-changing) data [6, 7]. Nevertheless, obtaining reliable accident data over a long enough period is not always possible, especially for recently deployed facilities. A reliable accident-based analysis takes a long time to establish and thus is not suitable for current urban traffic system development. In addition, many characteristics of the urban traffic system may change over time (e.g., traffic demand volumes, road alignments, traffic mix, etc.), and this might require an expedited method to assess the existing traffic conditions. Accordingly, using conflict analysis as a method of safety assessment is preferable, as it makes analyzing the safety

improvement before implementing any treatment in the real world possible.

However, the geometric configuration of an HOV facility has significant impacts on the safety performance [7]. For instance, conducting the before-after study of converting the continuous access to limited access of lane changes in HOV lanes has shown a significant decrease in conflict occurrence. Therefore, the HOV facilities with limited access are expected to be safer than those with continuous access. To validate this conclusion, more studies must be conducted. However, there is limited opportunity for researchers to conduct before-after studies of road facilities with respect to the geometric modification, because they are too infrequent. Therefore, utilizing simulation tools may be an effective remedial measure to overcome the limitation of data availability and to evaluate the impacts of potential geometric alignment changes of existing facilities. Several studies have introduced the evaluation of safety or capacity of HOV facilities utilizing microsimulation [3, 8, 9]. However, these studies mainly focused on the analysis results of the study areas. Therefore, it is necessary to develop a systematic assessment method for HOV lanes. In particular, the HOV deployment on arterials in the proximity of the terminals and parking lots can be conducted using real-word data to calibrate a microscopic simulation model.

In this study, a VISSIM microsimulation model is developed to test the safety and operational efficiency of an urban HOV facility near a bus terminal in Québec, Canada. This model is calibrated by employing a metaheuristic optimization algorithm–Whale Optimization Algorithm (WOA)—to minimize the deviation of simulations results from the observed data. Two general alternative network designs are proposed for comparison analysis (i.e., one modifies the existing road geometric alignment; another one proposes a change in the existing traffic control strategy). To assess the road safety impact of the proposed alternative designs, the Surrogate Safety Assessment Model (SSAM) is applied to compare the simulated vehicle conflicts between the existing network and the alternative solutions. The results indicate that the status quo of the study area exhibits a safety problem due to high interactions between buses and passenger cars. The proposed alternative geometry design efficiently eliminates the traffic conflict. In addition, the alternative control design scheme significantly reduces the public transit delay.

2. Literature Review

Traditionally, most traffic safety studies employed statistical analysis of accident records within a given study area [10–13]. Several studies pointed out the drawbacks of using authority reported crash data for safety evaluation, for example, the lack of ability to evaluate the safety of traffic facilities yet to be built or to assess the traffic remediation solution yet to be applied in the field. In addition, the seldom and random occurrence of traffic accidents lead to the slowness of establishing analysis [14] or the lack of ability to deduce the crash process [15, 16]. On account of these drawbacks, an alternative safety evaluation approach which includes the computer microsimulation modeling of vehicle interactions was developed over the past couple of decades. This approach was possible mainly due to the advancements in computing technologies that allowed the development of enhanced traffic simulation models to be able to replicate vehicle interactions through modeling complex driving behaviors [16, 17]. A significant advantage of simulation-based safety analysis is that microsimulation models can easily generate and measure various safety performance indicators [18, 19]. The typical safety performance indicator is the vehicular conflict, given that conflicts can be observed more frequently than crashes and that their frequency is expected to be correlated with the crash occurrence [14, 20–22]. Various studies have validated the statistical significance and correlation between conflicts and accidents [23–26].

A dedicated tool, namely, SSAM was developed by Federal Highway Administration (FHWA) to automatically identify, classify, and evaluate the severity of the simulated traffic conflicts [14]. Several studies showed that by combining VISSIM and SSAM a reliable tool for traffic safety evaluation can be used, provided that a consistency between the field observed and simulated conflicts is observed [27, 28]. Another study proposed a two-step calibration procedure of VISSIM (Wiedemann model) to enhance correlation between simulated and field-measured conflicts [29]. Therefore, if the simulation model is properly calibrated, it can be used to represent reliably the real-world traffic network in terms of both operation and safety parameters.

3. Methodology

3.1. Modeling of Geometry and Flow. Typically, more detailed information contained in the simulation model contributes to capturing more reliably the traffic conditions at a given study area. This is especially important for a traffic safety simulation model, which requires good accuracy of both simulated capacity and vehicle performance.

The basic input to this model is represented by the road characteristics (i.e., the number of lanes on each direction, the lane separation type, and the position of access). In this study, the links and connectors of the study area were built in VISSIM by means of an aerial photo from Google Maps®. Some details of the geometry, for example, the access position of the public transit terminal, were measured on the field and were compared with the field-recorded videos to ensure the accuracy. Similarly, the position of the reserved lane was collected on the field and included in the simulation model.

Traffic flow is another important input parameter as it relates to the road capacity, one of the potential calibration variables. Traffic flows were measured using the videos recorded at the study area—the following data was collected: the vehicle counts of each lane, vehicle routes within the study area, and the vehicle types (e.g., bus, truck, and passenger cars). In this study, in order to smooth out random variations in flows, while maintaining good precision, the vehicle flows were recorded and input into the model in five-minute increments. An additional five-minute period without vehicle demand was included at the end of each simulation scenario to avoid truncating the analysis period observed in the field. To model the observed vehicle composition, road users were

identified and classified into three categories, passenger cars, buses, and trucks, respectively. The basic vehicle characteristics, for example, the acceleration rate, vehicle length, and vehicle weight of each vehicle type, can be modeled separately in VISSIM so as to reflect the traffic more realistically. To determine individual vehicle routes, vehicles were tracked in from the videos generated by three cameras that were used to cover the whole study area. The route of each vehicle in the simulation was assigned in strict accordance with the path observed on the video recordings to ensure a realistic representation of the study area.

3.2. Modeling of Traffic Signal. The peak hour traffic signal cycle length and the red, amber, and green time intervals on each direction were collected on the field and modeled in VISSIM. In this study, a fix-cycled signal program was built and set at the intersection to replicate the traffic light at the study area. Some additional signal control strategy was used in this study to improve the network performance; for example, a fix signal cycle contains a protected left-turn phase at the intersection and a pulse-triggered signal at the public transit terminal.

To improve the efficiency of public transit, a pulse-triggered signal control was implemented by adding a detector at the exit of the terminal and signal heads linked with the detector near the terminal. An add-on signals design model, namely, Vehicle Actuated Programming (VAP) was programmed to control this actuated signal. Typically, a signal phase of permanent green on the main street and permanent red on the minor road is toggled when no buses are detected. Meanwhile, when the existing buses are detected by the sensor, the signal is programmed to switch to the complementary phase (i.e., green signal on the minor road and red on the main road), thus protecting the movements of buses crossing through multiple lanes.

3.3. Modeling of Right of Way without Signal Control. In VISSIM priority rules are defined to capture the conflicting traffic flows that are not controlled by signals. In this study, the priority rules were set at the entry and the exit zones of the bus terminal, in order to realistically model the access and egress movements of buses as they were observed in the video recordings. Typically, the buses travel to and from the terminal, yielding to the vehicles traveling along the main arterial, and stop in position near the access or exit until acceptable gaps occur on both directions on the main road. Two thresholds are set for the p*riority rules* to confine the crossing of the yielding vehicles, respectively, the *minimum headway* and the *minimum gap time*. A yielding vehicle will stop before the stop line until both predetermined thresholds are achieved. The values of the thresholds are determined by reviewing all the accepted gaps and headways by the crossing buses from the video.

The conflict areas are automatically generated in VISSIM where links or connectors overlap. In this study, the priority rules at the conflict areas were set to capture the vehicles approaching the conflict area from the minor road and yielding those from the main road, as typically observed in the field. The gap time needed for crossing at the conflict area was determined similarly by reviewing the video recordings.

Another important VISSIM calibration parameter is the *avoid blocking* value, which defines the ratio of vehicles that do not stop in the middle of a junction. This value is defaulted to be 100% in VISSIM; in other words, all the vehicles will follow the rule, not to block the junctions, if there is stopping traffic ahead. However, by reviewing the video recorded at the study area, no vehicle obeyed this rule. Therefore, to reflect the real conditions, this value is set to 0% for all the conflict areas in simulation models used in this study.

3.4. Modeling of Driving Behavior. Properly modeling of the field observed driving behavior is critical for road safety evaluation, since it directly influences the vehicle interactions in a micro level. Microsimulation tool VISSIM adopted Wiedemann car following model as the main portion for modeling the vehicle longitudinal movement and rule-based laws for modeling of vehicle lateral movement and lane change behavior.

In this study, the Wiedemann 74 model is selected to simulate the urban motorized traffic as suggested by the VISSIM user's manual [30]. This model contains three adjustable parameters, respectively, the *average standstill distance*, the *additive part of safety distance*, and *multiplicative part of safety distance*. *Average standstill distance* defines the average desired distance between two cars. *Additive part of safety distance* and *multiplicative part of safety distance* represent the values used for the computation of the desired safety distance. For the initial simulation, the values of these three parameters are usually defined with the default value. However, they must be calibrated later to suite the real driving behaviors of the study site.

The lane change behaviors are defined by a rule-based model in VISSIM. In this model, the critical parameter that decides whether a lane change would be executed is the *minimum headway*. A vehicle can only change lane when there is a distance gap arrival at the adjacent lane that is bigger than the predetermined minimum headway. Otherwise, it has to either travel continuously or stop and wait until the occurrence of an enough gap for it in order to merge according to its predefined route. In this study, the value of the *minimum headway* was determined by reviewing the videos.

Another noticeable parameter defined in the lane change model is the *advanced merging*; this option is selected in this study; thus more vehicles can change lanes earlier when following their routes, as encountered in the videos.

3.5. Measurement of Vehicle Speed Distribution by Feature-Based Tracking. Vehicle speed distribution is an important input parameter for safety simulation. While potentially more accurate, individual vehicle speed on multiple lanes is usually difficult to measure on the field simultaneously with radar devices. Therefore, an alternative method was applied in this study to measure the vehicle speed, which is the video-based feature tracking.

An open-sourced software project, namely, *Traffic Intelligence*, was used to automatically track and measure the speed of the vehicles caught by the video at the study

Figure 1: Points selected on the video frame to compute homography file.

site [31]. *Traffic Intelligence* consists of a set of tools that work cooperatively for traffic data processing and analysis, including camera image calibration, feature tracking, and trajectory data analysis.

The feature-based tracking algorithm utilizes a homography file that projects the camera image space to the real-world ground plane. The homography file was created by utilizing a video frame and a corresponding aerial photo with known scale (pixels per meter). In this study, an aerial photo of the study site from Google Maps with known scale of 0.21 pixels per meter was adopted. In total ten noncollinear visible points on the video frame were positioned on the aerial photo; thus, the video image was projected to the aerial photo, and the vehicles tracked in the video were deemed to be tracked in the real-world plane with their speeds. Figure 1 shows the points projected to the aerial photo from the video frame.

Based on the computed homography file, the feature tracking program can be run. The predetermined number of features of each vehicle in the video was detected and tracked frame by frame until the vehicle leaves the video capture area. In order to suppress the interference of the shadows, a mask image was created and toggled with the video image; therefore only the features within the white range of the mask image can be detected, and the shadows can be filtered out. The features that move consistently were then grouped together to generate the trajectory file of each vehicle, and all the trajectories generated from the video were written into a database. The average speed of each vehicle can be easily read by processing their trajectories. Figure 2 shows the feature tracking process by *Traffic Intelligence*.

3.6. Model Calibration. In order to determine the optimum values for the calibration parameters, an objective function should be defined based on the error between observed data and simulated data. The objective function is the deviation of the simulated gap distribution from the real observed gap distribution. In order to test this goodness of fit (objective), the Chi-square test was employed. In this study, the westbound vehicle gap distribution on the GP lane near the bus terminal was taken as the criterion to calibrate the

Figure 2: Feature tracking process by *Traffic Intelligence*.

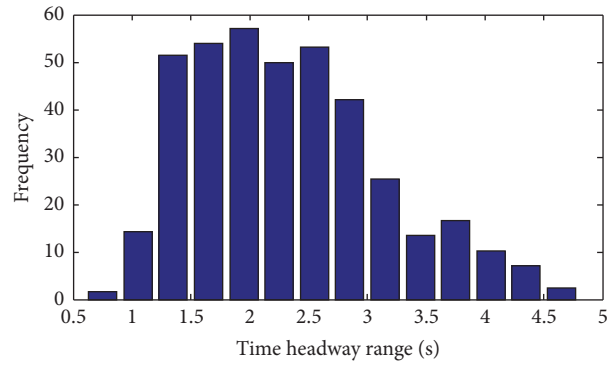

Figure 3: Observed vehicle gap distribution.

model, because the vehicle time gap directly reflects the car following behavior. The real vehicle gaps were observed manually from the video using the *MPC player* that provides milliseconds accuracy. Because the vehicles travel westbound pass through a signalized intersection before they enter the cameras field of view, to eliminate the impact of the red time at the intersection, the time gaps bigger than 5 seconds were ignored. The distribution of all the observed gaps that are smaller or equal to 5 seconds was recorded in a histogram with a sample rate of 0.3 seconds. Figure 3 shows the observed vehicle gap distribution.

In this paper, the Whale Optimization Algorithm (WOA), a metaheuristic nature-based algorithm, is applied to calibrate the model. The deviation of the simulated headway distribution from its' observed distribution is considered as the objective function to be minimized during the calibration process. WOA is inspired by hunting behavior of humpback whales. It is defined as "the simulated hunting behavior with random or the best search agent to chase the prey and the use of a spiral to simulate bubble-net attacking mechanism of humpback whales" [32]. The hunting behavior of whales is representative of the procedure of this algorithm.

The three parameters of the Wiedemann 74 model in VISSIM (i.e., average standstill distance (ASSD), additive part of safety distance (APSD), and multiplicative part of safety distance (MPSD)) which has the highest impact on the model have been selected to be calibrated. Using MATLAB, an optimization toolbox connecting to COM-interface of VISSIM by M-file programming in MATLAB, the calibration process has been accomplished. After 190 simulation runs, the optimal values of parameters were determined to be as

follows: ASSD = 1.156, APSD = 0.637, and MPSD = 8.079. For diverse random seeds, the simulation results showed these optimal parameters lead to statistically matching the observed headway distributions with the simulated ones at 90% confidence level. It is worth mentioning that the simple way to optimize the cost function is exploring the whole possible region of the parameters to find the global minimum, which is extremely time-consuming. For this case study, these optimization parameters took values within the following intervals: ASSD between 0 and 2, APSD between 0 and 1, and MPSD between 0 and 10. By exploring these intervals, the optimal values were found after nearly 1000 simulation runs.

The lateral movement of buses that merge into the main traffic from HOV lane or travel across the road when an acceptable gap was identified was also calibrated by adjusting the parameters of the priority rule. The minimum gap time and distance headway were set to 6 seconds and 20 meters, respectively, similar to the values observed in the recorded videos. It is noticeable that a part of the terminal-bound buses changed lanes between the reserved HOV lane and the adjacent GP lane before the intersection; this behavior is reflected in the simulation model.

3.7. Simulation Output. VISSIM provides direct output of various kinds of simulation results. In this study, the vehicle delay and trajectory were analyzed to evaluate the operational efficiency and safety of the study area.

Vehicle delay data can be generated by setting *vehicle travel time* on the defined vehicle routes, which are defined by a *Starting Point* and an *End Point*, respectively. For the vehicles that pass through the *Starting Point* and the *End Point*, successively, the travel time delays are automatically calculated. The vehicle delays of the interested vehicle routes were then analyzed to evaluate the operational efficiency of the network.

The trajectories of all the simulated vehicles can be generated by VISSIM, and the recorded trajectory data was then analyzed using SSAM, to evaluate the vehicle conflicts within the network. For each simulation run, different simulation random seeds were applied, and the output results were averaged for analysis purposes. This simulation setup scenario accounts for the stochastic properties of the simulation model, thus reflecting real-world traffic behavior more realistically.

3.8. Analyzing Vehicle Conflicts Using SSAM. The vehicle trajectory data collected from VISSIM was used in SSAM to assess the vehicle conflicts detected in the study area. Most studies evaluate traffic safety through two surrogate measures, Time to Collision (TTC) and Postencroachment Time (PET). Values below a commonly accepted threshold of either TTC or PET value indicates a higher probability of collision. SSAM is able to automatically estimate the TTC and PET values of each vehicle interaction and thus to record all potential conflicts. In this study, the TTC and PET were set to 1.5 seconds and 5 seconds, respectively, the values frequently established by previous research studies [20, 33].

The detected conflicts were classified into three types, based on the predetermined conflict angles, namely, *crossing*, *lane changing*, and *rear ending*, respectively. The thresholds of the conflict angles were adjusted to 2 degree and 45 degree as suggested by previous studies [8]. Basically, detected conflict which has a conflict angle of 2 degrees or less is defined as *rear ending* conflict; if the conflict angle is between 2 and 45 degrees, it is detected as *lane changing*; while if the conflict angle is bigger than 45 degrees, it is recorded as the *crossing type*. However, due to the peculiarity of geometry of each study area, the link information of all the output conflicts, which was also detected by SSAM, was manually checked to properly determine their type. The three types of conflicts were recorded for subsequent comparative safety analysis.

A built-in filter of SSAM can be applied to screen out the conflicts caused by each measured movement by reading the corresponding link information. The spots where conflicts were detected can be plotted automatically on the toggled network image by positioning the VISSIM network coordinates. The conflicts of different types can be showed in different shapes or colors on the togged map to give a visual estimate of the hotspot areas (i.e., conflicts' frequency and density).

3.9. Summary. The methodology presented in this study introduces a simulation-based approach to evaluate road network safety and efficiency. To apply this methodology, the field traffic conditions are collected, and the detailed information including the field geometry, control strategy, flow, and driving behavior is reviewed. Such basic information is then integrated in a VISSIM simulation model. With an important model parameter, the vehicle speed distributions are obtained using a feature tracking program, namely, *Traffic Intelligence*. The model is properly calibrated until the output vehicle time gap distribution compared well with the field observed vehicle gap distribution by applying the Chi-square test. The model output vehicle delays are reviewed for network operational efficiency analysis, and the model output vehicle trajectory files are analyzed by SSAM to determine the conflict within the study area thus giving the safety level of the site. Figure 4 shows the flow chart of the methodology used in this study for traffic safety and operational efficiency evaluation.

4. Case Study

4.1. Study Area Description. The study area used in this study is a segment of Rte-116, a suburban highway in Lévis, Québec. Evaluations of traffic safety and operations were made at a specific location along the four-lane east-west arterial segment that includes one GP lane and one HOV lane, in both directions. The eastbound reserved lane allows buses and passenger cars with three or more passengers, while the westbound direction has a bus-only lane. The current design of this facility is such that the westbound buses arriving at or departing from the terminal have to travel across the four-lane undivided road. Figure 5 shows the current paths of the buses using the terminal.

The traffic video feeds of vehicles accessing the terminal, the commuter parking lot, and traveling along Rte-116 were collected via GoPro HD video cameras that were installed

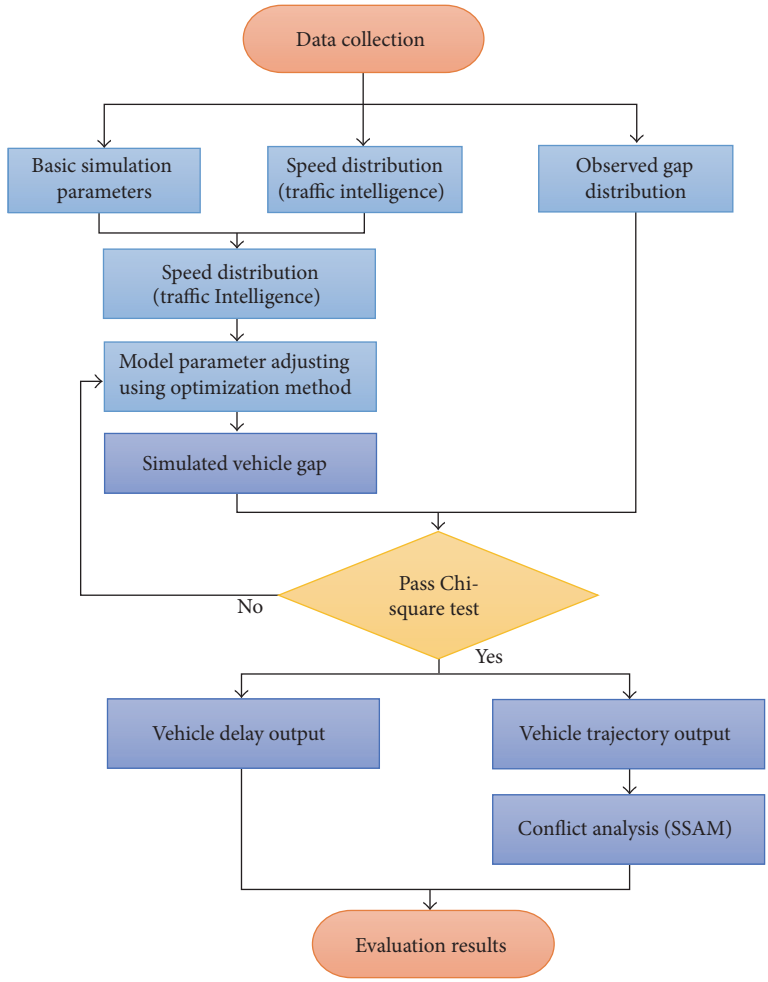

Figure 4: Framework of evaluation procedure.

on top of extendable masts along the roadway. Cameras 1 and 2 were both installed at the same location with views opposing each other. The orientations of these two cameras were adjusted to capture east-west traffic that interacts with both access points into and out of the bus terminal. Camera 3 was installed at the proximity of the commuter parking lot entry/exit gate, to capture interactions between main road traffic and vehicles to and from the parking. The positions of the cameras are shown in Figure 5. The video traffic data of the PM peak hour (4:30 pm~5:30 pm) was used in the final analysis of this study.

A probe vehicle was driven several times along the study segments with an arbitrarily selected constant speed. The known speed values were used to calibrate the postprocessing speed detection measuring software, *Traffic Intelligence*. A fixed 88-second cycle of the traffic signal along Rte-116 at the adjacent intersection (i.e., 40 seconds, red, 40 seconds, green, and 4 seconds, yellow) was measured in the field and used in the simulation model of the study area.

The video files from each camera were processed in 5-minute increments to manually determine the distribution of traffic flows during the analysis period. Vehicles were

Figure 5: Paths of the terminal-bound buses.

distinguished into four types: passenger cars (on the GP lane), buses, trucks, and reserved lane users, respectively. This definition of the traffic mix was necessary to capture more reliably the vehicle interactions in the traffic simulation model (different vehicle types exhibit different driving behaviors in terms of acceleration, minimum headway, etc.). Tables 1 and 2 show a classification of westbound and eastbound

Table 1: Observed traffic flow during the peak hour (4:30 pm~5:30 pm).

Time	Average vehicle flows (vehicles/hour)							
	Westbound				Eastbound			
	Car	Bus	Truck	HOV	Car	Bus	Truck	HOV
4:30 pm~5:30 pm	663	16	3	7	338	5	4	36

Table 2: Access and egress vehicles during the peak hour (4:30 pm~5:30 pm).

Time	Average vehicle flows (vehicles/hour)							
	Westbound				Eastbound			
	Bus		Parking car		Bus		Parking car	
	Access	Egress	Access	Egress	Access	Egress	Access	Egress
4:30 pm~5:30 pm	10	14	0	37	7	3	4	18

Table 3: Vehicles characteristics.

Vehicle type	Length (meter)	Width (meter)	Weight (ton)	Maximum acceleration (m/s^2)	Maximum deceleration (m/s^2)
Car and HOV	3.75–4.76	1.85–2.07	-	3.5	−7.5
Bus	11.54	3.17	4–12	1.24	−7.5
Truck	13.94	2.63	2.8–40	2.5	−5.5

traffic flows along the highway, as well as access/egress of the buses using the terminal during the afternoon peak period.

Traffic Intelligence was utilized to measure the vehicle speed. Calibration of the video analysis software was performed using various mask pictures to filter the shadows of the moving vehicles until the measured speeds of the probe vehicle were identical to the observed values. The vehicle speed distributions of both westbound and eastbound vehicles were recorded every five minutes and used as simulation input parameters.

4.2. Modeling Existing Configuration and Traffic Conditions (Status Quo). The peak hour traffic was modeled in VISSIM to evaluate traffic safety and operations of the observed arterial segment. Vehicle modals used in the simulation are selected by VISSIM automatically. The vehicle characteristics of the case study are shown in Table 3. To account for the effects of stochastic variation of the model's parameters, ten different simulations with different random seeds were ran, and the average values were used in the analysis.

The average vehicle delay (excluding signal waiting time at intersection) was measured for three types of movements, using the *vehicle travel time measurements* tool. *Movement 1* identifies the westbound traffic on the GP lane. *Movement 2* is associated with westbound buses entering the terminal (i.e., buses merging from HOV lane into the GP lane and then crossing the two eastbound lanes). *Movement 3* represents westbound buses leaving the terminal (i.e., buses that cross all the four lanes to enter the highway). Vehicle trajectory files were also generated for conflict analysis.

In addition, to evaluate the impact of expected increase in traffic flow on traffic operations (i.e., average vehicle delay) and safety (i.e., conflicts frequency), the same simulation model was used to evaluate similar scenarios, assuming the traffic volume increases in the future by 10%, 20%, and 30% from the current values. Figure 6 represents a snapshot of the VISSIM simulation model using the existing geometric alignment and traffic operations conditions.

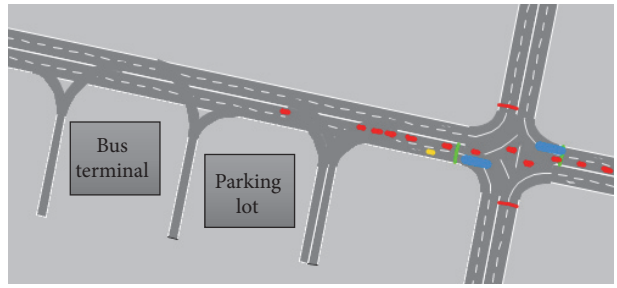

Figure 6: The status quo network modeled in VISSIM.

4.3. Simulations of Alternative Geometry/Control Designs. The main concern related to traffic safety at the investigated study area pertains to the placement of the reserved lanes on the outside lanes. This configuration leads to multiple lanes crossing when left turns are needed and high occurrence of vehicle interactions was observed especially during congested traffic conditions.

Two alternative designs have been tested to evaluate their potential to mitigate traffic safety and operations issues. Figure 7 shows the VISSIM network layout of the first alternative design. In this model, westbound buses were prohibited to enter or exit the terminal by crossing the highway directly. Instead, an adjacent roadway segment was inserted along the south side of bus terminal, which is directly connected to the minor road. To serve the terminal-bound buses, ten seconds of left-turning signal phase was provided at the intersection on the main road. Similarly, for each

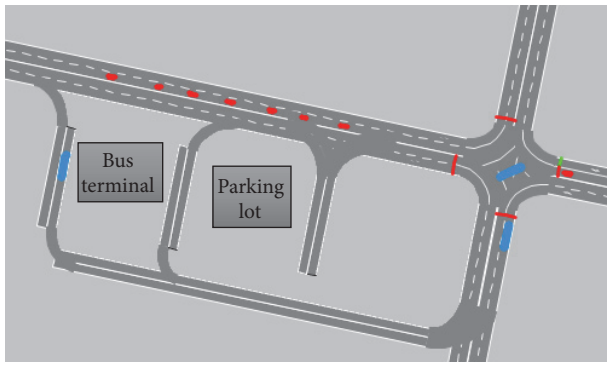

Figure 7: VISSIM network of alternative road geometry design.

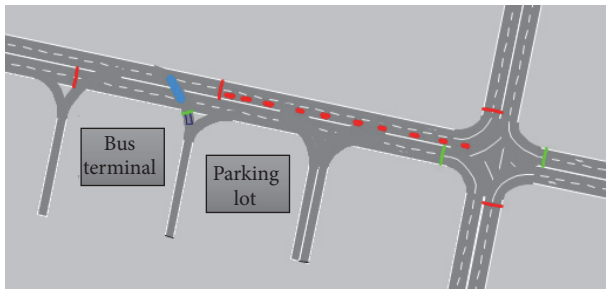

Figure 8: VISSIM network of alternative control design.

traffic demand alternative (i.e., current status, 10%, 20%, and 30% increments of vehicular traffic volume), the collected peak hour vehicle flows and speed distributions were used to model the network using ten simulation random seeds. The individual vehicle trajectories and delay measurements of the same movements evaluated for the status quo configuration were collected and used for comparison analysis. Figure 8 shows the VISSIM network layout of the second alternative design. In this model, a loop detector that controls a signal set was added to the existing network. This system was used to control the egress of westbound buses as they leave the terminal. The add-on signal control model VAP was created to program the signal timing. The detector was placed near the exit of the bus terminal. As long as buses are not in the proximity of the sensor, the signal indicates green for the main road to allow east-west traffic and red for the bus exit to prevent the egress buses from traveling across the road directly. When buses are detected at the terminal, exit signal turns green for them and red for traffic on the main road, which allows for protected turns. The red signal on the main road lasts for 10 seconds from the last bus detected and then turns back to green until the next detection. The same vehicle hourly flows previously processed were used in this simulation scenario, and the same ten different simulation random seeds were applied. The delay measurements of the same types of movements and trajectory data were collected for comparative analysis.

4.4. Surrogate Safety Measures of Vehicle Conflicts. SSAM was applied to assess the vehicle conflicts detected in the

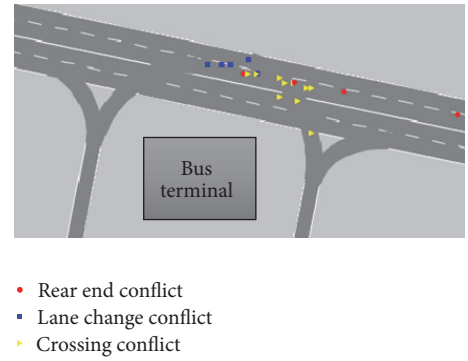

Figure 9: Conflicts near bus terminal plots on original network.

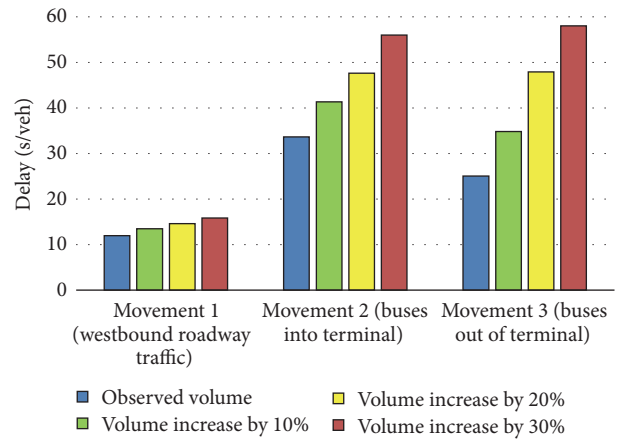

Figure 10: Effects of increasing traffic flow on average delay per vehicle.

study area for safety analysis. A built-in filter of SSAM was applied to screen out the conflicts caused by each measured movement by reading the corresponding link information. The spots where conflicts were detected were plotted automatically on the toggled network image by utilizing the VISSIM network coordinates. The conflicts of different types were showed in different shapes on the togged map. Figure 9 shows the spatial distribution of conflicts caused by measured movements near the bus terminal plotted on the original network.

4.5. Comparison Analysis of Safety and Operation. Figures 10 and 11 represent the impact of different traffic volumes on traffic operations (delay) and safety (conflicts).

As intuitively expected, more traffic demand leads to increased average delay. It also shows that of the three types of vehicle interactions analyzed movements labeled 2 and 3 (i.e., associated with buses entering and leaving the terminal) are affected by significantly higher delay than the vehicles moving along the east-west roadway. This is explained by the fact that buses have to make left turns from/into the arterial, and consequently they do not have the default right of way. In addition, traffic safety analysis (i.e., evaluation of vehicular interactions through the SSAM tool) shows that, for all levels of traffic demand, the majority (more than 85%) of vehicular

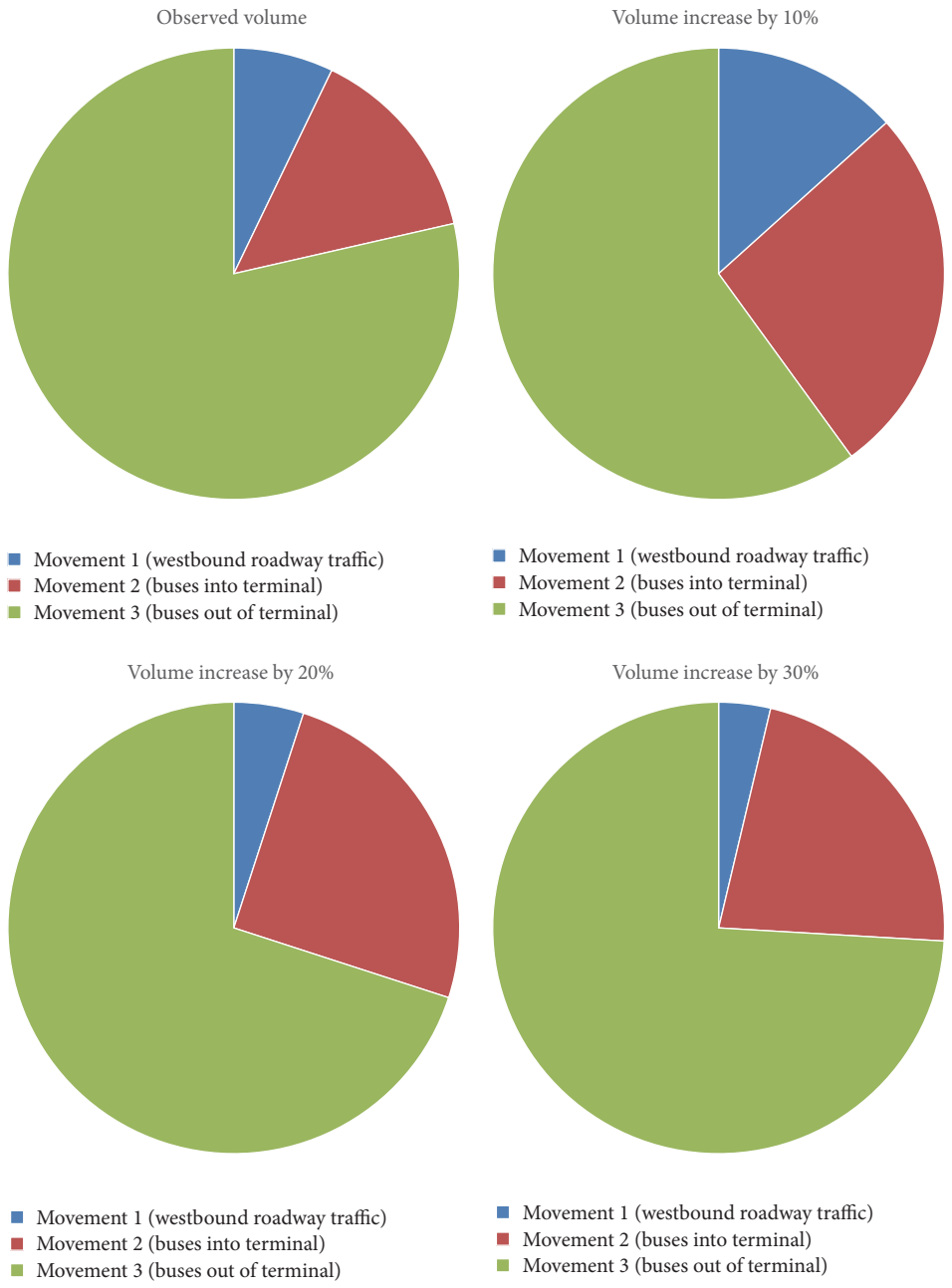

Figure 11: Sensitivity analysis of conflicts distribution (current configuration).

conflicts were crossing conflicts associated with the same movements of buses that enter or leave the terminal facility. Moreover, lane-changing conflicts were observed between buses moving from the reserved lane into the GP lane to engage in left-turning maneuvers towards the terminal.

Figure 12 shows the effects of different traffic volumes on traffic operations (magnitude of delay) and safety (frequency of conflicts) when the first alternative scenario was used. As expected, by including a separation median between the two directions of traffic, all vehicular conflicts associated with left-turn movements into and out of the terminal are eliminated. The sensitivity analysis demonstrates that traffic operations are not impacted by this design. It can be seen that there is a minor positive effect on the average vehicular delay for movement 1 (vehicles traveling westbound on Rte-116), but there is a significant positive effect on the average delay of buses accessing the terminal (i.e., a reduction in delay of about 85%). However, this alternative scenario brings a trade-off for the movements of buses exiting the terminal that are hindered for most traffic flow levels. The additional delay encountered by buses leaving the terminal is due to the fact that, for this design, the westbound egress buses must use

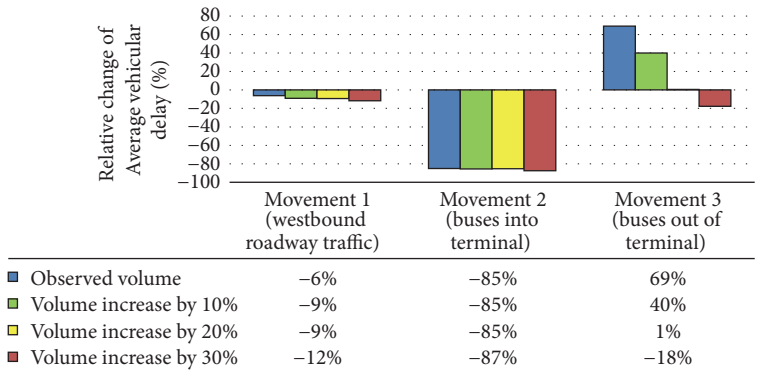

Figure 12: Effects of first alternative design on the average delay (separation median).

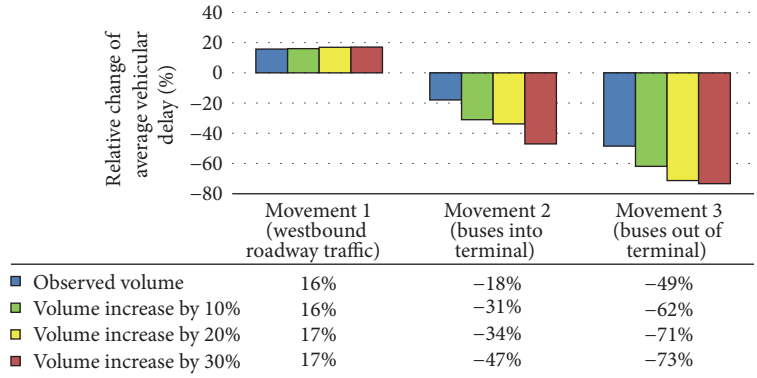

Figure 13: Effects of second alternative design on the average delay (traffic control).

the nearby intersection, and the traffic signal timing was not optimized to accommodate left-turning buses from the minor street.

The results for the second alternative design (i.e., controlling the access/egress of buses for Movements 2 and 3 via a bus-triggered traffic control signal, in order to reduce the vehicle interactions with the buses) are shown in Figure 13. It can be seen that this alternative design reduces considerably the delay of buses in and out of the terminal (Movements 2 and 3), while it increases by less than 17% the delay of vehicles traveling westbound along the arterial (Movement 1).

More importantly, the vehicular conflict analysis of these results shows the elimination of the crossing conflicts (Movements 2 and 3) related to buses accessing/leaving the terminal by turning left across the HOV and GP lanes. In addition, this design has no impact on the low conflict occurrence of Movement 1 (vehicles moving westbound on the arterial).

Several aspects of the proposed alternative designs are discussed at the end of this section. The delay of the traffic flow moving westbound on the arterial during the peak period was compared across all three simulation scenarios (i.e., current design, separation barrier, and traffic control alternative). It was found that the traffic control alternative leads to the most negative impact on the vehicular delay. In addition, conflict occurrence between the current design and the proposed traffic control design is not significantly different, due to breaking at red light; it is expected that rear ending conflicts might be more severe. On the other hand, rerouting buses through the intersection via the minor street seems to be the best option, because it eliminates completely all conflicts of left-turning vehicles while its impact on traffic operations might not be significant, since it can be mitigated with optimizing the traffic signal timing plan at the intersection.

To conclude, the existing geometric and traffic signal configurations show that there is a high occurrence of vehicular conflicts for left-turn buses approaching terminal. It can be seen from the results above that, by using the alternative designs, these types of conflicts are eliminated. In addition, the proposed alterations to existing alignment provide benefits for traffic operations because they reduce significantly the average vehicular delay. However, when traffic signals are used to control for protected left-turn buses that are rerouted through the adjacent intersection, an additional analysis of signal delay and optimization is necessary.

Similarly, the analysis of the measured movement 3 (i.e., westbound buses leaving from terminal) identifies a large number of crossing conflicts within the east-west traffic on the main arterial. Elimination of these conflicts can be achieved if this movement is protected either through the traffic signal sensitive to the buses present at the terminal exit,

or by using the barrier separated geometry that reroutes the buses via the adjacent intersection. The results indicate that the network with alternative control design is the best for departing buses (i.e., the delay is the smallest).

As expected, the sensitivity analysis shows that an increased main arterial traffic volume leads to negative effects on the conflict frequency and average vehicular delay, regardless of the design used, while the alternative designs provide elimination or significant reduction in conflicts.

5. Concluding Remarks

This study proposed two general alternative geometry and control designs to improve the operation and safety of High Occupancy Vehicle (HOV) lanes near the bus terminals and parking lots. A VISSIM simulation model was created using the observed field geometry, control strategy, and vehicle flows, and then the vehicle priority rules and driving behaviors were calibrated to reflect correlated parameters observed on the field. An important model parameter, the vehicle speed distribution, was measured by feature-based tracking technique using an open-sourced program, namely, *Traffic Intelligence*. The model was calibrated using a meta-heuristic optimization algorithm (i.e., Whale Optimization Algorithm) with respect to the field-measured vehicles headway distributions. The results showed that this algorithm converged to the optimal parameters faster than searching whole parameters' intervals. The output delay data was used for operational efficiency analysis, and the output trajectory data was analyzed by SSAM to determine the number of vehicle conflicts within the study area. This procedure was applied to test the safety and operational efficiency of an HOV road segment in Lévis, Québec. The peak hour safety and operational traffic conditions of the status quo and of two alternative designs (i.e., geometry and control designs) were analyzed. The results indicate that the existing network configuration exhibits significant safety issues due to the crossing conflicts along the path of buses approaching the terminal across the four-lane arterial road. It was shown that one of the investigated alternative designs may enable the terminal-bound buses to travel on a different path to efficiently eliminate critical vehicular conflict. In addition, it was shown that the alternative control design can be used to reduce the bus delay by giving priority to public transit. It is expected that this methodology can be successfully applied to other similar reserved lanes facilities in the vicinity of the bus stations and parking lots.

Disclosure

All the viewpoints and errors expressed in this research are solely those of the authors.

Conflicts of Interest

The authors declare that there are no conflicts of interest regarding the publication of this paper.

Acknowledgments

This study was funded by Ministère des Transports du Québec (MTQ) through research Project R706.1. The authors would like to thank Matin Giahi Foomani and Gia Hung Lieu from Concordia University for the help in data collection.

References

[1] C. Fuhs and J. Obenberger, "Development of high-occupancy vehicle facilities: Review of national trends," *Transportation Research Record*, no. 1781, pp. 1–9, 2002.

[2] M. Menendez and C. F. Daganzo, "Effects of HOV lanes on freeway bottlenecks," *Transportation Research Part B: Methodological*, vol. 41, no. 8, pp. 809–822, 2007.

[3] A. Guin, M. Hunter, and R. Guensler, "Analysis of reduction in effective capacities of high-occupancy vehicle lanes related to traffic behavior," *Transportation Research Record*, no. 2065, pp. 47–53, 2008.

[4] J. I. Bauer, C. A. McKellar, J. M. Bunker, and J. Wikman, "High occupancy vehicle lanes-an overall evaluation including Brisbane case studies," in *Proceedings of the 2005 AITPM National Conference*, J. Douglas, Ed., pp. 229–244.

[5] T. F. Golob, W. W. Recker, and D. W. Levine, "Safety of high-occupancy vehicle lanes without physical separation," *Journal of Transportation Engineering*, vol. 115, no. 6, pp. 591–607, 1989.

[6] K. Jang, K. Chung, D. R. Ragland, and C.-Y. Chan, "Safety performance of high-occupancy-vehicle facilities," *Transportation Research Record*, no. 2099, pp. 132–140, 2009.

[7] X. Qi, G. Wu, K. Boriboonsomsin, and M. J. Barth, "Empirical study of lane-changing characteristics on high-occupancy-vehicle facilities with different types of access control based on aerial survey data," *Journal of Transportation Engineering*, vol. 142, no. 1, Article ID 04015034, 2016.

[8] H. Tao, M. G. Foomani, and C. Alecsandru, "A two-step microscopic traffic safety evaluation model of reserved lanes facilities: an arterial case study," in *Transportation Research Board 94th Annual Meeting No. 15-3635*, 2015.

[9] V. Thamizh Arasan and P. Vedagiri, "Microsimulation study of the effect of exclusive bus lanes on heterogeneous traffic flow," *Journal of Urban Planning and Development*, vol. 136, no. 1, Article ID 009001QUP, pp. 50–58, 2010.

[10] B. N. Persaud, R. A. Retting, P. E. Garder, and D. Lord, *Observational BeforeAfter Study of the Safety Effect of US*, Transportation Research Board, National Research Council, 2001.

[11] D. Gettman and L. Head, "Surrogate safety measures from traffic simulation models," *Transportation Research Record*, no. 1840, pp. 104–115, 2003.

[12] S. Srinivasan, P. Haas, P. Alluri, A. Gan, and J. Bonneson, "Crash prediction method for freeway segments 2 with high occupancy vehicle (HOV) lanes 3," in *Transportation Research Board 95th Annual Meeting (No. 16-6333)*, 2016.

[13] R. Elvik, "The predictive validity of empirical Bayes estimates of road safety," *Accident Analysis & Prevention*, vol. 40, no. 6, pp. 1964–1969, 2008.

[14] D. Gettman, L. Pu, T. Sayed, and S. G. Shelby, *Surrogate Safety Assessment Model and Validation: Final Report*, 2008, No. FHWA-HRT-08-051.

[15] A. Laureshyn, Å. Svensson, and C. Hydén, "Evaluation of traffic safety, based on micro-level behavioural data: theoretical

framework and first implementation," *Accident Analysis & Prevention*, vol. 42, no. 6, pp. 1637–1646, 2010.

[16] W. Young, A. Sobhani, M. G. Lenné, and M. Sarvi, "Simulation of safety: A review of the state of the art in road safety simulation modelling," *Accident Analysis & Prevention*, vol. 66, pp. 89–103, 2014.

[17] J. Archer, "Developing the potential of micro-simulation modelling for traffic safety assessment," in *Proceedings of the 13th ICTCT Workshop*, vol. 44, 2000.

[18] J. Archer, *Methods for the Assessment and Prediction of Traffic Safety at Urban Intersections and Their Application in Micro-Simulation Modelling*, Royal Institute of Technology, 2004.

[19] A. Sobhani, W. Young, and M. Sarvi, "A simulation based approach to assess the safety performance of road locations," *Transportation Research Part C: Emerging Technologies*, vol. 32, pp. 144–158, 2013.

[20] C. Hydén, *The Development of a Method for Traffic Safety Evaluation: The Swedish Traffic Conflicts Technique*, Bulletin Lund Institute of Technology, 1987.

[21] S. J. Older and B. R. Spicer, "Traffic conflicts—a development in accident research," *Human Factors: The Journal of Human Factors and Ergonomics Society*, vol. 18, no. 4, pp. 335–350, 1976.

[22] F. H. Amundsen and C. Hyden, "Proceedings of first workshop on traffic conflicts," in *Proceedings of Workshop on Traffic Conflicts*, TTI, Oslo, Norway, 1977.

[23] S. R. Perkins and J. L. Harris, "Traffic conflict characteristics-accident potential at intersections," in *Proceedings of the Traffic Safety and presented at the 47th Annual Meeting*, pp. 35–43, Highway Research Board, 1968.

[24] M. R. Parker and C. V. Zegeer, *Traffic Conflict Techniques for Safety and Operations: Engineers Guide*, 1989.

[25] E. Hauer and P. Garder, "Research into the validity of the traffic conflicts technique," *Accident Analysis & Prevention*, vol. 18, no. 6, pp. 471–481, 1986.

[26] K. El-Basyouny and T. Sayed, "Safety performance functions using traffic conflicts," *Safety Science*, vol. 51, no. 1, pp. 160–164, 2013.

[27] R. Fan, H. Yu, P. Liu, and W. Wang, "Using VISSIM simulation model and surrogate safety assessment model for estimating field measured traffic conflicts at freeway merge areas," *IET Intelligent Transport Systems*, vol. 7, no. 1, pp. 68–77, 2013.

[28] F. Huang, P. Liu, H. Yu, and W. Wang, "Identifying if VISSIM simulation model and SSAM provide reasonable estimates for field measured traffic conflicts at signalized intersections," *Accident Analysis & Prevention*, vol. 50, pp. 1014–1024, 2013.

[29] M. Essa and T. Sayed, "Simulated traffic conflicts: do they accurately represent field-measured conflicts?" *Transportation Research Record*, vol. 2514, pp. 48–57, 2015.

[30] *PTV VISSIM 6 User Manual*, Karlsrule, Germany, 2013.

[31] S. Jackson, L. Miranda-Moreno, P. St-Aubin, and N. Saunier, "Flexible, mobile video camera system and open source video analysis software for road safety and behavioral analysis," *Transportation Research Record*, no. 2365, pp. 90–98, 2013.

[32] S. Mirjalili and A. Lewis, "The whale optimization algorithm," *Advances in Engineering Software*, vol. 95, pp. 51–67, 2016.

[33] G. R. Brown, "Traffic conflicts for road user safety studies," *Canadian Journal of Civil Engineering*, vol. 21, no. 1, pp. 1–15, 1994.

Hindawi
Journal of Advanced Transportation
Volume 2018, Article ID 2702360, 9 pages
https://doi.org/10.1155/2018/2702360

Research Article

Investigating the Differences of Single-Vehicle and Multivehicle Accident Probability Using Mixed Logit Model

Bowen Dong,[1] **Xiaoxiang Ma**,[1] **Feng Chen**,[1] **and Suren Chen**[2]

[1]*College of Traffic Engineering and Key Laboratory of Road & Traffic Engineering of the Ministry of Education, Tongji University, 4800 Cao'an Road, Shanghai 201804, China*
[2]*Department of Civil & Environmental Engineering, Colorado State University, Fort Collins, CO 80523, USA*

Correspondence should be addressed to Feng Chen; fengchen@tongji.edu.cn

Received 15 June 2017; Accepted 27 November 2017; Published 17 January 2018

Academic Editor: Helai Huang

Road traffic accidents are believed to be associated with not only road geometric feature and traffic characteristic, but also weather condition. To address these safety issues, it is of paramount importance to understand how these factors affect the occurrences of the crashes. Existing studies have suggested that the mechanisms of single-vehicle (SV) accidents and multivehicle (MV) accidents can be very different. Few studies were conducted to examine the difference of SV and MV accident probability by addressing unobserved heterogeneity at the same time. To investigate the different contributing factors on SV and MV, a mixed logit model is employed using disaggregated data with the response variable categorized as no accidents, SV accidents, and MV accidents. The results indicate that, in addition to speed gap, length of segment, and wet road surfaces which are significant for both SV and MV accidents, most of other variables are significant only for MV accidents. Traffic, road, and surface characteristics are main influence factors of SV and MV accident possibility. Hourly traffic volume, inside shoulder width, and wet road surface are found to produce statistically significant random parameters. Their effects on the possibility of SV and MV accident vary across different road segments.

1. Introduction

Given the economic costs and human casualties motor vehicle crashes continue to claim, traffic safety remains a hot topic among researchers across the world. Over the last decades, traffic safety researchers have spent tremendous effort and time to gain a better understanding of the contributory factors towards motor vehicle crash [1–6]. Despite the progress, there are many knowledge gaps yet to be filled in safety-related studies. One of these gaps pertains to the differences between single-vehicle and multivehicle crashes. As shown by previous studies [7–9], the mechanisms of single-vehicle (SV) accidents and multivehicle (MV) accidents are inherently different. Knipling [8] pointed out that single-vehicle and multivehicle crashes were related to different kinds of driver errors. Specifically, single-vehicle crashes usually resulted from loss of vehicle control that is associated with driver misbehavior. Multivehicle crashes, on the other hand, are most often caused by driver errors when interacting with other vehicles. It is therefore important to identify different contributing factors between single-vehicle and multivehicle crashes, which further offers insights for countermeasures to mitigate SV and MV crash risk, respectively. Along with this line of research, separate models were developed at first for SV and MV crashes to account for the difference between them [7, 9–12]. However, those models largely ignored the shared unobserved effects between SV and MV crashes, which is problematic and leads to inconsistent estimates [13]. To account for these shared heterogeneities between SV and MV crashes, researchers have proposed advanced models such as bivariate Poisson-gamma/lognormal models to study SV and MV accidents jointly [14–17]. These previous studies mainly employed count data models and had undoubtedly provided many useful finding which contributed to the overall understanding of the characteristics of SV and MV accidents.

Though many safety studies have already been conducted, the investigations on the mechanism of SV and

MV crashes especially those using disaggregate data are still lacking. Besides, methods other than Poisson-based frequency models are yet to be explored to bring a new understanding on SV and MV crashes. The objective of this study is mainly to investigate the difference of contributing factors between SV and MV accidents using disaggregate data. To this end, a comprehensive database is first established which includes road geometric features, traffic status, and environmental conditions that are processed on an hourly basis. Then, mixed logit models where the response variable is categorized as no accidents, SV accidents, and MV accidents are employed to address unobserved heterogeneity. Unlike previous aggregated studies that suffer from loss of time-varying information [4], this paper adopts refined-scale panel data to capture the time-varying information as well as to make the short-term prediction. To the authors' knowledge, there is rarely reported study so far on using the mixed logit model to analyze short-term SV and MV accidents risk. By using mixed logit models to examine SV and MV crash risk in short period, this study can address the unobserved heterogeneity and potentially provide new insights regarding the mechanisms of SV and MV crashes.

The remainder of this paper is organized as follows. Previous studies on SV and MV crashes and mixed logit model are briefly summarized in Section 2. In Section 3, a description of data is presented, followed by Section 4, where a detailed explanation of the mixed logit model structure used in this study is outlined. Section 5 presents the model results. Finally, Section 6 summarizes the conclusions and future research directions.

2. Previous Research

2.1. Studies on SV and MV Crashes. SV and MV crashes often refer to different types of accidents. To be specific, SV usually involves run-off-road crash and hitting objects, while MV usually relates to accidents such as rear-end crashes and sideswipes. Therefore, traffic safety researchers have long established that the etiologies of SV and MV crashes are different. Past studies have examined the different features of SV and MV crashes. For example, Mensah and Hauer [9] were among the first to investigate single-vehicle and multivehicle crashes. They developed separate models for SV and two-vehicle crashes and concluded that two separate models for SV and two-vehicle crashes outperformed the model that aggregated SV and two-vehicle crashes together.

Shankar et al. [18] investigated the effects of road geometric design and environmental and seasonal characteristics on SV and MV crashes. Different types of accident data and the various risk factors such as curve number and precipitation from a 61-km highway section were collected. They found that the separate models for SV and MV crashes can better explain the data than the model that pools all the crash data together.

F. Chen and S. Chen [19] examined the injury severities of truck-involved crashes on rural highways based on the distinct models for different crash types. Mixed logit models were used to investigate different risk factors including the driver, temporal, environmental, and roadway characteristics. Their results showed that SV and MV models have their respective contributing factors. The likelihood ratio test was conducted to verify the significance of separate models over the combined model, and the results indicated that separate models are superior.

These past studies have shown that it is beneficial to develop separate models for SV and MV crashes. However, the models adopted in those studies failed to account for the dependence between SV and MV crashes. By developing separate models, possible unobserved effects shared by SV and MV crashes were typically ignored [4]. To account for the dependence between crash types, researchers have proposed multivariate models to study SV and MV accidents jointly. For instance, Yu and Abdel-Aty [17] employed Bayesian bivariate Poisson-lognormal model and hierarchical Poisson models to examine the different characteristic of SV and MV crashes.

Geedipally and Lord [15] investigated the difference of confidence intervals between disaggregated models and the combined model of SV and MV crashes. Five-year crash data on multilane undivided highways were used to develop bivariate Poisson-gamma models for crash prediction. They discovered that the univariate models provide narrower confidence intervals than the bivariate model.

Ma et al. [16] proposed a random effect bivariate Poisson-lognormal model to investigate the effect of geometric features, weather, and traffic conditions on crash occurrence. Their results indicated that the proposed model could address the different levels of correlations between SV and MV crashes.

These abovementioned studies have contributed to the general understanding of SV and MV crashes. Most of these studies adopted Poisson-based models such as Poisson-gamma and Poisson-lognormal models to predict crash frequency. In this study, the difference of single-vehicle and multivehicle crashes will be reexamined from a different perspective. Advanced discrete choice model, that is, mixed logit model, is developed using real-time crash-related information that is processed into hourly records.

2.2. Mixed Logit Model. Over the past two decades, researchers have developed various methods to analyze the risk factors related to traffic crash frequency. Count data models such as Poisson, Negative Binomial, and Poisson-lognormal models are predominantly employed for such purposes [4]. Discrete choice models, on the other hand, are mainly used to investigate injury severity levels. For example, Barua and Tay [20] developed an ordered logit model to study the injury severities of bus crashes in Bangladesh. Xu et al. [21] used spatial logit model to examine the impact of possible risk factor on the injury severity of pedestrians in the crashes which occurred at signalized intersections.

Among various discrete choice models, mixed logit model, that is, the random parameter logit model, has become popular in injury severity studies [19, 22, 23]. It relaxes the independence of irrelevant alternatives assumption for multinomial logit model and offers great capability to capture unobserved heterogeneity in crash data. For instance, Haleem

and Gan [23] developed a mixed logit model to investigate the injury severities of urban freeway crashes in Florida. The role of vehicle types, driver's age, and sides of impact on each injury severity are assessed to unfold their respective effects. Based on the results, two major strategies were suggested to reduce the impacts of adverse factor. Hao and Kamga [24] use ten-year crash data which occurred at highway-rail grade crossings to analyze the effect of lighting on driver injury severities based on mixed logit models. The authors established separate models for lighted intersection and unlighted intersection and found that there are common and different significant attributes for the two situations and suggested that it is necessary to focus more on how drivers react to emergencies at unlighted highway-rail intersections. These studies have all demonstrated the great potential of mixed logit models in crash analyses. By allowing the parameters to vary across observations, mixed logit models enable analysts to discover complex relationships between injury severity and its contributing factors.

2.3. Real-Time Crash Prediction. Despite the preponderance of literature in safety research, most studies are focused on crash predictions on aggregate levels based on yearly records [1, 4, 14, 15, 18, 25]. Those studies employed highly aggregated data, thus being unable to provide guidance for proactive intervention. Real-time crash risk prediction which seeks to identify crash precursor, on the other hand, shows a great appeal for proactive traffic management. It has become a hot topic and been frequently examined by researchers in recent years [17, 26, 27].

However, the literature on real-time crash estimation is not without limitation. To begin with, the real-time safety analysis often requires traffic turbulence measures 5–10 minutes before the crash. Therefore, one key assumption for real-time risk evaluation requires the error of reported crash time to be small. Imprialou and Quddus [28] investigated in detail the quality of police-reported crash data. The results revealed that the reported crash time which ended at zero or five minutes over the course of 1 hour was unproportionally high, with an even higher spike at the thirtieth minute. It is therefore possible that some crashes occurred earlier than the reported time. They concluded that such inaccuracy in reported crash time might significantly compromise the validity of real-time safety studies. Schlögl and Stütz [29] summarized important issues associated with data uncertainty in road safety studies. They pointed out that it is untenable to use time unit smaller than 1 hour due to rounding errors in reported crash time and called for more hourly based studies. Moreover, Roshandel et al. [27] summarized the opportunities and challenges facing real-time risk prediction. They reviewed real-time safety literature and revealed problems such as inconsistent results from different studies and poor predictive performance. Another shortcoming relates to the nature of matched case-control design, which is a major tool for real-time crash prediction. The readers are referred to Roshandel et al. [27] for a detailed discussion.

Given that the aggregated models are incapable of guiding proactive traffic management and that the real-time safety studies suffer from abovementioned shortcomings, this paper tries to find a middle ground that can balance both sides. By employing the crash-related data processed into hourly records, this study can be far less sensitive to the inaccuracy in reported crash time yet still being able to provide short-term (1 hour) crash prediction for proactive traffic management.

3. Data Description

The selected highway stretch is a part of I-25 in Colorado, which starts at Mile Marker 188.49 and ends at Mile Marker 221.03. The overall length of this stretch is 55.93 miles. The data set used in this research mainly consists of the following four sources: (1) one-year detailed crash data obtained from Colorado State Patrol; (2) highway geometric characteristic and pavement condition data obtained from Roadway Characteristic Inventory; (3) refined-scale (in 20-minute intervals) weather and surface condition data from Road Weather Information System; (4) real-time (in 2-minute intervals) traffic data detected by the traffic monitoring stations on I-25.

In previous studies, crash data are usually processed into relatively large time interval. Such aggregation suffers from loss of the time-varying information and leads to estimation bias. To avoid these problems, the crash-related data are processed into relatively short time intervals (one hour) in the current study. The road segments are divided based on the location of traffic stations and further segmented according to the variation of geometric characteristics. For instance, if one of the main characteristics, such as speed limit, changes, this segment will be divided into two new segments. In this way, this study developed 57 road segments, 29 of which are northbound and the others are southbound. The crash data were mapped to roadway segments and processed into hourly records. Then they were matched with the traffic and weather data. The response variable resulted in four possible outcomes: (1) no accident; (2) SV accident; (3) MV accident; and (4) SV mixed with MV accident. However, there were only five out of 328,398 total observations which ended with the fourth outcome (SV mixed with MV). Due to its scarcity, the fourth outcome does not warrant a standalone category in the mixed logit model. Besides, the SV mixed with MV accident resembles the MV accident more than SV accident in terms of etiology. The resulting response variable is therefore defined as three categories, which are no accident, SV accidents, and MV accidents.

There are many detailed geometric variables in the dataset including segment length (miles), number of lanes, number of merging ramps per lane per mile, rutting condition, curvature (degree), and inside shoulder width (feet). Some important traffic control information like speed limit is also collected. There are five weather stations on the study stretch of I-25, which can provide road surface and weather data at a twenty-minute interval. The weather data of each segment are evaluated from the closest station. There are more than 20 monitoring stations that are almost evenly distributed on the road section. The traffic speed and volume data recorded by these stations at 2-minute interval are processed

Table 1: Descriptive statistics of response and significant explanatory variables.

Variable	Mean	Std. dev.	Minimum	Maximum
Crash type	0.008	0.121	0	2
Temporal characteristic				
Night	0.431	na	0	1
Weekend	0.271	na	0	1
November	0.095	na	0	1
Time of sunset	0.062	na	0	1
4 a.m.-5 a.m.	0.040	na	0	1
Traffic characteristic				
Low speed limit indicator (1 if speed limit is less than 55 miles per hour, 0 otherwise)	0.369	na	0	1
Speed gap (speed limit minus traffic speed) (mph)	2.642	5.533	0	69.18
Hourly traffic volume (in thousands per hour)	2.916	2.101	0.03	14.988
Truck percentage (%)	6.215	1.922	2.8	10.7
Road characteristic				
Number of entering ramps per lane per mile	0.252	0.215	0	0.926
Number of lanes	4.159	0.562	3	5
Curvature (degree)	0.947	0.681	0	2.260
length of segment (miles)	1.014	0.769	0.236	4.5
Long remaining service life of rutting (1 if the value of rut is higher than 99, 0 otherwise)	0.225	na	0	1
Inside shoulder width (in feet)	9.006	2.583	5	15
Environmental and road surface characteristic				
Cross wind speed	4.146	3.906	0	31.98
Visibility	1.075	0.136	0	1.1
Wet road surface	0.082	na	0	1
Chemical wet road surface	0.037	na	0	1

into hourly record. More details about how the data were processed can be found in a study by Chen et al. [30]. The descriptive statistics of response and explanatory variables are summarized in Table 1.

4. Methodology

For traditional crash prediction model, the effects of all the explanatory variables were assumed to be fixed across observations. Therefore, the unobserved heterogeneities were ignored. To address the problem, this study adopted mixed logit models to examine the risk factors and their degree of influence on the SV and MV accident. The model structure of mixed logit model is specified in the following section.

Since the data set used in this study is processed to panel data structure with multiple hourly observations from the same roadway segment, the number of all the observations is expressed as N:

$$N = \sum_{j=1}^{J} t_j = \sum_{t=1}^{T} j_t, \tag{1}$$

where t_j means the total number of observations in the site of j; j_t means the total number of observations in the time period of t; J and T mean the number of segments and time periods, respectively. In contrast to previous studies that used cross-sectional data [31], this study adopts panel data structure and specifies the random parameter on road segment level.

Let $P_{n_{jt}}(i)$ be the probability of crash category I (no accident, single-vehicle accident, and multivehicle accident) which occurred on observation n_{jt}:

$$P_{n_{jt}}(i) = P\left(\beta_i X_{n_{jt}} + \varepsilon_{n_{jt}i} \geq \beta_{i'} X_{n_{jt}} + \varepsilon_{n_{jt}i'}\right) \quad \forall i' \in I,\ i' \neq i, \tag{2}$$

where $n_{jt} = 1, \ldots, N$, which means the observation on the jth road segment at the tth hour. I is the set of all the possible crash categories which are mutually exclusive. i and i' are different crash categories. β_i and $\beta_{i'}$ mean the parameter vectors of crash categories i and i'. $X_{n_{jt}}$ is the vector of all the contribution variables for the observation n_{jt}, which have an influence on the possibilities of crash categories i and i'. $\varepsilon_{n_{jt}i}$ and $\varepsilon_{n_{jt}i'}$ are random components (also called error terms) that explain the unobserved effects on crash categories of the jth road segment at tth hour.

Assuming that $\varepsilon_{n_{jt}i}$ follows a type I extreme-value distribution [32], this results in a multinomial logit model which can be defined as

$$P_{n_{jt}}(i) = \frac{e^{\beta_i X_{n_{jt}}}}{\sum_{\forall i' \in I} e^{\beta_{i'} X_{n_{jt}}}}, \quad (3)$$

where the parameter β_i can be estimated using the maximum likelihood method.

The mixed logit model is introduced by relaxing the parameters β_i of the multinomial logit model to be variable across hours t. The distribution of random parameter is specified as follows:

$$\beta_{ki} \sim N\left(\overline{\beta_{ki}}, \sigma_{\beta_{ki}}\right) \quad \text{if } \beta_{ki} \text{ is a random parameter,} \quad (4)$$

where k is the index of explanatory variables for the crash category of level i; β_{ki} is the kth parameter in β_i at crash level i; $N(\overline{\beta_{ki}}, \sigma_{\beta_{ki}})$ means that β_{ki} obeys a normal distribution which varies across different hours; $\overline{\beta_{ki}}$ and $\sigma_{\beta_{ki}}$ are the mean and standard deviation of β_{ki}. In this case, the mixed logit model is specified on a panel data structure where multiple observations are nested within each segment under different hours. The resulting mixed logit model is given as follows:

$$P_{n_{jt}}(i) = \int \frac{e^{\beta_i X_{n_{jt}}}}{\sum_{\forall i' \in I} e^{\beta_i X_{n_{jt}}}} f(\beta \mid \varphi)\, \mathrm{d}\beta, \quad (5)$$

where $f(\beta \mid \varphi)$ is the density function of β with parameter vector φ. The likelihood function of mixed logit model was programmed using the NLMIXED procedure in SAS software. In previous studies [19, 22], the normal distribution was found to best fit the data compared to other distributions, including lognormal, triangular, and uniform distribution. Therefore, only normal distribution is considered herein.

5. Results

In this study, the no accident category is chosen as the base category. Hence, the estimated parameters of mixed logit model indicate the difference between the base category (no accident) and the corresponding category (SV accidents or MV accidents). To examine whether it is reasonable to divide the crash type into three categories, models with three crash categories and four crash categories are both established, respectively, for comparing. Detailed model estimation results are summarized in Tables 2 and 3. Many risk factors from different aspects (road geometric, traffic status, and environment characteristics) are shown to have significant influence on the SV and MV crash risk.

AIC (Akaike information criterion) and BIC (Bayesian information criterion), which weigh model fit against model complexity, are used to compare the performance of the two models. The model of three crash categories has relatively lower AIC and BIC than the model of four categories. This result somehow provides empirical evidence that three crash categories are better than four crash categories. Therefore, the following analysis is mainly based on the results shown in Table 2.

Table 2: The estimated results of mixed logit model with three crash categories.

Variable	Estimated parameter	t-statistic
Constant [SV]	−7.255	−16.38
Constant [MV]	−8.608	−9.9
Temporal characteristic		
Weekend [MV]	0.135	2.07
November [MV]	0.322	3.43
4 a.m.-5 a.m. [MV]	−1.698	−2.92
Traffic characteristic		
Low speed limit indicator [MV]	0.654	3.2
Speed gap [SV]	0.045	4.68
Speed gap [MV]	0.084	31.62
Hourly traffic volume [MV]	0.823	12.61
Truck percentage [MV]	−0.056	−1.94
Road characteristic		
Number of entering ramps per lane per mile [MV]	−1.138	−3.04
Curvature [MV]	0.360	2.43
Length of segment [SV]	0.787	6.01
Length of segment [MV]	0.823	5.5
Long remaining service life of rutting [MV]	0.422	2.44
Environmental and road surface characteristic		
Visibility [SV]	−0.821	−2.18
Wet road surface [SV]	0.676	2.56
Wet road surface [MV]	−0.330	−2.04
Chemical wet road surface [MV]	0.429	3.01
Random parameters		
Mean of log of hourly traffic volume [MV]	0.823	12.61
Std. dev. of log of hourly traffic volume (normal distribution)	0.160	2.29
Mean of inside shoulder width [MV]	0.032	0.95
Std. dev. of inside shoulder width (normal distribution)	0.047	5.89
Mean of wet road surface [MV]	−0.330	−2.04
Std. dev. of wet road surface (normal distribution)	0.608	3.35
Fit statistics		
−2 log likelihood	15476	
AIC (smaller is better)	15532	
BIC (smaller is better)	15589	

According to model estimation results, three explanatory variables are found to be better treated as random parameters (significant at the level of 95% with t-statistics 2.29, 5.89, and 3.35, respectively). From Table 2, the parameter associated with the hourly traffic volume of MV crash category is normally distributed with mean 0.8228 and standard deviation

Table 3: The estimated results of mixed logit model with four crash categories.

Variable	Estimated parameter	t-statistic
Constant [SV]	−7.254	−16.38
Constant [MV]	−8.587	−9.79
Constant [SV and MV]	−12.398	−16.62
Temporal characteristic		
Weekend [MV]	0.134	2.05
November [MV]	0.319	3.35
4 a.m.-5 a.m. [MV]	−1.678	−2.89
Traffic characteristic		
Low speed limit indicator [MV]	0.653	3.17
Speed gap [SV]	0.045	4.68
Speed gap [MV]	0.083	31.29
Speed gap [SV and MV]	0.140	5.56
Hourly traffic volume [MV]	0.822	10.92
Truck percentage [MV]	−0.058	−2.01
Road characteristic		
Number of entering ramps per lane per mile [MV]	−1.140	−3.02
Curvature [MV]	0.363	2.43
Length of segment [SV]	0.786	6
Length of segment [MV]	0.812	5.39
Long remaining service life of rutting [MV]	0.427	2.44
Environmental and road surface characteristic		
Visibility [SV]	−0.822	−2.18
Wet road surface [SV]	0.674	2.55
Wet road surface [MV]	−0.342	−2.1
Chemical wet road surface [MV]	0.419	2.91
Random parameters		
Mean of log of hourly traffic volume [MV]	0.823	10.92
Std. dev. of log of hourly traffic volume (normal distribution)	0.162	2.3
Mean of inside shoulder width [MV]	0.032	0.91
Std. dev. of inside shoulder width (normal distribution)	0.047	5.91
Mean of wet road surface [MV]	−0.342	−2.10
Std. dev. of wet road surface (normal distribution)	0.614	3.38
Fit statistics		
−2 log likelihood	15536	
AIC (smaller is better)	15598	
BIC (smaller is better)	15661	

0.1602. The distribution of hourly traffic volume of MV crash is shown in Figure 1. This indicates the increase of hourly traffic volume will raise the possibility of multivehicle crash in nearly all (99.99%) of the road segments. This result is consistent with people's perceptions/experience and is in line with previous studies [16, 33]. Besides, the random parameter indicates that the impact of hourly traffic volume on MV crash possibility is different across road segments. The same variable is not significant in SV crash category, which means hourly traffic volume has no significant effect on single-vehicle crashes. The difference of significant parameters reveals that some essential differences do exist between single-vehicle crashes and multivehicle crashes.

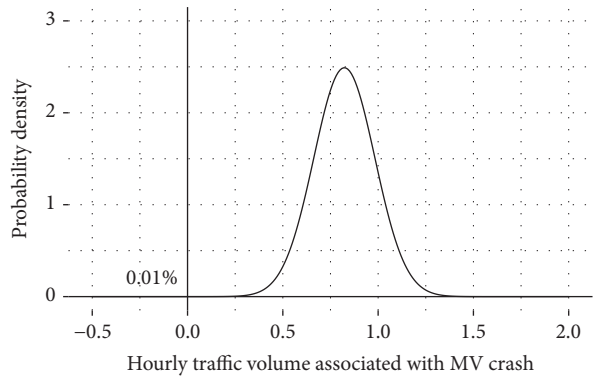

Figure 1: Distribution of hourly traffic volume associated with MV crash.

Inside shoulder width is also found to have random effect on different road segments for MV accidents. According to the results, the estimated mean of the parameter is not statistically significant, which may be considered as a problem. Nevertheless, a recent study by Behnood and Mannering [34] pointed out that when the standard deviation of a random parameter is significant, the mean of the random parameter does not need to be significant as well. From Table 2, the parameter of the inside shoulder width of MV crash category is normally distributed with mean 0.0318 and standard deviation 0.0472. The corresponding distribution is shown in Figure 2, which shows that 75% of the distribution is greater than zero and 25% is less than zero. This means that wider inside shoulder is associated with higher probability of MV accidents in 75% of the road segments and lower probability of MV accidents in the rest 25% of the road segments. This finding can possibly be explained by the tradeoff between forgiving geometric design and risky driving. On the one hand, wider inside shoulder tolerates more driver errors. On the other hand, it is possible that when inside shoulder exceeds a certain threshold, drivers may be more likely to take risky actions such as passing and speeding, according to risk compensation theory [35].

The parameter of the wet road surface of MV crash category is normally distributed with mean −0.3303 and standard deviation 0.6076. As shown in Figure 3, 29% of the distribution is greater than zero and 71% is less than zero. When the road surface gets wet, nearly three-quarters of the hours are related to lower likelihood of MV accidents, while the other hours are related to higher risk of MV accidents. Moreover, wet road surface is positively correlated to SV accidents, which means that wet road surface usually leads to more SV accidents. Such phenomena may be caused by some

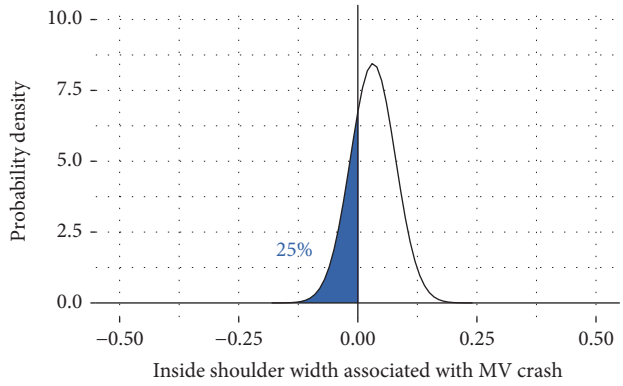

Figure 2: Distribution of insider shoulder width associated with MV crash.

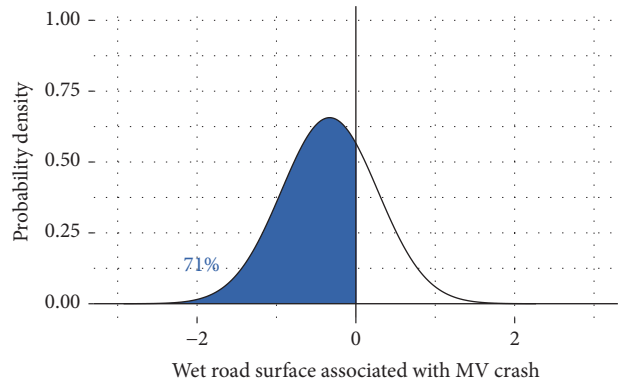

Figure 3: Distribution of wet road surface associated with MV crash.

unobserved heterogeneity of driver behavior. On wet road surface, the skid resistance decreases which increases crash risks. At the same time, wet road surface is often concurrent with rainy condition when drivers tend to maintain a longer distance between vehicles. The crash risk is therefore a result of increased driver attentiveness and reduced skid resistance. As a result, wet road surface leads to mixed effects on MV crash.

5.1. Temporal Characteristics. It can be found from Table 2 that the temporal factors do not have a strong impact on the possibility of SV accidents. As for MV accidents, the results indicate that the MV crashes are more likely to occur on weekends and less likely to occur during 4 a.m. to 5 a.m. Compared to other months, the likelihood of MV crashes is larger in November. This may be associated with some harmful impacts caused by the sudden storm and temperature change in November, 2010 [30].

5.2. Traffic Characteristic. Speed limit indicator is used to evaluate the effect of speed limit on traffic safety. This study uses a dummy indicator to express the speed limit. If the legal speed limit is smaller than 55, then the value equals 1, otherwise equals 0. The results show that low speed limit will increase the possibility of multivehicle crashes. Some researchers also found that low speed limit will increase crash possibility [36], but they failed to reveal its different effects on SV and MV accidents.

The speed gap variable denotes the difference between the average speed and the speed limit, which can represent the congestion level to some extent. As shown in Table 2, the results indicate that both SV and MV vehicle crashes are more likely to occur when the speed gap gets larger. This finding is partially similar to those in some previous studies [17]. In addition, the increase of truck ratio will decrease the likelihood of multivehicle crashes, which is in accordance with the conclusions drawn by Anastasopoulos and Mannering [37].

5.3. Road and Pavement Characteristic. Several road characteristics are found to have significant influence on SV and MV crash risks. The length of road segment tends to increase the likelihood of both SV and MV crash, which is consistent with the research by Venkataraman et al. [38]. More merging ramps per lane per mile will decrease the likelihood of multivehicle crashes, which may be attributed to the careful driving behavior on roads consisting of more merging ramps. The same indicator has also been investigated in previous studies. Pei et al. [39] also found that an increase in the merging and diverging ramp number leads to fewer accidents, while some other researchers [37] made opposite conclusions. The difference of their conclusion may be due to their aggregate model structure, which does not consider the different mechanism between SV and MV accidents. This inconsistency among past findings points to the very need to investigate SV and MV crashes separately and uncover their respective risk factors.

A similar result is also found for the curvature variable. In this study, the results imply that higher curvature will cause higher multivehicle crash risks. Albeit some researchers found that the degree of curvature can be beneficial for traffic safety [17, 39], other researchers found it positively correlated with the crash likelihood [36, 40].

As for pavement conditions, it can be found that the possibility of multivehicle crashes will decrease on segments with longer remaining service live of rut. This is probably because drivers have a tendency to drive carefully on the road with deeper rut and is consistent with past studies [30].

5.4. Environmental and Surface Characteristic. Turning to surface characteristic, wet road surface and chemical wet road surface are both shown to be associated with increased possibility of single-vehicle crash. Chemical wet road surface leads to more multivehicle crashes, while the effect of wet road surface will change across road segments because of its random nature, which has been discussed above.

From Table 2, higher visibility is related to decreased possibility of single-vehicle crashes. According to the results, other environment characteristics, such as cross wind, temperature, and humidity, are not significant. This phenomenon is plausible because the selected stretch of I-25 is relatively flat and spans across Denver metro. On highways located at mountainous terrains subjected to complex weather, the

environment characteristics may impose significant influence on traffic safety.

6. Discussion and Conclusion

In this study, mixed logit models are developed to examine the difference of SV and MV accident probability using hourly based disaggregated crash data. One-year accident data, detailed traffic data, weather condition, road geometry, and surface condition data on I-25 from the state of Colorado were collected to establish a refined-scale panel data structure. The refined-scale is used to capture the potential information lost in aggregate data. Many risk factors are found to have varying effects on SV and MV accident probability.

These findings contribute to the literature on the risk factors that are associated with the different mechanisms of SV and MV crash. Different from the former researches which model the SV and MV accidents frequencies separately or jointly, this study uses mixed logit model to study the risk of both SV and MV crashes. Therefore, the results of this paper can provide guidance to develop more rational and effective segment management measures and accident prevention strategies. In addition, some findings are also helpful for the evaluation and improvement of the designs of existing transportation infrastructure.

The main conclusions associated with the risk factors and their different effects on SV and MV accident are summarized as follows.

(1) Speed gap, length of segment, and wet road surface are found to have significant effects on both SV and MV accident possibility. In addition to these indicators, most of other variables including time of weekends, November, low speed limit indicator, hourly traffic volume, truck percentage, and chemical wet road surface are significant for only MV accidents. Visibility indicator is significant for only SV accidents.

(2) For I-25, the main influence factors of SV and MV accident possibility are traffic, road, and surface characteristics. Other temporal and environment characteristics like weekends, special period, and visibility also have certain effects on the possibility of SV and MV accidents, respectively.

(3) The model results indicate that hourly traffic volume, inside shoulder width, and wet road surface are random parameters with normal distribution for multivehicle crash probability. So the impacts of these variables on MV accident are proved to be different across road segments.

Without doubt, there are also some limitation existing in the present study. The conclusions conducted here are mainly based on the data from part of I-25, which may be not suitable for other highways. In order to get more precise and universal rules on the possibility of SV and MV accidents, further studies should be conducted on different types of highways.

Conflicts of Interest

The authors declare that they have no conflicts of interest.

Acknowledgments

This work was supported by the National Natural Science Foundation of China under Grant nos. 51508409 and 71531011, the Program for Young Excellent Talents in Tongji University, and the Fundamental Research Funds for the Central Universities. The authors would like to express their gratitude to the United States Department of Transportation and Colorado Department of Transportation and Colorado State Patrol for the detailed data.

References

[1] C. Y. Chan, B. Huang, X. Yan, and S. Richards, "Investigating effects of asphalt pavement conditions on traffic accidents in Tennessee based on the pavement management system (PMS)," *Journal of Advanced Transportation*, vol. 44, no. 3, pp. 150–161, 2010.

[2] J. Weng and Q. Meng, "Rear-end crash potential estimation in the work zone merging areas," *Journal of Advanced Transportation*, vol. 48, no. 3, pp. 238–249, 2014.

[3] S. M. Rifaat and H. C. Chin, "Accident severity analysis using ordered probit model," *Journal of Advanced Transportation*, vol. 41, no. 1, pp. 91–114, 2007.

[4] D. Lord and F. Mannering, "The statistical analysis of crash-frequency data: a review and assessment of methodological alternatives," *Transportation Research Part A: Policy and Practice*, vol. 44, no. 5, pp. 291–305, 2010.

[5] R. Tay and S. M. Rifaat, "Factors contributing to the severity of intersection crashes," *Journal of Advanced Transportation*, vol. 41, no. 3, pp. 244–265, 2007.

[6] L. Mussone and K. Kim, "The analysis of motor vehicle crash clusters using the vector quantization technique," *Journal of Advanced Transportation*, vol. 44, no. 3, pp. 162–175, 2010.

[7] T. Jonsson, J. N. Ivan, and C. Zhang, "Crash prediction models for intersections on rural multilane highways: Differences by collision type," *Transportation Research Record*, no. 2019, pp. 91–98, 2007.

[8] R. R. Knipling, "Car-truck crashes in the national motor vehicle crash causation study," in *Proceedings of the Transportation Research Board (TRB) 92nd Annual Meeting*, vol. 13, 2013.

[9] A. Mensah and E. Hauer, "Two problems of averaging arising in the estimation of the relationship between accidents and traffic flow," *Transportation Research Record*, vol. 1635, pp. 37–43, 1998.

[10] X. Ye, R. M. Pendyala, S. P. Washington, K. Konduri, and J. Oh, "A simultaneous equations model of crash frequency by collision type for rural intersections," *Safety Science*, vol. 47, no. 3, pp. 443–452, 2009.

[11] J. Ivan, "New approach for including traffic volumes in crash rate analysis and forecasting," *Transportation Research Record*, vol. 1897, pp. 134–141, 2004.

[12] M. Griffith, "Safety evaluation of rolled-in continuous shoulder rumble strips installed on freeways," *Transportation Research Record*, vol. 1665, no. 1, pp. 28–34, 1999.

[13] F. L. Mannering and C. R. Bhat, "Analytic methods in accident research: methodological frontier and future directions," *Analytic Methods in Accident Research*, vol. 1, pp. 1–22, 2014.

[14] S. R. Geedipally and D. Lord, "Identifying hot spots by modeling single-vehicle and multivehicle crashes separately," *Transportation Research Record*, no. 2147, pp. 97–104, 2010.

[15] S. R. Geedipally and D. Lord, "Investigating the effect of modeling single-vehicle and multi-vehicle crashes separately on confidence intervals of Poisson-gamma models," *Accident Analysis & Prevention*, vol. 42, no. 4, pp. 1273–1282, 2010.

[16] X. Ma, S. Chen, and F. Chen, "Correlated random-effects bivariate poisson lognormal model to study single-vehicle and multivehicle crashes," *Journal of Transportation Engineering*, vol. 142, no. 11, 2016.

[17] R. Yu and M. Abdel-Aty, "Multi-level Bayesian analyses for single- and multi-vehicle freeway crashes," *Accident Analysis & Prevention*, vol. 58, pp. 97–105, 2013.

[18] V. Shankar, F. Mannering, and W. Barfield, "Effect of roadway geometrics and environmental factors on rural freeway accident frequencies," *Accident Analysis & Prevention*, vol. 27, no. 3, pp. 371–389, 1995.

[19] F. Chen and S. Chen, "Injury severities of truck drivers in single- and multi-vehicle accidents on rural highways," *Accident Analysis & Prevention*, vol. 43, no. 5, pp. 1677–1688, 2011.

[20] U. Barua and R. Tay, "Severity of urban transit bus crashes in Bangladesh," *Journal of Advanced Transportation*, vol. 44, no. 1, pp. 34–41, 2010.

[21] X. Xu, S. Xie, S. C. Wong, P. Xu, H. Huang, and X. Pei, "Severity of pedestrian injuries due to traffic crashes at signalized intersections in Hong Kong: a Bayesian spatial logit model," *Journal of Advanced Transportation*, vol. 50, no. 8, pp. 2015–2028, 2016.

[22] J. C. Milton, V. N. Shankar, and F. L. Mannering, "Highway accident severities and the mixed logit model: an exploratory empirical analysis," *Accident Analysis & Prevention*, vol. 40, no. 1, pp. 260–266, 2008.

[23] K. Haleem and A. Gan, "Effect of driver's age and side of impact on crash severity along urban freeways: A mixed logit approach," *Journal of Safety Research*, vol. 46, pp. 67–76, 2013.

[24] W. Hao and C. Kamga, "The effects of lighting on driver's injury severity at highway-rail grade crossings," *Journal of Advanced Transportation*, vol. 50, no. 4, pp. 446–458, 2016.

[25] C. Xu, P. Liu, W. Wang, and Y. Zhang, "Real-time identification of traffic conditions prone to injury and non-injury crashes on freeways using genetic programming," *Journal of Advanced Transportation*, vol. 50, no. 5, pp. 701–716, 2016.

[26] M. Abdel-Aty, N. Uddin, A. Pande, F. Abdalla, and L. Hsia, "Predicting freeway crashes from loop detector data by matched case-control logistic regression," *Transportation Research Record*, vol. 1897, no. 1, pp. 88–95, 2004.

[27] S. Roshandel, Z. Zheng, and S. Washington, "Impact of real-time traffic characteristics on freeway crash occurrence: Systematic review and meta-analysis," *Accident Analysis & Prevention*, vol. 79, pp. 198–211, 2015.

[28] M. Imprialou and M. Quddus, "Crash data quality for road safety research: Current state and future directions," *Accident Analysis & Prevention*, 2016.

[29] M. Schlögl and R. Stütz, "Methodological considerations with data uncertainty in road safety analysis," *Accident Analysis & Prevention*, 2016.

[30] F. Chen, X. Ma, and S. Chen, "Refined-scale panel data crash rate analysis using random-effects tobit model," *Accident Analysis & Prevention*, vol. 73, pp. 323–332, 2014.

[31] F. L. Mannering, V. Shankar, and C. R. Bhat, "Unobserved heterogeneity and the statistical analysis of highway accident data," *Analytic Methods in Accident Research*, vol. 11, pp. 1–16, 2016.

[32] D. McFadden and K. Train, "Mixed MNL models for discrete response," *Journal of Applied Econometrics*, vol. 15, no. 5, pp. 447–470, 2000.

[33] Y. Qi, B. L. Smith, and J. Guo, "Freeway accident likelihood prediction using a panel data analysis approach," *Journal of Transportation Engineering*, vol. 133, no. 3, pp. 149–156, 2007.

[34] A. Behnood and F. Mannering, "The effect of passengers on driver-injury severities in single-vehicle crashes: A random parameters heterogeneity-in-means approach," *Analytic Methods in Accident Research*, vol. 14, pp. 41–54, 2017.

[35] C. Winston, V. Maheshri, and F. Mannering, "An exploration of the offset hypothesis using disaggregate data: the case of airbags and antilock brakes," *Journal of Risk and Uncertainty*, vol. 32, no. 2, pp. 83–90, 2006.

[36] Y. Kweon and K. Kockelman, "Safety effects of speed limit changes: use of panel models, including speed, use, and design variables," *Transportation Research Record*, vol. 1908, pp. 148–158, 2005.

[37] P. C. Anastasopoulos and F. L. Mannering, "A note on modeling vehicle accident frequencies with random-parameters count models," *Accident Analysis & Prevention*, vol. 41, no. 1, pp. 153–159, 2009.

[38] N. S. Venkataraman, G. F. Ulfarsson, and V. N. Shankar, "Random parameter models of interstate crash frequencies by severity, number of vehicles involved, collision and location type," *Accident Analysis & Prevention*, vol. 59, pp. 309–318, 2013.

[39] X. Pei, S. C. Wong, and N. N. Sze, "The roles of exposure and speed in road safety analysis," *Accident Analysis & Prevention*, vol. 48, pp. 464–471, 2012.

[40] L. Ewan, A. Al-Kaisy, and F. Hossain, "Safety effects of road geometry and roadside features on low-volume roads in Oregon," *Transportation Research Record*, vol. 2580, pp. 47–55, 2016.

Hindawi
Journal of Advanced Transportation
Volume 2018, Article ID 8645709, 10 pages
https://doi.org/10.1155/2018/8645709

Research Article

Modeling Lane-Changing Behavior in Freeway Off-Ramp Areas from the Shanghai Naturalistic Driving Study

Lanfang Zhang, Cheng Chen, Jiayan Zhang, Shouen Fang, Jinming You, and Jingqiu Guo

Key Laboratory of Road and Traffic Engineering of the Ministry of Education, Tongji University, Shanghai, China

Correspondence should be addressed to Jingqiu Guo; guojingqiu@hotmail.com

Received 16 June 2017; Revised 14 October 2017; Accepted 19 November 2017; Published 14 January 2018

Academic Editor: Chunjiao Dong

The objective of this study is to investigate lane-changing characteristics in freeway off-ramp areas using Shanghai Naturalistic Driving Study (SH-NDS) data, considering a four-lane freeway stretch in various traffic conditions. In SH-NDS, the behavior of drivers is observed unobtrusively in a natural setting for a long period of time. We identified 433 lane-changing events with valid time series data from the whole dataset. Based on the logit model developed to analyze the choice of target lanes, a likelihood analysis of lane-changing behavior was graphed with respect to three traffic conditions: free flow, medium flow, and heavy flow. The results suggested that lane-changing behavior of exiting vehicles is the consequence of the balance between route plan (mandatory incentive) and expectation to improve driving condition (discretionary incentive). In higher traffic density, the latter seems to play a significant role. Furthermore, we found that lane-change from the slow lane to the fast lane would lead to higher speed variance value, which indicates a higher crash risk. The findings contribute to a better understanding on drivers' natural driving behavior in freeway off-ramp areas and can provide important insight into road network design and safety management strategies.

1. Introduction

Innovative technologies and traffic data sources provide great potential to extend advanced strategies and methods in road safety research. Advances in traffic safety modeling and analysis will play an important role in reducing road crashes and improving traffic operations. Lane-changing's adverse impact on traffic safety has been investigated and confirmed. Recent studies in traffic management have shown that lane-changing maneuvers are a major source of traffic disturbance on a multilane freeway [1]. Such maneuvers are also critical to road safety as 40% of freeway accidents happened in ramp areas, particularly in off-ramp sections [2]. A better understanding of lane-change events can also improve design of the human-machine interface in driving assistance systems.

Up to now, lane-changing characteristics and influencing factors in urban roads or freeways have been studied from the perspectives of driver behavior [3] and road and traffic conditions [4, 5]. In these studies, lane-changes can be classified as either mandatory or discretionary according to driving incentives [6]. Generally traffic outflows do mandatory lane-changing (e.g., off-ramp or to avoid a block), while through traffic conduct discretionary lane-changing when drivers perceive that driving conditions in the target lane are better. So far there has been little research on the modeling of integrated mandatory and discretionary lane-changing strategies in freeway off-ramp areas.

Traffic on the fast lane must change to the shoulder lane before exiting a ramp on a freeway. Usually mandatory lane-changing to the shoulder lane is performed by the departure vehicles far enough before the off-ramp area. However, in actual traffic conditions, queue-jumping behavior occurs frequently when approaching an off-ramp and significantly affects traffic capacity and stability, which is neglected in most simulation programs. Furthermore, trade-offs between mandatory and discretionary incentives are limited. For example, when considering a mandatory lane-changing to exit a ramp, a driver may decide to overtake a heavy vehicle in front first (e.g., executing a discretionary lane-change first). Advances in data collection technologies, (e.g., the naturalistic driving system), giving access to high-resolution vehicular

data, provide an opportunity for us to fully understand the highly complex lane-changing procedure, particularly the trade-off decisions. Thus, it is valuable to conduct a comprehensively empirical study on lane-changing decision-making in freeway off-ramp areas.

The major lane-changing modeling methods consist of two distinct forms: lane-change decision model and lane-change influence model. For lane-changing decisions, Gipps introduced the original lane-changing model on urban roads which considered traffic signals, obstructions, and heavy vehicles [7], then several refined models based on Gipps were developed and extended to freeways [8, 9]. Ahmed et al. [10] employed random utility theory in lane-changing behavior modeling and a lane-changing choice was defined as a sequence of three steps: decision to consider a lane-change, choice of left or right lane, and search for an acceptable gap to execute the decision. Ahmed [11] extended the mandatory LC model to accommodate congested traffic, where forced merging behavior frequently occurs because of lacking of normally acceptable gaps. Toledo [12] developed a discrete choice framework to model integrated lane-changes and estimated the parameters. Other analysis methods of lane-changing behavior include risk-based models [13], as well as intelligent algorithms such as artificial neural networks [14] and fuzzy inference [15]. For example, Balal et al. [16] applied a fuzzy inference system to model a driver's binary decision to or not to execute a discretionary freeway lane-change. Research on the lane-changing behavior indicates that slower preceding vehicles would in many situations tempt the following drivers to consider overtaking, and 95% of drivers would choose to do lane-changing only if the rear spacing on the target lane is bigger than 15 meters and speeds are higher than the following vehicles on the target lane [17, 18]. Zheng [19] categorizes the major LC models in the literature into two groups: models that aim to capture the LC decision-making process and models that aim to quantify LC's impact on traffic.

Under the condition of dense traffic, a vehicle attempting a lane-change needs cooperation from at least one following vehicle in the target lane. Hidas [9] developed a cooperative lane-changing model based on a "driver courtesy" concept. By comprehensively reviewing previous works, Kesting et al. [20] proposed the model MOBIL (Minimizing Overall Braking Induced by Lane-changes) to address cooperative lane-changing of intelligent vehicles. Based on MOBIL, other researchers further studied intelligent lane-changing models [19]. On the empirical side, the studies of lane-changing behavior were far less extensive than those of longitudinal behavior (such as car following) due to the lack of comprehensive vehicle trajectory data. The emergence of connected vehicle technology offers some great opportunities.

Previous studies rely on theoretical calculation, traffic simulation, or driving simulator and field experiment to collect lane-changing behavior data. To overcome the restriction of driving simulation and field experiment such as short test horizon and limited controlled settings [21], the 100-car Naturalistic Driving Study (NDS) was the first large-scale NDS conducted in the US [22, 23], followed by the 60-Taxi NDS in Japan [24]. The UDRIVE Naturalistic Driving Study was conducted from 2012 to 2016 in seven countries in Europe [25]. Naturalistic Driving Study, undertaken in natural conditions (no interference, no appearance of researchers, and during daily driving) [26, 27], provides the opportunity to observe the actual driving process with an unobtrusive high-precision data acquisition system. In comparison to the intensive efforts on driver behavior and microsimulation, lane-changing modeling using naturalistic driving data is still a relatively undeveloped area. Frequent and substantial lane-changes based on individual decisions and preferences can certainly affect traffic flow and road safety. Improper lane-changing has been identified as a main source of congestion and collisions [28]. It is a challenging task to fully understand the mechanism for lane-changes at freeway exits and it requires data of heterogeneous traffic conditions with varying degrees of driver behavior and perception.

However, real-time lane-changing characteristics cannot be obtained in most of the existing studies. Limited investigations have been made to identify hazardous lane-changing behavior; thus few of the models can be applied in real-time driving assistance systems. Lane-changing risk has been investigated as a surrogate safety measure to predict crash potentials in a mesoway. Typically, traffic data from loop detectors has been utilized to predict potential lane-changing related crashes and studies indicated that difference in occupancy of adjacent lanes was significantly associated with the crash potential [29]. Individual vehicular information was extracted for a surrogate index of crash risk and results showed the measure was effective in predicting traffic crash occurrence [30, 31]. Thus, naturalistic driving data provide the opportunity for researchers to fully investigate the safety factors in lane-changing.

The ongoing Shanghai Naturalistic Driving Study (SH-NDS) is a joint effort by Tongji University, General Motor China and Virginia Tech Transportation Institute. The objective of the SH-NDS is to investigate how drivers interact with vehicle, roadway, traffic conditions, and traffic control devices in China. Also SH-NDS offers the opportunity to investigate similarities and differences between Chinese drivers and drivers from other countries. Typically, a naturalistic observation vehicle was equipped with devices that continuously monitor various aspects of driving behavior, including information about vehicle movements (e.g., acceleration and deceleration, position on the road, and driving speed), about the driver (e.g., eye, head and hand movements), and about the direct environment (e.g., time headway, traffic density, road, and weather conditions).

The objective of this study is to investigate lane-changing characteristics in freeway off-ramp areas using SH-NDS data, considering a four-lane freeway stretch in various traffic conditions. This paper is organized as follows. Section 2 presents data collection and sampling; a description of the model structure is presented after that. The homogeneity and heterogeneity analysis as well as the safety assessment of lane-changing are discussed in Section 3. The last part concludes with remarks on the potential scope of future studies.

Figure 1: Four camera views in SH-NDS data acquisition system: forward view (left), in-cabin driver face view (upper left), instrument panel and steering wheel view (upper right), and rear view (bottom right).

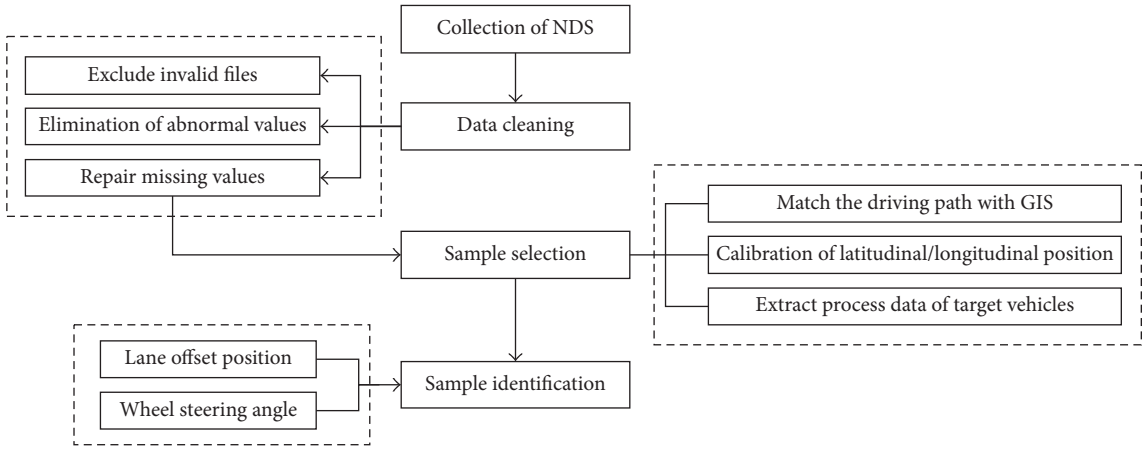

Figure 2: The procedure of data collection and extraction.

2. Method

2.1. Shanghai Naturalistic Driving Study Data. In this Shanghai naturalistic observation study, driving behavior was observed unobtrusively in a natural setting for a long period of time. A total of 60 drivers from the Shanghai metropolitan area have been involved since the end of 2012. They are between 35 and 50 years old, holding valid driving licenses, and with more than five years' driving experience. Participants were required to drive no less than 40 kilometers per day on average. Each participant drove the assigned vehicle, and every day the route was determined by themselves according to the needs of work and nonwork, without the presence of any researcher.

The instrumented vehicles were fitted with unobtrusive data acquisition systems consisting of GPS, high frequency video camera, triple axis accelerometer, Doppler radar, and lane offset system. The vehicle data acquisition system recorded data when the car was running and in-motion. The resultant dataset consisted of approximately 750,000 km of driving data (comprising more than 80,000 hours of video data). Each driver was assigned to one of five instrumented vehicles and drove the car for three months. After a participant completed her/his time in this study, a different driver was assigned to the test car until the data collection process was completed for all participants.

Original naturalistic driving data are characterized by a large number of parameters. In this dataset, there are more than 10,000 CSV files which contain the information acquired from single trips. For the purpose of this study, lane-changing data in freeway off-ramp areas were chosen as (1) vehicle trajectory data and motion characteristics (e.g., speed, acceleration) in a selected freeway off-ramp segment; (2) neighboring traffic around the objective, which refers to surrounding vehicles' motion information within the scope of instrumented radar; (3) videos recorded by four in-vehicle cameras during the full process of ramp exiting, as shown in Figure 1, consisting of forward and rear views, steering wheel view, and driver's face.

The procedure of data collection and extraction is shown in Figure 2. The first task was data cleaning. In this paper, on the basis of a large number of field data analyses, an outliers monitoring method was proposed based on a self-learning Pauta criterion [32], which is the method of three times standard deviation to eliminate outliers. The outlier correction method was based on linear interpolation. The second step is to extract departure samples in the freeway

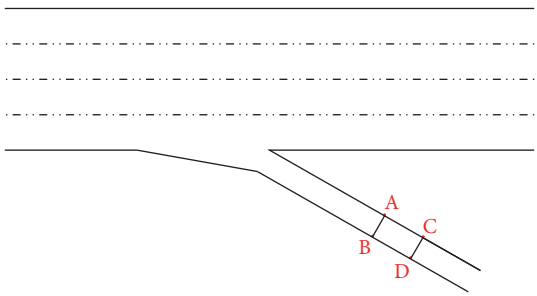

Figure 3: Schematic illustration of a study area.

off-ramp sections. We consider a four-lane stretch of freeway. Figure 3 is an illustration of the study area. After matching the driving path to real road sections in GIS according to actual longitude and latitude data during the trips, we framed the range of the off-ramp in all the freeway exits in the dataset by calibrating the longitude and latitude position of points A to D. To ensure that all selected off-ramp events are under the same road conditions, we set up the criteria: a straight four-lane freeway stretch, distance of adjacent exits no less than 4 km, and being in fine weather conditions. Missing data due to limitations of the data collection were also accounted.

2.2. Identification of Lane-Changing Samples. Lane-changing behavior can be identified by one or more of the following episodes. (1) Driver initiates a steering input to change the direction of the vehicle. (2) The vehicle begins to move laterally relative to the lane. (3) The vehicle leaves the current lane at least temporarily [33]. To determine the initiation point of a lane-changing action, a search algorithm was adopted, in which lane offset position and steering wheel angle were applied as indexes to extract data associated with lane-change events. In addition, data analyzers manually inspected video of the triggered driving episodes and identified any valid lane-changes in qualified freeway off-ramp segments.

In general, the target lane of a lane-changing maneuver is the lane the driver perceives as best to be in, depending upon the prevalent driving conditions and her/his trip plan. In this study, the target lane is defined as the lane next to the vehicle. One of the lane offset position parameters is LO, which indicates the offset between the vehicle center line and the center line of the current lane, detected by the lane offset system. For example, as shown in Figure 4, a positive value of LO means the vehicle is offset to the right side of the current lane center, and a negative LO implies a left offset from the lane center line. Furthermore, once the test vehicle's center line crosses the current lane boundary (either the left or the right side), instrumented sensors automatically identify the new lane's center line; therefore the sign of LO value will turn to the opposite and appears as a sudden change. Thus single and serial lane-changing behavior can be differentiated according to the sudden change of the LO values. Steering wheel angle is taken as secondary index for verification. Totally 433 valid lane-changing samples were extracted from the dataset.

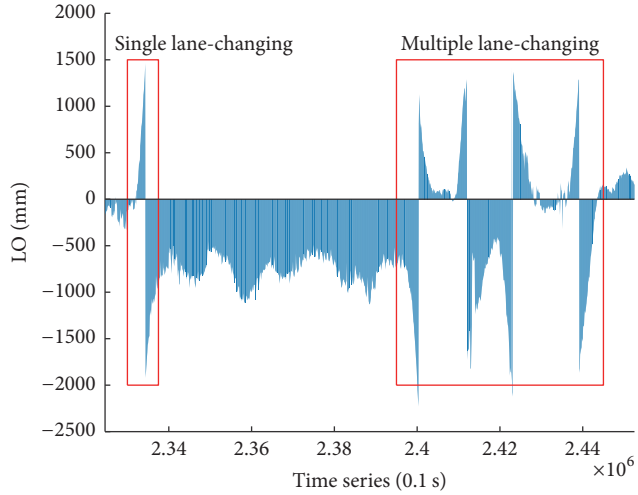

Figure 4: An example of LO values in the dataset.

2.3. Preliminary Analysis of Lane-Changing Data. Figure 5 presents a typical scenario among the 433 samples. For convenience, the left-most lane is defined as the 1st lane and the right-most lane is defined as the 4th lane.

To explore the spatial distribution of lane-changing behavior in freeway off-ramp areas, we classified the 433 lane-changing events into three groups: changing from Lane 1 to Lane 2, from Lane 2 to Lane 3, and from Lane 3 to Lane 4. According to the initial position of a lane-change event, cumulative frequency can be plotted to show spatial attributes of lane-changes in different lanes (see Figure 6). The x-axis expresses the distance from an initial lane-changing position to the ramp. It can be shown that the number of lane-changes needed in order to exit the ramp is significantly correlated to the distance from initial lane-changing point to ramp. Based on the statistics of the samples, 85 percentile of lane-changes were made in the range, respectively, 2,300 m to 470 m in Lane 1, 1,800 m to 415 m in Lane 2, and 1,200 m to 290 m in Lane 3, as presented in Figure 7.

2.4. Modeling Lane-Changing Decisions. When test vehicles are driving on Lane 1 or Lane 4, drivers can only change in a single direction; hence, we finally selected 319 valid lane-changing actions starting from either Lane 2 or Lane 3. For the purpose of this study, variables influencing the target lane choice in freeway off-ramp areas are explained in Table 1.

Here, we followed Ahmed [11] and Toledo [12]'s LCD discrete choice framework. The target lane (TL) choice denotes the immediate lane of the test driver, depending on the driving route information and traffic environment. Due to the nature of the binary outcome, the target lane choice set includes two alternatives: either change to the left lane (LL) or the right lane (RL). To explain drivers' choice of these two alternatives, the concept of utility is used for measuring the satisfaction degree of changing to a target lane in specific traffic condition and driving route. The utility of LC for driver n is defined as in

$$U_n^i = \sum \beta^i X_n^i + v_n \alpha^i + \varepsilon_n^i, \quad (1)$$

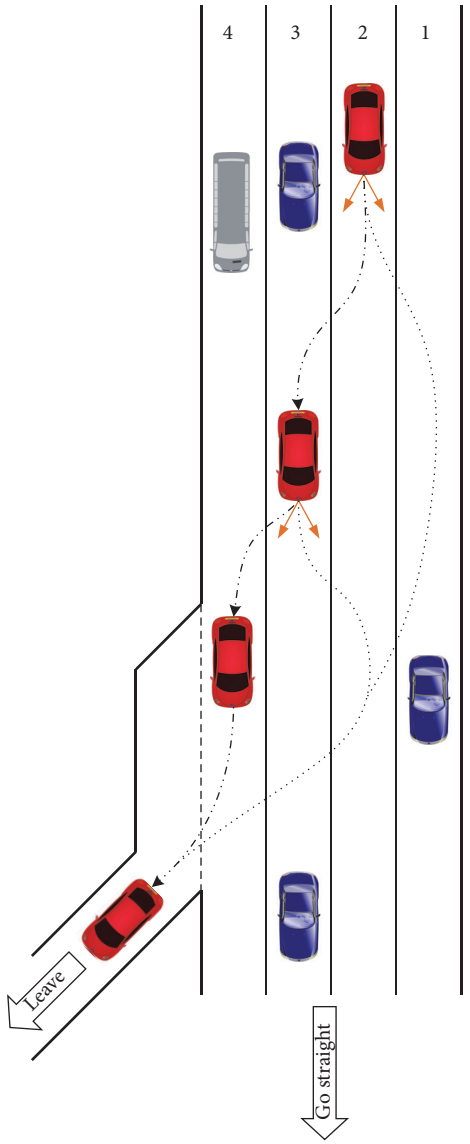

Figure 5: The lane-changing process in freeway off-ramp areas.

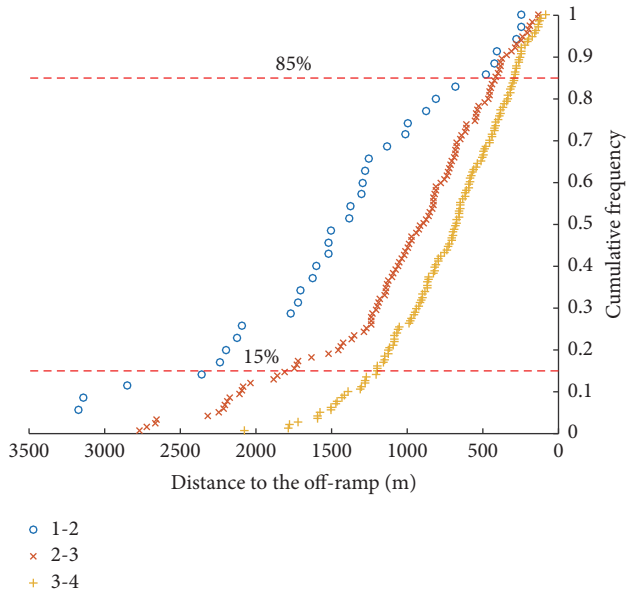

Figure 6: Cumulative frequency graph of lane-changing longitudinal position on different lanes.

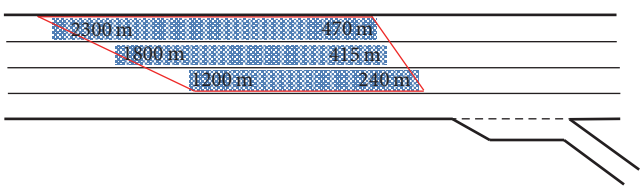

Figure 7: Range based on the 85 percentiles of lane-changing actions in each lane.

where U_n^i is the utility for driver n; $i \in \mathrm{TL} = \{\mathrm{LL}, \mathrm{RL}\}$; X_n^i is a vector of explanatory variables; β^i is the corresponding coefficient to X_n^i; and ε_n^i is the random error term for a given individual, as well as across individuals. v_n is an individual specific random term that can represent observable/unobservable characteristics. α^i are the parameters of v_n. It may be noted that, due to the limitation of data collection, in estimation not all the α^i values can be identified.

Under the assumption that individual n chooses an alternative that maximizes his/her satisfaction, alternative i is chosen if and only if $U_{in} \geq U_{jn}$. Assuming the term ε_n^i follows an IID Gumbel distribution, the probability of individual n choosing alternative i can be expressed by a logit model as

$$P_n(\mathrm{TL} = i) = \frac{\exp\left(V_n^i \mid v_n\right)}{\sum_{j \in \mathrm{TL}} \exp\left(V_n^j \mid v_n\right)}, \quad (2)$$

where $V_n^i \mid v_n$ are the conditional systematic utilities of the choice alternatives.

As mentioned in the previous section, lane-change utility functions depend on explanatory variables including driving route information, traffic environment, as well as driver characteristics. Due to the sampling criteria, the sample size of left lane-change (LL) choices is relatively small. Thus, LL was defined as alternative $Y = 1$. Although driver characteristics (e.g., driving style) naturally have significant impacts on various aspects of lane-changing decisions, data are not available in most field tests; nevertheless, their parameters can be captured by the individual specific term v_n [6, 12].

3. Results

3.1. Model Estimation. Several model diagnostics were used to check model goodness-of-fit and the statistical significance for each explanatory variable. A total of 20 variables were initially tested in the logit model and only 6 of them were found to be statistically significant. The final logit model was estimated with six explanatory variables as shown in Table 2. Whereas GT_l (Gap Time to the front vehicle on the left lane) was statistically significant at only the 90% confidence

Table 1: Potential factors contributing to the lane change.

Category	Factor	Data source
(1) Trip plan	Numbers of lane changes needed in order to exit the ramp	Determined by video of front view
	Relative distance to the off-ramp at the initial point of a lane-changing event	Calculated from the time series data
(2) Traffic environment	Density and speed of traffic in the lane, distribution of heavy vehicles, driving regulations, and so on	Video camera and Doppler radar
	Relative speed and gaps of the subject vehicle with respect to surrounding cars	We use Gap Time (GT) as index to reflect neighboring conditions GT = $D/\Delta v$
(3) Driver and vehicle characteristics	Demographic variables, physical conditions, driving experience	Questionnaire

Table 2: Model estimation results.

Variable	Descriptions	Definitions	Estimate	p value
$^{*}\delta_{(\Delta CL)}$	The number of lane-changes required to be in the correct lane	$\delta_{(\Delta CL)} = 1$ or $\delta_{(\Delta CL)} = 2$	−1.986	<0.001
$^{*}S$	The distance to the point where the driver needs to be off-ramp	unit: m	0.003	<0.001
$^{*}M_r$	The front vehicle type on the right lane	heavy vehicles = 1; others = 0	1.802	<0.001
$^{*}\mathrm{GT}_m$	Gap Time to the front vehicle in current lane	$\frac{d_{nm}}{v_m - v_n}$	−0.094	<0.001
GT_l	Gap Time to the front vehicle on the left lane	$\frac{d_{nl}}{v_l - v_n}$	0.053	0.078
$^{*}\mathrm{GT}_r$	Gap Time to the front vehicle on the right lane	$\frac{d_{nr}}{v_r - v_n}$	−0.058	0.002
	Number of observations		319	
	log likelihood		−91.8	
	AIC		197.6	

Note. $*$ means that the variable is significant at 95% level. In China heavy vehicles cannot drive on fast lanes; thus only vehicle type on right-side was considered.

level, all other five independent variables were statistically significant at the 95% level with p value less than 0.05.

Driving route information variables are important in this model. The effect of the path selection is represented by $\delta_{(\Delta CL)}$ and S which capture the number of lane-changes required to be in the correct lane and the distance to the point where the driver needs to be in a specific position (an exit). In line with expectation the estimated coefficient of this $\delta_{(\Delta CL)}$ is negative, which means the utility of a LL choice decreases with the number of lane-changes the driver needs to perform in order to complete the desired path plan. In contrast, the utility can be magnified when the distance to the off-ramp increases, where the coefficient of S is positive.

Another group of variables capture surrounding driving conditions on drivers' lane-changing decisions. These consist of the relative speed and spacing with respect to the vehicles in front in the current lane, in the lanes to the left and to the right of the test vehicle. A positive and significant coefficient of M_r captures drivers' tendency to avoid following a heavy vehicle, as heavy vehicles generally drive at lower speed and require greater braking distance. Both significant and negative coefficients of GT_m and GT_r indicate that when traffic neighboring conditions in the current and right lanes meet drivers' expectation, the left lane is generally not their preference.

GT_l is only statistically significant at 90% level and has a positive estimated coefficient. A possible explanation can be correlated with generally better level-of-service in Lane 1 (fast lane) and Lane 2 on the left. Driver characteristics such as age and gender did not play a significant role in lane-changing in this experiment. Contrary to priori expectations, gap time to the lagging vehicle on an adjacent lane did not have a significant effect on lane-changes in the estimation. This may reflect the trade-offs between mandatory and discretionary considerations in an off-ramp segment. In order to check model prediction accuracy, a classification matrix was used to compare predicted outcomes to the observed outcomes. According to it, the model successfully predicted 86.21% of the lane-changing behavior in off-ramp areas, which confirms that the logit model gave a good fit to the dataset.

3.2. Analysis of the Target Lane-Changing Probability Distribution. Ramps have been regarded as a major source of conflicts and congestion on freeways [34]. Near off-ramp areas are potential locations for bottleneck formation when the fraction of vehicles attempting to change to the lanes that are connected to their destinations is high. A diverging operation involves two interactive traffic streams: the freeway traffic and the ramp traffic. Two aspects need to be taken into account while studying lane-changing at ramps: the incentive and safety. This part discusses both types of characteristics in our experiment.

As discussed, important explanatory variables affecting the target lane choices came from route plan and neighboring

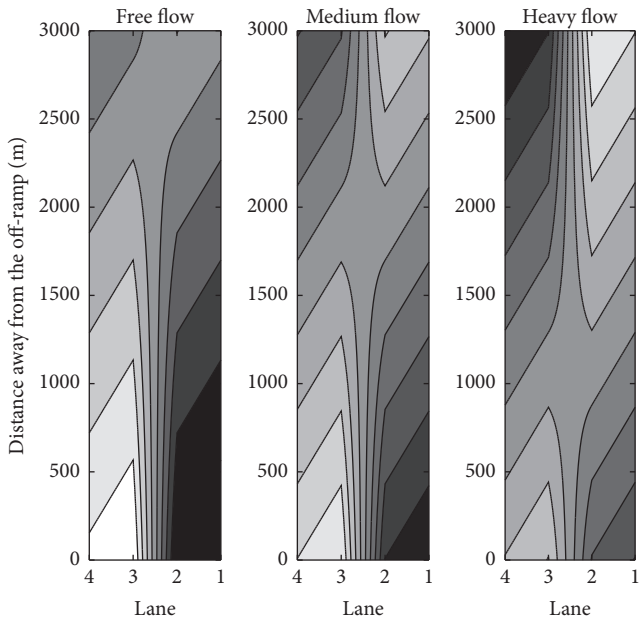

Figure 8: Lane-changing prob. sketch diagram in freeway off-ramp areas.

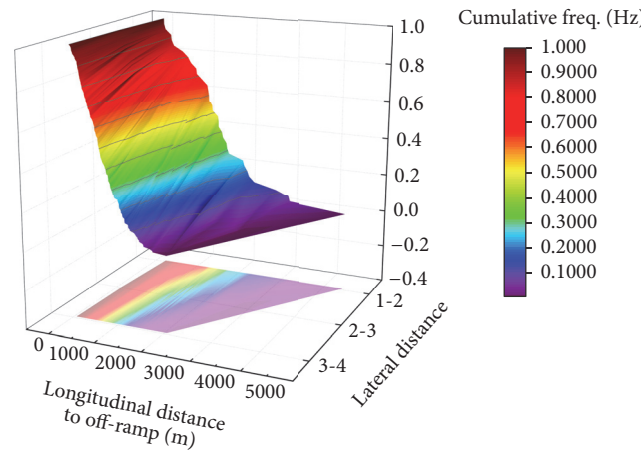

Figure 9: Spatial attributes with respect to cumulative frequency of lane-changes.

conditions. However, for a section of road, especially with a specific driving scenario (e.g., off-ramp), general traffic attributes, such as density and speed of traffic in the segment, also play a role for the lane-changes. Using time series DAS data, the information is available for estimation at discrete points on the test freeway segment. In a likelihood function of lane-changing behavior, a distribution of the distances from 3 km upstream to the off-ramp point was studied. For the sake of simplicity, we classified traffic into three levels: free flow, medium flow, and heavy flow.

We aim to quantify various traffic flows' impact on lane-changing. As shown in Figure 8, covering the three different traffic flow conditions, the lower right and top left corners with respect to the fast lane near the off-ramp and the shoulder lane far upstream of the off-ramp in a driving scenario have relatively low probability values. Correspondingly, the majority of mandatory lane-changes happened in the light gray area mainly along the three minor diagonals. In other words, we found the most likely lane-changing trajectory where drivers choose to change from lane 2 to lane 3 and at the last moment divert to lane 4 before arriving at the off-ramp, as displayed in Figure 5.

Our approach is innovative in the sense that the spatial and traffic attributes with respect to cumulative lane-changing rates can be measured in a quantitative and simultaneous manner. As the density is low, drivers start to carry out right lane-changing at earlier points. An explanation of this phenomenon can be that, in free flow, drivers are more likely to change lane to the right in advance without decreasing the feeling of comfort. Another interesting finding is that the more dense the traffic, the higher the wish to claim a position in the fast lane first. This implies that a driver postponing a response to a mandatory LC may have a higher propensity to perform discretionary LC. This can explain why, for an increasing density, a growth of lane-changes from the middle to the fast lane was found in the upstream stretch. The possible reason for these results is that when traffic density increases, vehicles at the upstream locations are more likely influenced by the pressure of surrounding vehicles and thus prefer to keep driving in the current lane or make a discretionary lane-change to the left. Hence they carry out right lane-changing actions for exiting only when approaching the off-ramp.

Furthermore, a lane-changing action will leave a gap in the original lane which may be used as gap to merge into by another vehicle. This case may happen more in higher density situations where vehicles are waiting for a gap and use this as soon as it becomes available. For some unobserved reason rather than the immediate traffic situations, a driver may decide on a particular lane-changing action [35], where there might be a trade-off between mandatory and discretionary. So if the fast lane for some reason is more attractive for the drivers, more vehicles change towards this fast lane. Even if it gets busier, the reason to go there can be still valid, and so drivers still move there in a dense situation. This theory is consistent with the results of the model estimates. Figure 9 displays spatial attributes (lateral and longitudinal distances to off-ramp) with respect to cumulative frequency of lane-changes.

3.3. Safety Assessment of Lane-Changing. Moreover, improper lane-changing action would result in potential safety hazards, such as rear-end crashes and sideswipe crashes. To put the lane-changing choice model into practice, safety assessment has been made to evaluate the potentially hazardous lane-changing behavior in this study.

There is a growing body of evidence to suggest a number of road safety benefits are associated with reduced speed variability between vehicles and reductions in 85th percentile speeds [36]. Specifically, increased speed variation may disturb homogenised traffic flow and increase the likelihood of conflict situations caused by human behavior [37].

Inspired by the findings, we applied the surrogate safety index Speed Variance (SV) of the following vehicle in the

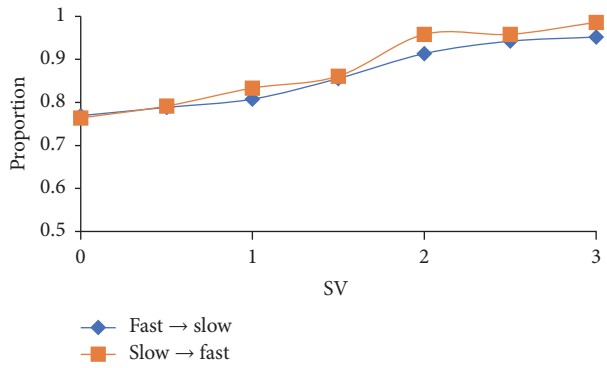

FIGURE 10: Cumulative frequency diagram of the speed variance of the lagging vehicle on the target lane.

target lane to assess the lane-changing behavior. The fundamental hypothesis concerning lane-changes is that any vehicle obeys a basic rule that lane-changing could be conducted only at least cost in speed reduction of neighboring vehicles; that is, a vehicle would change lane only if neighboring vehicles in the target lane would not have to slow down too much because of the lane-changing. Interestingly, in SH-NDS data, drivers are often cautious when they attempt to change lanes, especially under higher traffic density.

The SV value was calculated as

$$\mathrm{SV} = \frac{V_t - V_0}{t}, \tag{3}$$

where V_t denotes the speed of the lagging vehicle in the target lane when the test vehicle starts to change lane; V_0 denotes the speed of the lagging vehicle in the target lane when the test vehicle has completed its action; t denotes the period of a lane-changing event. A cumulative frequency diagram of the SV values is displayed in Figure 10.

According to Figure 10, a large majority of lagging vehicles will not be impacted by the lane-changing events. In such circumstances, lane-change maneuvers are not supposed to interfere with the motion of neighboring vehicles on the adjacent lane. In contrast, under a more congested traffic and aggressive lane-changing scenario, the lagging vehicles have to decelerate to avoid a potential rear-end or sideswipe collision. In an extreme case, when the SV values are great enough, the driver of the lagging vehicle may feel a surge of anxiety. Figure 10 also indicates that lane-changes from the slow lane to the fast lane lead to slightly higher SV values. This result is consistent with the expectation that, when the vehicle's running speed is higher, a bigger spacing between the preceding vehicle and the lagging vehicle is required for a safe lane-change. The threshold values of SV were selected to identify the risky lane-changing actions based in the dataset. The 85 percentile value of the SV values can be utilized as the threshold in normal road conditions [38, 39]. Lane-changes from the slow lane to the fast lane (e.g., Lane 3 to Lane 2) relate to a slightly greater 85 percentile speed variation value than lane-changes from the fast lane to the slow lane (e.g., lane 2 to lane 3) (1.324 versus 1.297). This result is consistent with the expectation and with other related works. A quantitative analysis of the safety assessment of lane-changes can contribute to the design of driving assistance systems. Once the improper lane-changing behavior has been identified, drivers can be alerted to the potential crash risk by in-vehicle driving assistance devices.

4. Conclusions

Studies of lane-changing behavior have been far less extensive than those of longitudinal driving behavior due to the lack of comprehensive vehicle trajectory data. For example, for the existing LC decision models, only a few have identified factors and developed lane-changing rules based on video evidence. Naturalistic driving study provides an opportunity to understand how drivers naturally interact with vehicle, roadway, and traffic environments. Naturalistic driving data have made it both technically and economically feasible to review kinematic information and driving behavior in natural surroundings on a large scale, through unobtrusive data gathering equipment and without experimental control.

Researchers have shown that lane-change maneuvers are primarily responsible for most of the traffic perturbations on multilane freeways. Therefore better understanding of lane-changing maneuvers is important in traffic studies, but this problem has not been satisfactorily investigated yet. In particular, in most off-ramp studies, lane-changes were considered as mandatory where the driver must leave the current lane. However, according to the data set of our naturalistic driving experiment and the analysis of this study, such classification of off-ramp lane-changing behavior seems to ignore trade-offs between mandatory and discretionary incentives. Applying a rigid lane-changing behavior model may result in unrealistic traffic flow characteristics. Only limited empirical studies have been done to accurately estimate the parameters of lane-changing models.

This study employed lane offset position and steering wheel angle as indexes to extract lane-changing samples in freeway off-ramp areas. Illustrated by the one-way four-lane freeway stretch, a logit model was developed to model the choice of target lanes. Parameters were estimated using vehicle trajectory data and individual characteristics. Estimations show that drivers' lane selection is impacted both by trip path variables and neighborhood traffic conditions. A likelihood analysis of lane-changing actions was graphed with respect to free flow, medium flow, and heavy flow.

The results suggest that lane-changing behavior of exiting vehicles is the consequence of the balance between route plan (mandatory incentive) and expectation to improve driving condition (discretionary incentive). In higher traffic density, the latter seems to play a significant role. The findings reveal the mechanism of lane-changing behavior near an off-ramp, which indicate the influencing factors as well as drivers' preferences in different traffic conditions. These can help improve driveway management in off-ramp areas and provide a reference for layout of guide signs. Therefore, traffic practitioners can take appropriate action, such as average speed enforcement and managed lane strategy, to make traffic smoother.

Near off-ramp sections, a lane-changing event may cause a harsh deceleration by the lagging vehicle and then may disrupt traffic and increase crashes and collisions. We applied the speed variance of the following vehicle in the target lane as a safety surrogate index. Moreover, lane-changing from slow lane to the fast lane would lead to a higher SV value. A series of thresholds are listed for real-time lane-changing safety assessment. It provides an opportunity to avoid potential rear-end or sideswipe crash. Further work is being conducted to study urban roadway stretches where the distance between ramps is shorter. For a more realistic and robust model, heterogeneity of vehicle composition in the roadway and geometry-specific effects should also be considered. Finally future studies need to also consider squeezed lane-changing behavior and driver negotiation with different off-ramps.

This is one of the first comprehensive studies using the Shanghai Naturalistic Driving Study data. The findings contribute to a better understanding of drivers' natural driving behavior in freeway off-ramp. This paper provides important insights into road network design and transportation safety strategies.

Conflicts of Interest

The authors declare that they have no conflicts of interest.

Acknowledgments

This work was supported in part by the Research and Application of Road Emergency Rehabilitation Equipment and Standard Project (2016YFC0802701), Shanghai Pujiang Program, the Fundamental Research Funds for the Central Universities, and the National Natural Science Foundation of China under Grant 71671126.

References

[1] J. A. Barria and S. Thajchayapong, "Detection and classification of traffic anomalies using microscopic traffic variables," *IEEE Transactions on Intelligent Transportation Systems*, vol. 12, no. 3, pp. 695–704, 2011.

[2] J. Lu, P. Liu, and B. Behzadi, "Safety Evaluation of Freeway Exit Ramp," in *Proceedings of the TRB Annual Meeting CD-ROM (07-1293)*, 2007.

[3] D. Sun and L. Elefteriadou, "Lane-changing behavior on urban streets: a focus group-based study," *Applied Ergonomics*, vol. 42, no. 5, pp. 682–691, 2011.

[4] D. J. Sun and L. Elefteriadou, "Lane changing behavior on urban streets: an 'in-vehicle' field experiment-based study," *Computer-Aided Civil and Infrastructure Engineering*, vol. 27, no. 7, pp. 525–542, 2012.

[5] T.-Q. Tang, S. C. Wong, H.-J. Huang, and P. Zhang, "Macroscopic modeling of lane-changing for two-lane traffic flow," *Journal of Advanced Transportation*, vol. 43, no. 3, pp. 245–273, 2009.

[6] T. Toledo, C. F. Choudhury, and M. E. Ben-Akiva, "Lane-changing model with explicit target lane choice," *Transportation Research Record*, no. 1934, pp. 157–165, 2005.

[7] P. G. Gipps, "A model for the structure of lane-changing decisions," *Transportation Research Part B: Methodological*, vol. 20, no. 5, pp. 403–414, 1986.

[8] Q. Yang and H. N. Koutsopoulos, "A microscopic traffic simulator for evaluation of dynamic traffic management systems," *Transportation Research Part C: Emerging Technologies*, vol. 4, no. 3, pp. 113–129, 1996.

[9] P. Hidas, "Modelling vehicle interactions in microscopic simulation of merging and weaving," *Transportation Research Part C: Emerging Technologies*, vol. 13, no. 1, pp. 37–62, 2005.

[10] K. I. Ahmed, M. E. Ben-Akiva, H. N. Koutsopoulos, and R. G. Mishalani, "Models of freeway lane changing and gap acceptance behavior," in *Proceedings of the 13th International Symposium on Transportation and Traffic Theory*, pp. 501–515, Lyon, France, 1996.

[11] K. I. Ahmed, *Modeling Drivers Acceleration and Lane Changing Behavior*, Massachusetts Institute of Technology, 1999.

[12] T. Toledo, *Integrated Driving Behavior Modeling [Ph.D. thesis]*, Department of Civil and Environmental Engineering, Massachusetts Institute of Technology, Boston, Mass, USA, 2007.

[13] S. H. Hamdar, *Modeling Driver Behavior as a Stochastic Hazard-based Risk-Taking Process [Ph.D. thesis]*, Northwestern University, Evanston, Ill, USA, 2009.

[14] C.-H. Wei, "Developing freeway lane-changing support systems using artificial neural networks," *Journal of Advanced Transportation*, vol. 35, no. 1, pp. 47–65, 2001.

[15] T. Mai, R. Jiang, and E. Chung, "A Cooperative Intelligent Transport Systems (C-ITS)-based lane-changing advisory for weaving sections," *Journal of Advanced Transportation*, vol. 50, no. 5, pp. 752–768, 2016.

[16] E. Balal, R. L. Cheu, and T. Sarkodie-Gyan, "A binary decision model for discretionary lane changing move based on fuzzy inference system," *Transportation Research Part C: Emerging Technologies*, vol. 67, pp. 47–61, 2016.

[17] S. E. Lee, E. C. B. Olsen, and W. W. Wierwille, "A comprehensive examination of naturalistic lane-changes," *Publication Dot Hs Virginia Tech Transportation Institute*, 2004.

[18] T. G. Oketch, "New modeling approach for mixed-traffic streams with nonmotorized vehicles," *Transportation Research Record*, no. 1705, pp. 61–69, 2000.

[19] Z. Zheng, "Recent developments and research needs in modeling lane changing," *Transportation Research Part B: Methodological*, vol. 60, pp. 16–32, 2014.

[20] A. Kesting, M. Treiber, and D. Helbing, "General lane-changing model MOBIL for car-following models," *Transportation Research Record*, vol. 1999, no. 1, pp. 86–94, 2007.

[21] D. Zhao, H. Peng, and K. Nobukawa, "Analysis of mandatory and discretionary lane change behaviors for heavy trucks," in *Proceedings of the 12th International Symposium on Advanced Vehicle Control*, Tokyo, Japan, 2014.

[22] T. Dingus, S. Klauer, V. Neale et al., "The 100-Car Naturalistic Driving Study, Phase II Results of the 100-Car Field Experiment," *Report no. DOT HS 810 593*, 2006.

[23] F. Guo, S. G. Klauer, J. M. Hankey, and T. A. Dingus, "Near crashes as crash surrogate for naturalistic Driving Studies," *Transportation Research Record*, no. 2147, pp. 66–74, 2010.

[24] N. Uchida, M. Kawakoshi, T. Tagawa, and T. Mochida, "An investigation of factors contributing to major crash types in Japan based on naturalistic driving data," *IATSS Research*, vol. 34, no. 1, pp. 22–30, 2010.

[25] Y. Barnard, F. Utesch, N. van Nes, R. Eenink, and M. Baumann, "The study design of UDRIVE: the naturalistic driving study across Europe for cars, trucks and scooters," *European Transport Research Review*, vol. 8, no. 2, article no. 14, 2016.

[26] G. M. Fitch and R. J. Hanowski, *Using Naturalistic Driving Research to Design, Test and Evaluate Driver Assistance Systems*, Handbook of Intelligent Vehicles, Springer London, Lodon, UK, 2012.

[27] K. D. Kusano, J. Montgomery, and H. C. Gabler, "Methodology for identifying car following events from naturalistic data," in *Proceedings of the 25th IEEE Intelligent Vehicles Symposium, IV 2014*, pp. 281–285, USA, June 2014.

[28] M. W. Levin and S. D. Boyles, "A multiclass cell transmission model for shared human and autonomous vehicle roads," *Transportation Research Part C: Emerging Technologies*, vol. 62, pp. 103–116, 2016.

[29] A. Pande and M. Abdel-Aty, "Assessment of freeway traffic parameters leading to lane-change related collisions," *Accident Analysis & Prevention*, vol. 38, no. 5, pp. 936–948, 2006.

[30] C. Dong, Q. Dong, B. Huang, W. Hu, and S. S. Nambisan, "Estimating factors contributing to frequency and severity of large truck–involved crashes," *Journal of Transportation Engineering Part A*, vol. 143, no. 8, 2017.

[31] H. D. Son, Y.-J. Kweon, and B. B. Park, "Development of crash prediction models with individual vehicular data," *Transportation Research Part C: Emerging Technologies*, vol. 19, no. 6, pp. 1353–1363, 2011.

[32] L. Li, Z. Wen, and Z. Wang, "Outlier detection and correction during the process of groundwater lever monitoring base on pauta criterion with self-learning and smooth processing," *Communications in Computer and Information Science*, vol. 643, pp. 497–503, 2016.

[33] S. E. Lee, E. C. B. Olsen, and W. W. Wierwille, "A comprehensive examination of Naturalistic Lane-changes," National Highway Traffic Safety Administration DOT HS-809 702, 2004.

[34] J. L. Evans, L. Elefteriadou, and N. Gautam, "Probability of breakdown at freeway merges using Markov chains," *Transportation Research Part B: Methodological*, vol. 35, no. 3, pp. 237–254, 2001.

[35] V. L. Knoop, S. P. Hoogendoorn, Y. Shiomi, and C. Buisson, "Quantifying the number of lane changes in traffic," *Transportation Research Record*, no. 2278, pp. 31–41, 2012.

[36] E. Cascetta, V. Punzo, and M. Montanino, "Empirical analysis of effects of automated section speed enforcement system on traffic flow at freeway bottlenecks," *Transportation Research Record*, no. 2260, pp. 83–93, 2011.

[37] D. W. Soole, B. C. Watson, and J. J. Fleiter, "Effects of average speed enforcement on speed compliance and crashes: A review of the literature," *Accident Analysis & Prevention*, vol. 54, pp. 46–56, 2013.

[38] A. Montella, L. L. Imbriani, V. Marzano, and F. Mauriello, "Effects on speed and safety of point-to-point speed enforcement systems: Evaluation on the urban motorway A56 Tangenziale di Napoli," *Accident Analysis & Prevention*, vol. 75, pp. 164–178, 2015.

[39] R. J. Porter, "Estimation of relationships between 85th percentile speeds, speed deviations, roadway and roadside geometry and traffic control in freeway work zones," *Dissertations & Theses - Gradworks*, 2007.

Hindawi
Journal of Advanced Transportation
Volume 2017, Article ID 1208170, 11 pages
https://doi.org/10.1155/2017/1208170

Research Article

Effects of Human-Centered Factors on Crash Injury Severities

Emmanuel Kofi Adanu[1] and Steven Jones[2]

[1]*Alabama Transportation Institute, The University of Alabama, Tuscaloosa, AL, USA*
[2]*Department of Civil, Construction and Environmental Engineering, The University of Alabama, Tuscaloosa, AL, USA*

Correspondence should be addressed to Emmanuel Kofi Adanu; ekadanu@crimson.ua.edu

Received 2 June 2017; Revised 20 November 2017; Accepted 29 November 2017; Published 20 December 2017

Academic Editor: Zhi-Chun Li

Factors related to drivers and their driving habits dominate the causation of traffic crashes. An in-depth understanding of the human factors that influence risky driving could be of particular importance to facilitate the application of effective countermeasures. This paper sought to investigate effects of human-centered crash contributing factors on crash outcomes. To select the methodology that best accounts for unobserved heterogeneity between crash outcomes, latent class (LC) logit model and random parameters logit (RPL) model were developed. Model estimation results generally show that serious injury crashes were more likely to involve unemployed drivers, no seatbelt use, old drivers, fatigued driving, and drivers with no valid license. Comparison of model fit statistics shows that the LC logit model outperformed the RPL model, as an alternative to the traditional multinomial logit (MNL) model.

1. Introduction

Road traffic crashes occur from a combination of factors related to elements of the transportation system, made up of the road and its environment, vehicles, and road users, with crash outcomes ranging from property damage to death. Some factors contribute to crash occurrence, while others influence the outcome (or severity) of the crash or both. While the effects of some crash causal factors such as speed are fairly obvious, they may be linked to other unobserved factors, such as a sensation seeking nature of the driver, which are not typically accounted for during the crash reporting process. Having a holistic understanding of crash causal factors and how they impact on severities are necessary to develop and target countermeasures.

There is a significant body of road safety literature dedicated to the study of factors affecting crash occurrence and severities. Multiple proposals on countermeasures have ranged from roadway reengineering, improved vehicle safety features, and strategies to influence driver behavior. The development of these proposals or countermeasures have been anchored on understanding the factors that affect the likelihood of crash occurrence and/or circumstances that influence the severity of the crash outcome. A critical component of road traffic crash analyses has been the examination of the driver. Some drivers have habits or choose to drive in ways that increase their likelihood of getting into a crash. For instance, driving styles such as choice of speed, threshold for overtaking, tolerance for gap acceptance, and adherence to traffic control have been strongly linked to certain groups of drivers [1]. According to [1], while certain groups of drivers may be disproportionately represented in crash statistics, this may be due to reasons not related to their risk of crash. One of the early attempts by researchers to gain in-depth understanding of crash causal factors was the Indiana Tri-Level Study. From this study, [2] observed that human errors and deficiencies were definite or probable cause in over 90% of the crashes examined. The leading direct human causes identified in the study included improper lookout (probable cause in 23% of accidents), excessive speed (17%), inattention (15%), improper evasive action (13%), and internal distraction (9%). In a similar study, [3] investigated specific driver behaviors and unsafe driving acts that lead to crashes. The study further assessed the situational, driver, and vehicle characteristics associated with these behaviors. They found human error to be the most frequently cited contributing

factor in 99.2% of crashes, followed by environmental (5.4%) and vehicle factors (0.5%). Thus, most crashes and their associated injuries and fatalities can be linked to some form of unsafe driving habits [3]. It is therefore important to examine the causal driver characteristics and also assess their driving behaviors that increase the likelihood of crash occurrence.

This paper investigates the effects of human-centered crash causal factors on crash outcomes. This is achieved by developing latent class logit (LC) and random parameters logit (RPL) models to identify how the human-related factors influence injury severity of crashes.

2. Human-Centered Traffic Safety

Driver-related behavioral factors and human errors dominate the causation of traffic crashes [2, 3, 6]. Driving behaviors and styles are influenced by external and driver-specific factors. Individual and societal characteristics which influence driving behavior in a way which can affect the chances of crash occurrence collectively constitute human factors in traffic safety. Driver characteristics (e.g., gender, race, and age), attitudes, beliefs, and personality traits (e.g., tolerance, caution, inattentiveness, perception of risk, and sensation seeking) are some human factors that influence driving habits [1, 7, 8]. Societal norms and cultural practices, such as adherence to traffic rules and regulations, on the other hand also play important roles in shaping driver attitudes and beliefs. These have impacts on driving styles and can affect traffic safety [9–14]. The National Highway Traffic Safety Administration (NHTSA) observed that cultural differences and sensitivities correlate with motor vehicle fatality and injury rates. In the US, for instance, racial and ethnic groups are disproportionately killed in traffic crashes compared with the much larger non-Hispanic White population [9]. The American Automobile Association explicitly studies traffic safety culture in the US [12]. Reference [15] documented differences in traffic safety culture in Iowa, [16] documented differences in traffic safety behavior across geographic regions in Alabama, and others [e.g., [13, 17]] have even compared traffic safety cultures across international boundaries. This means that, with other things being equal, some human-centered characteristics and behaviors put some groups of the driving population at greater risk of getting into traffic crashes.

In an attempt to explore the causal link between human factors and the likelihood of crashes, [18] distinguished behavior-related factors into two major categories: those that reduce the capability of a driver to perform driving tasks (e.g., inexperience, accident proneness, and alcohol and drug use) and those factors that influence risk taking while driving (e.g., habitual disregard of traffic laws and regulations). Differences in the behavioral factors exist among different demographic groups. For instance, [19] observed that alcohol was less likely to be a factor in traffic crashes involving older drivers, while the primary problems with young drivers are risk taking and lack of skill. Crashes among young drivers are more likely to involve a single vehicle, one or more driving errors, and speed as a factor or involve alcohol abuse. Reference [20] has also observed that young males are more prone to excessive speeding influenced by peer pressure. Female drivers on the other hand are more prone to driving errors [21]. Reference [22] studied the impact of distracted driving on safety and traffic flow. Their study has shown that drivers are likely to drive in a manner that negatively affects traffic safety and traffic flow if they are distracted, regardless of driver age. Other studies have shown that inexperienced drivers are more susceptible to errors and are slower to recover after being distracted [21, 23]. Reference [24] conducted a study to examine the effects of personality factors assessed during adolescence on persistent risky driving behavior and traffic crash involvement among young adults. They found that, for males, aggression, traditionalism, and alienation were the personality traits most frequently associated with risky driving behavior and crash risk. Willfully flouting driving laws and regulations may be indicative of risk taking behavior. Reference [25] identified that unlicensed drivers were at significantly higher risk of car crash injury than those holding a valid license. Beyond the individual characteristics, certain driving styles and behaviors also affect the severity of the crash. For instance, seatbelt nonuse has been associated with increased risk of injury and death in a crash. Reference [26] estimates reveal that more than half of teen drivers (13–19 years) and adults aged 20–44 years who died in crashes in 2014 were unrestrained at the time of the crash. Faster driving speeds are also known to increase the likelihood of crash occurrence and also the severity of the crash consequences. Speeding-related fatalities constituted approximately a third of total traffic fatalities across the United States between 2005 and 2014 [27]. Impairment by alcohol and other drugs, driver distraction and inattention have been cited frequently as contributing factors in crashes and these can also affect the severity of the crash outcome [e.g., [2, 3, 28, 29]]. Statistics show that alcohol-impaired-driving fatalities accounted for a third of all crash fatalities in the United States in 2014 [29]. Driver inattention has also been extensively linked to crash occurrence. Nearly 10 percent of fatal crashes, 18 percent of injury crashes, and 16 percent of all police-reported motor vehicle traffic crashes in 2014 were reported be distracted driving related [30].

Considering that human factors are responsible for the highest proportion of traffic crashes, it would seem that human-centered countermeasures would be worth pursuing. Indeed, [31] reported that crash countermeasures achieve best results when they influence driver behavior. Human-centered countermeasures may take the form of improved driver training and testing, education campaigns aimed at changing driving practices, legislation to control driver behavior, and improvements to the design of road systems and automobiles [1]. Promoting a culture of safe road user behavior is required to achieve sustained reductions in road traffic injuries.

3. Crash Injury Severity Models

The primary emphasis of crash injury severity studies is to identify factors that influence the severity of crash outcomes. Safety researchers have relied on myriad statistical modeling techniques, applied to postcrash records and other noncrash specific data, to gain data-driven knowledge and

Table 1: Summary statistics of the variables used for model building.

Variable name	Description	Mean (standard deviation)
Crash severity	Serious injury/minor injury	0.30/0.70
Driver error	Primary cause: error attributed to driver (1 = yes, 0 = no)	0.49 (0.50)
DUI	Primary cause: DUI (1 = yes, 0 = no)	0.09 (0.29)
Speed	Primary cause: speeding (1 = yes, 0 = no)	0.11 (0.32)
Distracted	Primary cause: distracted driving (1 = yes, 0 = no)	0.11 (0.31)
Fatigue	Driver condition at time of crash: fatigued (1 = yes, 0 = no)	0.06 (0.23)
Invalid license	License status of causal driver: invalid license (1 = yes, 0 = no)	0.07 (0.26)
No seatbelt	Seatbelt use: no seatbelt (1 = yes, 0 = no)	0.11 (0.31)
Female	Driver gender: female (1 = yes, 0 = no)	0.44 (0.50)
Black	Driver race: African American (1 = yes, 0 = no)	0.24 (0.43)
Young	Driver age: less than 30 (1 = yes, 0 = no)	0.42 (0.49)
Old	Driver age: more than 60 (1 = yes, 0 = no)	0.15 (0.36)
Unemployed	Driver employment status: unemployed (1 = yes, 0 = no)	0.30 (0.46)

understanding into crash causal circumstances. Reference [32] has shown that interest in identifying factors that affect crash injury severity has increased considerably in the last few years, perhaps, due to the availability of data and proliferation of advanced statistical packages. Depending on data characteristics and scope of studies, researchers have the option of choosing from a wide range of statistical tools for crash severity studies.

Discrete-choice (logit and probit) models have been used extensively over the years to analyze crash injury severity due to the classification of the severities into discrete outcomes. These methodologies have been applied to study safety of different roadway facilities and have included variables that describe the crash circumstances, environmental conditions, roadway, vehicle, and driver characteristics. For instance, [33] used nested logit formulation to predict crash severity on a section of rural interstate in Washington State. This study investigated the effect of environmental conditions, highway design, crash type, driver characteristics, and vehicle attributes on crash severity. References [34, 35] also applied nested logit techniques to analyze crash severity at unsignalized intersections and at roundabouts, respectively. Other logit modeling techniques that have been used in injury severity studies include binary logistic models [36–40], ordered logit models [41–44], multinomial logit [45, 46], mixed logit [5, 47], and heterogeneous models [44]. Logit models are however not able to handle random variations and are not applicable to panel data with temporally correlated errors. They also do not allow any pattern of substitution [48]. Probit models address these limitations. Ordered probit model is the most used type of probit models in crash severity analysis [e.g., [34, 49–51]]. Reference [52] used ordered probit modeling techniques to isolate factors that contribute to injuries in older drivers involved in crashes. Reference [53] analyzed crashes at signalized intersections to determine the expected injury severity level using ordered probit model. Data mining techniques have also been used to analyze traffic crash injury severity. For instance, [54, 55] used classification and regression trees and [56] used Chi-squared automatic interaction detection to analyze crash severities. Other advanced methodologies used in literature include Bayesian networks [e.g., [57, 58]], neural networks [e.g., [59, 60]], and linear genetic programming [e.g., [61]]. Latent class approach has recently been used for analyzing driver injury severities [62–64].

The fundamental characteristics of crash data and purpose of study dictate the choice of tool or methodology [65]. Many other methods have been used for crash injury severity studies. This discussion is by no means exhaustive on the subject. Reference [65], for instance, presents a comprehensive review of crash injury severity models and methodological approaches. Similarly, [32] undertook a meta-analysis and presented documentation on the characteristics and limitations of different modeling methods for safety researchers.

4. Data Description

This study is based on 2011–2015 injury-related crash data, for the State of Alabama, obtained from the Critical Analysis Reporting Environment (CARE) system developed by the Center for Advanced Public Safety at the University of Alabama for the Alabama Department of Transport (ALDOT). Each crash record contained all details related to a crash recorded by the police at the time of the crash, including details of the drivers (e.g., gender, age, and race) and vehicles (e.g., make, model, and age) involved, description of the roadway environment (facility type, presence of curvature or grade, traffic control, etc.), and environmental conditions (weather, lighting, rural versus urban, etc.). The data was filtered to select crashes that were reported to have human-centered factors as their primary contributing circumstance. These human-centered factors consist of driving styles, decisions, and activities undertaken by the driver, which led to the crash. For each crash event, information on the driver's license status and seatbelt use was obtained. Demographic information of the causal driver was also obtained. Observations with missing values were omitted from the dataset, resulting in a total of 87,326 observations. Table 1 shows the summary statistics of the variables available for model building and analysis.

Two categories of severity were adopted as is often done in crash injury severity studies [e.g., [16, 36–40]]. Serious injury crashes (defined as fatal or incapacitating injury, where an incapacitating injury implies that the victim is unable to leave the scene of the crash without physical assistance to do so) comprised 30% of the data and minor injury crashes (defined as nonincapacitating injury or possible injury) made up 70% of the crash observations. Crashes involving some form of driver error (defined to include aggressive driving, failure to yield, following too close, and ran traffic control device) made up approximately half of injury crashes. About 44% of injury crashes were reported to involve women. A third of the drivers involved in injury crashes were unemployed and about 42% of the drivers were less than 30 years old. Some 9% of the drivers were under the influence of drugs, alcohol, or medication, while 11% involved speeding.

5. Methodology

Unobserved heterogeneity is a critical issue in traffic safety research. Ignoring the moderating effect of unobserved variables can lead to biased estimates and incorrect inferences if inappropriate methods are used [66, 67]. Limiting the impact of a variable to its statistical significance in a model can mean eliminating some otherwise risky factors. Reference [68] observed that an insignificant variable in one model may be due to lack of observations. On the other hand, significance of a variable in an injury severity model is not an automatic indication that it is an important etiologic factor.

The ordinal nature of reporting crash injury severities makes ordered probit and logit models appropriate [51, 69]. However, these model forms can restrict the way variables influence outcome probabilities, possibly leading to incorrect inferences [37, 70]. Compared to the traditional ordered probability models, multinomial logit (MNL) models have a flexible structure which allows each severity outcome to have a different function for capturing the probabilities of injury severities [66, 71, 72]. Notwithstanding this, the MNL model is deficient in its application as it is susceptible to correlation of unobserved effects from one crash severity level to the next. Such correlation leads to a violation of the model's independence of irrelevant alternatives (IIA) property [70]. Also, the assumption that random terms in the crash severity functions in MNL models are independent and identically distributed (IID) is often violated in practice because crash severity functions do not contain a complete list of all contributing factors. Even though nested logit models can capture some unobserved effects shared by some injury severity outcomes, they cannot address unobserved heterogeneity in the data. Random parameters (mixed logit) models and latent class (finite mixture) logit models have the ability to capture the unobserved heterogeneity by allowing parameters to differ across observations [47, 67, 73]. For this study, injury severity analysis was performed to investigate the effects of some human-related explanatory factors on the likelihood of the occurrence of serious or minor injury severities.

5.1. Injury Severity Analysis. A traditional MNL injury severity model was first developed to identify how the human-centered variables influence crash outcomes. RPL and LC logit models were then estimated to address the heterogeneity challenges inherent in the MNL model. Estimation results for the RPL and the LC logit models are then compared to select the best fitting alternative model to the MNL model.

5.1.1. Random Parameters Logit Model. RPL model allows for heterogeneity within observed crash data by varying the elements of the vector of estimable parameters, β_i. The outcome specific constants and elements of β_i may either be fixed or randomly distributed over all parameters with fixed means. The random parameters logit model formulation is obtained from the standard MNL by introducing random parameters with $f(\beta_i \mid \varphi)$, where φ is a vector of parameters of the chosen density function (mean and variance) [48, 70, 74] as

$$P_n(i \mid \varphi) = \int \frac{\exp(\beta_i X_{in})}{\sum_{\forall I} \exp(\beta_i X_{in})} f(\beta_i \mid \varphi)\, d\beta_i, \quad (1)$$

and $P_n(i \mid \varphi)$ is the probability of injury severity i conditional on $f(\beta_i \mid \varphi)$.

For model estimation, β_i can now account for unobserved heterogeneity of the impact of X on injury severity outcome probabilities, with the density function $f(\beta \mid \varphi)$ used to determine β_i. Random parameters logit probabilities are weighted average for some different values of β across observations where some elements of the parameter vector β are fixed parameters and some may be randomly distributed. A continuous distribution relating how parameters vary across crash observations is assumed by the researcher. For this study, the normal distribution is assumed for model estimation [5].

5.1.2. Latent Class Logit Model. LC logit model offers an alternative perspective to the random parameters logit model in terms of accommodating heterogeneity [67, 73, 75]. This model replaces the continuous distribution assumption of random parameter model with a discrete distribution in which unobserved heterogeneity is captured by membership of distinct classes [75, 76]. A latent class logit model allows the driver injury severity to have C different classes so that each of the classes will have their own parameters with the probability given by [77]

$$P_n(c) = \frac{\exp(\alpha_c Z_n)}{\sum_{\forall C} \exp(\alpha_c Z_n)}, \quad (2)$$

where Z_n represents a vector that shows the probabilities of c for crash n, C is the possible classes c, and α_c represents the estimable parameters (class-specific parameters). The probability of driver having injury severity i is given by

$$P_n(i) = \sum_{\forall C} P_n(c) * P_n(i/c), \quad (3)$$

where $P_n(i/c)$ is the probability of drivers to have injury severity level i for crash n in class c. Based on the two equations above, the latent class logit model for class c will be

$$P_n(i/c) = \frac{\exp(\beta_{ic} X_{in})}{\sum_{\forall I} \exp(\beta_{ic} X_{in})}, \quad (4)$$

where I represents the possible number of injury severity levels and β_{ic} is a class-specific parameter vector that takes a finite set of values.

The latent class logit model can be estimated with maximum likelihood procedures [75]. The latent class method however does not account for the possibility of variation within a class since it assumes homogeneous characteristics of the within-class observations [76]. References [78, 79] present the random parameter latent class model as an extension of the latent class logit model to capture interactions with observed contextual effects within the latent classes.

Marginal effects are typically computed to reveal the relative impact of explanatory variables on the dependent variable. Marginal effect in a latent class logit model is computed for each class as the difference in the estimated probabilities with the indicator changing from zero to one, while keeping all the other variables at their means. Reference [80] has shown that the direct and cross-marginal effects can be computed respectively as follows:

$$\frac{\partial P_{ni}}{\partial x_{nik}} = \beta_{ik} P_{ni} \left(1 - P_{ni}\right), \qquad \frac{\partial P_{nq}}{\partial x_{nik}} = -\beta_{ik} P_{ni} P_{nq}. \tag{5}$$

The direct marginal effect shows the effect of a unit change in x_{nik} on the probability, P_{ni}, for crash n to result in severity i. The cross-marginal effect shows the impact of a unit change in variable k of alternative i ($i \neq q$) on the probability P_{nq} for crash n to result in outcome q. According to [80, 81], the final marginal effect of an explanatory variable is the sum of the marginal effects for each class weighted by their posterior latent class probabilities. It should be noted that there are no definitive rules for selecting a set number of latent classes to be modeled [81]. It is documented, however, that too many classes can negatively affect model convergence and complicate model interpretation [82]. It has been suggested to add one class at a time until further addition does not enhance intuitive interpretation and data fit [75, 82]. To select the model that best fits the data, likelihood ratio tests may be performed to compare models with different number of classes [75], or based on the Bayesian Information Criterion (BIC) computed for the two models [83–86]. Recent studies of crash injury severities have used the BIC measure to determine the number of classes [63, 64, 66]. The BIC for a given empirical model is equal to

$$\mathrm{BIC} = -2LL + KLn\left(Q\right), \tag{6}$$

where LL is the log-likelihood at convergence, K is the number of parameters, and Q is the number of observations. Lower BIC values indicate a better model fit.

6. Estimation Results

Examination of the classes of human-centered factors among injury crashes revealed interesting information on what behaviors contribute to injury crashes and, to some extent, what types of drivers exhibit them. In order to develop a more nuanced understanding of how human-centered factors affected crash severity, a series of analyses were conducted to examine the extent to which the various parameters are useful in estimating crash injury severity. A total of 12 variables were used for model building. Table 2 shows the estimation results for the RPL and the LC logit models. Since the RPL and LC logit models are improved extensions of the standard MNL model, results for the MNL model have also been shown to confirm this.

The MNL model reveals that crashes involving fatigue, drivers with invalid license, no seatbelt use, and old and unemployed drivers were more likely to result into serious injury while driver error, DUI, speed, and distracted driving-related crashes were more likely to lead to minor injuries. The MNL model also shows that female drivers, young drivers, and African American drivers were more likely be involved in minor injury crashes. The effects of the parameters in the MNL model are fixed across severity levels. This implies that variables are assumed to influence either minor injuries or serious injuries, not both. The RPL model, however, reveals that driver error, speeding, distracted driving, no seatbelt use, and young driver indicators were random variables. The random variables significantly contributed to both serious and minor injury crashes. This means that some proportion of crashes involving a random variable, for instance, driver error, resulted in serious injuries and some proportion resulted in minor injuries.

Two distinct classes with homogeneous attributes were identified to be significant for the LC logit model: latent class 1 (LC 1) with probability of 0.72 and latent class 2 (LC 2) with probability of 0.28. The two-class model was selected over an estimated three-class model based on BIC: the two- and three-class models had BIC values of 98032 and 98154, respectively. An inspection of the constant term defined for the serious injury function indicates that a crash in LC 1 is more likely to result in serious injury than a crash in LC 2. One interesting observation was that old drivers had high chance of being involved in serious injury crashes regardless of the latent class. Driver error, DUI, speed, and distracted driving-related crashes were less likely to lead to minor injuries in LC 2 but more likely to result in minor injuries in LC 1. Similarly, crashes involving females, African American, and young drivers were likely to result in serious injury in LC 2 and minor injury in LC 1. Unemployed drivers were more likely to be involved in serious injury crashes in LC 1 but less likely to be involved in the same in LC 2.

The marginal effects (Table 3) show that older drivers and crashes involving no seatbelt use, respectively, had 0.73% and 1.89% higher likelihood of resulting in serious injury. Injury crashes involving unemployed drivers, drivers with invalid license, and fatigued driving, respectively, had 4.19%, 0.32%, and 0.05% higher chance of lead to serious injury outcome. This result also indicates that drivers with no employment are perhaps more likely to drive with invalid license. Another interesting result from marginal effects is that though a high proportion of the injury crashes were attributed to driver error, DUI, and speeding, their outcomes were more likely to be minor injury.

A comparison of the fit statistics (e.g., McFadden pseudo R^2 = 0.069, 0.183, 0.193 for MNL, RPL, and LC logit models,

Table 2: Model estimation results.

Variable	MNL		RPL		LC 1		LC 2	
	Serious injury	Minor injury	Serious injury	Minor injury	Serious injury	Minor injury	Serious injury	Minor injury
Constant	−0.26 (−13.23)		−0.12 (−4.45)		0.69 (11.94)		−20.67 (−0.06)	
Driver error		0.95 (50.05)		2.19 (7.61)^{rp}		1.64 (23.24)		−17.71 (−0.05)
DUI		0.26 (8.99)		0.43 (9.43)		1.26 (8.40)		−19.83 (−0.06)
Speed		0.39 (14.93)		0.94 (4.13)^{rp}		0.83 (11.60)		−16.92 (−0.05)
Distracted		1.26 (41.57)		6.10 (5.74)^{rp}		2.48 (29.16)		−9.81 (−0.53)
Fatigue	0.14 (4.35)		0.02 (0.47)		−2.19 (−12.81)		47.11 (0.00)	
Invalid license	0.10 (3.44)		0.13 (2.71)		0.09 (1.41)		0.35 (1.21)	
No seatbelt	1.01 (41.70)		2.46 (8.71)^{rp}		1.59 (21.19)		−1.64 (−3.52)	
Female		0.17 (10.90)		0.26 (9.09)		0.26 (8.10)		−0.28 (−1.50)
Black		0.12 (6.77)		0.17 (5.89)		0.18 (5.29)		−0.04 (−0.21)
Young		0.23 (13.38)		0.55 (6.58)^{rp}		0.43 (10.21)		−1.16 (−4.19)
Old	0.11 (4.77)		0.11 (3.42)		0.11 (2.11)		0.50 (1.34)	
Unemployed	0.22 (12.74)		0.38 (11.56)		0.40 (10.85)		−0.60 (−2.55)	
Latent class probability					0.72 (74.94)		0.28 (29.71)	
Log-likelihood at zero			−60529.77				−60529.77	
Log-likelihood at convergence	−49584.82		−49451.9				−48868.27	
McFadden pseudo R^2	0.069		0.183				0.193	
BIC							98032	

Halton draw of 200 was used for the RPL model [4]. The random parameters found in the RPL model (indicated by rp superscripts) were assumed to be normally distributed [see [5]] and had statistically significant standard deviations at 0.05 significance levels.

Table 3: Marginal effects of the variables on probabilities of the severity outcomes (%).

	Driver error	DUI	Speed	Distracted	Fatigue	Invalid license	No seatbelt	Female	Black	Young	Old	Unemployed
Serious injury	−13.18%	−1.50%	−1.28%	−0.88%	0.05%	0.32%	1.89%	−4.93%	−1.73%	−1.99%	0.73%	4.19%
Minor injury	3.80%	0.94%	0.78%	0.37%	−0.03%	−0.18%	−1.73%	1.95%	0.69%	1.17%	−0.35%	−2.24%

resp.) suggests a stronger support for the LC logit model over the MNL and RPL models. Similar conclusions have been reported by other researchers [e.g., see [75, 81, 87, 88]]. An attempt was made to develop LC random parameters logit model for this study. However, none of the random parameters had statistically significant standard deviations. There was also no significant improvement in model fit statistics when compared with the LC logit model.

7. Conclusion

In this paper, latent class logit and random parameters models were developed as alternatives to the traditional multinomial logit model for human-centered crash injury severity analysis to account for unobserved heterogeneity. The study was based on 2011–2015 injury-related crash data, for the State of Alabama, and considered only crashes that had human-centered primary causal factors. Two crash injury outcomes were examined: serious injury (fatal and incapacitating injury) and minor injury (non-incapacitating and possible injuries). Twelve variables were used to build the models.

Comparison of fit statistics shows that the two-class latent class logit model outperformed the random parameters model, as an alternative to the traditional MNL model. This result is generally in line with past studies in this area. An attempt was made to identify random parameters for the LC logit model. However, none of the random parameters had statistically significant standard deviations. There was also no significant improvement in model fit statistics when compared with the LC logit model.

Both the RPL and LC models showed that six specific driving behaviors significantly contributed to the occurrence of serious crashes, driver error, speeding, DUI, distracted driving, fatigue driving, and not wearing a seatbelt. These conclusions suggest that targeted outreach and education campaigns designed to address these specific behaviors (or combinations thereof) could reduce serious crashes [e.g., [1, 7, 18, 23, 24]]. The analyses also showed that focusing education efforts on specific driver types (i.e., demographic groups) may also be effective in reducing serious crashes in Alabama. And finally, some of the behaviors may be positively impacted with increased or enhanced enforcement [e.g., [1, 14, 89]].

Human-centered (i.e., driving behavioral related) inferences from the current study are limited to the driving population of the State of Alabama. Nonetheless, there are general observations and conclusions documented herein that expand the understanding of the relationship between drivers and the severity outcomes of crashes.

Conflicts of Interest

The authors declare that there are no conflicts of interest regarding the publication of this paper.

Acknowledgments

The authors would like to acknowledge the Southeastern Transportation Center and the Alabama Transportation Institute for support of this research.

References

[1] J. Elander, R. West, and D. French, "Behavioral correlates of individual differences in road-traffic crash risk: an examination of methods and findings," *Psychological Bulletin*, vol. 113, no. 2, pp. 279–294, 1993.

[2] J. R. Treat, N. S. Tumbas, S. T. McDonald et al., "Tri-level study of the causes of traffic accidents: final report, vol. 1: causal factor tabulations and assessments," DOT HS-805 085, Indiana University: Institute for Research in Public Safety, Bloomington, Ind, USA, 1979.

[3] D. L. Hendricks, J. C. Fell, and M. Freedman, "The relative frequency of unsafe driving acts in serious traffic crashes," DTNH22-94-C-05020, NHTSA, Washington, DC, USA, 1999.

[4] C. R. Bhat, "Simulation estimation of mixed discrete choice models using randomized and scrambled Halton sequences," *Transportation Research Part B: Methodological*, vol. 37, no. 9, pp. 837–855, 2003.

[5] J. C. Milton, V. N. Shankar, and F. L. Mannering, "Highway accident severities and the mixed logit model: an exploratory empirical analysis," *Accident Analysis & Prevention*, vol. 40, no. 1, pp. 260–266, 2008.

[6] W. A. Tillmann and G. E. Hobbs, "The accident-prone automobile driver: a study of the psychiatric and social background," *The American Journal of Psychiatry*, vol. 106, no. 5, pp. 321–331, 1949.

[7] J. E. Donovan, "Young adult drinking-driving: behavioral and psychosocial correlates," *Journal of Studies on Alcohol*, vol. 54, no. 5, pp. 600–613, 1993.

[8] J. Yu and W. R. Williford, "Alcohol and risk/sensation seeking: specifying a causal model on high-risk driving," *Journal of Addictive Diseases*, vol. 12, no. 1, pp. 79–96, 1993.

[9] National Highway Traffic Safety Administration, Race and ethnicity in fatal motor vehicle traffic crashes 1999–2004, 2016, https://crashstats.nhtsa.dot.gov/Api/Public/ViewPublication/809956.

[10] E. Gaygisiz, "Cultural values and governance quality as correlates of road traffic fatalities: a nation level analysis," *Accident Analysis & Prevention*, vol. 42, no. 6, pp. 1894–1901, 2010.

[11] P. Stanojević, D. Jovanović, and T. Lajunen, "Influence of traffic enforcement on the attitudes and behavior of drivers," *Accident Analysis & Prevention*, vol. 52, pp. 29–38, 2013.

[12] American Automobile Association, "2015 traffic safety culture index," Tech. Rep., AAA Foundation for Traffic Safety, Washington, DC, USA, 2016.

[13] P. Atchley, J. Shi, and T. Yamamoto, "Cultural foundations of safety culture: a comparison of traffic safety culture in China, Japan and the United States," *Transportation Research Part F: Traffic Psychology and Behaviour*, vol. 26, pp. 317–325, 2014.

[14] C. Schlembach, G. Furian, and C. Brandstätter, "Traffic (safety) culture and alcohol use: cultural patterns in the light of results of the SARTRE 4 study," *European Transport Research Review*, vol. 8, no. 1, article 7, pp. 1–12, 2016.

[15] C. Albrecht, W. Li, and K. Gkritza, "Improving traffic safety culture in Iowa—phase II," Tech. Rep. 11-398, Center for Transportation Research and Education, Iowa State University, Ames, Iowa, USA, 2013.

[16] E. K. Adanu, R. Smith, L. Powell, and S. Jones, "Multilevel analysis of the role of human factors in regional disparities in crash outcomes," *Accident Analysis & Prevention*, vol. 109, pp. 10–17, 2017.

[17] I. O. Lund and T. Rundmo, "Cross-cultural comparisons of traffic safety, risk perception, attitudes and behaviour," *Safety Science*, vol. 47, no. 4, pp. 547–553, 2009.

[18] E. Petridou and M. Moustaki, "Human factors in the causation of road traffic crashes," *European Journal of Epidemiology*, vol. 16, no. 9, pp. 819–826, 2000.

[19] G. McGwin Jr. and D. B. Brown, "Characteristics of traffic crashes among young, middle-aged, and older drivers," *Accident Analysis & Prevention*, vol. 31, no. 3, pp. 181–198, 1999.

[20] M. Møller and S. Haustein, "Peer influence on speeding behaviour among male drivers aged 18 and 28," *Accident Analysis & Prevention*, vol. 64, pp. 92–99, 2014.

[21] J. Shi, Y. Bai, X. Ying, and P. Atchley, "Aberrant driving behaviors: a study of drivers in Beijing," *Accident Analysis & Prevention*, vol. 42, no. 4, pp. 1031–1040, 2010.

[22] D. Stavrinos, J. L. Jones, A. A. Garner et al., "Impact of distracted driving on safety and traffic flow," *Accident Analysis & Prevention*, vol. 61, pp. 63–70, 2013.

[23] J. A. Groeger, "Youthfulness, inexperience, and sleep loss: the problems young drivers face and those they pose for us," *Injury Prevention*, vol. 12, supplement 1, pp. i19–i24, 2006.

[24] P. Gulliver and D. Begg, "Personality factors as predictors of persistent risky driving behavior and crash involvement among young adults," *Injury Prevention*, vol. 13, no. 6, pp. 376–381, 2007.

[25] S. Blows, R. Q. Ivers, J. Connor, S. Ameratunga, M. Woodward, and R. Norton, "Unlicensed drivers and car crash injury," *Traffic Injury Prevention*, vol. 6, no. 3, pp. 230–234, 2005.

[26] National Highway Traffic Safety Administration, "Traffic safety facts: 2014 data—occupant protection," DOT HS 812 262, National Highway Traffic Safety Administration, Washington, DC, USA, 2016, https://crashstats.nhtsa.dot.gov/Api/Public/ViewPublication/812262.

[27] National Highway Traffic Safety Administration, Traffic Safety Facts: Speeding, 2017, https://crashstats.nhtsa.dot.gov/Api/Public/ViewPublication/812021.

[28] S. G. Klauer, J. Sudweeks, J. S. Hickman, and V. L. Neale, "How risky is it? An assessment of the relative risk of engaging in potentially unsafe driving behaviors," Tech. Rep., AAA Foundation for Traffic Safety, Washington, DC, USA, 2006, https://www.aaafoundation.org/sites/default/files/RiskyDrivingReport.pdf.

[29] National Highway Traffic Safety Administration, "Traffic safety facts: alcohol-impaired driving," Traffic Safety Administration, National Highway Traffic Safety Administration, Washington, DC, USA, 2015, https://crashstats.nhtsa.dot.gov/Api/Public/ViewPublication/812231.

[30] National Center for Statistics and Analysis, "Distracted driving: 2013 data, in traffic safety research notes," DOT HS 812 132, National Highway Traffic Safety Administration, Washington, DC, USA, 2015.

[31] K. W. Ogden, *Safer Roads: A Guide to Road Safety Engineering*, Ashgate Publishing Ltd, Melbourne, Australia, 1996.

[32] R. O. Mujalli and J. De Ona, "Injury severity models for motor vehicle accidents: a review," *Proceedings of the Institution of Civil Engineers: Transport*, vol. 166, no. 5, pp. 255–270, 2013.

[33] V. Shankar and F. Mannering, "An exploratory multinomial logit analysis of single-vehicle motorcycle accident severity," *Journal of Safety Research*, vol. 27, no. 3, pp. 183–194, 1996.

[34] K. Haleem and M. Abdel-Aty, "Examining traffic crash injury severity at unsignalized intersections," *Journal of Safety Research*, vol. 41, no. 4, pp. 347–357, 2010.

[35] S. Daniels, T. Brijs, E. Nuyts, and G. Wets, "Externality of risk and crash severity at roundabouts," *Accident Analysis & Prevention*, vol. 42, no. 6, pp. 1966–1973, 2010.

[36] S. Dissanayake, "Comparison of severity affecting factors between young and older drivers involved in single vehicle crashes," *IATSS Research*, vol. 28, no. 2, pp. 48–54, 2004.

[37] P. Savolainen and F. Mannering, "Probabilistic models of motorcyclists' injury severities in single- and multi-vehicle crashes," *Accident Analysis & Prevention*, vol. 39, no. 5, pp. 955–963, 2007.

[38] C. Peek-Asa, C. Britton, T. Young, M. Pawlovich, and S. Falb, "Teenage driver crash incidence and factors influencing crash injury by rurality," *Journal of Safety Research*, vol. 41, no. 6, pp. 487–492, 2010.

[39] D. W. Kononen, C. A. C. Flannagan, and S. C. Wang, "Identification and validation of a logistic regression model for predicting serious injuries associated with motor vehicle crashes," *Accident Analysis & Prevention*, vol. 43, no. 1, pp. 112–122, 2011.

[40] X. Xu, S. Xie, S. C. Wong, P. Xu, H. Huang, and X. Pei, "Severity of pedestrian injuries due to traffic crashes at signalized intersections in Hong Kong: a Bayesian spatial logit model," *Journal of Advanced Transportation*, vol. 50, no. 8, pp. 2015–2028, 2016.

[41] H. T. Abdelwahab and M. A. Abdel-Aty, "Development of artificial neural network models to predict driver injury severity in traffic accidents at signalized intersections," *Transportation Research Record*, vol. 1746, pp. 6–13, 2001.

[42] A. J. Khattak and M. Rocha, "Are SUVs 'Supremely Unsafe Vehicles'? analysis of rollovers and injuries with sport utility vehicles," *Transportation Research Record*, vol. 1840, pp. 167–177, 2003.

[43] S. Jung, X. Qin, and D. A. Noyce, "Rainfall effect on single-vehicle crash severities using polychotomous response models," *Accident Analysis & Prevention*, vol. 42, no. 1, pp. 213–224, 2010.

[44] M. A. Quddus, C. Wang, and S. G. Ison, "Road traffic congestion and crash severity: econometric analysis using ordered response models," *Journal of Transportation Engineering*, vol. 136, no. 5, pp. 424–435, 2010.

[45] N. V. Malyshkina and F. L. Mannering, "Markov switching multinomial logit model: An application to accident-injury severities," *Accident Analysis & Prevention*, vol. 41, no. 4, pp. 829–838, 2009.

[46] W. H. Schneider, P. T. Savolainen, and K. Zimmerman, "Driver injury severity resulting from single-vehicle crashes along horizontal curves on rural two-lane highways," *Transportation Research Record*, no. 2102, pp. 85–92, 2009.

[47] A. Morgan and F. L. Mannering, "The effects of road-surface conditions, age, and gender on driver-injury severities," *Accident Analysis & Prevention*, vol. 43, no. 5, pp. 1852–1863, 2011.

[48] K. E. Train, *Discrete Choice Methods with Simulation*, Cambridge University Press, New York, NY, USA, 2009.

[49] Y. Xie, Y. Zhang, and F. Liang, "Crash injury severity analysis using Bayesian ordered probit models," *Journal of Transportation Engineering*, vol. 135, no. 1, pp. 18–25, 2009.

[50] Z. Wang, H. Chen, and J. J. Lu, "Exploring impacts of factors contributing to injury severity at freeway diverge areas," *Transportation Research Record*, no. 2102, pp. 43–52, 2009.

[51] X. Zhu and S. Srinivasan, "A comprehensive analysis of factors influencing the injury severity of large-truck crashes," *Accident Analysis & Prevention*, vol. 43, no. 1, pp. 49–57, 2011.

[52] A. J. Khattak, M. D. Pawlovich, R. R. Souleyrette, and S. L. Hallmark, "Factors related to more severe older driver traffic crash injuries," *Journal of Transportation Engineering*, vol. 128, no. 3, pp. 243–249, 2002.

[53] M. Abdel-Aty and J. Keller, "Exploring the overall and specific crash severity levels at signalized intersections," *Accident Analysis & Prevention*, vol. 37, no. 3, pp. 417–425, 2005.

[54] F. M. Council and J. R. Stewart, "Severity indexes for roadside objects," *Transportation Research Record*, no. 1528, pp. 87–96, 1996.

[55] L.-Y. Chang and H.-W. Wang, "Analysis of traffic injury severity: an application of non-parametric classification tree techniques," *Accident Analysis & Prevention*, vol. 38, no. 5, pp. 1019–1027, 2006.

[56] W.-H. Chen and P. P. Jovanis, "Method for identifying factors contributing to driver-injury severity in traffic crashes," *Transportation Research Record*, vol. 1717, pp. 1–9, 2000.

[57] M. Simoncic, "A Bayesian network model of two-car accidents," *Journal of Transportation and Statistics*, vol. 7, no. 2-3, pp. 13–25, 2005.

[58] J. De Oña, R. O. Mujalli, and F. J. Calvo, "Analysis of traffic accident injury severity on Spanish rural highways using Bayesian networks," *Accident Analysis & Prevention*, vol. 43, no. 1, pp. 402–411, 2011.

[59] M. Abdel-Aty and H. Abdelwahab, "Modeling rear-end collisions including the role of driver's visibility and light truck vehicles using a nested logit structure," *Accident Analysis & Prevention*, vol. 36, no. 3, pp. 447–456, 2004.

[60] D. Delen, R. Sharda, and M. Bessonov, "Identifying significant predictors of injury severity in traffic accidents using a series of artificial neural networks," *Accident Analysis & Prevention*, vol. 38, no. 3, pp. 434–444, 2006.

[61] A. Das and M. Abdel-Aty, "A genetic programming approach to explore the crash severity on multi-lane roads," *Accident Analysis & Prevention*, vol. 42, no. 2, pp. 548–557, 2010.

[62] Y. Xiong and F. L. Mannering, "The heterogeneous effects of guardian supervision on adolescent driver-injury severities: a finite-mixture random-parameters approach," *Transportation Research Part B: Methodological*, vol. 49, pp. 39–54, 2013.

[63] H.-C. Chu, "Assessing factors causing severe injuries in crashes of high-deck buses in long-distance driving on freeways," *Accident Analysis & Prevention*, vol. 62, pp. 130–136, 2014.

[64] S. Yasmin, N. Eluru, C. R. Bhat, and R. Tay, "A latent segmentation based generalized ordered logit model to examine factors influencing driver injury severity," *Analytic Methods in Accident Research*, vol. 1, pp. 23–38, 2014.

[65] P. T. Savolainen, F. L. Mannering, D. Lord, and M. A. Quddus, "The statistical analysis of highway crash-injury severities: a review and assessment of methodological alternatives," *Accident Analysis & Prevention*, vol. 43, no. 5, pp. 1666–1676, 2011.

[66] M. S. Shaheed and K. Gkritza, "A latent class analysis of single-vehicle motorcycle crash severity outcomes," *Analytic Methods in Accident Research*, vol. 2, pp. 30–38, 2014.

[67] F. L. Mannering, V. Shankar, and C. R. Bhat, "Unobserved heterogeneity and the statistical analysis of highway accident data," *Analytic Methods in Accident Research*, vol. 11, pp. 1–16, 2016.

[68] G. F. Ulfarsson and F. L. Mannering, "Differences in male and female injury severities in sport-utility vehicle, minivan, pickup and passenger car accidents," *Accident Analysis & Prevention*, vol. 36, no. 2, pp. 135–147, 2004.

[69] M. Islam and S. Hernandez, "Large truck-involved crashes: Exploratory injury severity analysis," *Journal of Transportation Engineering*, vol. 139, no. 6, pp. 596–604, 2013.

[70] S. P. Washington, M. G. Karlaftis, and F. L. Mannering, *Statistical and Econometric Methods for Transportation Data Analysis*, CRC Press, Boca Raton, Fla, USA, 2nd edition, 2011.

[71] N. V. Malyshkina and F. Mannering, "Effect of increases in speed limits on severities of injuries in accidents," *Transportation Research Record*, no. 2083, pp. 122–127, 2008.

[72] S. Jones, S. Gurupackiam, and J. Walsh, "Factors influencing the severity of crashes caused by motorcyclists: analysis of data from Alabama," *Journal of Transportation Engineering*, vol. 139, no. 9, pp. 949–956, 2013.

[73] A. Behnood and F. L. Mannering, "The temporal stability of factors affecting driver-injury severities in single-vehicle crashes: some empirical evidence," *Analytic Methods in Accident Research*, vol. 8, pp. 7–32, 2015.

[74] D. McFadden and K. Train, "Mixed MNL models for discrete response," *Journal of Applied Econometrics*, vol. 15, no. 5, pp. 447–470, 2000.

[75] W. H. Greene and D. A. Hensher, "A latent class model for discrete choice analysis: contrasts with mixed logit," *Transportation Research Part B: Methodological*, vol. 37, no. 8, pp. 681–698, 2003.

[76] F. L. Mannering and C. R. Bhat, "Analytic methods in accident research: methodological frontier and future directions," *Analytic Methods in Accident Research*, vol. 1, pp. 1–22, 2014.

[77] A. Behnood, A. M. Roshandeh, and F. L. Mannering, "Latent class analysis of the effects of age, gender, and alcohol consumption on driver-injury severities," *Analytic Methods in Accident Research*, vol. 3-4, pp. 56–91, 2014.

[78] W. H. Greene and D. A. Hensher, "Revealing additional dimensions of preference heterogeneity in a latent class mixed multinomial logit model," *Applied Economics*, vol. 45, no. 14, pp. 1897–1902, 2013.

[79] A. Bujosa, A. Riera, and R. L. Hicks, "Combining discrete and continuous representations of preference heterogeneity: a latent class approach," *Environmental and Resource Economics*, vol. 47, no. 4, pp. 477–493, 2010.

[80] W. H. Greene, *NLOGIT Version 4.0 Reference Guide*, Econometric Software, Inc, Plainview, NY, USA, 2007.

[81] Y. Xie, K. Zhao, and N. Huynh, "Analysis of driver injury severity in rural single-vehicle crashes," *Accident Analysis & Prevention*, vol. 47, pp. 36–44, 2012.

[82] N. Eluru, M. Bagheri, L. F. Miranda-Moreno, and L. Fu, "A latent class modeling approach for identifying vehicle driver injury severity factors at highway-railway crossings," *Accident Analysis & Prevention*, vol. 47, pp. 119–127, 2012.

[83] P. C. Boxall and W. L. Adamowicz, "Understanding heterogeneous preferences in random utility models: a latent class approach," *Environmental and Resource Economics*, vol. 23, no. 4, pp. 421–446, 2002.

[84] K. Roeder, K. G. Lynch, and D. S. Nagin, "Modeling uncertainty in latent class membership: a case study in criminology," *Journal of the American Statistical Association*, vol. 94, no. 447, pp. 766–776, 1999.

[85] N. Dean and A. E. Raftery, "Latent class analysis variable selection," *Annals of the Institute of Statistical Mathematics*, vol. 62, no. 1, pp. 11–35, 2010.

[86] K. L. Nylund, T. Asparouhov, and B. O. Muthén, "Deciding on the number of classes in latent class analysis and growth mixture modeling: a Monte Carlo simulation study," *Structural Equation Modeling: A Multidisciplinary Journal*, vol. 14, no. 4, pp. 535–569, 2007.

[87] J. Shen, "Latent class model or mixed logit model? a comparison by transport mode choice data," *Applied Economics*, vol. 41, no. 22, pp. 2915–2924, 2009.

[88] C.-H. Wen, W.-C. Wang, and C. Fu, "Latent class nested logit model for analyzing high-speed rail access mode choice," *Transportation Research Part E: Logistics and Transportation Review*, vol. 48, no. 2, pp. 545–554, 2012.

[89] J. K. Simandl, A. J. Graettinger, R. K. Smith, S. Jones, and T. E. Barnett, "Making use of big data to evaluate the effectiveness of selective law enforcement in reducing crashes," *Transportation Research Record*, vol. 2584, pp. 8–15, 2016.

Hindawi
Journal of Advanced Transportation
Volume 2017, Article ID 8376572, 9 pages
https://doi.org/10.1155/2017/8376572

Research Article

A Novel Surrogate Safety Indicator Based on Constant Initial Acceleration and Reaction Time Assumption

Adrian Fazekas, Friederike Hennecke, Eszter Kalló, and Markus Oeser

Institute of Highway Engineering, RWTH Aachen University, Aachen, Germany

Correspondence should be addressed to Adrian Fazekas; fazekas@isac.rwth-aachen.de

Received 2 June 2017; Revised 25 October 2017; Accepted 1 November 2017; Published 13 December 2017

Academic Editor: David F. Llorca

The development of surrogate safety measures has drawn significant research interest in the field of traffic safety analysis. Innovative data sources such as video-based traffic surveillance systems have made it possible to collect large amounts of microscopic traffic data. By deriving traffic safety indicators such as the Deceleration Rate to Avoid a Crash (DRAC) statements concerning traffic safety over a determined road section can be made. This work presents the derivation of a novel surrogate safety indicator based on a Constant Initial Acceleration and reaction time assumption which considers the interaction between vehicles and describes the traffic safety of a road section. The evaluation is based on a video-based microscopic traffic data collection. To examine the efficiency, the new developed indicator is compared to the original Deceleration Rate to Avoid a Crash (DRAC) and the modified indicator (MDRAC) which includes the reaction time. The results showed that the new indicator is more sensitive in detecting critical situations than the other indicators and in addition describes the conflict situations more realistically.

1. Introduction

As advances in vehicle technologies lead to a continuous reduction of accident counts in traffic, applications of traffic conflict technologies have received increasing attention in the field of traffic safety research. Amundsen [1] defines a traffic conflict as "an observable situation in which two or more road users approach each other in space and time for such an extent that there is a risk of collision if their movement remain unchanged."

A detailed analysis of traffic conflicts can give us a better insight into crash occurrence and thus leads to more efficient traffic safety measures. With the use of conflict indicators, such as the Deceleration Rate to Avoid a Crash, the relevant conflict situations can be identified.

Many of the indicators covered by existing research publications assume an unchanged speed and direction of the conflicting vehicles [2]. This however insufficiently describes the complex reciprocal behavior of the individual vehicles. Furthermore, many of these indicators have boundary conditions on speed. Because of this, car interactions are considered to be safe as long as the following vehicle has a lower speed compared to the leader although the two vehicles might have high speeds and small gaps between each other [3]. Moreover, the reaction time of the road users is often neglected [4].

In this paper, a modified indicator for conflict situations is presented by considering a reasonable reaction time and a more realistic acceleration behavior in the analytical description. The modified indicator is derived and compared with existing indicators based on a data-set of microscopic traffic data collected by computer-vision-based technologies. Furthermore, a discussion of the results is conducted to analyze the benefits of the modified indicator and also further possible developments are presented.

2. Literature Review

Critical safety road sections mostly have an inhomogeneous traffic flow characterized by large speed differences leading to an increase in the number and severity of acceleration and deceleration phases [5, 6]. A homogenization of the traffic flow can positively increase the safety level on such road sections.

The Deceleration Rate to Avoid a Crash (DRAC) is a suitable method to identify critical road sections, as it covers

the varying speeds of individual vehicles and derives suitable deceleration phases for the following vehicle [7–9].

DRAC is defined as the minimum required deceleration rate which a vehicle has to apply to avoid a crash with the leading vehicle.

One important factor in the analysis of traffic safety is the minimum time required for the drivers to react to certain situations, also called Perception Reaction Time (PRT).

Kuang et al. [4] argue that the initial determination of DRAC does not consider the PRT of the following vehicle. They modify this specific safety indicator by implementing a factor including PRT. They reach the conclusion that the Modified DRAC (MDRAC) improves crash prediction performance. Wang and Stamatiadis [10–12] have successfully considered the PRT in a number of their studies when evaluating road safety at intersections.

Besides the area of surrogate safety analysis the PRT has been also the focus of other research fields including the planning of roads [13], the associated traffic light systems, and their switching times [14, 15].

Even back in 1936, Greenshields [16] conducted a study on the determination of the probability distribution of reaction time. Reaction times are normally approximated with lognormal probability distribution with the parameters μ and σ^2 [17, 18]. In an extended study survey, Green [19] noticed that due to the numerous influencing factors the determination of a uniform reaction time is very difficult.

Another argument often found across publications is the fact that the DRAC is only considering identical movement direction of the conflicting vehicles. Therefore, Wang and Stamatiadis [10] derived the MDRAC for typical crossing and lane-change conflicts.

In order to reach a conclusion about whether a situation is critical or not, the DRAC or the MDRAC has to be compared with a threshold value [20, 21]. If the identified DRAC or MDRAC is higher than the given threshold the situation is derived to be critical.

3. Analytical Methods

DRAC is defined as the minimum required deceleration rate of the following vehicle to avoid a crash with the leading vehicle. The assumption in the original form of the indicator is that the speed of the leading vehicle remains constant. Mathematically, the DRAC is the squared speed difference between the following V_2 and the leading vehicle V_1 divided by their (net) distance gap D_{1-2} [10, 22–24].

$$\mathrm{DRAC} = \begin{cases} \dfrac{(V_2 - V_1)^2}{2D_{1-2}}, & \text{if } V_2 > V_1 \\ 0, & \text{otherwise.} \end{cases} \quad (1)$$

Kuang et al. [4] add the reaction time of the vehicle following the DRAC obtaining the Modified DRAC (MDRAC). This parameter is calculated as follows:

$$\mathrm{MDRAC} = \begin{cases} \dfrac{V_2 - V_1}{2\,(\mathrm{TTC} - R)}, & \text{if } \mathrm{TTC} > R \\ \infty, & \text{otherwise.} \end{cases} \quad \forall V_2 > V_1 \quad (2)$$

In (2) R denotes the PRT and TTC represents the time-to-collision value at an initial time ($t = 0$). TTC is defined as the time remaining until a collision between two vehicles occurs [25] assuming a linear trajectory based on the last known speed value:

$$\mathrm{TTC} = \begin{cases} \dfrac{D_{1-2}}{V_2 - V_1}, & \text{if } V_2 > V_1 \\ \infty, & \text{otherwise.} \end{cases} \quad (3)$$

Besides the TTC, the reaction time R in (2) has a significant influence on the resulting values. Thus, it is sensible to conduct more thorough investigation on this parameter. Green [19] worked on the determination of the reaction time and came to the conclusion that the shortest reaction time is between 0.7 and 0.75 seconds. For the reaction on unexpected but usual signals, such as the activation of the brake lights, approximately 1.25 seconds are necessary. For unexpected events the reaction time is approximately 1.5 seconds. Morita et al. [26] determined throughout their experiments that the reaction time of the following driver lies between 1.3 and 1.6 seconds when the leading vehicle starts breaking and activates the brake lights. Zhang et al. [27] estimate the reaction time on unexpected incidents with visual indications to 1.13 seconds with a standard deviation of 0.52 seconds and on those without visual indications to 1.25 seconds with a standard deviation of 0.60 seconds. For a 90% percentile the value would be 1.8 or 2.02 seconds. Therefore, two reaction times have been considered for this study. Reaction time values of 1.3 and 2.02 seconds were used for unexpected incidents with and without visual indications, respectively.

As described in the introductory chapters, Mahmud et al. [28] pointed out the fact that the calculation of the DRAC is based on the hypothetical assumption that the speed of the leading vehicle is constant. Furthermore, the trajectory of the second vehicle is also assumed to rely on a constant speed until the time of the reaction. These assumptions or omissions do not adequately cover the complexity of the real driving situation as thorough investigations carried out by Wiedemann [29] have shown that naturalistic driving behavior consists of continuous change of acceleration and speed. This leads to a periodical change in distance between vehicles and also indicates that the driving speed will seldom be constant.

Due to the fact that the DRAC and the MDRAC do not realistically represent the driving behavior by using a constant speed during the time periods in which vehicles are not reacting, the derived values tend to show a lower level of risk. Thus, the only assumption regarding the speed of the vehicles is that they do not change their acceleration or deceleration unless reacting to a new situation. Assumptions on the leading or following vehicle's hypothetical actions are not considered.

By combining the reaction time described above with the more realistic assumption on the acceleration behavior, this work presents a novel indicator for describing risk called Deceleration Rate to Avoid a Crash using Constant Initial Acceleration (DCIA). The detailed derivation of this indicator will be subsequently presented.

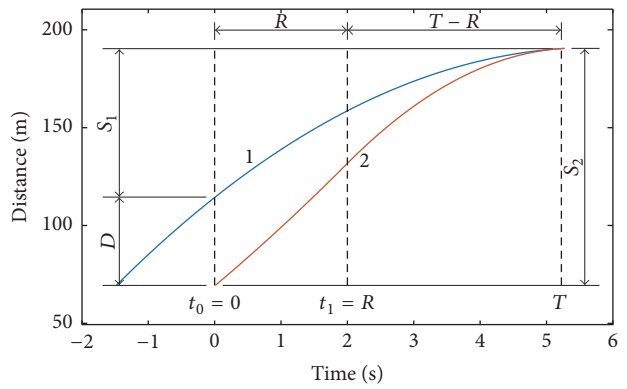

Figure 1: Distance-time diagram of the conflict situation. The trajectories of the leading and following vehicle are labeled with the numbers 1 and 2, respectively. The considered time period for the indicator starts at the initial time $t_0 = 0$ with a reaction of the following vehicle at time $t_1 = R$.

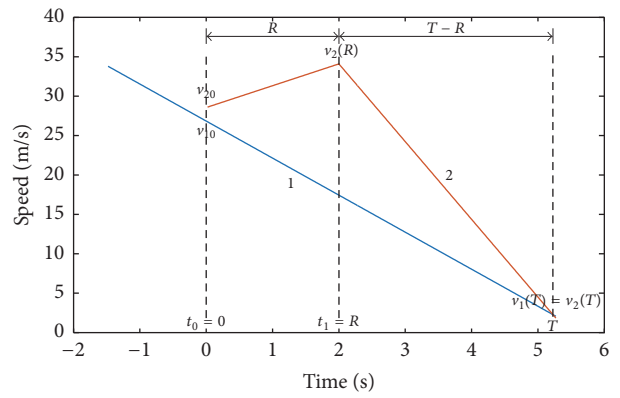

Figure 2: Speed-time profile for the conflict situation. The profiles are numbered with 1 and 2 for the leading and following vehicles, respectively, while v_{10} and v_{20} are the corresponding initial speeds.

Figure 1 illustrates the distance-time diagram of the considered situation. As shown in the diagram, the following vehicle keeps a constant acceleration until it reacts on the deceleration of the leading vehicle. From this moment the following vehicle will start decelerating with the DCIA value in a way that the net distance between the vehicles at time T is infinitely small and their speeds are equal. This means that the DCIA is the minimal deceleration of the following vehicle so that a collision is avoided.

The mathematical derivation of the DCIA is based on the logic that the distance S_2 traveled by the following vehicle is equal to the sum of distances S_1 of the leading one at the moment T with the net distance gap D at time t_0.

$$S_1(T) + D = S_2(T). \tag{4}$$

During an arbitrary time t the leading vehicle travels the distance S_1:

$$S_1(t) = v_{10}t + \frac{d_{10}t^2}{2}, \tag{5}$$

where v_{10} is the speed and d_{10} is the acceleration of vehicle 1 at time t_0.

The distance, which has been covered by vehicle 2 in the period t after the reaction time R, is composed of the distance traveled during the reaction time R and the distance traveled in the time period $t - R$.

$$S_2(t) = v_{20}R + \frac{d_{20}R^2}{2} + v_2(t-R) + \frac{\mathrm{DCIA}(t-R)^2}{2}, \tag{6}$$

where v_{20} is the speed and d_{20} the acceleration at time t_0, v_2 is the speed after the reaction time, and d_2 is the necessary deceleration rate to prevent a collision or to be able to drive at an infinitely small distance behind the leading vehicle at its speed.

The DCIA can be determined by substituting (5) and (6) into (4). The required deceleration to avoid an accident is thus calculated according to the following formula:

$$\mathrm{DCIA} = \frac{2\left(v_{10}T + d_{10}T^2/2 + D - v_{20}R - d_{20}R^2/2 - v_2(T-R)\right)}{(T-R)^2}. \tag{7}$$

In addition to the deceleration rate, the time T is another unknown parameter in this equation. The following contexts are known for the determination of T.

The speed of vehicle 1 at an arbitrary time t is

$$v_1(t) = d_{10}t + v_{10}. \tag{8}$$

The speed of vehicle 2 at the time $t_1 = R$ is

$$v_2(R) = d_{20}R + v_{20}. \tag{9}$$

The speed of vehicle 2 at the time t after reacting is

$$v_2(t) = d_2(t-R) + v_2(t). \tag{10}$$

According to the definition of the DRAC, the following vehicle should be delayed in such a way that the two vehicles must travel at the same speed at an infinitely small distance one after another, so that $v_1(T) = v_2(T)$ must apply (see Figure 2).

Therefore,

$$d_{10}T + v_{10} = \mathrm{DCIA}(T-R) + d_{20}R + v_{20}. \tag{11}$$

Transformed according to DCIA, the following equation is obtained (see Figure 3):

$$\mathrm{DCIA} = \frac{d_{10}T + v_{10} - d_{20}R - v_{20}}{T-R}. \tag{12}$$

T results from (7) and (12):

$$T = \frac{v_{20}R - v_{10}R - 2D}{v_{10} - d_{10}R - v_{20} + d_{20}R}. \tag{13}$$

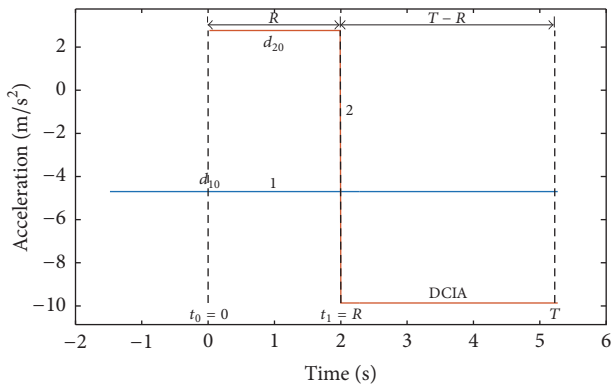

FIGURE 3: Acceleration-time profile for the conflict situation. The profiles are numbered with 1 and 2 for the leading and following vehicles, respectively, while d_{10} and d_{20} are the corresponding initial acceleration.

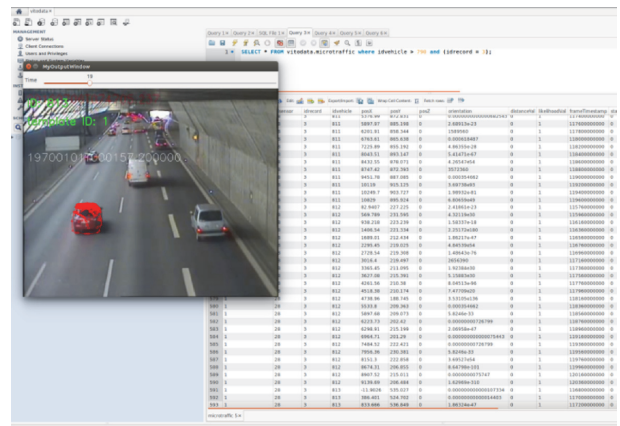

FIGURE 4: Manual position estimation tool GUI. A specific point cloud is moved on the street surface to best fit a vehicle position. The chosen position is then written into a database for further analysis.

In contrast to DRAC and MDRAC, DCIA is also suitable for scenarios where the speed of the following vehicle is lower than that of the leading vehicle. Because the DCIA does not assume constant speed profiles but rather a constant acceleration, it is able to identify risky interactions where the following vehicle has a lower speed but a much higher acceleration than the leading vehicle and in combination with a small headway it would come to a crash.

According to AASHTO [20], a traffic situation is considered critical when the DRAC exceeds 3.4 m/s^2. Archer [30] proposes a threshold for critical situation of 3.35 m/s^2. Guido et al. [7] have also chosen a threshold of 3.35 m/s^2 in their study on the traffic safety of a roundabout.

For the evaluation of the DCIA a value less than or equal to 0 means that a collision is prevented without intervention by the following vehicle. A negative value shows the minimum deceleration rate required to avoid a collision by adjusting the speed. In accordance with the studies referenced above a deceleration value greater than 3.4 m/s^2 was chosen as a threshold to indicate a critical situation.

4. Field Data

In order to evaluate the methods described above, the conflict indicators are derived from microscopic traffic data. These were extracted from videos recorded within the research project ESIMAS [31] from surveillance cameras in an enclosure tunnel on the German motorway A3, which has 3 lanes. The surveillance cameras are located above the lanes towards Frankfurt also covering an exit lane. The considered section is subject to a speed limit of 100 km/h.

The video material used for evaluation was recorded from 7:35 a.m. until 7:55 a.m. in summer time with good lighting conditions. It includes traffic jams due to the rush hour traffic.

The derivation of the microscopic traffic data has been performed with software being developed at the Institute of Highway Engineering (RWTH Aachen University) within the research project AUTUKAR regarding automatic video analysis in tunnel surveillance systems (Figure 4). The analysis methods consist of a 3D model based vehicle detection, classification, and tracking of individual vehicles [32]. The 3D models are point clouds of different vehicle types which are being used to match image features of the real vehicles present in the video. The projection of the point clouds into the two-dimensional image is performed by first assessing the intrinsic and extrinsic parameters of the camera matrix. The assumptions used are that the street is planar and the projection of the vehicle point clouds can only be performed onto this plane. For each vehicle point cloud, an anchor point is computed as the mean point of the outer contour after projecting the point cloud onto the bottom plane. The vehicle positions are determined manually with a graphical user interface by selecting the optimal position of the anchor on the street surface so that the point cloud best matches the image of the vehicle on the street. An automatic analysis is also possible where an image processing based likelihood function finds the position with the best match. While the automatic assessment delivers a higher amount of data, occlusion may lead to false tracking and position estimation. As the main focus of this work is the safety assessment rather than automatic position estimation manual evaluation was used. This gives the best humanly possible accuracy in the position estimation, so that a better analysis of the safety indicator effect can be performed. This manual tagging is also used as proof for the validation of computer vision techniques throughout different research areas.

The accuracy of the data is mostly dependent on the camera calibration itself. An inaccurate camera calibration would lead to inaccurate transformation of pixel coordinates to street surface coordinates and thus to inaccurate distances between vehicles. To determine the calibration matrix, features of the road surface like the lane boundary markings. Based on these markings, virtual positions on the streets are used for calibration as their relative positions can be calculated. The calibration algorithm optimizes the calibration parameters until the back-projection of the input points shows a high accuracy [33]. Thus accuracy of the position estimation is dependent on the accuracy assumed road marking geometry such as the lane width, lengths of

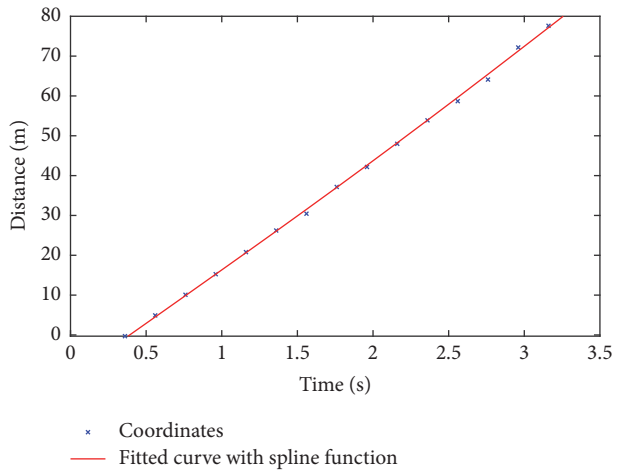

Figure 5: A vehicle trajectory with crosses being originally chosen positions and the line being the fitted smoothing spline, which was used for a new oversampling.

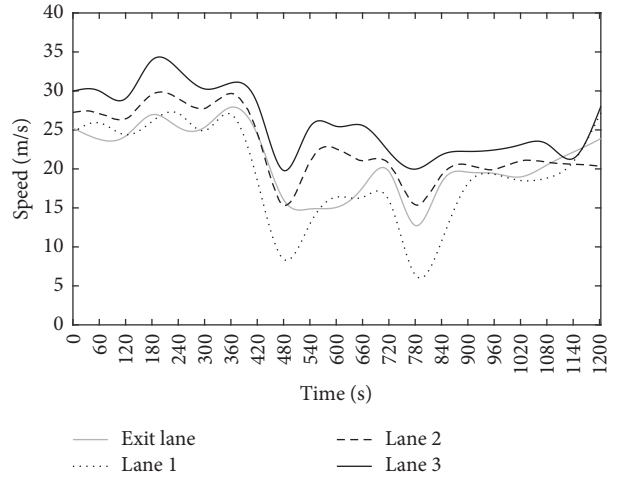

Figure 6: Speed-time diagram for the exit lane and the right, middle, and left lane numbered 1, 2, and 3, respectively, above the considered time interval.

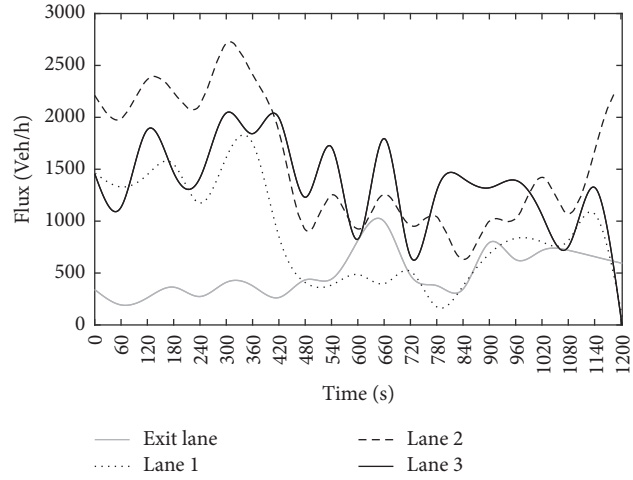

Figure 7: Traffic flux diagram.

the markings, and the gaps between them. Due to the traffic and other safety precautions, another point estimation for t camera calibration is not possible.

The manual position estimation consists of the first step of choosing the right point cloud which fits best to the real vehicle. After specifying the vehicle type, the position is chosen in different frames, and the two-dimensional coordinates on the street surface with the corresponding timestamp are written into a database. It is important to point out that, with the chosen point cloud, the real length and width of the vehicles are known, which are also used in the calculation of the net distances for the safety indicator assessment.

The coordinates of the vehicles have been imported into MATLAB where the trajectories of the vehicles were estimated by fitting a smoothing spline over the sampled coordinates (Figure 5). When the considered section shows a left curvature, the splines were adjusted, respectively. Using the fitted smoothing splines rather than the original sampled positions, a new sampling time of 0.1 s could be used for the estimation of the safety indicator. For the estimation of the traffic parameters, such as speed, the values along the smoothing spline are used so that at each 0.1 s sample the current speed of the vehicle can be estimated.

5. Results and Discussion

In order to be able to conduct a thorough validation and discussion of the derived safety indicator, a general macroscopic analysis of the traffic included in the video data needs to be first undertaken.

1,290 vehicles passed through the 80-meter evaluation section in 20 minutes including 115 lane changes. In addition, 1,174 vehicle pairs were identified, which are characterized by the fact that the two consecutive vehicles on the same lane were both present in the 80-meter section at the same time. For the vehicle positions a sampling period of 0.1 s has been chosen, which has resulted in a total of 16,036 rear-end scenarios. Out of the entire set of rear-end scenarios 5,842 were recorded on lane 2.

Figures 6, 7, and 8 show the speed profile, traffic flux, and traffic density for each of the four lanes over the regarded time period, respectively. The values have been determined by running average over 60 previous seconds. In case of speed the values are also a mean over all vehicles present in the considered section.

The traffic is in a free flowing state during the first 300 seconds. The speeds ranged, depending on the considered lane, from approx. 90 to 125 km/h. Afterwards there was a significant drop in the traffic speed and flux. In the video material it can be seen that the vehicles slowed down due to an event at a further position along the highway section, which resulted in a recognizable change in the speed behavior.

As from second 420 onwards, a traffic backlog was recorded on lane 1. Starting with second 540, the speed slowly increased and the traffic flow improved. In second 580, a vehicle with a blue flashing light was detected that supports

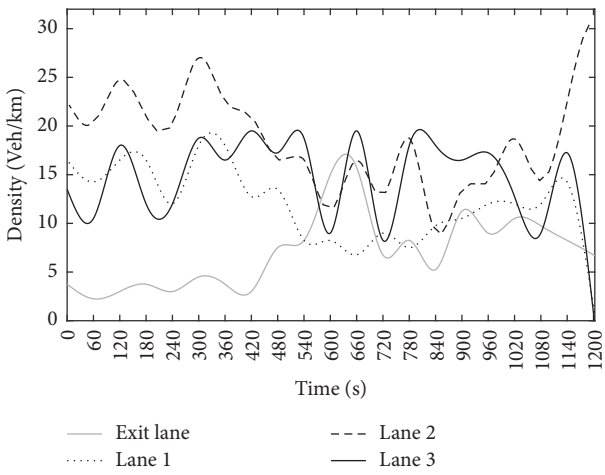

Figure 8: Traffic density diagram.

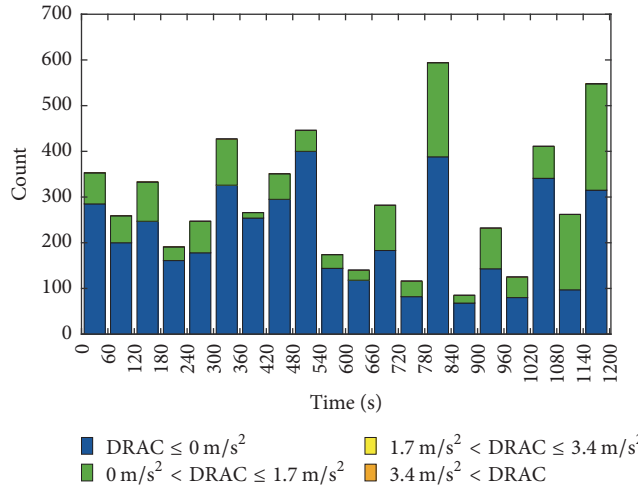

Figure 9: DRAC values categorized in four groups over the considered time interval in lane 2.

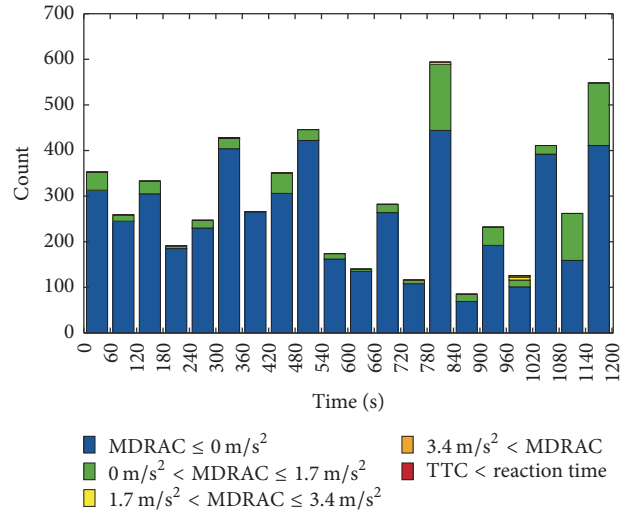

Figure 10: MDRAC values calculated with PRT = 1.3 s categorized in four groups over the considered time interval in lane 2.

the assumption that an event had occurred in a subsequent section. Based on the traffic parameter graphs of the exit lane it can be seen that after the presence of the blue light many of the vehicles leave the highway. From second 700 onwards, a drop in the speed profile is again observed. From second 750 the traffic density increases in lane 1 and from second 800 onwards it also increases in the other lanes. As from second 840, the speed slowly increases again and the traffic flow improved to a stable traffic state.

With the aim of testing the impact of the PRT and the constant acceleration/deceleration, the performances of traditional and modified surrogate indicators are compared.

The traffic in lane 2 serves as a data base for the derivation of the microscopic traffic safety parameters, since the majority of the vehicles were monitored in this lane. In addition, there is a reduced occlusion compared to lane 1 where high vehicles such as trucks and busses tend to lead to a less accurate position estimation.

In Figures 9–13 the entire height of the bar shows the amount of existing rear-end situations over the defined time intervals. It becomes clear that a higher traffic density leads to a high number of rear-end situations. This is due to the fact that many vehicles are located in this section, and thus many vehicle pairs are registered for assessment. In addition, it can be seen that particularly many rear-end situations occur in the periods of slow moving traffic between seconds 300 to 540 and seconds 780 to 840. However, the high number of rear-end situations does not automatically lead to many critical situations as vehicles tend to drive at low speeds.

Furthermore, the rear-end situations are classified into different criticality groups based on thresholds of the required deceleration rates. The number and proportion of rear-end situations in different groups are marked by different color representations inside the bars in the figures. If the determined safety parameter exceeds the threshold value of 3.4 m/s^2 this indicates a critical situation.

As the original DRAC does not exceed the threshold of 3.4 m/s^2 no critical conflicts were identified using this safety indicator (Figure 9). However, it is apparent that starting from second 660 increasingly more rear-end situations occurred where a slight deceleration was necessary to avoid a critical situation.

The modified version of the DRAC, MDRAC, was calculated with two different reaction times, 1.3 seconds and 2.02 seconds. The MDRAC is only calculated when $v_2 > v_1$ and TTC $> R$. However, the number of occurrences where $R >$ TTC can be relevant, as this may indicate an extremely critical situation. This of course does not implicitly mean that an accident occurs but follows from the theoretical assumption of constant speed while the reaction time is measured from the timestamp of the current assessment. For this reason, both criteria are considered.

In Figure 10 the MDRAC was calculated with $R = 1.3$ s while in Figure 11 the reaction time value was $R = 2.02$ s.

It can be seen that values between 1.7 and 3.4 m/s^2 (almost critical situations) can be found at 960 to 1020 seconds

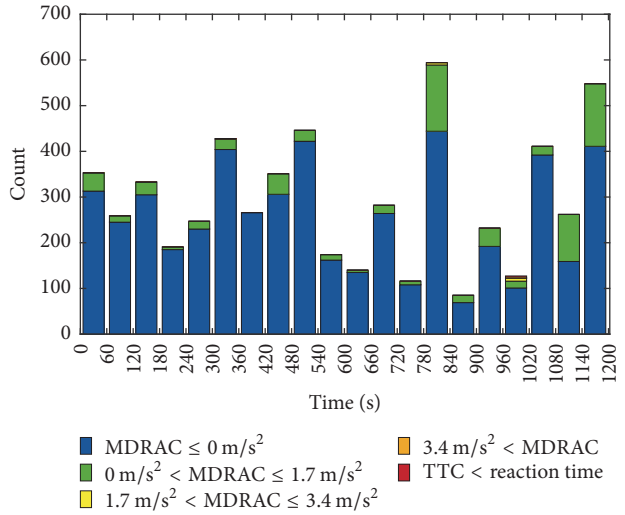

Figure 11: MDRAC values calculated with PRT = 2.02 s categorized in four groups over the considered time interval in lane 2.

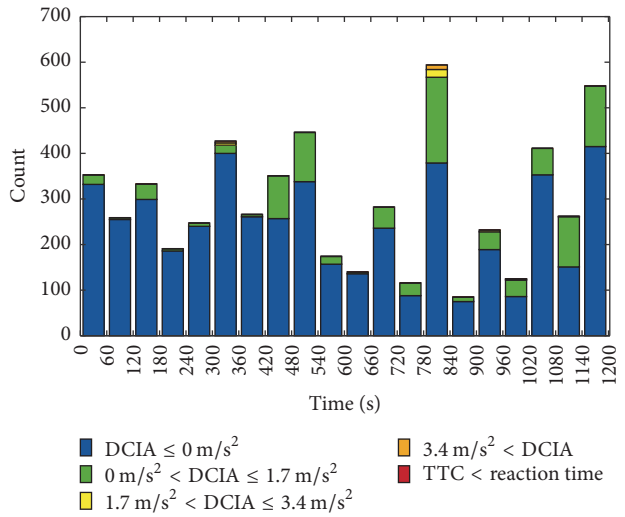

Figure 12: DCIA values calculated with PRT = 1.3 s categorized in four groups over the considered time interval in lane 2.

when the reaction time used is 1.3 seconds (Figure 10). Additionally to this time interval the safety parameter also shows occurrences of values in this criticality group at 780 to 840 seconds when the reaction time is 2.02 seconds (Figure 11). The MDRAC with a reaction time of 2.02 seconds identifies a critical traffic situation at 780–840 seconds.

For further discussions and validation of the DCIA, considering a constant deceleration rather than constant speed has been derived from the data with reaction times of 1.3 seconds and 2.02 seconds (Figures 12 and 13).

Compared to the MDRAC with a reaction time of 1.3 seconds the DCIA results in more critical situations when using the same reaction time. While MDRAC only once identified occurrences of almost critical situations at seconds 960 to 1020, DCIA registers critical situations at seconds 300 to 360, seconds 780 to 840, and second 960 to 1020, as well as

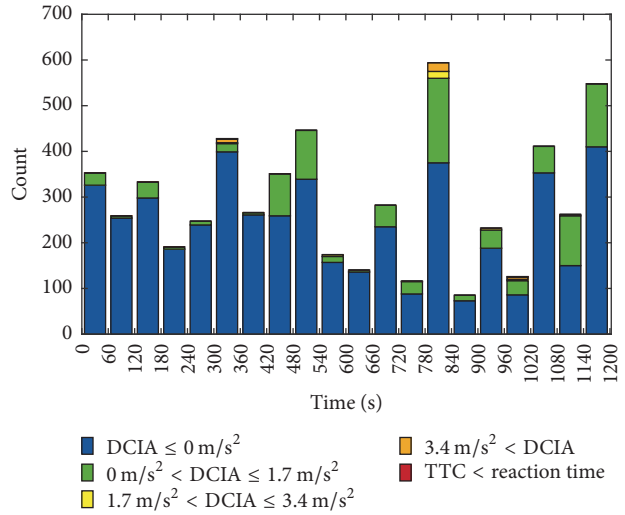

Figure 13: DCIA values calculated with PRT = 2.02 s categorized in four groups over the considered time interval in lane 2.

almost critical situations at seconds 900 to 960 and seconds 1080 to 1140.

The phenomenon that the DCIA is more sensitive to critical situations compared to MDRAC is also shown in the comparison between MDRAC and DCIA with a response time of 2.02 seconds. DCIA identifies more critical situations and even 2 situations where the reaction time exceeds the time to collision (TTC).

Overall, it is clear that in the periods of traffic disturbances greater amounts of general rear-end as well as critical rear-end situations occur. On the basis of the critical situations in the period of 960 to 1020 seconds, in which the traffic is almost moving, it can be seen that critical situations or accidents can also occur under normally good circumstances and are attributable to the driving behavior of the vehicle drivers.

The critical situations (deceleration > 3.4 m/s^2) were subjected to a detailed analysis. Thereby it was found that four pairs of vehicles are involved in the critical situations, which have differently often led to exceeding the threshold depending on the indicator used (see Table 1). While no critical vehicle combination has occurred using DRAC and MDRAC with PRT = 1.3 s, there was one occurrence with MDRAC with PRT = 2.02 s, three occurrences with DCIA with PRT = 1.3 s, and four with DCIA with PRT = 2.02 s.

In addition, it was possible to ascertain through analyzing the video material that two of the four vehicle combinations are lane changes. Although the indicators show that these situations are critical, accelerating before changing the lane for an overtake is a sensible driving behavior which should not be classified as a critical situation.

6. Conclusion

In this paper a novel surrogate safety indicator was presented which rather than assuming a constant speed for the conflict prediction only uses a constant acceleration and also includes a theoretical reaction time of the road users.

Table 1: Detailed information about the four identified critical situations.

Vehicle-IDs	Time	Safety indicator	Situation
1034/1036	964	MDRAC, PRT = 2.0 s DCIA, PRT = 1.3 s DCIA, PRT = 2.0 s	Lane-change
374/375	333	DCIA, PRT = 1.3 s DCIA, PRT = 2.0 s	Rear-end
872/874	798	DCIA, PRT = 1.3 s DCIA, PRT = 2.0 s	Rear-end
866/868	792	DCIA, PRT = 2.0 s	Lane-change

The DRAC, MDRAC, and DCIA were assessed using a database of 3D microscopic traffic data gathered from video material by using innovative image processing techniques. A thorough comparison of the three indicators showed that the DCIA is more sensitive in detecting critical situation throughout all criticality groups. The discussion showed that the DCIA is considerably more realistic regarding the description of the dynamic conflict situation.

It was shown that critical situations more often occur at traffic disturbances. Nevertheless, the data showed that critical conflict situations may also occur under circumstances including free flowing traffic due to dangerous driving behavior.

As two of the four identified critical situations detected by the DCIA turned out to be uncritical lane changes, more sophisticated safety indicators need to be developed which can cope with the 3D trajectories of the vehicles. Furthermore, the video-based traffic safety data collection and the subsequent data showed huge potential for safety analysis; thus a higher data volume should be gathered. Further research work should be conducted by comparing large data volumes to real crash data which would lead to a more comprehensive indicator validation.

Conflicts of Interest

The authors declare that they have no conflicts of interest.

Acknowledgments

This research is a part of the project "Basic Evaluation for Simulation-Based Crash-Risk-Models: Multi-Scale Modelling Using Dynamic Traffic Flow States" supported by the German Research Directory (Deutsche Forschungsgemeinschaft, DFG). The data-material is based upon work conducted in the project ESIMAS supported by the German Federal Ministry for Economic Affairs and Energy.

References

[1] F. H. Amundsen, "Proceedings, First Workshop on Traffic Conflicts," in *Proceedings of the First Workshop on Traffic Conflicts (Oslo '77)*, Tekniska Högskolan i Lund, TØI, Oslo, Norway, 1977.

[2] A. R. van der Horst, *A Time-Based Analysis of Road User Behaviour in Normal And Critical Encounters*, Technische Universität Delft, 1990.

[3] Y. Kuang, X. Qu, and S. Wang, "A tree-structured crash surrogate measure for freeways," *Accident, Analysis & Prevention*, vol. 77, pp. 137–148, 2015.

[4] Y. Kuang, X. Qu, J. Weng, and A. Etemad-Shahidi, "How does the driver's perception reaction time affect the performances of crash surrogate measures?" *PLoS ONE*, vol. 10, no. 9, Article ID e0138617, 2015.

[5] S. Almqvist, C. Hydén, and R. Risser, "Use of speed limiters in cars for increased safety and a better environment," *Transportation Research Record: Journal of the Transportation Research Board*, no. 1318, pp. 34–39, 1991.

[6] Q. Meng and J. Weng, "Evaluation of rear-end crash risk at work zone using work zone traffic data," *Accident, Analysis & Prevention*, vol. 43, no. 4, pp. 1291–1300, 2011.

[7] G. Guido, F. F. Saccomanno, A. Vitale, V. Astarita, and D. C. Festa, "Comparing safety performance measures obtained from video capture data," *Journal of Transportation Engineering*, vol. 137, no. 7, pp. 481–492, 2011.

[8] V. Astarita, G. Guido, A. Vitale, and V. P. Giofré, "A new microsimulation model for the evaluation of traffic safety performances," *European Transport/Trasporti Europei*, no. 51, pp. 1–16, 2012.

[9] D. Gettman and L. Head, "Surrogate safety measures from traffic simulation models," *Transportation Research Record*, no. 1840, pp. 104–115, 2003.

[10] C. Wang and N. Stamatiadis, "Surrogate safety measure for simulation-based conflict study," *Transportation Research Record*, no. 2386, pp. 72–80, 2013.

[11] C. Wang and N. Stamatiadis, "Derivation of a new surrogate measure of crash severity," *Transportation Research Record*, vol. 2432, pp. 37–45, 2014.

[12] C. Wang and N. Stamatiadis, "Evaluation of a simulation-based surrogate safety metric," *Accident, Analysis & Prevention*, vol. 71, pp. 82–92, 2014.

[13] D. B. Fambro, K. Fitzpatrick, and R. J. Koppa, "New stopping sight distance model for use in highway geometric design," *Transportation Research Record*, no. 1701, pp. 1–8, 2000.

[14] H. Rakha, I. El-Shawarby, and J. R. Setti, "Characterizing driver behavior on signalized intersection approaches at the onset of a yellow-phase trigger," *IEEE Transactions on Intelligent Transportation Systems*, vol. 8, no. 4, pp. 630–640, 2007.

[15] F. Wang, K. Tang, and K. Li, "A stochastic computational model for yellow time determination and its application," *Journal of Advanced Transportation*, vol. 49, no. 3, pp. 457–474, 2015.

[16] B. D. Greenshields, "Reaction time in automobile driving," *Journal of Applied Psychology*, vol. 20, no. 3, pp. 353–359, 1936.

[17] G. Taoka, "Break reaction times of unalerted drivers," *ITE Journal* , vol. 59, no. 3, pp. 19–21, 1989.

[18] H. Summala, "Brake reaction times and driver behavior analysis," *Transportation Human Factors*, vol. 2, no. 3, pp. 217–226, 2000.

[19] M. Green, ""How long does it take to stop?" methodological analysis of driver perception-brake times," *Transportation Human Factors*, vol. 2, no. 3, pp. 195–216, 2000.

[20] American Association of State Highway and Transportation Officials, "A Policy on Geometric Design of Highways and Streets," AASHTO, 2004.

[21] J. Archer, *Methods for the Assessment and Prediction of Traffic Safety at Urban Intersections and their Application in Micro-simulation Modelling*, Academic Thesis, Royal Institute of Technology Stockholm, 2004.

[22] A. R. Mamdoohi, M. F. Zavareh, C. Hydén, and T. Nordfjærn, "Comparative analysis of safety performance indicators based on inductive loop detector data," *PROMET—Traffic & Transportation*, vol. 26, no. 2, pp. 139–149, 2014.

[23] L. T. Truong, M. Sarvi, G. Currie, and T. M. Garoni, "How many simulation runs are required to achieve statistically confident results: a case study of simulation-based surrogate safety measures," in *Proceedings of the 18th IEEE International Conference on Intelligent Transportation Systems (ITSC '15)*, pp. 274–278, Gran Canaria, Spain, September 2015.

[24] G. Guido, V. Astarita, V. Giofré, and A. Vitale, "Safety performance measures: a comparison between microsimulation and observational data," in *Proceedings of the 14th Meeting of the Euro Working Group on Transp. - In Quest for Adv. Models, Tools, and Methods for Transp. and Logist., EWGT, 26th Mini-EURO Conf. - Intelligent Decis. Making in Transp. and Logist., MEC, 1st Eur. Sci. Conf. on Air Transp. - RH*, vol. 20, pp. 217–225, September 2011.

[25] Y. Kuang and X. Qu, "A Review of Crash Surrogate Events," in *Proceedings of the 2nd International Conference on Vulnerability and Risk Analysis and Management, ICVRAM 2014 and the 6th International Symposium on Uncertainty Modeling and Analysis (ISUMA '14)*, pp. 2254–2264, July 2014.

[26] K. Morita, M. Sekine, and T. Okada, "Factors with the greatest influence on drivers' judgment of when to apply brakes," in *Proceedings of the 2006 SICE-ICASE International Joint Conference*, pp. 5044–5049, Busan, Korea, October 2006.

[27] Y. Zhang, E. K. Antonsson, and K. Grote, "A new threat assessment measure for collision avoidance systems," in *Proceedings of the IEEE Intelligent Transportation Systems Conference (ITSC '06)*, pp. 968–975, September 2006.

[28] S. M. S. Mahmud, L. Ferreira, M. S. Hoque, and A. Tavassoli, "Application of proximal surrogate indicators for safety evaluation: a review of recent developments and research needs," *IATSS Research*, 2016.

[29] R. Wiedemann, *Simulation des Straßenverkehrsflusses*, Universität Karlsruhe, 1974.

[30] J. Archer, *Indicators for Traffic Safety Assessment And Prediction And Their Application in Micro-Simulation Modelling: A Study of Urban And Suburban Intersections*, Royal Institute of Technology Stockholm, 2005.

[31] Bundesanstalt für Straßenwesen, "Echtzeit-Sicherheits-Management-System für Straßentunnel (ESIMAS)," http://www.esimas.de/.

[32] A. Fazekas, M. Bommes, and M. Oeser, "Vehicle Tracking using 3D Particle Filter in Tunnel Surveillance and Incident Detection," in *Proceedings of the 3rd International Conference on : Models and Technologies for Intelligent Transportation Systems 2013*, vol. no. 3, pp. 213–222, 2013.

[33] Z. Zhang, "A flexible new technique for camera calibration," *IEEE Transactions on Pattern Analysis and Machine Intelligence*, vol. 22, no. 11, pp. 1330–1334, 2000.

Hindawi
Journal of Advanced Transportation
Volume 2017, Article ID 9862949, 14 pages
https://doi.org/10.1155/2017/9862949

Research Article

A Novel Approach for Operating Speed Continuous Predication Based on Alignment Space Comprehensive Index

Ying Yan,[1] Gengping Li,[1] Jinjun Tang,[2] and Zhongyin Guo[3]

[1]*School of Automobile, Chang'an University, Xi'an, China*
[2]*School of Traffic and Transportation Engineering, Key Laboratory of Smart Transport in Hunan Province, Central South University, Changsha, China*
[3]*College of Transportation Engineering, Tongji University, Shanghai, China*

Correspondence should be addressed to Jinjun Tang; jinjuntang@csu.edu.cn

Received 1 June 2017; Revised 18 September 2017; Accepted 30 October 2017; Published 12 December 2017

Academic Editor: Chunjiao Dong

Operating speed is a critical indicator for road alignment consistency design and safety evaluation. Although extensive studies have been conducted on operating speed prediction, few models can finish practical continuous prediction at each point along alignment on multilane highways. This study proposes a novel method to estimate the operating speed for multilane highways in China from the aspect of the three-dimensional alignment combination. Operating speed data collected in field experiments on 304 different alignment combination sections are detected by means of Global Positioning System. First, the alignment comprehensive index (ACI) is designed and introduced to describe the function accounting for alignment continuity and driving safety. The variables used in ACI include horizontal curve radius, change rate of curvature, deflection angle of curve, grade, and lane width. Second, the influence range of front and rear alignment on speed is determined on the basis of drivers' fixation range and dynamical properties of vehicles. Furthermore, a prediction model based on exponential relationships between road alignment and speeds is designed to predict the speed of passenger cars and trucks. Finally, three common criteria are utilized to evaluate the effectiveness of the prediction models. The results indicate that the prediction models outperform the other two operating speed models for their higher prediction accuracy.

1. Introduction

Human-orient and safety supremacy are currently the new guidance during the period of highway construction. The traditional design speed-based alignment design approach usually only specifies the minimum value of one isolated alignment element. This designing method is prone to be inconsistent with successive elements of a road. Large amount of practical studies highlights the fact that inconsistent alignment might cause a sudden change in the characteristics of the roadway, which would lead to critical driving errors and crash risks [1, 2]. A consistent alignment design is required to meet drivers' expectations and promotes harmonious driving behaviors. Since a number of experimental surveys state that the actual speeds adopted by drivers are considerably higher than those used to determine road design standards [3, 4], several countries recommend the analysis of the design consistency or safety evaluation in order to check excessive differences of operating speed on successive elements along the road [5–7]. It is noticed that the operating speed profile is the most useful tool to achieve this goal [7]. For example, Interactive Highway Safety Design Model (IHSDM) developed by the US Federal Highway Administration is wildly used for comprehensive safety assessment [8]. The current version of IHSDM checks the operating speed profile against two consistency criteria. Operating speed is an expressive parameter of driver's behavior influenced by multiple factors, such as alignment, vehicle dynamical properties, traffic flow composition, traffic management and control measures, climate, and sight distance. The 85th percentile of the free-flow speed distribution is commonly used to represent operating speed for design consistency evaluation [1, 8].

There are extensive literatures on operating speed prediction models in which the variables and the model constructions vary considerably. Most models focus on horizontal

curve by assuming constant speed on curves and therefore deceleration and acceleration that occur entirely on the approach tangent and on the departure tangent [3]. Lamm et al. [9] considered the curve radius to be the most significant indicator in determining the operating speed and used it as the dominant independent variable to predict operating speed on horizontal curves. They also established a process and a classification system to evaluate horizontal design consistency. Islam and Seneviratne [10] reported the differences on feature points of alignment and established the operating speed regression model on three sites of curve. McFadden and Elefteriadou [11] combined the degree of curvature, length of curve, deflection angle, and the speed on approach tangent to make a regression analysis. Krammes et al. [12] developed an operating speed prediction model in which all the variables are related to the geometry characteristics of the curve to evaluate horizontal alignment consistency based on data collected from 138 curves. Bucchi et al. [13] conducted the estimation of operating speed on large grade sections and sharp curve with radius from 25 m to 170 m for the rural road. Some similar speed profile models mostly used curve radius (radius or degree of curvature) as the predictor [11, 14–17].

Meanwhile, previous works introduced the vertical alignment influences on operating speed [18]. Jessen et al. [19] studied the potential influences of mileage, grade of vertical curve, crash barrier, intersection, lane width, and volume on operating speed by collecting the car data on 70 vertical curves. Fambro et al. [20] presented that the sight distance was constrained by the vertical curvature which consequently determined the operating speed. Moreover, vertical grade, vertical curve type, and rate of vertical curvature were considered in the prediction models. The methodology in the IHSDM adopted these equations [8]. Gibreel et al. [21] investigated the operating data on three-dimensional alignments involving sag and crest vertical curves in Ontario and set up the reliable operating speed prediction models for two-lane highways. In addition, other models using statistical methods including simple linear regression, multiple linear regressions, and nonlinear regression were built up on the basis of analysis between alignment variables and operating speed [22–24]. By contrast, Brazil model [25] was put forward according to the mechanical properties and driving behaviors. This model also presented the clear explanation for the restriction factors to improve the accuracy of prediction. Moreover, artificial neural network and simulation technique were introduced to estimate operating speed [26, 27].

Numerous studies have been completed for passenger car operating speed prediction and design consistency on rural two-lane highways [13, 16]. Relatively few researches, however, are conducted for trucks on multilane highways [28, 29]. J. E. Leisch and J. P. Leisch [30] found that an increase in vertical grade or length of vertical curve had much significant influence on truck speed than car speed. They also suggested that the speed profile models for trucks can be constructed by considering both horizontal and vertical alignments. In this regard, another concern has to be stressed. Most of the existing two-dimensional (2D) models which only considered horizontal and vertical curve have much lower values of coefficient of determination due to the cross section missed in the model [6, 12, 17]. Gibreel et al. [21] proposed that the maximum differences between the predicted and the observed speed using three-dimensional (3D) model and 2D model on some sites reached 35%. In addition, most existing models are based on spot speed data collected by measuring the individual speeds of a sample of the vehicles passing a given spot [31]. They assumed that constant speed occurs on curves and therefore deceleration and acceleration entirely occur on the approach tangent and on the departure tangent. With these assumptions, spot speed data are collected at the center of the horizontal curve and at the midpoint of the preceding tangent. However, the maximum and minimum speeds may not occur, respectively, at the center of tangents and curves. Since the speed data are not collected at the beginning and the ending deceleration or acceleration points, these models do not accurately represent drivers' behavior. Therefore, previous works mainly calculated the speed of the feature points (i.e., the midpoint of horizontal curve or preceding tangent) of alignment using spot speed data which is usually accompanied by human error and cosine error [10]. In fact, the analysis of an individual point may blur the change pattern of operating speed and disregard the continuity of speed variation. On the basis of the overall state of the art, few of them can conduct the operating speed at each point along the road [16, 20].

In terms of limitations in aforementioned methods, it is challenging to design different approaches to explore a comprehensive representation of the operating speed. The report E-C151 of the Transportation Research Board [32], a thorough review of the operating speed all over the world which also underlined the requirements for novel speed models for different countries because speed behavior was influenced by multiple factors, significantly differs among regions. Recently, limited studies on continuous operating speed prediction were developed through relationships analysis between speed at all points and geometry alignment [31, 33–35]. These models provided a potential for a more accurate investigation of driver's behavior.

The main objective of the research in this paper is to propose a continuous operating speed prediction model for passenger cars and trucks on multilane highways. This new methodology, for the first time, formulates a three-dimensional alignment comprehensive index (ACI) combined with driver's visual characteristics and vehicle dynamic properties to achieve higher accurate and reliable speed estimation at each point along the roadway. This could be useful for researchers to evaluate alignment design consistency and determine alignment features.

2. Methodology

2.1. Basic Hypotheses. Operating speed is affected by multiple factors. How to find the key information from complex influence factors is critical for accurate prediction. Based on the analysis of the relation among operating speed, alignment, and other influence factors, the basic hypotheses are summarized as follows:

① Operating speed varies with the change of road condition along the driving direction.

② The comprehensive influence of alignment on operating speed is not only mutually independent, but also not equivalent to a simple linear overlay. As a quantitative indicator to characterize horizontal, vertical, and cross section alignment, the road alignment comprehensive index is related to the speed variation.

③ Operating speed on a certain section is related to alignment features on this section and also affected by the range of a certain length of alignment between rear segment and front segment.

These three assumptions which focus on the influences of front and rear alignment on operating speed are in line with the general driving rules of vehicles run on highway. Meanwhile, the continuity of operating speed in space is also taken into account.

2.2. Three-Dimensional Alignment Comprehensive Index (ACI) Description Model

2.2.1. Alignment Comprehensive Index. An ACI is defined as a mathematical indicator f which can characterize the influence of indices on alignment continuity and driving safety by considering the three-dimensional geometric features of horizontal, vertical, and cross section alignment.

It is indicated that one point corresponds to a unique value of f which describes the comprehensive geometry features of various indices on each point and also reflects the amount of the information perceived by drivers. According to the influence of alignment on the driving safety, the consistent relationship between alignment and f is represented as a smaller value of f contributes to better alignment. In other words, the alignment corresponding to a smaller f will be more benefit for driving.

The key idea of method lies in setting up the horizontal, vertical, and cross section alignment model, respectively, and then integrating them into the ACI description model. According to the definition of ACI and the works in [31], the most significant independent variables influencing the operating speed and corresponding to each point have been taken into account.

2.2.2. Horizontal Alignment Description Model. Three variables including radius, change rate of curvature, and deflection angle of curve are considered in the horizontal alignment description model. Generally, these three variables can represent lateral force, rotation rate of the steering wheel, and deflection angle of driver's vision. When vehicles travel on a horizontal curve with greater curvature, the worse lateral stability may be generated due to the larger centrifugal [36]. The mutations of curvature are prone to driving risk even crashes. Thus, the consistent relationship between curvature and f can be determined as the larger the curvature, the smaller f. Similarly, the more rapidly the curvature changes on a spiral curve, the greater the impact on the driver is because of the workload on adjusting the steering wheels and ultimately the greater likelihood of danger. Generally, drivers need to shift their eyes or turn their heads to focus on a front point as the trajectory changes. A sharp change of deflection angel of curve would aggravate range of driver's vision. This is also harmful for safe driving. Therefore, f increases as these two variables become larger.

The relationship between each individual indices and the intermediary variable is applied to transform and unify the change laws of each index and the comprehensive index. The vertical and cross section correction model also use the same research ideas, in which speed is often taken as the intermediary variable.

In some traditional regression models, the speed at a given radius is formulated as an ordinary linear model ($V = a - b/R$) or power model ($V = aR^b$). Combining with the test data, the relation between operating speed and radius are analyzed by using these two forms function firstly. It can be concluded that power model has limitation with radius less than 250 m. The variation is too slight to reflect the influence of radius on operating speed. However, it is apparently rare for highways with radius less than 250 m. On the contrary, the speed variation in linear model is too strong and even negative value occurs with the radius less than 700 m. However, this is a frequent occurrence that the radius of horizontal curve is less than 700 m. Thus, power function is adopted to demonstrate the relation between f and radius. Moreover, exponential model [9, 11, 12] is widely used to predict the variation of operating speed with change rate of curvature and deflection angle of curve. Based on above analyzes of each indicator, these models can be generalized as (1) by using a multiple exponential with linearized function to form the horizontal ACI (f_H) model:

$$f_H = mR^n \exp\left(a_1 \mathrm{CCR} + b_1 \mathrm{DF}\right), \tag{1}$$

where R is curvature; CCR represents change rate of curvature; DF denotes deflection angle of curve; m, n, a_1, and b_1 are parameters.

2.2.3. Vertical Alignment Description Model. In the vertical alignment description model, grade is considered as the main variable. It can be concluded that the driving safety would become worse as the grade increases no matter on downhill or uphill due to the insufficient sighting distance or speeding. From the point of the definition of the consistent relationship between f and alignment index, f increases with the increase of grade. Although the variation of f with grade is easy to know, the quantitative relation still remains unclear. That is, the intermediary variable, speed with the absolute value of grade, has a distinct trend. According to the initial data analysis, speed decreases as grade varies from downhill to uphill. So the correlation between grade and the vertical ACI (f_V) is firstly expressed as linear regression is analyzed [20]. However, in fact, speed varies slightly when the grade ranges between −2% and 2%, whereas the grade is greater than 3% or less than −3%, and the variation of speed increases with nonlinear function. Moreover, for the positive and negative grade, the corresponding f_V has a different value range.

Consequently, the vertical ACI model (see (2)) is developed based on the improvements of the linear regression equation:

$$f_V = a_2 i\,|i| + b_2 i + c_2, \tag{2}$$

where i is grade; a_2, b_2, and c_2 are parameters.

2.2.4. Cross Section Alignment Correction Model. In the cross section alignment model, the five independent variables are utilized in model, including lane width, lane number, widths of right and left shoulder, and the adjustment coefficient which represents the variation of pavement width because of the transition from common road to bridge or tunnel. Generally, the interaction between adjacent vehicles along the driving direction is smaller on the wider roadway. Such driving environment also offers greater driving convenience and freedom due to a wider vision field. It indicates that wider roadway is more favorable to the traffic. In other words, f decreases with the increase of lane width, lane number, and the left and right shoulder width. However, operating speed increases as the width of pavement becomes large. In the findings of Harwood et al. [37], the regression relationship between speed reduction and cross section is presented. It also suggests cumulative effects on the speed due to variations in lane and shoulder width [17]. For example, for a given cross section composed by a lane width smaller than 3.6 m and a shoulder width smaller than 1.8 m, the reduction in speed is the sum of the individual effects caused by each variable. On the basis of field investigation, the cross section ACI (f_C) model is set up in terms of the width standard of eight-lane highway and the reduction percentage of speed related to cross section width as

$$\begin{aligned} f_C &= \beta \cdot \ln\left(a_3 B^2 + b_3 B + c_3\right) + \xi, \\ B &= n_3 \cdot L + w_1 + w_2, \end{aligned} \tag{3}$$

where β, a_3, b_3, and c_3 are the parameters; ξ is the adjustment coefficient of the bridge and tunnel; B is the total width of single carriageway section; L is the width of a single lane; n_3 is the number of lanes; w_1 and w_2 are the widths of the left and right road shoulders.

2.2.5. Model Integration. A horizontal alignment in a roadway refers to the alignment or how "straight" the roadway section is. A vertical alignment refers to a roadway's change in elevation or the "flatness" of the roadway. With respect to the road information perceived by drivers, it is not only related to alignment itself but also involved operating speed. In this paper, the challenge is how to quantify the road alignment information and integrate the horizontal, vertical, and cross section alignment ACI into a 3D ACI description model serving for the operating speed prediction. Because people's perception to the distance, shape, and speed of the objects in real space depends on continuous learning and experience [20], it is really difficult to achieve effective identification performance. Currently, the perspective images are generally used to depict the road section from high view (bird's eye view). However, the analysis of these images is qualitative and subjective [38].

It is worth mentioning that tangent is a radial ray expanded from a vanishing point in the fields of vision of drivers [39]. Tangent is the most recognizable shape for drivers, and the understanding of other alignment is usually acquired based on the comparison with tangent. Drivers could firstly predict the consistency between the front and the current horizontal alignment, focusing primarily on the operating speed rather than on the direction. Through a change of sight distance, drivers can attain information about vertical alignment. Given the fact that the cross section alignment rarely changes, the perceptions of drivers in different cross sections are nearly the same and are less dependent on the change of horizontal and vertical alignments.

During construct ACI model, we consider the following several reasons: first, in some traditional regression models, the speed at a given radius, change rate of curvature, and deflection angle of curve are formulated as an ordinary linear model, power model, or exponential model [9, 11, 12]. We referenced these model forms and generalized these models by using a multiple exponential with linearized function to form the horizontal ACI (f_H) model.

Second, we found speed decreased as grade varied from downhill to uphill. So we analyze the correlation between grade and the vertical ACI using the linear regression firstly [20]. However, in fact, speed varies slightly when the grade is between −2% and 2%, whereas the grade is greater than 3% or less than −3%, and the variation of speed increases with nonlinear function. Moreover, for the positive and negative grade, the corresponding f_V has a different value range. Consequently, the vertical ACI model (see (2)) is developed based on the improvements of the linear regression equation.

Third, in the findings of Harwood et al. [37], the regression relationship between speed reduction and cross section is presented. It also suggests cumulative effects on the speed due to variations in lane and shoulder width [17]. On the basis of field investigation, the cross section ACI (f_c) model is set up in terms of the width standard of eight-lane highway and the reduction percentage of speed related to cross section width.

Moreover, the challenge in this study is how to integrate the horizontal, vertical, and cross section alignment ACI into a 3D ACI description model. By considering alignment design features, several research findings and the cross section alignment adjustment form mentioned in Highway Capacity Manual 2010 [40], and the ACI description model is put forward based on the sensitivity to each alignment index.

After repeated trial calculation and parameters calibration, the three-dimensional alignment comprehensive index description function is set up finally. The ACI description model is put forward based on the sensitivity to each alignment index as shown in

$$f = f_H f_V + f_C. \tag{4}$$

The reasons we choose these indicators are shown as follows: First, on the basis of data analysis, we studied the correlation among the single index, operating speed, and traffic safety, including length of tangent, radius of horizontal curve (curvature), curvature rate, curve length deflection

angle of horizontal curve, grade, length of vertical grade, and lane width. Then, we selected the indexes which were often used to establish operating speed model in the related achievements at home and aboard. In summary, the indexes which have great influence on operating speed and safety were selected preliminarily.

Secondly, according to the characteristics of road alignment, these indexes can be divided into two categories. One category is the section design index corresponding to the milepost, mainly including radius, curvature rate, curve length deflection angle of horizontal curve, grade, lane number, lane width, and shoulder width. Another category is the indexes along the roadway, such as tangent length, curve length, length of vertical curve length, and spiral length.

The alignment comprehensive index is based on the road section, so the model of ACI mainly considers the first category indexes, and the second category indexes will be selected in the operating speed prediction model.

2.3. Determination of Influence Range. This study emphasizes a continuous speed prediction which is more accurate than other researches on operating speed with a single alignment index. The section speed is selected as objects through discretizing the continuously variable operating speed. Although the alignment comprehensive index and operating speed are divided into points, the operating speed on a certain section is always related to the front and rear alignments within a certain length. The speed of one point is the cumulative result of speed variation on rear alignment that has already traveled. On the other hand, a certain range of alignment ahead decides the driver's expectation of acceleration and deceleration based on the perception of the visual information obtained at the present moment. So the influence range of front and rear alignment on current section speed should be determined.

The visual characteristics of drivers are the most important factor affecting the change in operating speed. The key step to determine the influence range of front alignment is to quantify environmental factors of visual information to a digital index, then using this digital index to analyze the influence of front alignment on operating speed.

Road alignment forms a visual sensitive area in the drivers' view plane, generally known as fixation range [41], including the invisible region, rear view region, and front view region. Using as the prejudgment of alignment conditions ahead, the front view region is the main influence range of the operating speed. Easa and He [42] showed that driver's visual demand interval was generally approximately 3 s. Therefore, 3 s trip is used as the starting point of the most sensitive position in driving process, which is the nearest point of the front alignment influence. Depending on the speed, driver vision is usually focused further as the speed increase. However, because of the influences of elevation fluctuation and sight distance on curves, the maximum fixation distance on curves may be closer than that on tangents. According to the current China Technical Standard of Highway Engineering (JTG B01-2014) [43], a certain stopping sight distance on curve segments is specified. When the design speed is 120 km/h, the recommended stopping sight distance is 210 m. Thus, 1.2 times stopping sight distance is adopted as the farthest fixation point of front alignment influence on the basis of general consideration. To take the maximum design speed 120 km/h into account, the influence range of front alignment is determined from 100 m to 250 m.

Operating speed on a current section is the result of cumulative speed change of the rear-traveled sections. The speed differences existing between the front and rear sections are induced by the acceleration and deceleration of a vehicle. Thus, the influence range of rear alignment can be approximately characterized by the acceleration and deceleration distance. According to several previous studies [44, 45], the deceleration or acceleration rates mainly depend on the radius of the curve and its locations. However, the acceleration and deceleration models using the spot speed data do not reflect driver's actual behavior because the starting and ending points of the speed transition can not be determined a priori. Therefore, the actual acceleration and deceleration rates cannot be accurately obtained. Moreover, the speed transition length depends more on driver characteristic (such as age, gender, purpose of the trip, and distance traveled) than on the alignment transition design [44].

Thanks to the continuous speed profiles observed for each individual trajectory, 15th and 85th percentile speeds are, respectively, 102 km/h and 123 km/h for car compared to 69 km/h and 81 km/h for truck. Because the probability of occurrence of speed decelerating from 85th percentile to 15th percentile is generally low, it is relatively conservative and safe to consider these speed intervals as the speed differences in deceleration process. Consequently, according to the recommended deceleration of 0.9 m/s^2 for cars and 0.35 m/s^2 for trucks in our project report [46], the influence range of the rear alignment can be determined as 200 m.

2.4. Structure of Prediction Model. From the given analysis, the operating speed V of current section contains the following two parts: V_1 and ΔV. The initial speed V_1 represents the accumulation of operating speed within the 200 m influence range of rear alignment. ΔV means acceleration or deceleration according to the alignment features within the effective fixation range from 100 m to 250 m ahead. These two variables are jointed to determine the operating speed V of current section, and the relationship can be expressed as

$$V = V_1 + \Delta V. \tag{5}$$

In (5), V_1 and ΔV are also determined by the accumulated values of ACI of the front and rear influence ranges. However, the influences of front and rear alignment on operating speed are different. Therefore, considering speed superposition principle, this study puts forward the form of speed prediction model as (6). The criteria used for identifying the prediction performance are based on the highest coefficient

Table 1: Site geometric design characteristics.

Variable	Minimum	Maximum	Mean	Standard deviation
Design speed (km/h)	60.00	120.00	108.32	15.62
Horizontal curve radius (m)	400.00	3500.00	868.05	218.65
Curve length (m)	284.22	1155.48	902.65	89.37
Deflection angle of horizontal curve	6.51	71.12	37.22	12.36
Length of spiral curve	135.00	1800.00	728.93	106.32
Tangent length (m)	121.00	2245.00	1253.28	185.21
Grade (%)	−5.40	5.00	0.63	2.57
Length of vertical grade (m)	160.00	1300.00	776.89	165.79
Lane number	4.00	8.00	6.75	0.93
Lane width (m)	3.50	3.75	3.70	0.12
Left shoulder width [hard/soft] (m)	[1.00/0.75]	[1.25/0.75]	[1.17/0.75]	[1.02/0]
Right shoulder width [hard/soft] (m)	[3.00/0.75]	[3.50/0.75]	[3.35/0.75]	[0.56/0]

of determination R^2, the significance of each predictor, and the logical explanation of the model

$$V = a \exp\left[bF_{(r200\,\mathrm{m})} + c\left(F_{(f250\,\mathrm{m})} - F_{(f100\,\mathrm{m})}\right)\right], \quad (6)$$

$$F_{(f250\,\mathrm{m})} = \left|\int_0^{250} f(l) \cdot dl\right|, \quad (7)$$

$$F_{(f100\,\mathrm{m})} = \left|\int_0^{100} f(l) \cdot dl\right|, \quad (8)$$

$$F_{(r200\,\mathrm{m})} = \left|\int_{-200}^{0} f(l) \cdot dl\right|, \quad (9)$$

where V is the operating speed on the current point; $f(l)$ represents the ACI function; $F_{(f250\,\mathrm{m})} - F_{(f100\,\mathrm{m})}$ is the ACI accumulated value in the influence range of front alignment; $F_{(r200\,\mathrm{m})}$ denotes the ACI accumulated value in the influence range of rear alignment; $F_{(f250\,\mathrm{m})}$, $F_{(f100\,\mathrm{m})}$, and $F_{(r200\,\mathrm{m})}$ can be calculated using (7), (8), and (9); a, b, and c are the coefficient; other parameters are introduced before.

3. Data Collection

Speed data were collected on Shenda Highway (eight-lane in two directions, design speed of 120 km/h), Shenshan Highway (six-lane in two directions, design speed of 120 km/h), and Shendan Highway (four-lane in two directions, design speed of 100 km/h, 80 km/h, and 60 km/h on different sites) for both directions in two time periods: from June to October 2013 and from March to May 2014, to establish prediction model. The testing data set used to validate the proposed model was collected on Taijiu Highway from April to May 2014.

The test sites consists of two types alignment combinations including 158 sections of a sag curve combined with a horizontal curve and 146 sections of a crest curve combined with a horizontal curve. In all cases, there exists a spiral transition between tangent and circular curve. The geometric design data were acquired from road alignment design documents. The data include radius of horizontal curve, deflection angle of horizontal curve, length of horizontal, vertical and spiral curve, grade, length of tangent, lane width, number of lane, shoulder width, and the milepost of each feature points. Table 1 summarizes the main geometric features of the test alignment.

There are several instruments for speed data collection, including Global Positioning System (GPS), radar gun, loop detector, video detection system, and infrared detector. By contrast with the features of each instruments, this study applied GPS devices placed on passenger cars and trucks to obtain the individual continuous operating speed profiles. Drivers were proved to be not biased by the presence of GPS device [32], and therefore the operating speed data collected in the test were reasonable to reflect the normal driving behavior. GPS also can provide high accuracy of the spatial coordinates with a frequency of 1 Hz. Therefore, it is possible to know the position and calculate the speed of each point.

The passenger cars or trucks which would travel through the observed sections were recruited in toll stations to participant this project. All the participants were informed that speed data would be used only for research purpose; thus they were free to select their speed according to their driving habits.

The experiments were carried out during daytime, off-peak periods, in sunny day, under free-flow conditions which are typically defined as having time headways of at least 5 or 6 s [18, 34], and on the condition of dry pavements. In the experiment, one test personnel sat in the rear of the car so as to record the nonfree flow conditions (i.e., car-following or lane-changing). In the further analysis, all the data influenced by the external factors were discarded in the data processing. More than 340 passenger cars and 287 trucks were investigated at each selected site, ensuring a minimum of 100 speed data of each type vehicle per direction at each point for operating speed estimation.

In order to explore the operating speed prediction models, the following speed data were processed subsequently based on the initial analysis of continuous speed profile of each vehicle and the reference of data collection position proposed by Gibreel et al. [21]:

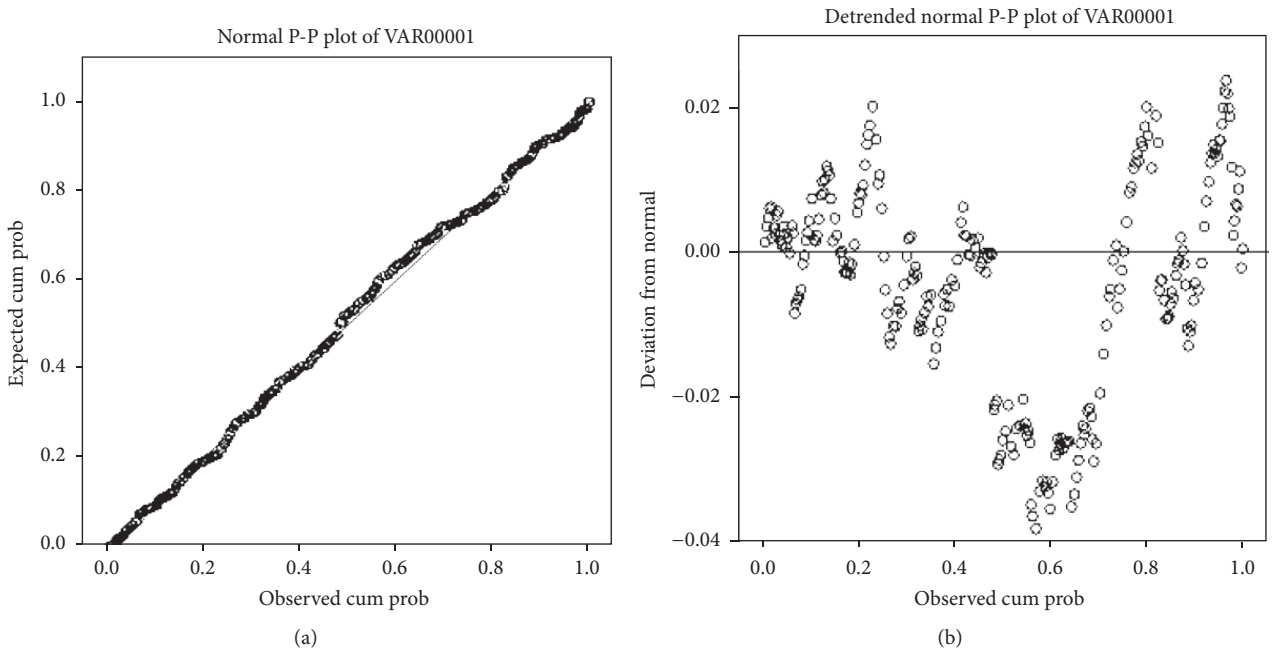

Figure 1: Normal probability plot of cars. (a) Cumulative probability distribution. (b) Deviation from Normal.

① Points were 0 m, 50 m, and 100 m on the approach tangent before the beginning of the spiral curve where drivers may change speed but not completely because of the effect of the 3D combination ahead.

② Point was the start point of a horizontal curve where drivers could finish the speed selection from a tangent to transition of a curve.

③ Points were the middle point of tangent, spiral curve, and horizontal curve.

④ Point was the end point of a horizontal curve and the beginning of spiral curve.

⑤ Points were 0 m, 50 m, and 100 m on the departure tangent after the end of spiral curve where drivers may select speed according to the transition from curve to tangent.

If the length of tangent is short, the processed points were reduced correspondingly. Furthermore, the 3σ statistical criterion [2] was used to check the homogeneity distribution around the mean and the maximum deviation of speed distribution equal to 3σ. Consequently, speed data from more than 2400 points were measured. Moreover, an important issue is to verify the speed distribution for each type site (i.e., tangent and curve) because it is found that speed distribution differed from the curve to the tangent [11].

The distribution characteristics of speed data are analyzed based on histogram features of overall frequency of speed sample. Normal, Weibull, Gamma, and Logistic distribution are applied to finish distribution fitting and frequency testing. Normal probability plot is applied to accomplish qualitative test and determine the preliminary distribution form. In Figure 1(a), the horizontal and vertical coordinates represent the theoretical and the actual cumulative probability, respectively. It can be seen that the data points in the graph coincide with the theoretical diagonal line. Figure 1(b) is the residual plot calculated based on normal distribution. The data are basically distributed over the horizontal line without regular fluctuations. This could be a hint that the data obey normal distribution. After using the Pearson's goodness fit test and Kolmogorov-Smirnov test, the tangents and curves are identified with Normal and Logistic distribution, respectively. Therefore, the operating speed that is 85th percentile speeds measured on 2400 points is available for further calculation.

4. Results Analysis and Discussion

4.1. Parameters Calibration and Sensitivity Analysis. First, according to the regulations of minimum and maximum radius of curve on highway, the influence weight in (1) is obtained. Second, the parameters in (2) are determined by using the limitations of grade in specification and influence ratio of grade on speed. Third, the coefficients in (3) are also fixed taking the reduction relation between pavement width and speed into consideration.

After repeated trial calculation and parameters calibration, the three-dimensional alignment comprehensive index description function is set up as follows:

$$f(l) = \left\{430 \cdot R^{-0.757} \exp\left[3000\mathrm{CCR} + 0.0005\mathrm{DF}\right]\right\} \cdot f_V + f_C, \tag{10}$$

$$f_V = 0.012 \cdot i \cdot |i| + 0.04 \cdot i + 1.0, \tag{11}$$

$$f_{\mathrm{CA}} = -28.57$$

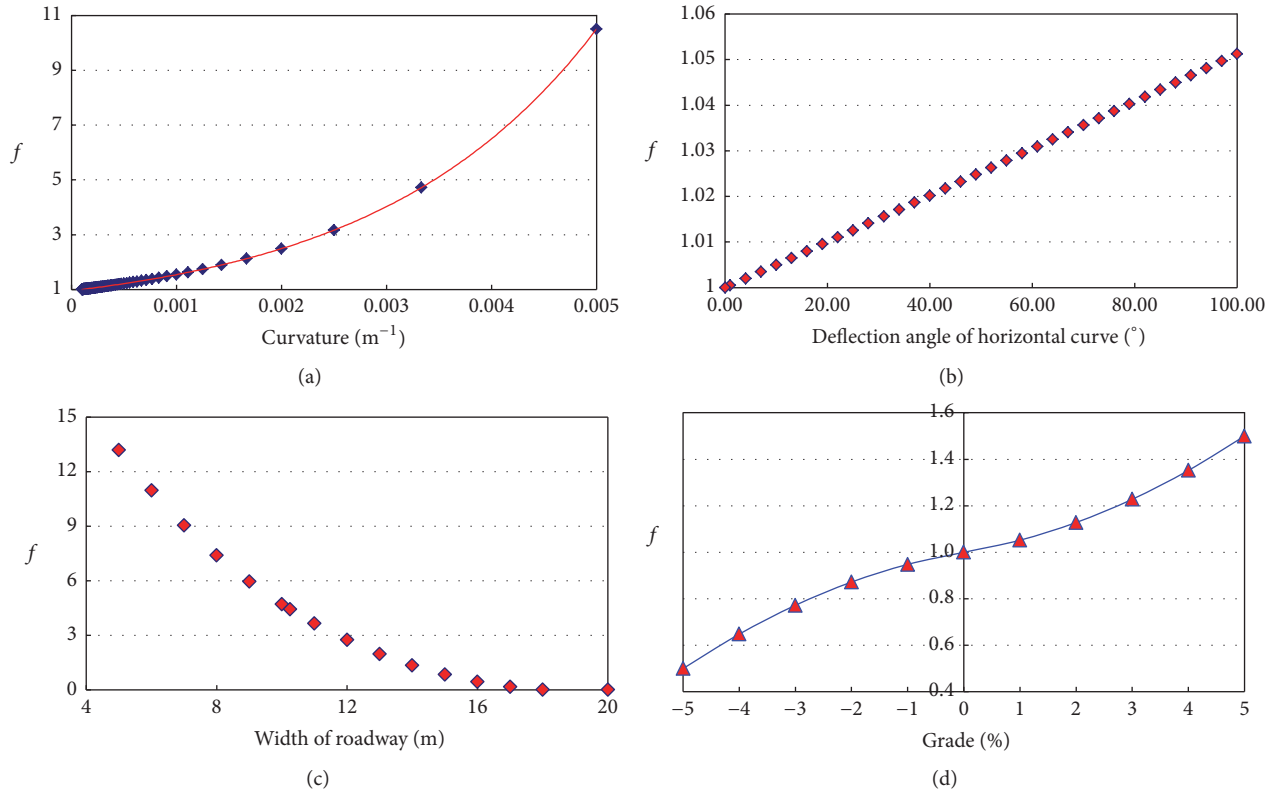

FIGURE 2: Relation between single index and f. (a) Curvature. (b) Deflection angle of horizontal curve. (c) Width of roadway. (d) Grade.

$$\cdot \ln\left(-0.00189 \cdot B^2 + 0.0719 \cdot B + 0.318\right) + \xi, \tag{12}$$

$$f_{CD} = -20.57 \cdot \ln\left(0.0078 \cdot B + 0.847\right) + \xi, \tag{13}$$

where f_{CA} and f_{CD} are the cross section alignment function for cars and trucks; the definitions of other parameters are the same as aforementioned.

In order to analyze the sensitivity of each index to f in the description model, a single key indicator is chosen as a variable. And then the other factors in the 3D ACI model are fixed. Thus, the variation of f with the single index can be seen in Figure 2.

It can be seen from Figure 2 that f on curves considerably increases with the increase in curvature. f is more sensitive to the curvature between 0.001 and 0.005 (i.e., radius is less than 1000 m). By contrast, f has little changes on curves with a curvature less than 0.001 (i.e., the radius is larger than 1000 m). It indicates that horizontal curve with radius of 4000 m or 5000 m already have very slight impact on driving which is close to the effect of tangent. Notably, deflection angle of horizontal curve and width of roadway markedly affects f.

Figure 2(d) shows f increases as a unilateral parabolic curve with the increase of grade. f has very obvious sensitivity to bigger grade because of the higher requirements of vehicle dynamic performance on uphill and acceleration behavior. However, the sensitivity of f is relatively weak with the grade ranging from −1% to 1%. In real driving, drivers' perceptions on such slope are usually not obvious.

Meanwhile, in order to further validate the sensitivity of ACI to alignment condition, K63 + 000–K83 + 000 and K63 + 300–K65 + 100 of Shendan Highway are selected to conduct relation analysis (Figures 3(a) and 3(b)). With (11), (12), and (13) substituted into (10), the ACI of this section can be obtained by using the actual alignment data.

From Figure 3(a), it can be seen that each point has different comprehensive index value as the alignment varies. In Figure 3(b), the number means the alignment combination type (i.e., 1: spiral curve, small grade; 2: spiral curve, small grade; 3: spiral curve, sag curve; 4: circular curve, sag curve; 5: circular curve, tangent grade; 6: circular curve, crest curve; 7: tangent, sag curve; 8: tangent, grade; 9: circular curve, large grade). For example, the road segment K63 + 314–K63 + 474 is located on the spiral curve and grade of 1.467%. The alignment comprehensive index gradually decreases while the curvature tends to be smaller. The segment K64 + 630–K64 + 854 is located on the tangent and crest curve. When grade becomes larger, the alignment comprehensive index increases slowly. Similarly, the segment after K64 + 854 is located on the tangent grade of 2% and the comprehensive index becomes stable and much smaller. It can be concluded that the results comply with consistence of the sensitivity analysis. In addition, we can see that, on the section with larger synthetic index, the variation of cumulative curve is also more obvious. This indicates that the alignment index

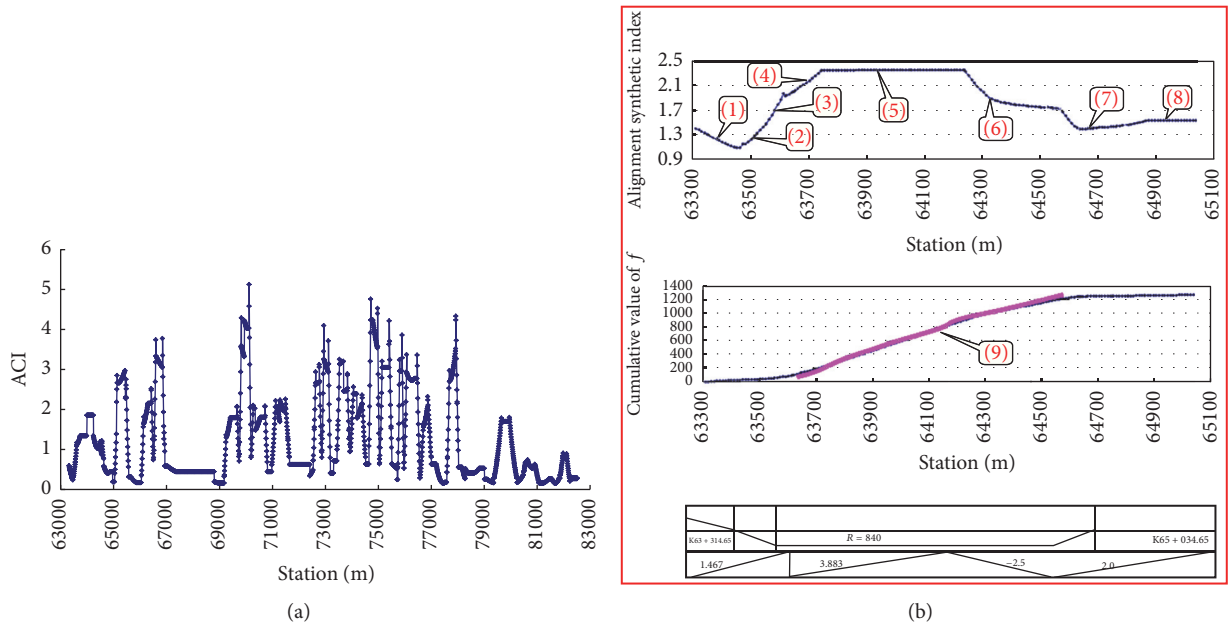

Figure 3: Alignment comprehensive index variations. (a) ACI at each point. (b) Distribution of cumulated alignment comprehensive index.

condition is good. On the contrary, the condition is poor. So the good corresponding relation among the alignment features, ACI, and ACI cumulative value can reflect the difference of alignment condition to a certain extent.

4.2. Establishment of Operating Speed Prediction Model. The alignment comprehensive indices are divided into two categories (i.e., I uphill and other indices and II downhill and other indices) due to the different influence degree of grade in vertical description model on operating speed.

Considering the point in integration theory, the cumulative value of the ACI in a certain length range using small spacing as a unit is equal to the integral of ACI in this length range. So during the calculation of the cumulative value of ACI, it can approximately take 1 m as a unit to calculate one ACI value and then to solve the accumulation value in a certain length range. It is worthy noting that the radius value is taken as 3000 on the tangent or on the curve with more than 3000 m radius since it may has little influence on driving behavior. Some operating speed data and the cumulative value of I alignment comprehensive index are shown in Table 2.

Through the analysis of operating speed variation with alignment index and coefficient calibration, the following operating speed prediction models which best fit the criteria of the regression analysis are established. The predicting speed for cars can be calculated by using (14) and (15). Accordingly, (16) are suitable for the speed estimation of trucks:

① Cars

$$V_{\mathrm{I,A}} = 141.03 \cdot \exp\left[-1.35 \times 10^{-4} \cdot \left(F_{(r200\,\mathrm{m})}\right) - 6.78 \times 10^{-5} \cdot \left(F_{(f250\,\mathrm{m})} - F_{(f100\,\mathrm{m})}\right)\right],$$
$$V_{\mathrm{II,A}} = 140.79 \cdot \exp\left[-9.44 \times 10^{-5} \cdot \left(F_{(r200\,\mathrm{m})}\right) - 1.07 \times 10^{-4} \cdot \left(F_{(f250\,\mathrm{m})} - F_{(f100\,\mathrm{m})}\right)\right]. \quad (14)$$

$$V_{\mathrm{I,A}} = 89.73 \cdot \exp\left[-1.42 \times 10^{-4} \cdot \left(F_{(r200\,\mathrm{m})}\right) - 1.24 \times 10^{-4} \cdot \left(F_{(f250\,\mathrm{m})} - F_{(f100\,\mathrm{m})}\right)\right],$$
$$V_{\mathrm{II,A}} = 89.26 \cdot \exp\left[-1.20 \times 10^{-4} \cdot \left(F_{(r200\,\mathrm{m})}\right) - 1.41 \times 10^{-4} \cdot \left(F_{(f250\,\mathrm{m})} - F_{(f100\,\mathrm{m})}\right)\right]. \quad (15)$$

② Trucks

$$V_{\mathrm{I,D}} = 89.73 \cdot \exp\left[-1.42 \times 10^{-4} \cdot \left(F_{(r200\,\mathrm{m})}\right) - 1.24 \times 10^{-4} \cdot \left(F_{(f250\,\mathrm{m})} - F_{(f100\,\mathrm{m})}\right)\right],$$
$$V_{\mathrm{II,D}} = 89.26 \cdot \exp\left[-1.20 \times 10^{-4} \cdot \left(F_{(r200\,\mathrm{m})}\right) - 1.41 \times 10^{-4} \cdot \left(F_{(f250\,\mathrm{m})} - F_{(f100\,\mathrm{m})}\right)\right]. \quad (16)$$

4.3. Validation of Effectiveness. Four statistical validation indicators are applied to evaluate the effectiveness of prediction model including Goodness of Fit test, F-test, Residual analysis, and t-test. The test results of I operating speed prediction model (see (14)) for cars as an example are listed at Table 3 and Figure 4.

In [34], the correlation coefficient R^2 between predicted average speed and variables including length of the horizontal curve, radius of the horizontal curve, and local longitudinal grade is 0.63. In [35], the correlation coefficient R^2 between predicted average speed and variables including averaged curvature, average of grade for upgrades, and average of grade for downgrades is 0.625. R^2 in this study is about 0.6523, which shows the relationship between ACI and speed is related when the great amount of data processed is taken into account. It is also indicated that the significance of model is good due to significance F much smaller than significant level of 0.05. The regression coefficients of the variables in the model are, respectively, 4.949, −0.00013, and −0.000068. This finding illustrates that variables pass the significance test. In addition, the facts that the points on the residual analysis

Table 2: Test data for cars.

Milepost	Grade (%)	$F_{(r200\,\mathrm{m})}$	$F_{(f250\,\mathrm{m})} - F_{(f100\,\mathrm{m})}$	Operating speed (km/h)
K65 + 985	1.47	1106.47	1252.86	111.82
K66 + 049	1.47	1103.77	1354.53	108.15
K66 + 095	1.97	1125.53	1393.17	114.22
K66 + 139	2.61	1228.09	1419.28	109.14
K66 + 281	4.64	1705.29	1203.53	110.35
K66 + 423	4.90	1890.35	1488.18	98.94
K66 + 465	4.90	1878.74	1617.33	98.76
K66 + 513	4.90	1740.86	1624.97	92.63
K69 + 105	1.09	1099.20	1162.30	113.32
K69 + 263	2.42	1191.36	1330.58	113.03
K69 + 565	5.00	1778.82	1160.20	106.55
K69 + 664	5.00	1790.49	1554.80	101.46
K69 + 752	5.00	1646.05	1626.90	97.16
K69 + 829	4.68	1642.82	1585.98	99.02
K69 + 900	4.20	1817.33	1556.34	96.14
K69 + 974	3.71	2129.76	1276.69	92.91
K70 + 119	3.40	2114.19	1183.25	94.90
K76 + 370	1.50	1866.46	1056.80	103.44
K76 + 469	1.50	1908.52	981.25	105.93
K76 + 575	1.17	1718.65	1112.75	108.10
K76 + 645	0.01	1456.53	1062.38	104.18
K77 + 555	1.62	1090.20	1346.95	110.63
K77 + 592	1.62	1096.66	1336.88	112.39
K79 + 366	1.39	1112.55	1061.81	114.87
K79 + 657	0.60	1450.03	1240.57	110.63
K79 + 725	0.60	1570.39	1240.58	105.58
K79 + 808	0.60	1644.95	1196.11	106.98
K79 + 885	0.60	1654.10	1087.42	109.76
K79 + 959	0.60	1654.24	952.85	107.44

Table 3: Statistical test of speed prediction model.

Goodness of fit test						
Multiple R				0.8077		
R square				0.6523		
Adjusted R square				0.6330		
Standard error				0.0362		
Observed value				39		
F-test						
	df	SS	MS	F	Significance F	
Regression analysis	2	0.0887	0.0444	33.7746	$5.51E-09$	
Residual	36	0.0473	0.0013			
Total	38	0.1360				
t-test						
	Coefficients	Standard error	t stat	P value	Low limit	Upper limit
Intercept	4.9490	0.0381	129.9758	$1.04E-49$	4.8718	5.0262
X variable 1	−0.0001	$1.86E-05$	−7.2385	$1.6E-08$	−0.0002	$-9.7E-05$
X variable 2	$-6.8E-05$	$2.46E-05$	−2.75481	0.0092	−0.0001	$-1.8E-05$

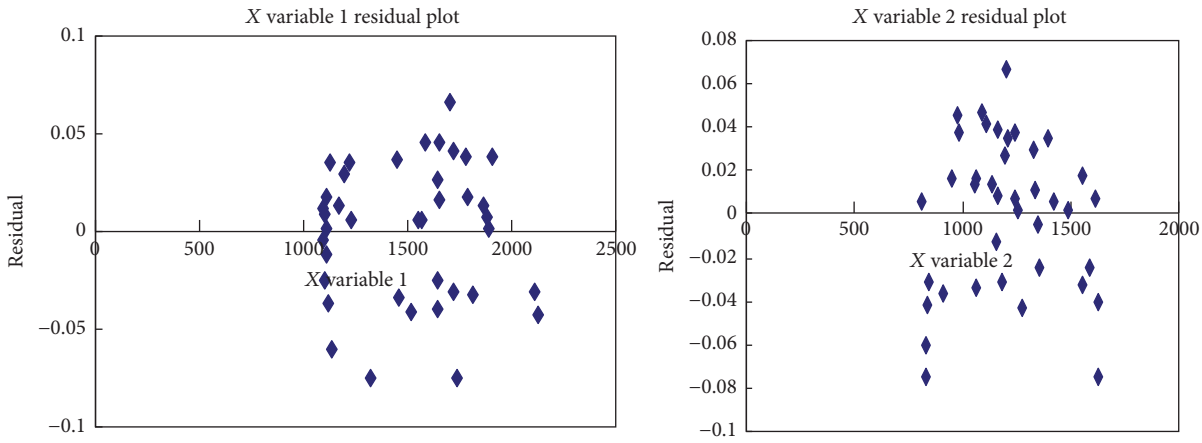

Figure 4: Residual analysis.

plot distribute on both side of x axis and the residual value is located between −2 and 2 present that the regression equation can better reflect the rules. For other models, testing results also demonstrate the effectiveness of proposed method.

In the following section, the results of the proposed prediction models are compared with the models proposed by Morris and Donnell [29] and the speed models recommended in Guidelines for Safety Audit of Highway (GSAH) (JTG/T B05-2004) [47] which is the only national profession standard for operating speed prediction and alignment consistency evaluation in China. Three common criteria are used to evaluate the prediction performance of different models: mean absolute error (MAE), root mean square error (RMSE), and mean absolute relative error (MARE). Moreover, the standard deviation (SD) is also used as the evaluation indicator. The four indicators are defined in (17), (18), (19), and (20):

$$\text{MAE} = \frac{1}{n}\sum_{i=1}^{n}\left|t_i - \widehat{t}_i\right|, \tag{17}$$

$$\text{RMSE} = \sqrt{\frac{1}{n}\sum_{i=1}^{n}\left(t_i - \widehat{t}_i\right)^2}, \tag{18}$$

$$\text{MARE}\,(\%) = \frac{1}{n}\sum_{i=1}^{n}\frac{\left|t_i - \widehat{t}_i\right|}{t_i} \times 100, \tag{19}$$

$$\text{SD} = \sqrt{\frac{1}{n}\sum_{i=1}^{n}\left(\widehat{t}_i - \overline{t}_i\right)^2}, \tag{20}$$

where n is the number of testing points, t_i and $\overline{t_i}$ denote the actual observed values and mean values of operating speed, respectively, and $\widehat{t_i}$ represents the predicting values of operating speed.

To consider different position of operating speed according to the GSAH model and proposed models in this paper, we finally compare the prediction results of three models at 480 points on 3D alignment with length of 12 km. From Table 4, it is indicated that the estimation errors for other two models which are calculated by using (17) through (20) are generally higher than those for the proposed models. Some comparison results of actual test speed data and prediction data are shown in Figure 5. Thus, the prediction models introduced in this study obviously outperform the GSAH models and Morris's models for its higher accuracy.

With respect to the consideration of vehicle dynamic properties into the model, operating speed on a current section is the result of cumulative speed change of the rear-traveled sections. The speed differences existing between the front and rear sections are induced by the acceleration and deceleration of a vehicle. Thus, the influence range of rear alignment can be approximately characterized by the acceleration and deceleration distance which is related to vehicle dynamic properties. Based on each vehicle trajectory and recommended deceleration rate, the influence range of the rear alignment can be determined as 200 m.

The related researches on how to quantify driver's visual information to a digital index are lacking. The deceleration rate of vehicles in China has significant differences from that in worldwide. At the same time, the influence range of rear alignment is also determined based on data analysis. Thus, we did not discuss more about these two considerations. In the case study, the other two models did not consider the influence of visual characteristics and vehicle dynamics; they just establish the relation between operating speed and alignment indexes. We think that the comparison results may reflect the accuracy of our model with these considerations.

5. Conclusions

One significant limitation in previous research work on highway alignment design consistency is that the existing operating speed prediction models are established mainly on 2D alignment or single index. Particularly when the road is characterized by different alignment combinations, the models may be inaccurate. Only some feature points, such as the middle point of a horizontal curve or the end point of a grade can be predicted correspondingly. Therefore, the

Table 4: Comparison results of three models.

Vehicle type	Criteria	Estimation methods		
		Proposed model	GSAH	Morris
Cars	MAE	2.69	4.45	10.29
	RMSE	3.54	6.03	13.67
	MARE (%)	4.38	6.98	10.28
	SD	10.7	15.32	18.21
Trucks	MAE	3.57	6.89	16.32
	RMSE	7.10	10.22	21.04
	MARE (%)	4.93	6.34	15.39
	SD	8.85	14.17	17.33

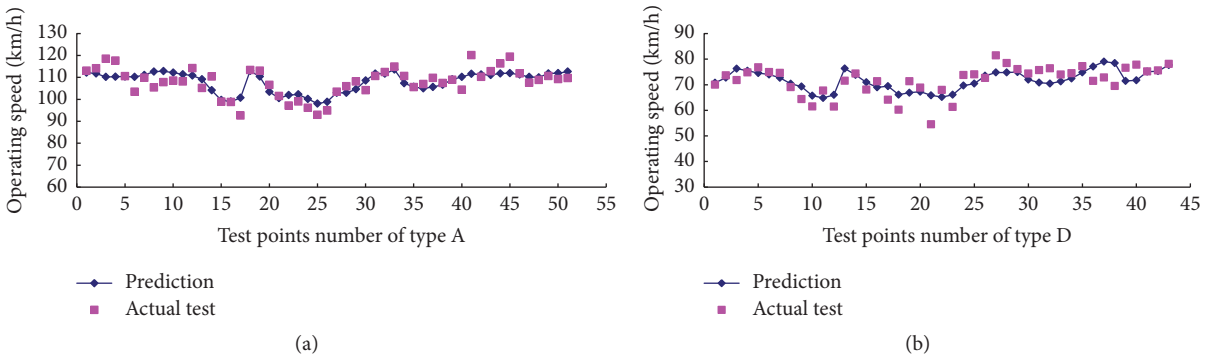

Figure 5: Comparison between predicted speed and actual speed. (a) Comparison for cars. (b) Comparison for trucks.

speed variation of passenger cars and trucks along each point of the road is studied using the actual test data and alignment indices.

The achievements of this study are twofold. The first one is the three-dimensional alignment comprehensive index description functions. These functions select curvature, change rate of curvature, curve angle, grade, and lane width as variables rather than a single index. Based on the principle of spatial geometry and the design characteristics of road alignment, the alignment description model is established by taking the horizontal and vertical indices as the primary models and the cross-sectional index as the correction model. The second process is to set up the relationship between alignment comprehensive index and operating speed for continuous prediction. During the establishment of this model, the visual requirement of driver and the different features of acceleration and deceleration of vehicles are also considered. This modeling procedure makes it possible to predict a reliable and continuous operating speed profile at each point along the alignment and to significantly improve the performance of consistency alignment design and safety evaluations. The prediction performance of the proposed model demonstrates its higher accuracy when compared with other models using the actual observed data.

Owing to the test data mainly collected on highways (bidirectional four to eight lanes) in plain area in China, the models reported in the paper can be used to predict continuous operating speed for passenger cars and trucks on the condition of three-dimensional alignment indexes along roadway which can be obtained. However, the models cannot predict the operating speeds in mountainous area or other type roads accurately. Application of the model outside China would require a new calibration based on local speed surveys because of the differences in driver behavior, roadway systems, and vehicle performances. Although design speed and speed limit have effect on operating speed to some extent, these factors are not considered in models. Substantially, highway alignment is a three-dimensional curve in Euclidean space. The interaction mechanism of multiple alignment indices on speed is very complicated. Hence, the methods of alignment comprehensive modeling are required further study. With the development of automotive technology, fusion of data collected from mobile and fixed sensors [48], and the improvement of road conditions, results of the prediction model may deviate from the actual values; thus, the model can be further examined, updated, and improved. Future efforts should focus on these factors in order to explore more efficient models.

Conflicts of Interest

The authors declare that there are no conflicts of interest regarding the publication of this paper.

Acknowledgments

The project is supported by National Natural Science Foundation of China (51308059 and 71701215), China Postdoctoral

Science Foundation (2015M581585), the Special Fund for Basic Scientific Research of Central Colleges, Chang'an University (310822152007), and Western Transportation Science and Technology Project of Ministry of Communications (2012318361110).

References

[1] F. Russo, S. A. Biancardo, and M. Busiello, "Operating speed as a key factor in studying the driver behaviour in a rural context," *Transport*, vol. 31, no. 2, pp. 260–270, 2016.

[2] G. Dell'acqua, M. Busiello, and F. Russo, "Safety data analysis to evaluate highway alignment consistency," *Transportation Research Record*, no. 2349, pp. 121–128, 2013.

[3] J. L. Ottesen and R. A. Krammes, "Speed-profile model for a design-consistency evaluation procedure in the United States," *Transportation Research Record: Journal of the Transportation Research Board*, no. 1701, pp. 76–85, 2000.

[4] N. J. Garber, "The effect of speed, flow, and geometric characteristics on crash rates for different types of Virginia highways," *Virginia Transportation Research Council*, vol. 1, pp. 10–15, 2000.

[5] German Road and Transportation Research Association, *Guidelines for the Design of Roads*, Berlin, 1984.

[6] J. Morrall and R. J. Talarico, "Side friction demanded and margins of safety on horizontal curves," *Transportation Research Record: Journal of the Transportation Research Board*, pp. 145–152, 1994.

[7] Transportation of Ontario, *Ontario Traffic Manual Book 7: Temporary Conditions*, Ontario, 2014.

[8] Turner-Fairbank Highway Research Center.: Interactive Highway Safety Design Model, Federal Highway Administration, Mclean, 2003.

[9] R. Lamm, E. M. Choueiri, J. C. Hayward, and A. Paluri, "Possible design procedure to promote design consistency in highway geometric design on two-lane rural roads," *Transportation Research Record*, no. 1195, pp. 111–122, 1988.

[10] M. N. Islam and P. N. Seneviratne, "Evaluation of design consistency of two-lane rural highways," *Journal of Transportation of the Institute of Transportation Engineers*, vol. 64, no. 2, pp. 28–31, 1994.

[11] J. McFadden and L. Elefteriadou, "Evaluating horizontal alignment design consistency of two-lane rural highways: development of new procedure," *Transportation Research Record*, no. 1737, pp. 9–17, 2000.

[12] R. A. Krammes et al., *HorizoNtal Alignment Design Consistency for Rural Two-Lane Highways*, Federal Highway Administration, 1994.

[13] A. Bucchi, K. Biasuzzi, and A. Simone, "Evaluation of design consistency: a new operating speed model for rural roads on grades," *Transportation Research Record: Journal of the Transportation Research Board*, vol. 1701, pp. 76–85, 2005.

[14] J. Tang, F. Liu, Y. Zou, W. Zhang, and Y. Wang, "An Improved Fuzzy Neural Network for Traffic Speed Prediction Considering Periodic Characteristic," *IEEE Transactions on Intelligent Transportation Systems*, 2017.

[15] P. Perco, "Influence of the general character of horizontal alignment on operating speed of two-lane rural roads," *Transportation Research Record*, no. 2075, pp. 16–23, 2008.

[16] A. A. Abdul-Mawjoud and G. G. Sofia, "Development of models for predicting speed on horizontal curves for two-lane rural highways," *Arabian Journal for Science and Engineering*, vol. 33, no. 2 B, pp. 365–377, 2008.

[17] Y. Yan, S. Zhang, J. Tang, and X. Wang, "Understanding characteristics in multivariate traffic flow time series from complex network structure," *Physica A: Statistical Mechanics and its Applications*, vol. 477, pp. 149–160, 2017.

[18] K. Fitzpatrick, *Design Speed, Operating Speed, and Posted Speed Practices*, Transportation Research Board, 2003.

[19] D. R. Jessen, K. S. Schurr, P. T. McCoy, G. Pesti, and R. R. Huff, "Operating speed prediction on crest vertical curves of rural two-lane highways in Nebraska," *Transportation Research Record: Journal of the Transportation Research Board*, no. 1751, pp. 67–75, 2001.

[20] D. B. Fambro, K. Fitzpatrick, and C. W. Russell, "Operating speed on crest vertical curves with limited stopping sight distance," *Transportation Research Record: Journal of the Transportation Research Board*, no. 1701, pp. 25–31, 2000.

[21] G. M. Gibreel, S. M. Easa, and I. A. El-Dimeery, "Prediction of operating speed on three-dimensional highway alignments," *Journal of Transportation Engineering*, vol. 127, no. 1, pp. 21–30, 2001.

[22] E. M. Choueiri, R. Lamm, J. H. Kloeckner, and T. Mailaender, "Safety aspects of individual design elements and their interactions on two-lane highways: international perspective," *Transportation Research Record*, no. 1445, pp. 34–46, 1994.

[23] J. Tang, F. Liu, W. Zhang, R. Ke, and Y. Zou, "Lane-changes prediction based on adaptive fuzzy neural network," *Expert Systems with Applications*, vol. 91, pp. 452–463, 2018.

[24] H. Gong and N. Stamatiadis, "Operating speed prediction models for horizontal curves on rural four-lane highways," *Transportation Research Record*, no. 2075, pp. 1–7, 2008.

[25] X. H. Li and Z. K. Yao, "Vehicle fuel consumption prediction model," *Journal of Tongji University*, vol. 20, no. 4, pp. 403–410, 1992.

[26] A. Calvi and F. Bella, "Modeling speed differential parameters in day and night environments using driving simulator," in *Proceedings of the 2014 9th International Symposium on Safety Science and Technology, ISSST 2014*, pp. 648–661, China, November 2014.

[27] A. M. Semeida, "Application of artificial neural networks for operating speed prediction at horizontal curves: a case study in Egypt," *Journal of Modern Transportation*, vol. 22, no. 1, pp. 20–29, 2014.

[28] E. T. Donnell, Y. Ni, M. Adolini, and L. Elefteriadou, "Speed prediction models for trucks on two-lane rural highways," *Transportation Research Record*, no. 1751, pp. 44–55, 2001.

[29] C. M. Morris and E. T. Donnell, "Passenger car and truck operating speed models on multilane highways with combinations of horizontal curves and steep grades," *Journal of Transportation Engineering*, vol. 140, no. 11, Article ID 04014058, 2014.

[30] J. E. Leisch and J. P. Leisch, "New concepts in design-speed application," *Transportation Research Record*, no. 631, pp. 15–23, 1977.

[31] A. Montella, F. Galante, F. Mauriello, and M. Aria, "Continuous speed profiles to investigate srivers' behavior on two-lane rural highways," *Transportation Research Record*, vol. 2521, pp. 3–11, 2015.

[32] Transportation Research Board (TRB), *Modeling operating speed. Synthesis report. Transportation Research Circular Number E-C151*, Transportation Research Board, Washington, D.C., 2011.

[33] A. M. P. Zuriaga, A. G. García, F. J. C. Torregrosa, and P. D'Attoma, "Modeling operating speed and deceleration on two-lane rural roads with global positioning system data," *Transportation Research Record*, no. 2171, pp. 11–20, 2010.

[34] F. Bella, A. Calvi, and P. D'Attoma, "Operating speed prediction for Italian two-lane rural roads using speed profiles from GPS data," in *Proceedings of the 4th road safety and simulation international conference*, Rome, 2013.

[35] S. Cafiso and G. Cerni, "New approach to defining continuous speed profile models for two-lane rural roads," *Transportation Research Record*, no. 2309, pp. 157–167, 2012.

[36] G. Reymond, A. Kemeny, J. Droulez, and A. Berthoz, "Role of lateral acceleration in curve driving: Driver model and experiments on a real vehicle and a driving simulator," *Human Factors: The Journal of the Human Factors and Ergonomics Society*, vol. 43, no. 3, pp. 483–495, 2001.

[37] D. W. Harwood, A. D. May, and I. B. Anderson, "Capacity and quality of service of two-Lane highways," *Transportation Research Board of the National Academies*, 1999.

[38] F. S. Mertzanis and V. J. Hatzi, "Model for sight distance calculation and three-dimensional alignment evaluation in divided and undivided highways," in *Proceedings of the 3rd international conference on road safety and simulation*, Indianapolis, 2011.

[39] T. Kim and H. Michael Zhang, "Interrelations of reaction time, driver sensitivity, and time headway in congested traffic," *Transportation Research Record*, no. 2249, pp. 52–61, 2011.

[40] TRB, *Highway Capacity Manual*, Transportation research board of the national academies, 2010.

[41] A. W. Inhoff, M. S. Solomon, B. A. Seymour, and R. Radach, "Eye position changes during reading fixations are spatially selective," *Vision Research*, vol. 48, no. 8, pp. 1027–1039, 2008.

[42] S. M. Easa and W. He, "Modeling driver visual demand on three-dimensional highway alignments," *Journal of Transportation Engineering*, vol. 132, no. 5, pp. 357–365, 2006.

[43] "JTG B01-2014: Technical Standard of Highway Engineering, 2015".

[44] A. M. Pérez-Zuriaga, F. J. Camacho-Torregrosa, and A. García, "Tangent-to-curve transition on two-lane rural roads based on continuous speed profiles," *Journal of Transportation Engineering*, vol. 139, no. 11, pp. 1048–1057, 2013.

[45] K. Fitzpatrick, L. Elefteriadou, D. Harwood et al., *Speed Prediction for Two-Lane Rural Highways*, FHWA, U.S. Department of Transportation, 2000.

[46] Y. Yan and Z. Y. Guo, *Alignment Consistency Evaluation Based on Operating Speed Prediction Models*, Tongji University, Shanghai Shi, China, 2009.

[47] H. T. Zhou, C. H. Yang, Z. Y. Guo et al., *Guidelines for Safety Audit of Highway*, JTG/T B05-2004, Ministry of Communications of the People's Republic of China, China, 2004.

[48] S. Zhang, J. Tang, H. Wang, Y. Wang, and S. An, "Revealing intra-urban travel patterns and service ranges from taxi trajectories," *Journal of Transport Geography*, vol. 61, pp. 72–86, 2017.

Hindawi
Journal of Advanced Transportation
Volume 2017, Article ID 5783696, 10 pages
https://doi.org/10.1155/2017/5783696

Research Article

Analyzing Traffic Crash Severity in Work Zones under Different Light Conditions

Xinxin Wei,[1] Xiang Shu,[2] Baoshan Huang,[2] Edward L. Taylor,[3] and Huaxin Chen[1]

[1]*School of Materials Science and Engineering, Chang'an University, Xi'an, Shaanxi 710061, China*
[2]*Department of Civil and Environmental Engineering, University of Tennessee, Knoxville, TN 37996, USA*
[3]*Construction Industry Research & Policy Center, Haslam College of Business, University of Tennessee, Knoxville, TN 37996, USA*

Correspondence should be addressed to Xiang Shu; xshu@utk.edu and Huaxin Chen; chx92070@163.com

Received 6 March 2017; Revised 24 July 2017; Accepted 12 September 2017; Published 4 December 2017

Academic Editor: Helai Huang

Previous studies have investigated various factors that contribute to the severity of work zone crashes. However, little has been done on the specific effects of light conditions. Using the data from the Enhanced Tennessee Roadway Information Management System (E-TRIMS), crashes that occurred in the Tennessee work zones during 2003–2015 are categorized into three light conditions: daylight, dark-lighted, and dark-not-lighted. One commonly used decision tree method—Classification and Regression Trees (CART)—is adopted to investigate the factors contributing to crash severity in highway work zones under these light conditions. The outcomes from the three decision trees with differing light conditions show significant differences in the ranking and importance of the factors considered in the study, thereby indicating the necessity of examining traffic crashes according to light conditions. By separately considering the crash characteristics under different light conditions, some new findings are obtained from this study. The study shows that an increase in the number of lanes increases the crash severity level in work zones during the day while decreasing the severity at night. Similarly, drugs and alcohol are found to increase the severity level significantly under the dark-not-lighted condition, while they have a limited influence under daylight and dark-lighted conditions.

1. Introduction

Work zones have been an important research topic because they have a substantial effect on a nation's economy and traffic flow. Statistics show the economic cost of a fatal crash was $1,398,916 in 2010 in the United States [1]. Based on this estimate, the annual cost of work zone fatalities is more than seven billion dollars per year. Moreover, considering the 26,000 nonfatal injury crashes and 60,000 property–damage-only (PDO) crashes that occur in work zones, additional billions of dollars of economic damage occur annually. At this time, the number of work zones is increasing. During peak construction season, approximately 20% of highway system is under construction and motorists may encounter a work zone every 100 miles [2].

To reduce adverse traffic impacts on the public, more and more work zones require night construction. An extensive survey conducted of 175 work zones in 13 states revealed that 58% of the work zones involved mostly daylight construction, 33% involved primarily night work, and the remaining 9% were active day and night [3]. This has raised concerns about whether work zones have influenced traffic safety at night.

Previous studies have found the night crash rate was higher than daylight crash rate in work zones [4–6]. Arditi et al. [7] used Illinois fatality crashes from work zones to investigate safety differences between night and daylight construction in the period 1996–2011, showing that night work zones were more hazardous. In one study, crash rates per million vehicle miles were higher in night work zones by 67 to 156 percent [8]. The differences in crash rate between day and night work zones suggest that both should be examined separately in varying light conditions. Although there is a consensus that the night crash rate has improved, there is debate about improvement in night crash severity.

Knowing crash risk factors is a key to create safe work zones. With more night work zones and the evident differences between day and night work zone crashes, there is an urgent need to investigate work zone crashes under different

light conditions and little research has been undertaken on this topic.

Severity is considered the most important crash outcome and is the core of this paper. This study analyzes crash injury severity in work zones with respect to its inherent casualties and not frequency. A decision tree method is used to model the severity of traffic accidents using available risk factors. Unlike most of the previous studies, in which light condition was treated as a single contributing factor, this study divides light conditions into three categories: daylight, dark-lighted, and dark-not-lighted. Three decision trees are built to reveal the relationship between crash severity and different contributing factors under differing light conditions in work zones.

2. Literature Review

2.1. Effects of Light Condition on Crashes. Light condition is a significant factor affecting traffic crashes. Previous studies have confirmed that adverse light conditions may increase both crash frequency and severity [4–6]. In fact, Gray et al. [4], Abdel-Aty [5], and Huang et al. [6] all reported that injury severity increases during darkness. Pande and Abdel-Aty [9] concluded that there is a significant correlation between lack of illumination and high crash severity. de Oña et al. [10, 11] pointed out that fatal accidents are associated with roadways with no lighting. Wanvik [12] found that good road lighting can decrease road accidents by one-half based upon a study of 763,000 injury accidents and 3.3 million property-damage accidents in Norway. Some studies (e.g., [13]) found that drivers are less likely to be injured in a construction work zone under darkness (with good illumination) than under daylight conditions. Moreover, researchers found that crash prediction models can reveal detailed information about contributing factors [14–16]. For example, Ullman et al. [17] found that some contributing factors are significant in a daytime crash rate model (e.g., low speed limit and the number of entering ramps per lane per mile), while others become significant in a nighttime model (e.g., snow and percentage of trucks). In summary, light condition has an important effect on traffic crashes but little has been done to explore the relationship between work zone crash severity and its contributing factors. More research efforts are needed in this area.

2.2. Decision Tree Method. Crash models are used to investigate the effects of risk factors on crashes in work zones. Regression models (such as logit and probit) have been widely employed [18–21]. In regression models, binary or multiple levels of severity are typically set as dependent variables and the risk factors affecting severity as independent variables. A common assumption for regression models is that there is no dependency among the risk factors. In addition, regression models need to assume a specific functional form to model the relationships between dependent and independent variables. Therefore, use of regression models is limited if the assumptions do not hold well [22].

In order to overcome the limitations of regression models, classification models using data-mining approaches have been applied to the risk factor analysis problem. Typically, severity level is set as a class variable and risk factors as feature variables [22–26]. The decision tree classifier is one classification model, and the three commonly used decision tree methods are Classification and Regression Trees (CART), the Iterative Dichotomiser 3 (ID3) algorithm [27], and the C4.5 algorithm [28]. The CART method [29] uses a split criterion based on the Gini Index. Quinlan's method uses Information Gain (IG) as a split criterion based on the entropy measure on probabilities [30]. Subsequently Quinlan [31] also presented the algorithm C4.5, which is an advanced version of ID3 with a split criterion, called the Information Gain Ratio (IGR), similar to the one used in the ID3 procedure that penalizes variables with many states. Among these methods, CART is the most widely used [25, 28, 32–36]. It should be noted, however, that compared to conventional statistical models, CART still has its limitations such as simplicity and difficulty in interpreting. Nonetheless, previous studies have confirmed that the CART algorithm can be adopted in crash severity analyses and provide a more precise result compared with other prediction models [34].

3. Method

From the above discussion, many modeling approaches have been used to investigate the effects of risk factors on crashes in work zones. Different modeling approaches have different advantages and disadvantages. In this study, the decision tree method is selected and the CART algorithm is used to generate a decision tree. The split criterion in the CART method is based on gini, which represents the diversity of a factor, and is calculated as follows:

$$\text{gini} = 1 - \sum_{i}^{n} p_i^2, \tag{1}$$

where i is the category of the target (injury or PDO), n is the total number of targets, and p is the percentage of injury or PDO. Since CART is a binary tree here, our total number of targets is two.

Gini is used to calculate the diversity of the beginning node, while the Ginidex is created to measure the heterogeneity of the following node. For each node, the Ginidex is calculated as follows:

$$\text{Ginidex}(x) = \sum_{j}^{n} p_{xij} \text{gini}\left(x_{ij}\right), \tag{2}$$

where x is the contributing factor like lane number and x_{ij} means the severity i of character j. For instance, i can be injury or PDO and j may represent lane number >2 or <2. Finally p_{xij} represents the percentage of x_{ij}.

In order to determine the next split node, the category with the largest diversity improvement is chosen:

$$\text{Maxnode} = \text{Max}\left\{\text{gini}_{\text{parent}} - \text{Ginidex}(x = i)_{\text{childi}}\right\}, \tag{3}$$

where $\text{gini}_{\text{parent}}$ is the gini of higher layer and Ginidex is the index of second layer. Then this process is repeated several

times until the improvement equals 0 or reaches the maximum level. Since large trees could lead to higher percentage of misclassification [22], decision trees with different layers are tried in this study. When a decision tree with two layers is built, it presents less information. When a four-layer tree is built, it appears that many nodes in the fourth layer contain less than 1% of the total crashes. According to previous research [28], if one node contains less than 1% of samples, the results are not reliable. Therefore, three layers are chosen as the maximum depth for a decision tree in this study.

One of the major advantages of decision tree analysis is the decision rule. Decision rules have logical structure like "If A, then B". While regression models show the impact of single factors, a decision tree can show the effect produced by a combination of several factors. In this study, decision rules are inferred when injury rate > 50%, or PDO rate > 80% and the population on that node > 1%. This is because the overall injury rate is approximately 20%–30%, and injury rates above 50% are extreme.

In order to feel confident of the results, the data used in this study are divided into two subsets: 70% of the data is used for training the model, while the remaining 30% is used for validation. The accuracy can be calculated as follows:

$$\text{Percentage Correct} = \frac{\sum_{i=1}^{n} \text{TP}_i}{\sum_{i=1}^{n} \text{TP}_i + \text{FN}_i} * 100, \quad (4)$$

where TP_i is true positive and FN_i is false negative.

In addition, the CART algorithm can also calculate the importance of each factor based on the improvement in Ginidex. The Importance Index (IM) is defined as follows:

$$\text{IM}\left(x_j\right) = \sum_{t=1}^{T} \frac{n_t}{N} \Delta\text{Ginidex}_{jt}, \quad (5)$$

where x_j is a variable, $\Delta\text{Ginidex}_{jt}$ is the reduction in Ginidex, n_t is the number of the observations in the dataset that belong to node t, T is the total number of nodes, and N is the total number of observations. The detailed calculation method and principles can be found in Montella et al. [25], Chang and Chien [35], and J. S. Lee and E. S. Lee [37].

4. Data

The data from the Enhanced Tennessee Roadway Information Management System (E-TRIMS) is used in the study. The crashes that happened in the work zones during 2003–2015 are used. There are five variables describing light conditions in the database including daylight, dark-lighted, dark-not-lighted, dusk, and dawn. The light conditions are based on the fixed streetlights in this study. Since the numbers of crashes under dusk and dawn conditions are relatively small (279 and 215, resp.), these data are excluded. Thus, a total number of 19941 crashes are analyzed. The class variable of the study is accident severity. The injury severity analyzed in the study includes that of drivers, passengers, and pedestrians.

When analyzing injury risk factors, it is desirable to include as many injury severity levels as possible because different factors may have different effects on the injury levels. However, among the 19941 crashes used in the study, fatal crashes only account for less than 1%. The number of fatal crashes is not high enough to conduct a reliable analysis. Therefore, several severity levels including fatal, incapacitating, and slight injuries are combined into a single injury level. Similar to previous studies [22], two levels of injury severity are used in the study: injury and property-damage-only (PDO). PDO refers to a crash where no one was injured but only the vehicle was damaged. Figure 1 shows the crash data according to two severity levels and three light conditions.

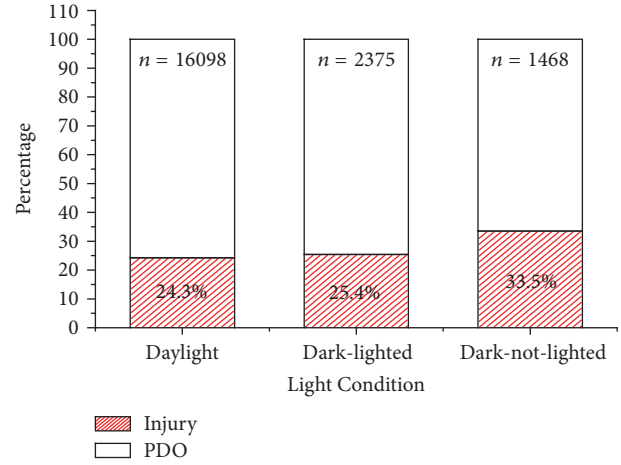

Figure 1: Crash severity distribution under different light conditions.

As demonstrated in Figure 1, the injury rate increases when light conditions worsen (24.3% < 25.4% < 33.5%). It can be seen that crashes under limited light conditions were more severe than those under dark-lighted condition, which is consistent with findings from other studies [4–6]. In order to investigate factors affecting work zone crashes under different light conditions, 15 variables are identified and presented in Table 1. In order to achieve more concise results, all the covariates are divided into two categories according to previous studies [20, 38, 39].

The variables describe characteristics related to the driver (at fault, drugs and alcohol, etc.), vehicle (body type), road (number of lanes, speed limit, terrain, and operation), and environment (weather condition, crash date, etc.). SPSS 19 is used to build the decision trees in the study.

5. Results and Discussion

5.1. Decision Trees under Different Light Conditions. Figure 2 and Table 2 present the results of the decision tree under the daylight condition. The first node is split by collision type, demonstrating that a head-on collision has a predicted injury probability more than twice that of other noncollision types (51.8% versus 23.5%). This is consistent with the findings from Kockelman and Kweon [19].

The lowest injury probability appears at node 8, with an injury rate of 11.7%. This node represents the most advantageous situation in daytime work zone crashes, indicating

Table 1: Description of variables.

Category	Variables	Description: code	Light condition		
			Daylight % (*n*)	Dark-lighted % (*n*)	Dark-not-lighted % (*n*)
Driver	At fault (AF)	No (N)	49.4% (7946)	42.2% (1003)	44.3% (651)
		Yes (Y)	50.6% (8152)	57.8% (1372)	55.7% (817)
	Drugs and alcohol (D&A)	No (N)	99.2% (15974)	93.7% (2225)	92.5% (1358)
		Yes (Y)	0.8% (124)	6.3% (150)	7.5% (110)
	Vehicle maneuver (VM)	Changing lanes or merging (CL)	25.3% (4065)	19.2% (456)	12.1% (178)
		Other (O)	74.7% (12033)	80.8% (1919)	87.9% (1290)
Vehicle	Body code (BC)	Not-truck-related (NT)	97.1% (15632)	98.8% (2347)	98.9% (1452)
		Truck-related (T)	2.9% (466)	1.2% (28)	1.1% (16)
Road	No. of lanes (NL)	<=2	20.0% (3218)	13.1% (312)	23.8% (350)
		>2	80.0% (12880)	86.9% (2063)	76.2% (1118)
	Speed Limit (SL)	<=40	50.9% (8188)	58.0% (1377)	39.2% (576)
		>40	49.1% (7910)	42.0% (998)	60.8% (892)
	Terrain (TR)	Flat (F)	6.9% (1118)	9.1% (215)	3.7% (54)
		Not flat (NF)	93.1% (14980)	90.9% (2160)	96.3% (1414)
	Operation (OP)	One-way (1)	0.8% (124)	0.7% (16)	0.3%(4)
		Two-way (2)	99.2% (15974)	99.3% (2359)	99.7% (1464)
Environment	Traffic control device (TCD)	At control (AC)	66.65% (10729)	68.67% (1631)	62.36% (918)
		Not at control (NAC)	33.35% (5369)	31.33% (744)	37.64% (554)
	Location (LC)	Along Roadway (AR)	41.4% (6662)	27.0% (641)	46.9% (688)
		At an Intersection (AI)	58.6% (9436)	73.0% (1734)	53.1% (780)
	Date of Crash	Other months (OM)	59.4% (9566)	77.9% (1849)	78.2% (1148)
		Summer vacation (SV)	40.6% (6532)	22.1% (526)	21.8% (320)
	Weather condition (WC)	Clear (C)	90.6% (14592)	85.7% (2035)	80.8% (1186)
		Not clear (NC)	9.4% (1506)	14.3% (340)	19.2% (282)
	Relation to first roadway (RFR)	Off roadway (OR)	4.7% (752)	10.6% (252)	20.0% (294)
		On roadway (OR)	95.3% (15346)	89.4% (2123)	80.0% (1174)
	Urban or rural (UR)	Rural (R)	15.8% (2538)	1.7% (40)	28.6% (420)
		Urban (U)	84.2% (13560)	98.3% (2335)	71.4% (1048)
	Manner of first collision (MFC)	Head-on (HO)	2.2% (358)	7.6% (181)	6.8% (100)
		Not-head-on (NHO)	97.8% (15740)	92.4% (2194)	93.2% (1368)

Table 2: Decision rules for crash severity of daylight condition.

Node	Rules [if (and. . .and. . .)]	Then	*P* (%)
2	If (CT = HO)	Injury	51.5
6	If (CT = HO) and (LC = AR)	Injury	59.5
8	If (CT = NHO) and (LC = AI) and (TR = FL)	PDO	88.2

that if the collision type is a non-head-on collision at an intersection and if a driver is involved in a collision, there would be an 11.7% chance of an injury and an 88.3% chance of a PDO crash on flat terrain. It should be noted that if the terrain is not flat, the predicted injury rate increases to 22.1%. One possible reason could be that flat terrain provides good visibility, which can slow crash speed and help decrease the severity level.

Of three decision rules inferred from the tree (see Table 3), two are injury rules. Note that both rules contain head-on collision, suggesting that avoiding head-on collisions is critical in lowering the daylight work zone crash severity. Measures like adopting hard barrier to separate traffic from two directions can be helpful.

Figure 3 and Table 3 present the results of the decision tree under the dark-lighted condition. In the same manner as discussed previously, collision type is the criterion based on which node 0 was split under the dark-lighted condition (Figure 3). It shows that head-on collisions account for a much higher percentage of injury crashes that occur under the dark-lighted condition.

However, compared to the daylight model, lane number plays a different role in the crash severity in the dark-lighted model. In the daylight model, an increase in lane number

Table 3: Decision rules for crash severity of dark-lighted condition.

Rule	Node	Rules [if (and. . .and. . .)]	Then	P (%)
(1)	2	If (CT = HO)	Injury	54.5
(2)	5	If (CT = HO) and (NL <= 2)	Injury	100
(3)	8	If (CY = NHO) and (NL > 2) and (WC = NC)	PDO	89.2

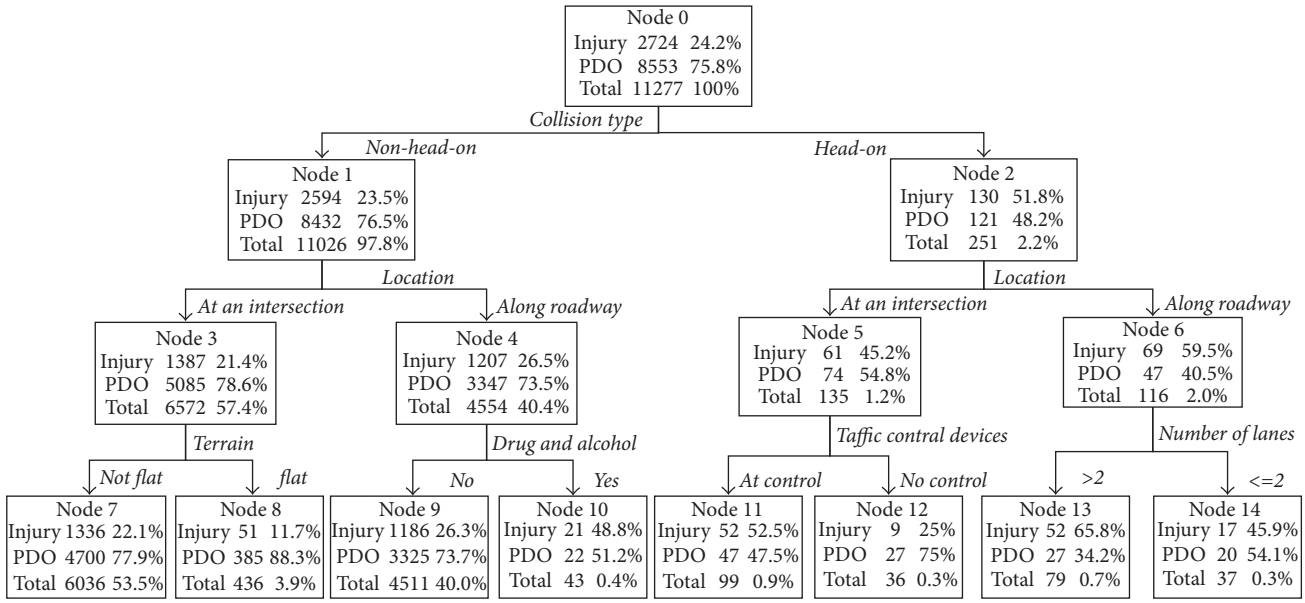

Figure 2: Decision tree under daylight condition.

increases the injury percentage of head-on collisions, while an increase in lane number decreases the injury rate in the dark-lighted model. Specifically, crashes occurring on narrow roads (<=2 lanes) predict a 100% injury rate in a head-on collision, whereas the predicted injury rate decreases to 47.4% on multilane roads. At the same time, the rate on narrow roads is 33.3%, while the rate on wider roads is 21.6% for non-head-on collisions. This phenomenon may be attributed to the changes in drivers' maneuvers under different light conditions. Weng and Meng [40] reported that drivers are more likely to be involved in risky driving maneuvers on multilane roads under daylight conditions, whereas at night most risky driving behavior occurred on narrower roads.

Node 8 gave the lowest predicted injury rate of 10.8%, indicating that the minimum severity case happens in non-head-on collisions on multiple lane (>2) roads when the weather condition is not clear under the dark-lighted condition.

Comparing node 9 and node 10, it can be seen that under the same conditions of multilane road and head-on collision, the use of a traffic control device significantly reduces the predicted injury rate by more than one-half (33.8% versus 69.8%). This indicates that a traffic control device is very helpful in lowering head-on crash severity on multilane roads under the dark-lighted condition. Therefore, it is highly recommended that traffic control devices be installed in work zones with multiple lanes under illumination.

Similar to the daylight model, three decision rules are obtained under the dark-lighted condition. However, the injury rate for the dark-lighted condition is slightly higher than that for the daylight condition. The fact that lane number plays an important role in work zone crashes under the dark-lighted condition may be due to decreased visibility (see rule (2) of Table 3).

Figure 4 and Table 4 present the results of the decision tree under the dark-not-lighted condition. Under dark-not-lighted condition, the darkest light condition, some significant changes in crash severity are found. Unlike the daylight and the dark- lighted decision tree models, the first partition node is not based on collision type but on speed limit. A higher speed limit (>40 miles/h) contributes to more severe crashes compared to a lower speed limit (<=40 miles/h) (37.9% versus 23%) for the dark-not-lighted condition. As we know, the dark-not-lighted condition is characterized by a sharp reduction of visibility that affects the driver's ability to perceive obstacles. With the high speed limit and limited visibility, drivers may have insufficient time to stop the vehicle.

The factor of drugs and alcohol shows a significant impact on crash severity under the dark-not-lighted condition. If a driver is under the influence, the predicted injury percentage climbs to 72.7% even with the speed limit lower than 40 miles/h. This rate reduces dramatically to 20.1% if the driver is not under the influence. This verifies the findings from

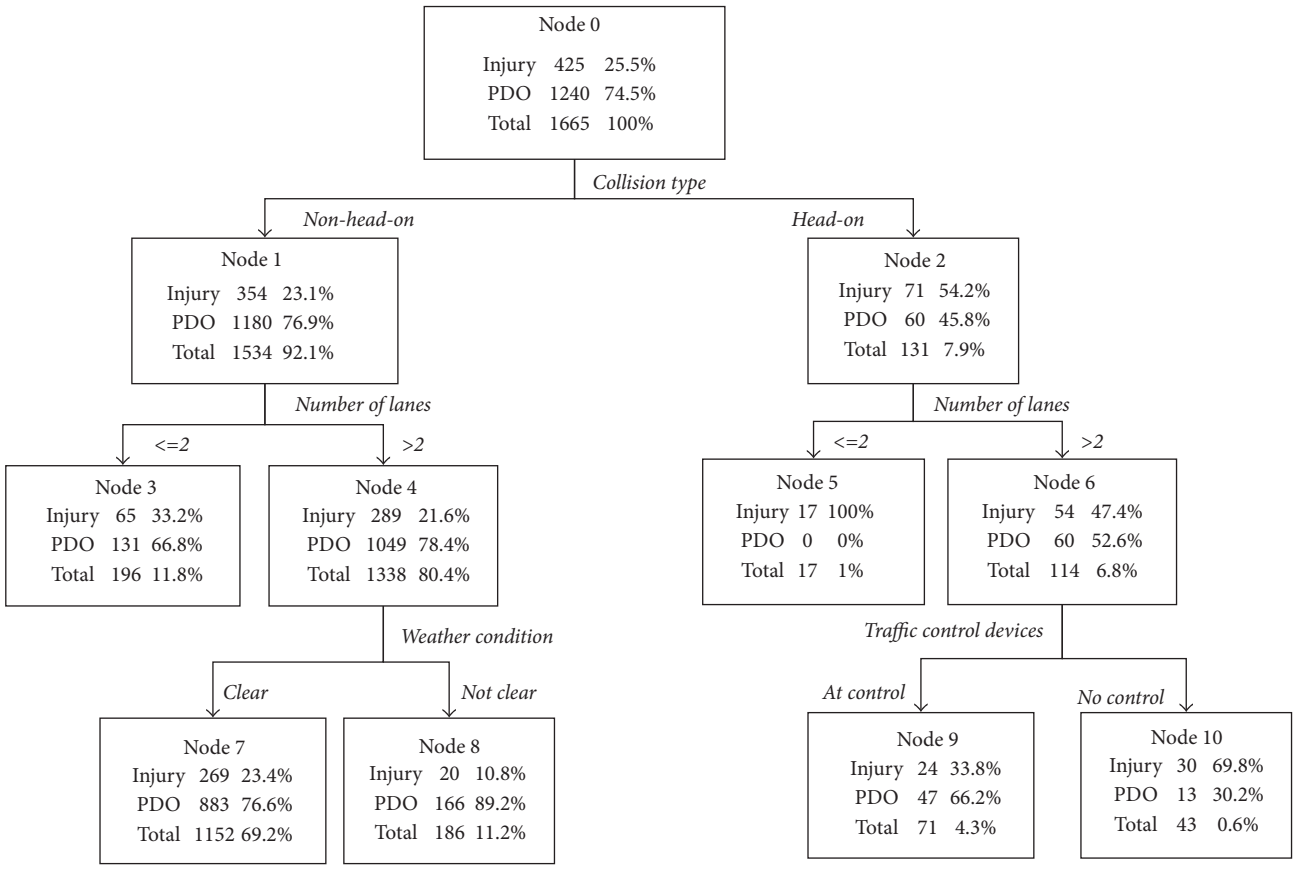

Figure 3: Decision tree under dark-lighted condition.

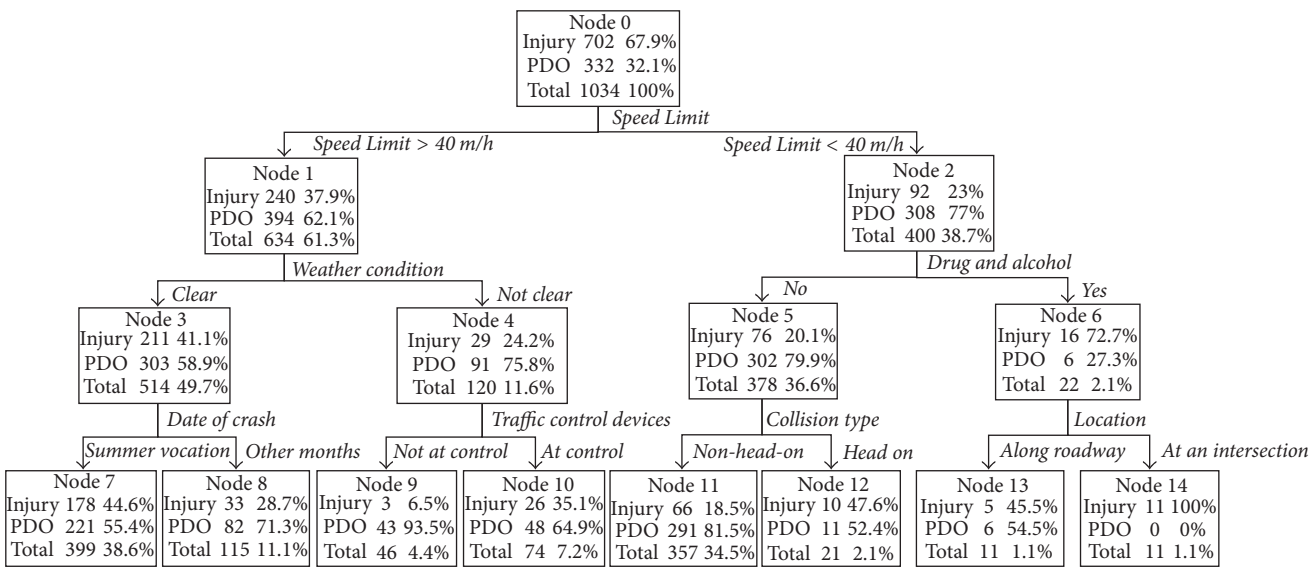

Figure 4: Classification tree under dark-not-lighted condition.

Table 4: Decision rules for crash severity of dark-not-lighted condition.

Rules	Node	Rules [if (and. . .and. . .)]	then	P (%)
(1)	6	If (SL <= 40) and (D & A =Y)	Injury	72.7
(2)	9	If (SL > 40) and (WC = NC) and (TCD = N)	PDO	93.5
(3)	11	If (SL <= 40) and (D & A = N) and (CT = NHO)	PDO	81.5
(4)	14	If (SL <= 40) and (D & A = Y) and (LC = AI)	Injury	100

Table 5: Rank of the importance of variables under different light conditions.

Rank	Daylight	Dark-lighted	Dark-not-lighted
(1)	Manner of first collision	Manner of first collision	Drugs and alcohol
(2)	Location	No. of lanes	Speed limit
(3)	Drugs and alcohol	Traffic control devices	Weather cond.
(4)	Terrain	Location	Traffic control devices
(5)	Urban or rural	Weather cond.	Date of crash
(6)	Traffic control devices	Drugs and alcohol	Manner of first collision
(7)	Speed limit	Relation to first roadway	Location
(8)	Date of crash	Urban or rural	No. of lanes
(9)	No. of lanes	Speed limit	Operation
(10)	Body code	Terrain	Body code
(11)	Relation to first roadway		Relation to first roadway
(12)	At fault		Urban or rural
(13)	Vehicle maneuver		

previous studies that drug and alcohol intake significantly increases the likelihood of severe injuries [41, 42] and further reveals that the impact of drugs and alcohol is significantly higher under the dark-not-lighted condition. One possible reason may be that drivers need to be more alert under this condition and impaired drivers under the influence are likely not to stop, change lanes to avoid obstacles, or otherwise avoid severe crashes.

Also, under the influence of drugs and alcohol, the injury rate of traffic crashes doubles at intersections compared to long open roadways at a speed limit less than 40 miles/h, indicating that intersections introduce additional risk under the dark-not-lighted condition. Node 9 shows the lowest injury rate of 6.5% under the dark-not-lighted condition, at a speed limit above 40 miles/h without traffic control devices. This is significantly different from the findings from Chang and Chien [35], which concluded that traffic control devices can enhance traffic safety. The reason for the seemingly contradictory findings may be due to the fact that traffic control devices usually appear at crash-prone sites where road conditions are more complex. It is improper to compare two places with different geometry features and traffic patterns. The effect of traffic control devices can only be validated by a before-after test in a future study.

Table 4 shows the decision rules inferred from the dark-not-lighted condition. Two of the rules are injury rules, indicating that the involvement of drugs and alcohol and a speed limit less than 40 miles/h are common in severe crashes. It is highly recommended that fines for driving under the influence be increased significantly in work zones including dark-not-lighted zones.

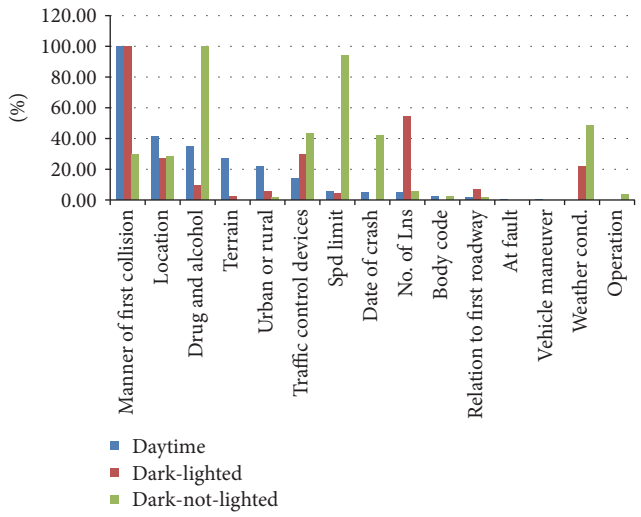

Figure 5: The importance of variables under different light conditions.

5.2. Comparison of the Importance of Variables. Table 5 and Figure 5 rank and compare the importance of various risk factors under different light conditions. For the daylight decision tree model, the top five factors contributing to crash severity are collision type, location, drugs and alcohol, terrain, and urban or rural location. For the dark-lighted model, the top five factors are collision type, number of lanes, traffic control devices, location, and weather condition. From the dark-not-lighted model, the top five factors are drugs and alcohol, speed limit, weather condition, traffic control devices, and

Table 6: Prediction Performance.

Sample	Observed	Predicted		
		Injury	PDO	Percentage correct
Daylight	Injury	46	1134	3.9%
	PDO	32	3609	99.1%
	Overall percentage	1.6%	98.4%	75.8%
Dark-lighted	Injury	19	159	10.7%
	PDO	9	523	98.3%
	Overall percentage	3.9%	96.1%	76.3%
Dark-not-lighted	Injury	5	155	3.1%
	PDO	0	274	100.0%
	Overall percentage	1.2%	98.8%	64.3%

date of crash. The ranking of the top five contributing factors is different under the three light conditions, indicating that the effects of the major contributing factors vary significantly under different light conditions within work zones. Table 5 also shows that vehicle body type, location (rural or unban), and road operation (one-way or two-way) do not show an important effect on crash severity in work zones. In order to achieve safer work zones, safety guidelines should be established according to different light conditions.

5.3. Validation. Table 6 presents the results from the validation of the decision trees. For all three models, the percentage predicted correctly was above 60%. This rate is higher than those reported in previous studies using the same method [35]. All three models are capable of predicting PDO crashes with an accuracy rate above 98%. On the other hand, these models show a poor ability to predict injury crashes with an accuracy ranging from 3.1% to 10.7%. This rate for predicting injuries is close to that reported in other studies using CART decision method [36]. The reason may lie in the dataset itself. There are more than 70% of the crashes that are PDO while only less than 30% belong to injury. In order to achieve the minimum error of the whole dataset, models or prediction methods tend to classify a result to PDO which is the major crash type.

6. Conclusions

In this study, three decision trees are generated using the CART method to investigate the factors contributing to crashes in work zones. The light-based individual decision tree models use detailed information of work zone crashes to identify risk factors. Identification of these factors then suggests mitigation measures that may help establish safer work zones. In the study, the following are found.

(i) The daylight model indicates that in head-on crashes occurring along roadways, as opposed to intersections, drivers are at a higher risk, up to 59.7%, of being involved in injury crash.

(ii) The dark-lighted model demonstrates that the injury rate of head-on crashes occurring on a narrow road (<=2 lanes) could reach 100%.

(iii) Under the dark-not-lighted condition, a combination of a speed limit less than 40 miles/h and drivers being under the influence of drugs and alcohol could lead to an injury rate of up to 72.7%.

By examining the effects of specific light conditions on crash severity, this study reveals some new findings never reported before. The study shows that if drivers are under the influence of drug/alcohol, they have a larger chance of being involved in severe crashes when passing a work zone without street light than a work zone with street light. This study reveals that collision type is the most important risk factor under daylight and dark-lighted conditions but not under dark-not-lighted condition. On the other hand, the study suggests that traffic control devices do not reduce crash severity under the dark-not-lighted condition, yet, they do under the dark-lighted condition. This implies that traffic control devices should be designed and used differently according to light conditions. Additionally, the number of roadway lanes shows opposite effects on crash severity under the daylight and the dark-not-lighted conditions. Specifically, under the daylight condition, an increase in the number of lanes may increase crash severity, whereas it may help reduce crash severity under the dark-not-lighted condition.

The CART decision tree method was found to be useful in revealing crash severity characteristics and the factors contributing to traffic crashes in work zones. In future work, these results may be helpful in developing work zone safety guidelines to mitigate crash severity. In addition, it will be of practical significance to use the decision tree method to investigate drivers' behavior under different light conditions.

Conflicts of Interest

The authors declare that there are no conflicts of interest regarding the publication of this paper.

Acknowledgments

The authors would like to thank the Construction Industry Research and Policy Center (CIRPC) for funding this research project. The first author would also like to thank the China Scholarship Council (CSC) for its financial support.

References

[1] L. J. Blincoe, T. R. Miller, E. Zaloshnja, and B. A. Lawrence, "The economic and societal impact of motor vehicle crashes, 2010," Report No. DOT HS 812 013, National Highway Traffic Safety Administration, Wash, USA, 2015.

[2] K. Wunderlich and D. Hardesty, *A Snapshot of Summer 2001 Work Zone Activity*, Federal Highway Administration, U.S. Department of Transportation, Wash, USA, 2003.

[3] J. E. Bryden and D. J. Mace, "A procedure for assessing and planning nighttime highway construction and maintenance," NCHRP Report 475, Transportation Research Board, National Research Council, Wash, USA, 2002.

[4] R. C. Gray, M. A. Quddus, and A. Evans, "Injury severity analysis of accidents involving young male drivers in Great Britain," *Journal of Safety Research*, vol. 39, no. 5, pp. 483–495, 2008.

[5] M. Abdel-Aty, "Analysis of driver injury severity levels at multiple locations using ordered probit models," *Journal of Safety Research*, vol. 34, no. 5, pp. 597–603, 2003.

[6] H. Huang, H. C. Chin, and M. M. Haque, "Severity of driver injury and vehicle damage in traffic crashes at intersections: a Bayesian hierarchical analysis," *Accident Analysis & Prevention*, vol. 40, no. 1, pp. 45–54, 2008.

[7] D. Arditi, M. A. Ayrancioglu, and J. Shi, "Effectiveness of safety vests in nighttime highway construction," *Journal of Transportation Engineering*, vol. 130, no. 6, pp. 725–732, 2004.

[8] E. C. Sullivan, "Accident Rates during Nighttime Construction," Report No. UCB-ITS-RR-89-11, Institute of Transportation Studies, University of California-Berkeley, Berkeley, Calif, USA, May 1989.

[9] A. Pande and M. Abdel-Aty, "Market basket analysis of crash data from large jurisdictions and its potential as a decision support tool," *Safety Science*, vol. 47, no. 1, pp. 145–154, 2009.

[10] J. de Oña, R. O. Mujalli, and F. J. Calvo, "Analysis of traffic accident injury on Spanish rural highways using Bayesian networks," *Accident Analysis & Prevention*, vol. 43, pp. 402–411, 2011.

[11] J. de Oña, G. López, and J. Abellán, "Extracting decision rules from police accident reports through decision trees," *Accident Analysis & Prevention*, vol. 50, pp. 1151–1160, 2013.

[12] P. O. Wanvik, "Effects of road lighting: an analysis based on Dutch accident statistics 1987-2006," *Accident Analysis & Prevention*, vol. 41, no. 1, pp. 123–128, 2009.

[13] J. Weng and Q. Meng, "Analysis of driver casualty risk for different work zone types," *Accident Analysis & Prevention*, vol. 43, no. 5, pp. 1811–1817, 2011.

[14] J. D. Bullough, E. T. Donnell, and M. S. Rea, "To illuminate or not to illuminate: roadway lighting as it affects traffic safety at intersections," *Accident Analysis & Prevention*, vol. 53, no. 1, pp. 65–77, 2013.

[15] R. R. Dinu and A. Veeraragavan, "Random parameter models for accident prediction on two-lane undivided highways in India," *Journal of Safety Research*, vol. 42, no. 1, pp. 39–42, 2011.

[16] E. T. Donnell, R. J. Porter, and V. N. Shankar, "A framework for estimating the safety effects of roadway lighting at intersections," *Safety Science*, vol. 48, no. 10, pp. 1436–1444, 2010.

[17] G. L. Ullman, M. D. Finley, J. E. Bryden, R. Srinivasan, and F. M. Council, "Traffic Safety Evaluation of Nighttime and Daytime Work Zones," NCHRP Report 627, Transportation research board, Wash, USA, 2008.

[18] A. S. Al-Ghamdi, "Using logistic regression to estimate the influence of accident factors on accident severity," *Accident Analysis & Prevention*, vol. 34, no. 6, pp. 729–741, 2002.

[19] K. M. Kockelman and Y.-J. Kweon, "Driver injury severity: an application of ordered probit models," *Accident Analysis & Prevention*, vol. 34, no. 3, pp. 313–321, 2002.

[20] N. N. Sze and S. C. Wong, "Diagnostic analysis of the logistic model for pedestrian injury severity in traffic crashes," *Accident Analysis & Prevention*, vol. 39, no. 6, pp. 1267–1278, 2007.

[21] C. Dong, D. B. Clarke, X. Yan, A. Khattak, and B. Huang, "Multivariate random-parameters zero-inflated negative binomial regression model: an application to estimate crash frequencies at intersections," *Accident Analysis & Prevention*, vol. 70, pp. 320–329, 2014.

[22] L.-Y. Chang and H.-W. Wang, "Analysis of traffic injury severity: an application of non-parametric classification tree techniques," *Accident Analysis & Prevention*, vol. 38, no. 5, pp. 1019–1027, 2006.

[23] T. Beshah and S. Hill, "Mining road traffic accident data to improve safety: role of road-related factors on accident severity in ethiopia," in *Proceedings of AAAIArtificial Intelligence for Development (AI-D '10)*, pp. 22–24, 2010.

[24] A. T. Kashani and A. S. Mohaymany, "Analysis of the traffic injury severity on two-lane, two-way rural roads based on classification tree models," *Safety Science*, vol. 49, no. 10, pp. 1314–1320, 2011.

[25] A. Montella, M. Aria, A. D'Ambrosio, and F. Mauriello, "Data-mining techniques for exploratory analysis of pedestrian crashes," *Transportation Research Record*, vol. 2237, no. 1, pp. 107–116, 2011.

[26] A. Montella, M. Aria, A. D'Ambrosio, and F. Mauriello, "Analysis of powered two-wheeler crashes in Italy by classification trees and rules discovery," *Accident Analysis & Prevention*, vol. 49, pp. 58–72, 2012.

[27] J. R. Quinlan, "Induction of decision trees," *Machine Learning*, vol. 1, no. 1, pp. 81–106, 1986.

[28] J. Abellán, G. López, and J. de Oña, "Analysis of traffic accident severity using decision rules via decision trees," *Expert Systems with Applications*, vol. 40, no. 15, pp. 6047–6054, 2013.

[29] L. Breiman, J. Friedman, R. Olshen, and C. Stone, *Classification and Regression Trees*, Chapman and Hall, Belmont, Calif, USA, 1984.

[30] C. E. Shannon, "A mathematical theory of communication," *Bell System Technical Journal*, vol. 27, no. 4, pp. 623–656, 1948.

[31] J. R. Quinlan, *C4.5: Programs for machine learning*, Morgan Kaufmann Publishers, San Mateo, Calif, USA, 1993.

[32] P. M. Kuhnert, K.-A. Do, and R. McClure, "Combining non-parametric models with logistic regression: an application to motor vehicle injury data," *Computational Statistics & Data Analysis*, vol. 34, no. 3, pp. 371–386, 2000.

[33] A. Pakgohar, R. S. Tabrizi, M. Khalili, and A. Esmaeili, "The role of human factor in incidence and severity of road crashes based on the CART and LR regression: a data mining approach," *Procedia Computer Science*, vol. 3, pp. 764–769, 2010.

[34] O. H. Kwon, W. Rhee, and Y. Yoon, "Application of classification algorithms for analysis of road safety risk factor dependencies," *Accident Analysis & Prevention*, vol. 75, pp. 1–15, 2015.

[35] L. Chang and J. Chien, "Analysis of driver injury severity in truck-involved accidents using a non-parametric classification tree model," *Safety Science*, vol. 51, no. 1, pp. 17–22, 2013.

[36] A. T. Kashani, A. Shariat-Mohaymany, and A. Ranjbari, "A data mining approach to identify key factors of traffic injury severity," *Promet - Traffic - Transportation*, vol. 23, no. 1, pp. 11–17, 2011.

[37] J. S. Lee and E. S. Lee, "Exploring the usefulness of a decision tree in predicting people's locations," *Procedia - Social and Behavioral Sciences*, vol. 140, pp. 447–451, 2014.

[38] R. Tay, "A random parameters probit model of urban and rural intersection crashes," *Accident Analysis & Prevention*, vol. 84, pp. 38–40, 2015.

[39] D. M. Cerwick, K. Gkritza, M. S. Shaheed, and Z. Hans, "A comparison of the mixed logit and latent class methods for crash severity analysis," *Analytic Methods in Accident Research*, vol. 3-4, pp. 11–27, 2014.

[40] J. Weng and Q. Meng, "Effects of environment, vehicle and driver characteristics on risky driving behavior at work zones," *Safety Science*, vol. 50, no. 4, pp. 1034–1042, 2012.

[41] S. P. Baker, E. R. Braver, L.-H. Chen, G. Li, and A. F. Williams, "Drinking histories of fatally injured drivers," *Injury Prevention*, vol. 8, no. 3, pp. 221–226, 2002.

[42] B. E. Smink, B. Ruiter, K. J. Lusthof, J. J. De Gier, D. R. A. Uges, and A. C. G. Egberts, "Drug use and the severity of a traffic accident," *Accident Analysis & Prevention*, vol. 37, no. 3, pp. 427–433, 2005.

Hindawi
Journal of Advanced Transportation
Volume 2017, Article ID 5230248, 9 pages
https://doi.org/10.1155/2017/5230248

Research Article

Developing a Clustering-Based Empirical Bayes Analysis Method for Hotspot Identification

Yajie Zou,[1] Xinzhi Zhong,[1] John Ash,[2] Ziqiang Zeng,[3,4] Yinhai Wang,[1] Yanxi Hao,[5] and Yichuan Peng[1]

[1] *The Key Laboratory of Road and Traffic Engineering, Ministry of Education, Tongji University, Shanghai 201804, China*
[2] *University of Washington, P.O. Box 352700, Seattle, WA 98195-2700, USA*
[3] *Uncertainty Decision-Making Laboratory, Sichuan University, Chengdu 610064, China*
[4] *Department of Civil and Environmental Engineering, University of Washington, Seattle, WA 98195, USA*
[5] *College of Urban Railway Transportation, Shanghai University of Engineering Science, 333 Longteng Road, Shanghai 201620, China*

Correspondence should be addressed to Yanxi Hao; haoyx0316@163.com and Yichuan Peng; yichuanpeng1982@hotmail.com

Received 15 June 2017; Revised 10 October 2017; Accepted 15 October 2017; Published 22 November 2017

Academic Editor: Chunjiao Dong

Hotspot identification (HSID) is a critical part of network-wide safety evaluations. Typical methods for ranking sites are often rooted in using the Empirical Bayes (EB) method to estimate safety from both observed crash records and predicted crash frequency based on similar sites. The performance of the EB method is highly related to the selection of a reference group of sites (i.e., roadway segments or intersections) similar to the target site from which safety performance functions (SPF) used to predict crash frequency will be developed. As crash data often contain underlying heterogeneity that, in essence, can make them appear to be generated from distinct subpopulations, methods are needed to select similar sites in a principled manner. To overcome this possible heterogeneity problem, EB-based HSID methods that use common clustering methodologies (e.g., mixture models, K-means, and hierarchical clustering) to select "similar" sites for building SPFs are developed. Performance of the clustering-based EB methods is then compared using real crash data. Here, HSID results, when computed on Texas undivided rural highway cash data, suggest that all three clustering-based EB analysis methods are preferred over the conventional statistical methods. Thus, properly classifying the road segments for heterogeneous crash data can further improve HSID accuracy.

1. Introduction

Network screening to identify sites (i.e., roadway segments or intersections) with promise for safety treatments is an important task in road safety management [1–7]. The identification of sites with promise, also known as crash hotspots or hazardous locations, is the first task in the overall safety management process [8]. One widely applied approach to this task is the popular Empirical Bayes (EB) method. The EB method is described and recommended in the *Highway Safety Manual* [9] for roadway safety management. This method is relatively insensitive to random fluctuations in the frequency of accidents with two clues combined, the observed crash frequency of the site and the expected number of crashes calculated from a safety performance function (SPF) for homogeneous sites (or the reference group) [10, 11]. The EB method can correct for regression-to-the-mean bias and refine the predicted mean of an entity [12]. Further, it is relatively simple to implement compared to the fully Bayesian approach.

Although the EB method has several advantages, there are a few issues associated with the methodology which may limit its widespread application. First, the selection of the reference population (i.e., similar sites) influences the accuracy of the EB method. When estimating the safety performance function, the crash data are usually obtained from distinct geographic sites to ensure a sufficient sample size for valid statistical estimation [10]. As a result, the aggregated crash data often contain heterogeneity. When conducting an EB analysis, the reference group must be similar to the target

group in terms of geometric design, traffic volume, and so on. Manually identifying such a reference group is a rather time consuming task for transportation safety analysts whose time could be better spent elsewhere. Second, the EB procedure is relatively complicated and requires a transportation safety analyst with considerable training and experience to implement it for a safety evaluation. Thus, the training investment required to prepare analysts to undertake EB evaluations can be a barrier. As a result, some quick and dirty conventional evaluation methods may be applied as a compromise of convenience, which may produce questionable results.

Given that the specification of correct reference groups is critical for the accuracy of the EB methodology, the primary objective of this research will examine different clustering algorithms (e.g., centroid-based clustering, connectivity-based clustering, and distribution-based clustering) and develop a procedure to identify appropriate reference groups for the EB analysis.

2. Hotspot Identification Methods Used in Comparison

2.1. Conventional Hotspot Identification Methods. One common HSID method is the accident frequency (AF) method. Sites are ranked based on AF and hotspots are defined as sites whose accident frequency exceeds some threshold value [13]. The problem of accounting for exposure in the AF method can be accommodated by considering accident rate (AR) instead of accident frequency. As such, AR methods have been used by some analysts and normalize accident frequency by traffic count. While AF and AR methods are easy to implement, they have difficulty accounting for randomness in crash data. As such, another popular HSID method was developed, that being the Empirical Bayes method presented by Abbess et al. [14]. Since its introduction decades ago, the EB method has been used numerous times in many safety studies [15–23]. One of the key advantages of using the EB method is that it accounts for the regression-to-the-mean (RTM) bias. The EB method can also help improve precision in cases where limited amounts of historical accident data are available for analysis at a given site. At its core, the EB method forecasts the expected crash count at a particular site as a weighted combination of (1) the accident count at the site based on historical data and (2) the estimated number of accidents at similar locations as determined from a regression model [24]. The regression model is generally referred to as a SPF and typically takes into account roadway and traffic characteristics (e.g., average daily traffic) at similar sites. To date, the most popular choice for the SPF has been a Negative Binomial regression model [25–27]. In terms of HSID via the EB method, EB estimates are computed for each site and then sites are ranked according to such estimates. Sites exceeding some thresholds are then considered as hotspots. Besides the EB method, another relatively common HSID method is rooted in so-called "accident reduction potential" (ARP). The ARP metric used for ranking sites was computed by subtracting the estimated accident count from the observed accident count at a given site, where the estimated accident count comes from a regression model developed from data at similar sites to the target. Among different HSID methods, the EB method is probably the most widely applied approach for screening sites with potential for safety treatment.

2.2. Clustering for Selection of Similar Sites. In the following section, we present three methods that can be used to group data into different clusters. As aforementioned, crash data often exhibit heterogeneity that can affect model estimates if not properly accounted for. The idea here is to cluster crash data into different groups that hopefully align to some degree with the underlying subpopulations from which the crash data are generated. Then, separate Negative Binomial (NB) regression models (i.e., SPFs) can be developed based on each cluster and EB estimates can then be computed using an SPF that hopefully considers sites that truly are "similar" to the site in question.

2.2.1. Generalized Finite Mixture of NB Regression Models. The generalized finite mixture of NB regression models with g components (GFMNB-g) assumes that y_i follows a mixture of NB distributions, as shown as follows [28]:

$$f_Y\left(y_i \mid \mathbf{x}_i, \boldsymbol{\Theta}\right) = \sum_{j=1}^{g} w_j \mathrm{NB}\left(\mu_{ij}, \phi_j\right) = \sum_{j=1}^{g} w_j \left[\frac{\Gamma\left(y_i + \phi_j\right)}{\Gamma\left(y_i + 1\right)\Gamma\left(\phi_j\right)}\left(\frac{\mu_{ij}}{\mu_{ij} + \phi_j}\right)^{y_i} \cdot \left(\frac{\phi_j}{\mu_{ij} + \phi_j}\right)^{\phi_j}\right], \tag{1}$$

$$E\left(y_i \mid \mathbf{x}_i, \boldsymbol{\Theta}\right) = \sum_{j=1}^{g} \mu_{ij} w_j, \tag{2}$$

$$\mathrm{Var}\left(y_i \mid \mathbf{x}_i, \boldsymbol{\Theta}\right) = E\left(y_i \mid \mathbf{x}_i, \boldsymbol{\Theta}\right) + \left(\sum_{j=1}^{g} w_j \mu_{ij}^2 \left(1 + \frac{1}{\phi_j}\right) - E\left(y_i \mid \mathbf{x}_i, \boldsymbol{\Theta}\right)^2\right), \tag{3}$$

where w_j is the weight of component j (weight parameter), with $w_j > 0$ and $\sum_{j=1}^{g} w_j = 1$; g is the number of components; $\mu_{ij} = \exp(\mathbf{x}_i \boldsymbol{\beta}_j)$, the mean rate of component j; $\mathbf{x}_i$ is a vector of covariates; $\boldsymbol{\beta}_j$ is a vector of the regression coefficients for component j; $\boldsymbol{\Theta} = \{(\phi_1, \ldots, \phi_g), (\boldsymbol{\beta}_1, \ldots, \boldsymbol{\beta}_g), \mathbf{w}\} = \{(\boldsymbol{\theta}_1, \ldots, \boldsymbol{\theta}_g), \mathbf{w}\}$ for $i = 1, 2, \ldots, n$; and $\boldsymbol{\theta}_j$ is vectors of parameters for the component j.

For GFMNB-g models, the equation for developing the weight parameter is shown in (4). By using a function of the covariates, the GFMNB-g model makes it possible for each site to have different weights for each component that depends on the site-specific values of the covariates. Zou et al.

[28] demonstrated how this additional flexibility can lead to better classification results

$$\frac{w_{ij}}{w_{ig}} = e^{\gamma_{0j}} e^{\boldsymbol{\gamma}_j \mathbf{x}_i}, \tag{4}$$

where w_{ij} is the estimated weight for component j at segment i; $\boldsymbol{\gamma}_j = (\gamma_{0j}, \gamma_{1j}, \gamma_{2j}, \ldots, \gamma_{mj})'$ are the estimated coefficients of component j and m is the number of unknown coefficients; and $\mathbf{x}_i$ is a vector of covariates.

2.2.2. K-Means Clustering. The K-means clustering algorithm is often attributed to Lloyd [29] and Anderson [30], and it is one of the most popular clustering algorithms in use today. Inputs to the algorithm are the data points; here, each data point can be viewed as one of the road segments in the crash data set and its corresponding descriptive variables (e.g., lane width and average daily traffic (ADT)). With the data in hand, K cluster centers are initialized. Cluster centers can be chosen as random points in the feature space (i.e., points that do not exist in the data set could be selected) and random data points in the feature space (i.e., only points in the dataset can be selected) or through a variety of other methods. For this project, the initialization using K random data points in the dataset was used. The algorithm then proceeds in an iterative process until it converges, where convergence is defined as the point at which the cluster assignments do not change. The first step in the iteration assigns each data point to the cluster such that the distance between that cluster center and the data point itself is smallest; the distance metric used for this work is Euclidean distance defined as shown in (5). Then, the second step recalculates the center for each cluster. Pseudocode for the algorithm is shown in the following:

$$d(x_i, x_{i'}) = \sum_{j=1}^{m} \left(x_{ij} - x_{i'j}\right)^2 = \left\|x_i - x_{i'}\right\|^2, \tag{5}$$

where $d(\cdot)$ is Euclidean distance between two points; i is data point index, ranging from $1:n$; j is variable index, ranging from $1:m$ for m variables; and $\|\cdot\|$ is the two norms of two data points.

K-Means Algorithm

Cluster-Assignment Step

$$C(i) = \underset{1\le k\le K}{\arg\min} \left\|x_i - m_k\right\|, \tag{6}$$

where $C(i)$ is cluster assignment for data point x_i; m_k is center of cluster k; and all other variables are defined as previous.

Center-Update Step

$$m_k = \frac{1}{|C(k)|} \sum_{i\in C(k)} x_i, \tag{7}$$

where $|C(k)|$ is cardinality (number of data points) in cluster $C(k)$ and all other variables are defined as previous.

2.2.3. Hierarchical Clustering. Hierarchical clustering methods differ from K-means clustering in that the results do not depend on the number of clusters used (i.e., the results will always be the same for a given number of clusters) nor an initialization. Rather, they are rooted in the use of a dissimilarity measure defined between clusters that is defined in terms of all possible pairwise combinations of data points within two given clusters. In this research, agglomerative (i.e., bottom-up) hierarchical clustering in the form of complete linkage clustering was considered. Agglomerative clustering methods (e.g., complete linkage, single linkage, and average linkage) take the data points (i.e., road segments and their corresponding descriptors) as inputs and begin with each data point as its own cluster; a lone data point forming its own cluster is also known as a singleton. For complete linkage clustering, the algorithm proceeds in a total of $n - 1$ steps (i.e., one step less than the total number of data points in the dataset) and at each step, the two clusters with the smallest intergroup dissimilarity measure are joined to form a new cluster. Thus, in each successive step, the number of clusters is reduced by one. For complete linkage clustering the intergroup dissimilarity is defined as follows [31]:

$$d(A, B) = \max_{i\in A, i'\in B} d_{ii'}, \tag{8}$$

where A, B are two arbitrary clusters and

$$d_{ii'} = \left\|x_i - x_{i'}\right\|. \tag{9}$$

Thus, for each step of the complete linkage clustering algorithm, the two clusters with the smallest value of the maximum between-cluster distance are joined.

2.3. Classification-Based EB Methods. At this point it is important to clarify the main contribution of this work. It is well-known that aggregated crash likely has some degree of heterogeneity, as if they are generated from multiple distinct subpopulations. As such, if one were able to try to capture this heterogeneity and group the data into different units, ideally based upon the subpopulations from which they were generated, better estimates of safety and HSID rankings could likely be obtained. Thus, three types of clustering algorithms (GFMNB-g model based, k-means clustering, and hierarchical clustering with complete linkage) are proposed to cluster the data into distinct subgroups that hopefully correspond to the subpopulations from which the data were generated. The main idea/application of clustering is to define groups (i.e., clusters) of data points such that all points assigned to/belonging to a given cluster are closer/more similar to the points in that cluster than any other cluster [31].

Clustering methods present an ideal means to represent/describe heterogeneity within crash data. As such, we apply clustering-based EB methods in this study as a new means of hotspot identification. For these methods, three types of clustering as aforementioned are considered, and the classification method for HSID purposes has four main steps as follows. First, the full set of input crash data is clustered into g clusters via the GFMNB-g model, k-means clustering algorithm, or hierarchical clustering algorithm. In this study,

the number of clusters considered is set equal to the number of components selected for the GFMNB-g model, which was itself selected on the basis of the Bayesian information criterion (BIC). Ultimately, however, the choice for selection of both number of clusters and number of components in the GFMNB-g model is up to the analyst. The second step of the algorithm involves splitting the data into g groups based on the results of the applied clustering algorithm. The third step of the algorithm calls for estimation of an NB regression model (i.e., SPF) for each of the g subgroups/clusters from the data and using these SPFs in further generation of EB estimates for each site. For example, if $g = 2$, two SPFs will be estimated and the data in each of the two groups will have EB estimates calculated through application of the corresponding SPF. Fourth and finally, the EB estimates for all sites across all g subgroups are aggregated and ranked, after which hotspots identification is based on threshold values or other methods. From this point forward, the classification-based HSID methods aforementioned will be referred to as follows: GFMNB-based EB method, the K-means-based EB method, and hierarchical-based EB method, respectively. A summary of the classification-based EB method for HSID is shown in Table 1.

2.4. Evaluation Criteria for Hotspot Identification Methods. For the purpose of evaluating the performance of HSID methods, some kind of standardized test procedures are needed. Ultimately, analysts will be concerned with an HSID method's capability to find accident prone sites and properly rank sites according to risk. These concerns are directly related to the overarching objective of prioritizing safety treatments at hotspots in a limited-funding environment. While a multitude of tests are available and determining which test is optimal may not be clear, one might argue that "good" performance (to be described in the forthcoming test descriptions) across multiple tests could be a reasonable indicator of a method's overall performance in HSID. As such, we consider three commonly used tests attributed to Cheng and Washington [32]: the Site Consistency Test (SCT), the Method Consistency Test (MCT), and the Total Rank Difference Test (TRDT). For more information about these three tests, interested readers are referred to Cheng and Washington [32].

3. Data and Analysis

3.1. Data Description. In order to examine the effectiveness of the methodology presented herein, the research team chose to work with a dataset used in many previous safety studies, which being the Texas rural undivided highway crash dataset. The dataset contains crash counts collected over 1,499 rural undivided highway segments over a span of five years, 1997–2001, for the National Cooperative Highway Research Program (NCHRP) 17–29 project [33]. Since the aforementioned tests for evaluation of the hotspot identification methods require data from different time periods for comparison purposes, the dataset comprised of 1,499 observations was broken down into two temporal subsets. The first subset, called "Time Period 1" henceforth, contains the data from the original dataset recorded for 1997 and 1998. The second subset, called "Time Period 2" henceforth, contains the data from the original dataset recorded for 1999, 2000, and 2001. Thus, the union of these two subsets is the original dataset with 1,499 points. Variables collected to describe the segments and be considered as independent variables in the analysis include average daily traffic during the analysis period (F), lane width (LW, in feet), total shoulder width (i.e., the sum of shoulder width on both sides of the roadway in feet, SW in feet), and curve density (i.e., the number of curves per mile, CD). The dependent variable in the analysis is the number of crashes observed on each segment over the analysis period, and another variable, segment length (L, in miles), was considered as an offset in the regression. Summary statistics on the dataset are presented in Table 2.

3.2. Modeling Results. To study classification-based EB methods, GFMNB-g models were developed from the crash records in Time Periods 1 and 2, respectively. Data in each time period was used to estimate the finite mixture models with g components; that is, g separate NB models were estimated for each type of mixture model that are combined together to form a weighted estimate. Then, the GMFNB-g model was used as the basis for the clustering-based EB methods. That is to say, the number of components used in the model was selected as the basis for the number of clusters to use for grouping the crash data under each of the aforementioned clustering methods.

When estimating the GFMNB-g models, perhaps the main problem is to determine how many components should be used in the model (i.e., to select g). In order to select the number of components for each model in each time period, the method presented in Park et al. [34] was applied in this study. Under this approach, the analyst builds finite mixture models with increasing numbers of components (from two upwards) and selects the final model (and number of components) through goodness-of-fit metrics, such as the Akaike Information Criterion (AIC) or the previously mentioned BIC, which balance the number of components and overall model fit (measured via log-likelihood). Eluru et al. [35] noted that BIC is more stringent than AIC in terms of applying a penalty based on number of components, and thus it may be more robust in terms of preventing overfitting. As such, BIC was selected as the means of choosing the number of components for the finite mixture models in each of the two time periods:

$$\text{BIC}_j = -2 * \text{loglikelihood}_j + g_j * \log(n), \quad (10)$$

where loglikelihood_j is the log-likelihood of model j; g is the number of components in finite mixture model j; and n is the sample size (i.e., number of sites in dataset).

In this study, GFMNB-g models were developed from the crash data in Time Periods 1 and 2 with increasing numbers of components $g = 2$, 3, or 4. Figure 1 indicates that use of $g = 2$ (i.e., finite mixture models with two components) leads to the best goodness-of-fit as indicated by the lowest value of BIC. Hence, the number of components is selected as $g = 2$ and

Table 1: Classification-based EB method for HSID.

Step	Description
(1)	Use the GFMNB-g model, K-means algorithm, or hierarchical clustering algorithm to cluster the data into g groups
(2)	Separate the data into g groups based on the results of clustering
(3)	Estimate g NB regression models, one for each of the g subgroups, and use the corresponding SPF to get EB estimates for each site
(4)	Aggregate the EB estimates for all sites, rank the sites, and identify hotspots

Table 2: Summary statistics for road segments in Texas rural undivided highways dataset.

Variable	Time Period 1 (1997 and 1998)			Time Period 2 (1999–2001)		
	Minimum	Maximum	Mean (SD†)	Minimum	Maximum	Mean (SD†)
Crash number	0	59	2.93 (4.81)	0	78	4.58 (7.81)
F	40	24000	6391 (3835.01)	43.33	25333.3	6761.8 (4149.84)
LW (ft)	9.75	16.5	12.57 (1.59)	9.75	16.5	12.57 (1.59)
SW (ft)	0	40	9.96 (8.02)	0	40	9.96 (8.02)
CD	0	18.07	1.43 (2.35)	0	18.07	1.43 (2.35)
L (miles)	0.1	6.28	0.55 (0.68)	0.1	6.28	0.55 (0.68)

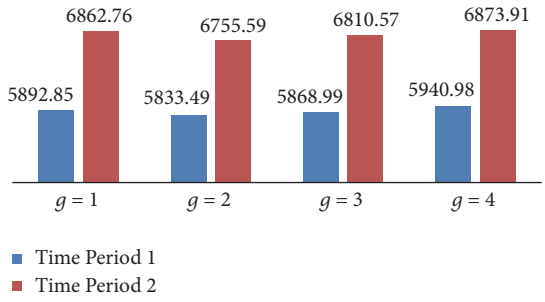

Figure 1: BIC values for GFMNB-g models.

the GFMNB-g models can now be indicated as GFMNB-2 models. It is important to note that, in general, $g = 2$ may not always be the optimal number of components and the choice will depend on the data. That said, BIC is a reasonable method to use to select g.

By examining Figure 1, one can see that the BIC values reported for the GFMNB-2 models are not as large as those for the regular NB model ($g = 1$) in the corresponding time period suggesting that the mixture models have better goodness-of-fit. Further, the choice of $g = 2$ based on BIC seems to suggest the existence of two distinct subpopulations within the crash data corresponding to each time period instead of a lone data population.

3.3. Grouping Results. According to the results of the GFMNB-g fitting procedure, it was determined that a GFMNB model with two components fit the data best. Thus, for each of the clustering-based-EB procedures for HSID, the full set of crash data was split into two groups for each time period (i.e., four groups total) from which NB models were estimated and corresponding EB estimates were calculated. That is to say, given the crash data for Time Periods 1 and 2, the three aforementioned clustering algorithms (i.e., k-means, hierarchical with complete linkage, and estimation of a GFMNB-g model) were applied to group the data from each time period into two clusters, for which EB estimates were computed.

Table 3 shows grouping results for each component, under each clustering method for both time periods considered in the study. For each component, the sample size along with the mean and standard deviation (SD) for each variable in the dataset (as described previously) is presented. From the table, it can be seen that, in general, mean values for the lane width, shoulder width, and segment length do not differ much between components. That said, in some cases, particularly for the groupings based on hierarchical clustering for Time Period 2, the mean number of crashes differs dramatically between components. Additionally, there is a substantial difference in the mean values of average daily traffic (F) between components for all clustering methods considered in both time periods. Such a trend suggests that the data considered here may come from underlying subpopulations where traffic volume is a defining characteristic for subpopulation membership and thus a good descriptor of the heterogeneity in the data.

With crash data clustered for each time period according to the three aforementioned clustering methods, EB estimates were then obtained after estimating an NB regression model for each of the two components corresponding to a given clustering method for a given time period. When interpreting results henceforth, one should consider the sample sizes used to estimate the NB models. For example, the sample size of "Component 1" (i.e., one grouping) for Time Period 2 as defined via hierarchical clustering with complete linkage has only 66 data points. Thus, modeling results associated with this group (namely, the results of the SPF and corresponding EB estimates) and the overall EB estimates for Time Period 2 as determined via hierarchical clustering (i.e., the aggregation of the EB estimates for components 1 and 2) should be interpreted with caution.

Table 3: Characteristics of each component.

Method	Component (sample)	Statistic	Crashes	F	LW	SW	L
			Time Period 1				
K-means	Component 1 (527)	Mean	5	10547.19	12.88	10.08	0.54
		SD	6.58	3013.67	1.76	8.45	0.6
	Component 2 (972)	Mean	1.796	4138.07	12.4	9.89	0.55
		SD	2.92	1820.303	1.46	7.77	0.69
Hierarchical	Component 1 (473)	Mean	5.063	10895.39	12.9577	10.24	0.53
		SD	6.58	2988.96	1.803	8.51	0.52
	Component 2 (1026)	Mean	1.939	4314.87	12.39	9.83	0.565
		SD	3.27	1924.28	1.44	7.778	0.72
GFMNB-2	Component 1 (738)	Mean	3	8191	12.58	11.22	0.29
		SD	4.45	3867.52	1.62	8.31	0.17
	Component 2 (761)	Mean	2.85	4646	12.57	8.74	0.81
		SD	5.13	2878.96	1.56	7.53	0.85
			Time Period 2				
K-means	Component 1 (972)	Mean	2.68	4364.14	12.4	9.89	0.55
		SD	4.71	2035.808	1.46	7.77	0.69
	Component 2 (527)	Mean	8.07	11184.04	12.88	10.08	0.54
		SD	10.6	3343.19	1.76	8.459	0.609
Hierarchical	Component 1 (66)	Mean	16.69	18144.65	13.59	12.39	0.64
		SD	17.71	3095.972	2.03	8.46	0.633
	Component 2 (1433)	Mean	4.02	6237.53	12.52	9.84	0.5496
		SD	6.52	3366.45	1.548	7.98	0.66
GFMNB-2	Component 1 (452)	Mean	6.27	9145.69	12.95	12.98	0.26
		SD	8.6	4457.79	1.74	8.12	0.15
	Component 2 (1047)	Mean	3.85	5732.65	12.41	8.66	0.68
		SD	7.33	3546.66	1.49	7.61	0.76

3.4. Test Results. In this section, evaluations of six different HSID methods, (1) AF, (2) AR, (3) EB (here, all data are considered as being from one population), (4) GFMNB-based EB method, (5)K-means-based EB method, and (6) hierarchical-based-EB method, are conducted using the three main tests from Cheng and Washington [32]. As all test procedures involve comparison across two different time periods, we use the time periods as defined in Table 2. Further, we consider three different scenarios in terms of the number of high-risk sites selected for consideration under each HSID method. These scenarios correspond to considering 1%, 5%, and 10% of all sites as high-risk (i.e., $c = 0.01$, 0.05, and 0.10). For example, in this study, when $c = 0.10$, a total of approximately 150 sites (i.e., ~10% of the 1,499 total sites) will be considered as high-risk, and their data will be used in calculation of the test statistics for the various HSID methods.

Table 4 shows the results of the six HSID methods considered under the Site Consistency Test. As aforementioned, the goal of the SCT is to measure consistency of a method in identifying sites as high-risk over time. The underlying principle is that high-risk sites should show consistently high crash counts over time, and thus the higher the value for the SCT statistic, the better performing the HSID method. From the table, it can be seen that the worst performing method across all cutoff levels for high-risk site identification (i.e., all c values) is the AR method. When one percent of sites are considered as high-risk, the conventional EB method, K-means-based EB method, and hierarchical-based EB method all perform equally well. For the cases in which 5% and 10% of sites are considered as high-risk, the K-means-based EB method is identified as the best performing HSID method according to the SCT. That said, in both of these cases, the value of the SCT test statistic for the hierarchical-based-EB method gives a value quite close to those obtained by the K-means-based method, indicating that it also seems to perform nearly as well in HSID.

The results of the six HSID methods being evaluated in terms of the Method Consistency Test are shown in Table 4. The MCT is designed to assess consistent identification of the same high-risk sites across different time periods. As such, the higher the value of the MCT test statistic, the better the performance of the HSID method (i.e., higher values imply that more sites were identified as high-risk in both time periods considered). From Table 4, one can see that, across all three cutoff levels for proportions of sites to consider as high-risk, the GFMNB-based EB method performs the best. That said, for the case in which 10% of sites are considered as high-risk, the K-means-based method performs just as well. Additionally, for all cutoff levels, the results of all clustering-based EB methods (e.g., GFMNB-, K-means-, and

Table 4: Results for various methods using three different tests.

Method	$c = 0.01$	$c = 0.05$	$c = 0.10$
Site Consistency Test (SCT)			
AF	269	1109	1911
AR	110	570	1051
EB	**361**	1376	2182
GFMNB-based EB method	329	1352	2115
K-means-based EB method	**361**	**1396**	**2186**
Hierarchical-based EB method	**361**	1395	2171
Method Consistency Test (MCT)			
AF	7	43	88
AR	2	27	63
EB	7	47	100
GFMNB-based EB method	**8**	**51**	**103**
K-means-based EB method	7	49	**103**
Hierarchical-based EB method	7	47	99
Total Rank Difference Test (TRDT)			
AF	365	7599	20721
AR	5944	24259	49548
EB	217	3543	14132
GFMNB-based EB method	**162**	**3226**	**10195**
K-means-based EB method	220	3273	12391
Hierarchical-based EB method	220	3420	14068

Note. Bold number indicates the best result.

hierarchical-based) exhibit quite similar performance. As was the case for the SCT, the AR method consistently performs the worst across all three cutoff levels for proportions of sites to be considered as high-risk.

Table 4 presents the results of the HSID-procedure evaluation under the Total Rank Difference Test. Again, this test is based on consistent identification of high-risk sites across time periods, but here, the rankings of sites identified as high-risk in one time period are compared to the rankings of the same sites in another time period. Hence, the smaller the value of the TRDT test statistic, the better the performance of the method in HSID. From the table, it can be seen that the GFMNB-based EB method yields the best HSID performance across all three cutoff levels of proportions of sites to be considered as high-risk. Under this test, the other clustering-based EB methods (e.g., K-means-based and hierarchical-based) outperform the naïve AF and AR methods across all cutoff values and also outperform the EB method for the 5% and 10% cutoffs. As was the case for the preceding two HSID performance tests, the AR method of HSID consistently performs the worst across all three cutoff levels of proportions of sites to be considered as high-risk.

Overall, the preceding tests indicate that the GFMNB-based EB method appears to exhibit the strongest HSID performance in all three tests and across the different cutoff levels of proportion of sites to be considered as high-risk. That said, the results obtained from the other clustering-based EB methods (e.g., K-means-based and hierarchical-based) are usually close and tend to outperform the AF, AR, and standard EB methods. From all tests, it appears that the AR method performs the worst. One possible explanation for this behavior may be that since the test sites are rural road segments, many may exhibit low ADT values and thus, as aforementioned, low-volume sites may be overrepresented as high-risk since the AR calculation normalizes by traffic count. Ultimately, HSID methods that themselves make use of the EB method when computing safety estimates prior to site ranking appear to perform better than the naïve AF and AR methods. This finding is consistent with many previous studies including [17, 36, 37].

3.5. Discussion. From the preceding analysis, it appears that the GFMNB-based EB procedure for HSID performs the best when evaluated with the three aforementioned test procedures [32] on the Texas rural undivided highway crash dataset. That said, it seems that all EB-based methods typically outperform the naïve methods, especially the AR HSID method. One possible reason the EB-based HSID methods may perform better is due their use of both the observed historical accident data and predicted accident count from similar sites with the SPF. Further, the EB methods are able to adjust for RTM bias. That said, the conventional EB method is not without its limitations for HSID. The main limitation, perhaps, arises when there is a substantial degree of heterogeneity in the crash data making it such that the crash data seem to arise from different subpopulations. Such heterogeneity could arise when large amounts of crash data collected from areas that differ dramatically geographically and with respect to a variety of other site-specific conditions. Oftentimes, crash data are aggregated in an effort to ensure

that sufficient sample sizes are available for model estimates (i.e., in an effort to reduce the standard error value of regression coefficients). In order to remedy this issue of not accounting for heterogeneity in the data, three clustering-based EB methods were proposed in this report. The idea behind these methods was to group the overall set of crash data (i.e., full list of study sites) into smaller subsets such that the site in each subset was more similar to sites within their groups than sites in other groups according to features, such as traffic volume, lane width, and other predictors. Further, it was hoped that such clustering could potentially help uncover the underlying groups/subpopulations from which the data could have been generated. Indeed, it appears that the clustering-based EB methods that applied *k*-means-, hierarchical-, and GFMNB-based clustering were able to analyze heterogeneous data and outperform more conventional methods in terms of HSID.

While the clustering-based EB methods for HSID have several benefits, they are not without their limitations. Perhaps the largest limitation of clustering-based EB methods is that, in some cases, they can cluster data into groups with relatively small sample sizes. Then, regression models (i.e., SPFs) developed from these small samples are more likely to exhibit their own issues such as biases in their coefficient estimates. This issue can further be compounded when analysts interpret the biased results and have the potential to make erroneous inferences/conclusions. As such, it is important that one be cognizant of the sample sizes of the clusters and what impacts they may have on model estimates and resulting inference [38]. Ultimately, as always, analysts are encouraged to interpret all results, especially those corresponding to regression models developed from small samples (e.g., 100 or less sites) with caution.

4. Conclusions

This study introduced three clustering-based EB methods for hotspot identification purposes. The clustering methods considered were the GFMNB-g model, *K*-means clustering, and hierarchical clustering with complete linkage. The newly developed clustering-based EB methods for HSID were compared in terms of performance to conventional HSID methods, including the EB method, as well as the naïve AF and AR method, with three methods comparing performance in HSID across different time periods as developed by Cheng and Washington [32]. When studying the HSID results based on applying the methodology to Texas undivided rural highway crash data, the results suggest that all three clustering-based EB analysis methods are preferred over the conventional statistical methods. Additionally, it seems that the accuracy of HSID can be enhanced by appropriately classifying roadway segments according to the heterogeneity of the crash data (i.e., clustering the data before developing SPFs for use in EB estimates). That said, one should always be cautious when classifying roadway segments into clusters as inappropriate classification of roadway segments can lead to erroneous results (e.g., biased coefficient estimates from SPFs developed from small sample sizes). Although the proposed clustering-based EB method is not yet ready for practical application, transportation safety analysts may use the clustering-based EB method to calculate the EB estimates and avoid manually identifying similar groups within the heterogeneous crash dataset, a task that may be difficult as the underlying subpopulations in the data are usually unknown. Future work could evaluate development of a performance measure to evaluate the overall HSID performance of the three clustering-based EB methods (i.e., to determine which clustering method is best and when it is best to use each).

Conflicts of Interest

The authors declare that they have no conflicts of interest.

Acknowledgments

The authors would like to thank Dr. Dominique Lord from Texas A&M University for graciously providing us with the Texas crash data. This research is sponsored jointly by the Pacific Northwest Transportation Consortium (Contract no. DTRT13-G-UTC40), the National Natural Science Foundation of China (Grant no. 51608386 and Grant no. 71601143), and Shanghai Sailing Program (Grant no. 16YF1411900).

References

[1] B. Persaud, C. Lyon, and T. Nguyen, "Empirical Bayes procedure for ranking sites for safety investigation by potential for safety improvement," *Transportation Research Record*, no. 1665, pp. 7–12, 1999.

[2] C. Dong, D. B. Clarke, X. Yan, A. Khattak, and B. Huang, "Multivariate random-parameters zero-inflated negative binomial regression model: an application to estimate crash frequencies at intersections," *Accident Analysis & Prevention*, vol. 70, pp. 320–329, 2014a.

[3] X. Ye, V. M. Garikapati, D. You, and R. M. Pendyala, "A practical method to test the validity of the standard Gumbel distribution in logit-based multinomial choice models of travel behavior," *Transportation Research Part B: Methodological*, 2017.

[4] C. C. Xu, P. Liu, W. Wang, and Z. B. Li, "Evaluation of the impacts of traffic states on crash risks on freeways," *Accident Analysis & Prevention*, vol. 47, pp. 162–171, 2012.

[5] Y. J. Zou, J. J. Tang, L. T. Wu, K. Henrickson, and Y. H. Wang, "Quantile analysis of factors influencing the time taken to clear road traffic incidents," in *Proceedings of the Institution of Civil Engineers-Transport*, vol. 170, pp. 296–304, 2017a.

[6] J. Tang, F. Liu, W. Zhang, R. Ke, and Y. Zou, "Lane-changes prediction based on adaptive fuzzy neural network," *Expert Systems with Applications*, vol. 91, pp. 452–463, 2018.

[7] L. Fawcett, N. Thorpe, J. Matthews, and K. Kremer, "A novel Bayesian hierarchical model for road safety hotspot prediction," *Accident Analysis & Prevention*, vol. 99, pp. 262–271, 2017.

[8] A. Montella, "A comparative analysis of hotspot identification methods," *Accident Analysis & Prevention*, vol. 42, no. 2, pp. 571–581, 2010.

[9] H. S. Manual, *American Association of State Highway and Transportation Officials (AASHTO)*, DC, Washington, Wash, USA, 2010.

[10] Y. Zou, K. Henrickson, L. Wu, Y. Wang, and Z. Zhang, "Application of the empirical Bayes method with the finite mixture model for identifying accident-prone spots," *Mathematical*

Problems in Engineering, vol. 2015, Article ID 958206, 10 pages, 2015.

[11] Y. J. Zou, H. Yang, Y. L. Zhang, J. J. Tang, and W. B. Zhang, "Mixture modeling of freeway speed and headway data using multivariate skew-t distributions," *Transportmetrica a-Transport Science*, vol. 13, pp. 657–678, 2017b.

[12] Y. Zou, D. Lord, Y. Zhang, and Y. Peng, "Comparison of sichel and negative binomial models in estimating empirical bayes estimates," *Transportation Research Record*, no. 2392, pp. 11–21, 2013.

[13] J. A. Deacon, C. V. Zegeer, and R. C. Deen, Identification of hazardous rural highway locations, 1974.

[14] C. Abbess, D. Jarrett, and C. C. Wright, "Accidents at blackspots: estimating the effectiveness of remedial treatment, with special reference to the 'regression-to-mean' effect," *Traffic Engineering & Control*, vol. 22, no. 10, pp. 535–542, 1981.

[15] Z. Xu and A. Y. Huang, "Safety benefits of converting HOV lanes to hot lanes: case study of the I-394 MnPASS," *Institute of Transportation Engineers. ITE Journal*, vol. 82, no. 2, pp. 32–37, 2012.

[16] L. Mountain, B. Fawaz, and D. Jarrett, "Accident prediction models for roads with minor junctions," *Accident Analysis & Prevention*, vol. 28, no. 6, pp. 695–707, 1996.

[17] L. Wu, Y. Zou, and D. Lord, "Comparison of sichel and negative binomial models in hot spot identification," *Transportation Research Record*, vol. 2460, no. 1, pp. 107–116, 2014.

[18] M. A. Mohammadi, V. A. Samaranayake, and G. H. Bham, "Safety effect of missouri's strategic highway safety plan: missouri's blueprint for safer roadways," *Transportation Research Record*, vol. 2465, pp. 33–39, 2014.

[19] W. Cheng, W. H. Lin, X. Jia, X. Wu, and J. Zhou, "Ranking cities for safety investigation by potential for safety improvement," *Journal of Transportation Safety & Security*, pp. 1–22, 2017.

[20] C. Xu, W. Wang, and P. Liu, "A genetic programming model for real-time crash prediction on freeways," *IEEE Transactions on Intelligent Transportation Systems*, vol. 14, no. 2, pp. 574–586, 2013.

[21] C. Dong, S. H. Richards, B. Huang, and X. Jiang, "Identifying the factors contributing to the severity of truck-involved crashes," *International Journal of Injury Control and Safety Promotion*, vol. 22, no. 2, pp. 116–126, 2015.

[22] J. J. Tang, F. Liu, Y. J. Zou, W. B. Zhang, and Y. H. Wang, "An improved fuzzy neural network for traffic speed prediction considering periodic characteristic," *IEEE Transactions on Intelligent Transportation Systems*, vol. 18, pp. 2340–2350, 2017.

[23] S. Zhang, J. J. Tang, H. X. Wang, Y. H. Wang, and S. An, "Revealing intra-urban travel patterns and service ranges from taxi trajectories," *Journal of Transport Geography*, vol. 61, pp. 72–86, 2017.

[24] E. Hauer, D. W. Harwood, F. M. Council, and M. S. Griffith, "Estimating safety by the empirical bayes method: a tutorial," *Transportation Research Record*, no. 1784, pp. 126–131, 2002.

[25] F. L. Mannering, V. Shankar, and C. R. Bhat, "Unobserved heterogeneity and the statistical analysis of highway accident data," *Analytic Methods in Accident Research*, vol. 11, pp. 1–16, 2016.

[26] F. L. Mannering and C. R. Bhat, "Analytic methods in accident research: methodological frontier and future directions," *Analytic Methods in Accident Research*, vol. 1, pp. 1–22, 2014.

[27] C. Dong, D. B. Clarke, S. H. Richards, and B. Huang, "Differences in passenger car and large truck involved crash frequencies at urban signalized intersections: an exploratory analysis," *Accident Analysis & Prevention*, vol. 62, pp. 87–94, 2014b.

[28] Y. Zou, Y. Zhang, and D. Lord, "Analyzing different functional forms of the varying weight parameter for finite mixture of negative binomial regression models," *Analytic Methods in Accident Research*, vol. 1, pp. 39–52, 2014.

[29] S. P. Lloyd, "Least squares quantization in PCM," *Institute of Electrical and Electronics Engineers Transactions on Information Theory*, vol. 28, no. 2, pp. 129–137, 1982.

[30] T. K. Anderson, "Kernel density estimation and K-means clustering to profile road accident hotspots," *Accident Analysis & Prevention*, vol. 41, no. 3, pp. 359–364, 2009.

[31] J. Z. Lu, "The elements of statistical learning: data mining, inference, and prediction," *Journal of the Royal Statistical Society: Series A (Statistics in Society)*, vol. 173, no. 3, pp. 693-694, 2010.

[32] W. Cheng and S. Washington, "New criteria for evaluating methods of identifying hot spots," *Transportation Research Record*, vol. 2083, pp. 76–85, 2008.

[33] D. Lord, S. Geedipally, B. Persaud et al., "Methodology to predict the safety performance of rural multilane highways [Final Report for NCHRP Project 17-29], 2008".

[34] B.-J. Park, D. Lord, and J. D. Hart, "Bias properties of Bayesian statistics in finite mixture of negative binomial regression models in crash data analysis," *Accident Analysis & Prevention*, vol. 42, no. 2, pp. 741–749, 2010.

[35] N. Eluru, M. Bagheri, L. F. Miranda-Moreno, and L. Fu, "A latent class modeling approach for identifying vehicle driver injury severity factors at highway-railway crossings," *Accident Analysis & Prevention*, vol. 47, pp. 119–127, 2012.

[36] W. Cheng and S. P. Washington, "Experimental evaluation of hotspot identification methods," *Accident Analysis & Prevention*, vol. 37, no. 5, pp. 870–881, 2005.

[37] L. Wu, D. Lord, and Y. Zou, "Validation of crash modification factors derived from cross-sectional studies with regression models," *Transportation Research Record*, vol. 2514, pp. 88–96, 2015.

[38] D. Lord, "Modeling motor vehicle crashes using Poisson-gamma models: examining the effects of low sample mean values and small sample size on the estimation of the fixed dispersion parameter," *Accident Analysis & Prevention*, vol. 38, no. 4, pp. 751–766, 2006.

Hindawi
Journal of Advanced Transportation
Volume 2017, Article ID 3192967, 8 pages
https://doi.org/10.1155/2017/3192967

Research Article

Turnout Fault Diagnosis through Dynamic Time Warping and Signal Normalization

Shize Huang,[1] Fan Zhang,[1] Rongjie Yu,[1,2] Wei Chen,[1] Fei Hu,[3] and Decun Dong[1]

[1]*Key Laboratory of Road and Traffic Engineering of Ministry of Education, Tongji University, Shanghai 201804, China*
[2]*State Key Laboratory of Rail Traffic Control and Safety, Beijing Jiaotong University, Beijing 100044, China*
[3]*Department of Electrical and Computer Engineering, University of Alabama, Tuscaloosa, AL 35487, USA*

Correspondence should be addressed to Rongjie Yu; yurongjie@tongji.edu.cn

Received 30 May 2017; Revised 27 August 2017; Accepted 20 September 2017; Published 23 October 2017

Academic Editor: N. N. Sze

Turnout is one key fundamental infrastructure in the railway signal system, which has great influence on the safety of railway systems. Currently, turnout fault diagnoses are conducted manually in China; engineers are obliged to observe the signals and make problem solving decisions. Thus, the accuracies of fault diagnoses totally depend on the engineers' experience although massive data are produced in real time by the turnout microcomputer-based monitoring systems. This paper aims to develop an intelligent diagnosis method for railway turnout through Dynamic Time Warping (DTW). We firstly extract the features of normal turnout operation current curve and normalize the collected turnout current curves. Then, five typical fault reference curves are ascertained through the microcomputer-based monitoring system, and DTW is used to identify the turnout current curve fault through test data. The analysis results based on the similarity data indicate that the analyzed five turnout fault types can be diagnosed automatically with 100% accuracy. Finally, the benefits of the proposed method and future research directions were discussed.

1. Introduction

Recently, the railway system has experienced rapid development all over the world [1] with both the freight and passenger traffic demands increasing. According to a report from the National Railway Administration of the People's Republic of China, the railway passenger and cargo transportation volume in China were 2.535 billion and 3.358 billion tons, respectively, in 2015 [2]. Therefore, due to the rapid development, the maintenance of the railway system has become a critical issue. Problems such as lack of relevant experienced professionals and heavy workloads to monitor the railway safety are emerging.

Turnout (shown in Figure 1), with high operation frequency, is the core component of the railway infrastructure since it is an essential device which moves the train from one track to another [3]. Turnout failures have caused several major railway accidents recently [4]. According to one report, more than 100 turnout failure events occurred in Changsha communication and signal division each year, and this accounted for 17.5% of all faults of the signaling equipment including turnout in the past five years [5].

Given the importance of the turnout system, microcomputer-based monitoring system (MMS) has been introduced to monitor the turnout state in real time in China. The MMS collects turnout operation current and voltage levels data; then engineers perform the failure diagnose analysis based on the displayed curves. The current manual diagnosis system has not only caused low diagnosis efficiency, but also increased the manpower and resources requirements [6]. In addition, the accuracy of the diagnosis mainly depends on the engineers' subjective experiences, where any misinterpretation of the data could lead to potential safety issues. Therefore, automatic turnout pattern detection methods are needed to identify the railway faults or failures.

Given the emerging issue, different methods have been utilized in the turnout failure diagnosis area. Zhao and Lu

Figure 1: Turnout system.

studied the turnout fault diagnosis system based on gray correlation analysis [7]. Roberts et al. used single throw mechanical equipment (STME) to detect the fault [8]. Neural network and fuzzy theory ([9–13]), Support Vector Machine (SVM), and improved SVM ([6, 14]) have also been applied for turnout fault diagnoses. Atamuradov et al. utilized Dynamic Time Warping (DTW) and expert systems to recognize three states including one healthy state and two failure states for turnout [15]. Ardakani et al. established the health assessment of the turnout by Principal Component Analysis (PCA) [16].

However, the abovementioned methods have several limitations for the targeted problem. For example, gray correlation analysis needs to choose suitable feature vectors or parameters that are hard to ascertain for large scale of fault types since a continuous search of large space is needed until the matching feature vector or parameter is identified. Besides, SVM-based methods cannot efficiently handle the large sample size. And expert system needs to have much a priori knowledge, which requires much manpower from experienced people to summarize the rules and knowledge based on years of experience. However, it is difficult to build a complete knowledge base due to more microcomputer-based monitoring systems and various environments and lack of rich experience. Besides, neural network and fuzzy theory models were developed based on large size of historical fault data, which is difficult to collect, and the model training process would be time consuming for tuning the model parameters.

Recently, Dynamic Time Warping (DTW) [17], a Dynamic Programming (DP) method which has originally been used in isolated word recognition area, has become popular. DTW calculates the distance between reference data and test data which has never been trained, and the smallest distance indicates the greatest similarity [18–20]. And it holds the benefits of requiring small amount of fault reference data, no need of selecting feature vectors, and requiring limited historical data and a priori knowledge. In this study, DTW was introduced to conduct the turnout fault diagnosis.

In addition to the analysis method, various data have been used in the literature, such as turnout operation current [21–23], turnout operation power [24], and data from sensors [25–27]. Most researchers choose the first two kinds of data since they can be obtained directly by the MMS. Moreover, the data from sensors requires the installation of extra sensors, which may be cost-prohibitive. Therefore, in this study, we utilize turnout operation current data to analyze the fault because current data can intuitively reflect the turnout fault while power data cannot.

Conventional methods to diagnose the fault based on turnout operation current data do not deal with current curve images. The turnout comes from different manufacturers, disparate MMSs, and diverse railway bureaus. Thus, the current curves images have much disturbance such as noise and grids which may seriously affect the accuracy of diagnosis results. Through the normalization of the current curve [28], we can effectively remove the noise in the image and diagnose the types of turnout faults.

Furthermore, in this study the single-action ZD6 turnout will be targeted given its wide range of applications. The operation current curves were collected from the MMS. We will first normalize the original turnout operation current curve and ascertain turnout reference templates. Then, the similarities between the reference templates and the test samples will be calculated through DTW. Each turnout diagnosis result would be recorded and finally the classification accuracy of the proposed approach will be evaluated.

The rest of this paper is organized as follows. Section 2 provides the meaning of the normal turnout operation current curve for each stage and introduces the method of image normalization method for turnout current curves. The method and principles of DTW and reference templates are explained in Section 3. Section 4 presents numerical experiments and result for the real turnout operation current curves to diagnose the faults, followed by the conclusions and discussions in Section 5.

2. Data Preparation

2.1. Turnout Operation Current Curve. Nowadays, MMS is the main approach to monitor the state of the turnout in China. Turnout operation current curve can intuitively reflect current changes of the switch machine. The operation process of the turnout can be divided into four stages: unlocking, conversion, locking, and slow release [12]. We can see the characteristics of the turnout operation current curve of different stages from Figure 2:

(1) Stage 1 (unlocking) (T_0-T_1): the motor starts with a large starting current which makes the curve rise suddenly. With the operation of the turnout system, the curve shows sharp decline and the turnout enters the unlocking stage.

(2) Stage 2 (conversion) (T_1-T_2): the current curve is smooth because the turnout operates smoothly during the conversion process.

(3) Stage 3 (locking) (T_2-T_3): the point moves to the other side of the rail and the current curve reduces to zero when the locking stage is finished.

(4) Stage 4 (slow release) (T_3-T_4): 1DQJ relay slows release and the current stays at zero continuously at slow release stage.

2.2. Image Standardization. Turnout operation current curves collected from different MMSs, diverse railway bureaus and various environments, may have much disturbance which causes fault detection errors. It is indispensable to process

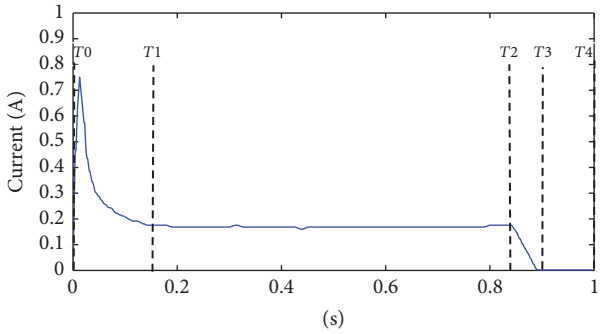

Figure 2: The turnout operation current curve.

turnout operation current curves and improve the accuracy of fault diagnosis. We need to remove the noise such that the disturbance in the images does not affect the experimental results. We have used the following procedure to remove the noise:

(1) Gray-scale transformation: it is a method of producing the gray value for each pixel of the original image according to a target condition. The gray value of the original image pixel is assumed as

$$D = f(x, y), \tag{1}$$

where D is the gray value of the original image pixel andxis abscissa andyis ordinate. Gray-scale enhancement is expressed as

$$f(x, y) = T[g(x, y)] \tag{2}$$

and $g(x, y)$ is the function of the image threshold.

(2) Binarization: the gray-scale image is converted into binary image which is a two-dimensional array ($M \times N$). The value of the pixel is set to 0 if the gray value is less than the threshold T; otherwise the value of the pixel is set to 1. The function of the image threshold is

$$g(x, y) = \begin{cases} 0 & f(x, y) \le T \\ 1 & f(x, y) > T. \end{cases} \tag{3}$$

(3) Noise removal: the first step is to find out the target region surrounded by the axis through the sum of the rows and columns in the two-dimensional array. Then isolated pixels are removed from the object region with open operations including erosion and dilation.

(4) Refinement: the denoising image may have multiple zero pixels in one column. And this situation would lead to the phenomenon that a moment corresponds to a number of current values in the coordinate transformation. It is assumed that the value of L pixel is 0, and the value R in that row is

$$R = \{r_1, r_2, r_3, \ldots, r_L\} \tag{4}$$

and r_1 is the value of 1 pixel.

The number of rows in the kth column with the value of pixel of 0 is

$$r_K = \frac{\sum_{i=1}^{L} r_i}{L} \tag{5}$$

and others are set to 1.

(5) Coordinate transformation: the purpose of the coordinate transformation is to convert the coordinate of the curve from the RO'C coordinate system to the tO'I coordinate system. We assume that the point M with coordinate (c_m, r_m) in the RO'C coordinate system has (t_m, I_m) in the tO'I coordinate system. Thus

$$\left(\frac{OM_1}{OB}\right)_{\text{RO'C}} = \left(\frac{OM_1}{OB}\right)_{\text{tO'I}}$$
$$\left(\frac{OM_2}{OA}\right)_{\text{RO'C}} = \left(\frac{OM_2}{OA}\right)_{\text{tO'I}}. \tag{6}$$

Point coordinate is

$$\left(\frac{c_m - c_1}{c_2 - c_1}\right) = \left(\frac{t_m - t_0}{t_b - t_0}\right)$$
$$\left(\frac{r_2 - r_m}{r_2 - r_1}\right) = \left(\frac{I_m - I_0}{I_a - t_0}\right). \tag{7}$$

c_1, c_2, r_1, and r_2 are the edge line of location for the target area and t_0, I_0, t_a, I_a, t_b, and I_b are set by engineers.

(6) Normalization: the normalization aims to zoom the data proportionally and place it in a specific interval in order to make the algorithm universal because the data comes from disparate systems and manufacturers. It eliminates the influence of different coordinates. For example, the range of t in one image is 0 to 5 and in another it is 0 to 8. The same type of switch machine made in different factories has different current values but the turnout operation current curves have the same tendency. The original data is transformed linearly and the results are mapped to [0, 1]. The transformation function is as follows:

$$X' = \frac{X - X_{\min}}{X_{\max} - X_{\min}}. \tag{8}$$

And X' is a point after normalization. X is original data. $X_{\max}$ is the maximum value. $X_{\min}$ is the minimum value.

The normalization process is shown in Figure 3. All of reference templates and test samples must be processed.

3. Methodology

3.1. Dynamic Time Warping (DTW). In this study, DTW was used to calculate the similarities between test samples and reference templates in order to diagnose the fault types.

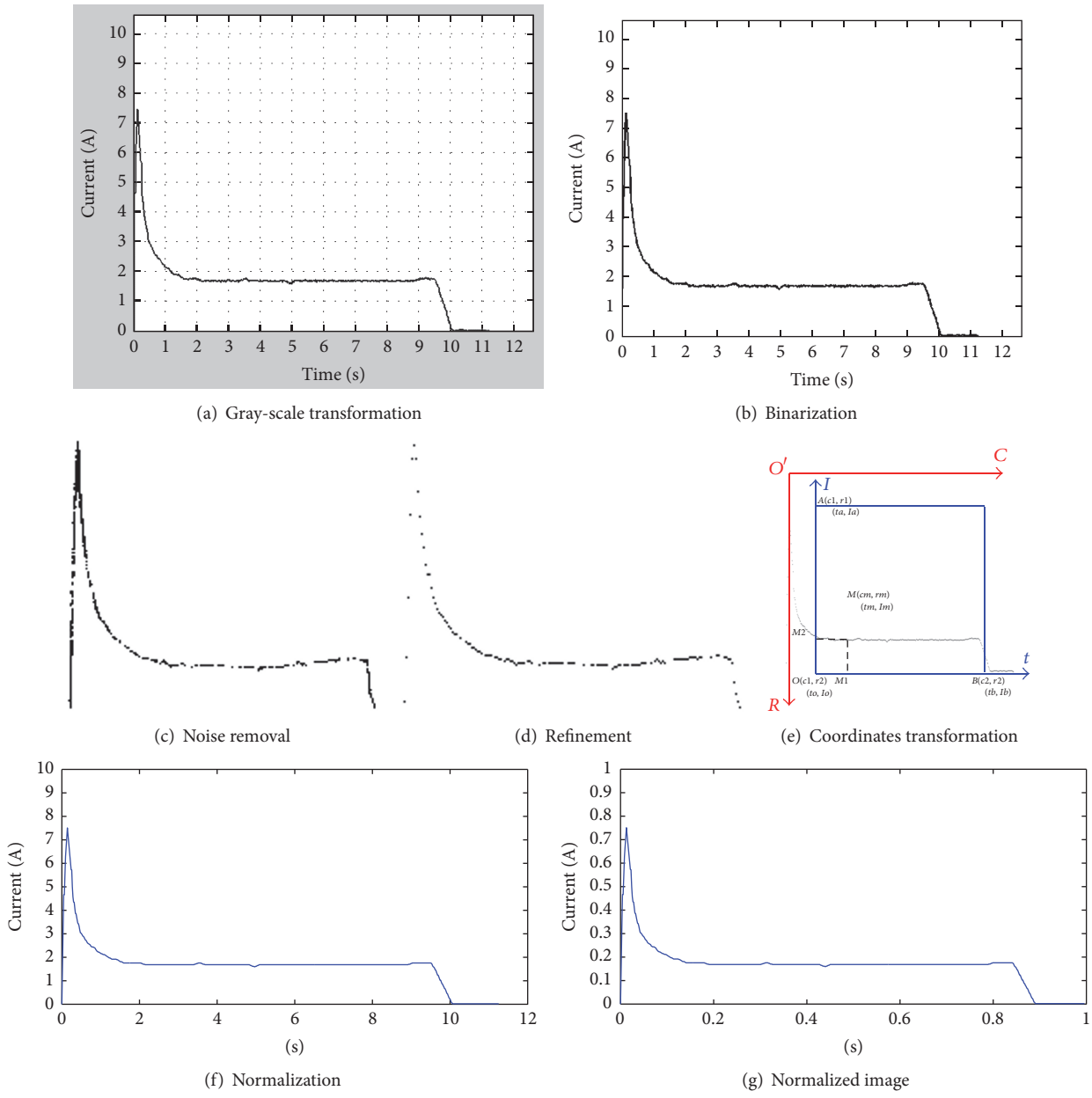

Figure 3: Image normalization process.

DTW was firstly introduced in the field of speech recognition to recognize the distortion of similar sounds, and it was a flexible distance-based curve comparison model which has been successfully applied to a wide range of time series data [17]. DTW is based on the idea of Dynamic Programming (DP), which can match different lengths of the time series and avoid mismatch between the peaks on curves even if the abscissa of peak is different. In Figure 4, the peak of the top line is point a. It is incorrect to simply consider that point a would correspond to point b' in the bottom curve. DTW can identify point b which corresponds to point a and then calculate the distance of two lines. It compares the similarity of two series by calculating a similarity matrix and searching for an optimal path with the minimum cumulative distance.

The path is not casually selected. The selected path must start from the lower left corner and end in the upper right corner, as shown in Figure 5. It is assumed that the grid points in the path are $(n_1, m_1), \ldots, (n_i, m_j), \ldots, (n_N, m_M)$. If the path has passed the point (n, m), the next passing point can only be one of the following three cases:

(1) $(n, m) = (n + 1, m)$.

(2) $(n, m) = (n + 1, m + 1)$.

(3) $(n, m) = (n, m + 1)$.

The path starts from the point (0, 0) to match the two sequences T and R. All the distances of points calculated before will be accumulated when it is reaching each point.

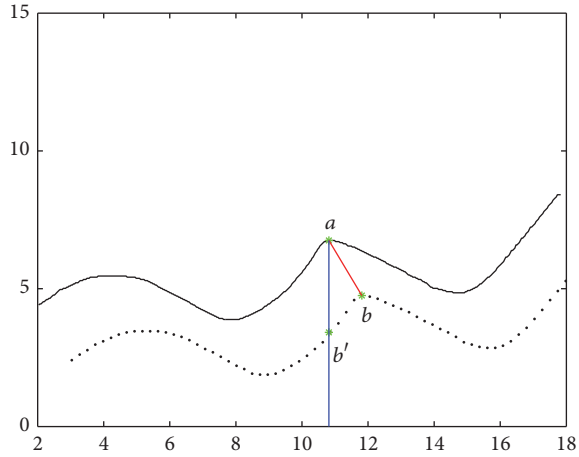

Figure 4: Match the peaks by using DTW.

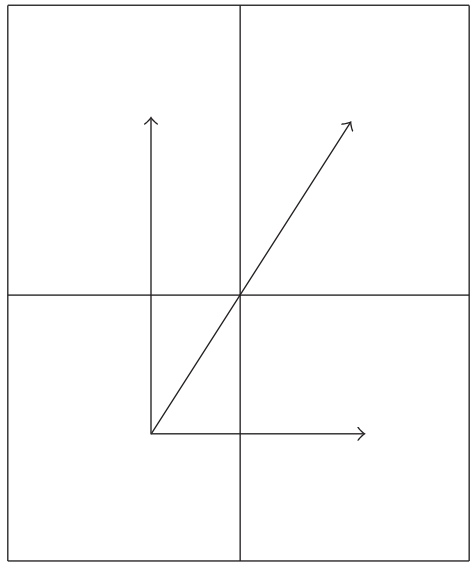

Figure 5: The selected path.

After reaching the end point (n, m), the optimal path is formed and the cumulative distance is the last total distance. The lower the cumulative distance between the time sequences is, the higher the similarity is [14]. Thus the minimum cumulative distance of the time sequences T and R is

$$D[(n,m)] = d[T(n), R(m)] + \min\{D(n+1,m), D(n+1,m+1), D(n,m+1)\}. \quad (9)$$

DTW algorithm compares the test samples with the reference templates directly without the need of knowing plenty of prior knowledge and historical data. It is a kind of practical method for fault diagnosis because this algorithm only needs several reference templates to diagnose the fault.

3.2. Confirming Reference Templates. A total of 5 ZD6 turnout fault type current curves were selected as the reference templates, which are shown in Figure 6.

Figure 6(a) presents the fault that the turnout suddenly stops running after starting. It can be seen that conversion time is short and locking line disappears. There are several potential reasons for that: (1) The switch machine action current is too small. (2) The switch machine has a poor performance. (3) The self-closing circuit of 1DQJ has faults that 1DQJ cannot continue after sucking up. The end of turnout jamming curve in Figure 6(b) is stable at a relatively high value. The reason for this is that there is foreign matter between the switch rail and the stock rail or the fault current of the switch machine is too small. Figure 6(c) shows the current curve when start-up circuit disconnects. The trend of this curve is almost straight without parabolic downward trend and the value of current stays at a high value. This failure is due to the mixed line of stator and rotor. Exceeding locking current curve (shown in Figure 6(d)) suddenly rises in the locking section. The reasons for this could be tight turnout adjustment, dirty slide plate, lack of oil in slide plate, the stock rail with a lateral move, and so on. Figure 6(e) shows the fault that automatic actuator is not flexible. This locking line of fault current curve is longer than normal curve and has a larger current value. The reason is that the turnout has been already locked and several shafts of the automatic actuator action are not flexible due to lack of oil. It causes the following: the automatic actuator operation becomes abnormal and the start connections cannot be disconnected.

4. Performance Analysis

In this study, a total of 260 current curves have been tested to verify the accuracy of proposed analysis method. Each test sample was compared with the 6 preselected reference templates including one normal template and 5 fault templates through DTW algorithm. Smaller distances between the test sample and reference templates indicate larger similarity. Shown as an example, the distances for 10 current curves between test samples and 6 kinds of reference templates are shown in Table 1. The system fault identification results are shown in Table 2.

From Table 1, we can find the smallest values in each row. That means that this curve has great similarity to the reference template where the smallest numbers are located. Thus, curves (1) and (9) indicate turnout jamming. Curves (2) and (6) represent that the turnout suddenly stops running after starting. Start-up circuit disconnection corresponds to curves (3) and (10). Exceeding locking current is for curves (5) and (8). Curves (4) and (7) indicate that automatic actuator is not flexible. We have verified in real experiments that all of our fault identification results are correct.

Table 2 shows the diagnosis results for the system. Each type of faults has 52 curves and the normal curve is 0 for total of 260 test samples.

Table 3 presents the accuracy of the system diagnosis result for 5 kinds of faults, and a 100% accuracy rate was achieved, while, in [15], the classification accuracy of fault detection decreased along with the increase of noise level. In this study, image normalization procedure is used to avoid the impact of noise and other interference on the result, and

Table 1: The distance between test samples and reference templates.

Curve	Normal	Turnout suddenly stops running after starting	Turnout jamming	Start-up circuit disconnection	Exceeding locking current	Automatic actuator is not flexible
(1)	83.74164	85.27251	0.07067	893.41762	138.01478	103.46032
(2)	73.65857	4.16262	1.79e + 308	1.79e + 308	1.79e + 308	1.79e + 308
(3)	137.36763	35.84982	482.30596	0.67117	271.46292	1.79e + 308
(4)	139.69423	110.73194	108.16510	1179.04733	68.79076	0.92959
(5)	157.70522	205.33733	316.96448	978.42134	85.86655	198.50005
(6)	79.33443	5.60595	1.79e + 308	1.79e + 308	1.79e + 308	1.79e + 308
(7)	124.28016	95.15331	107.97440	1199.03284	62.16355	2.54591
(8)	169.02205	216.35205	324.22023	1001.80220	97.32649	204.93660
(9)	79.1762	81.5792	0.3843	888.6765	134.7714	105.8146
(10)	132.39715	33.21258	464.77556	1.59861	261.00913	1.797e + 308

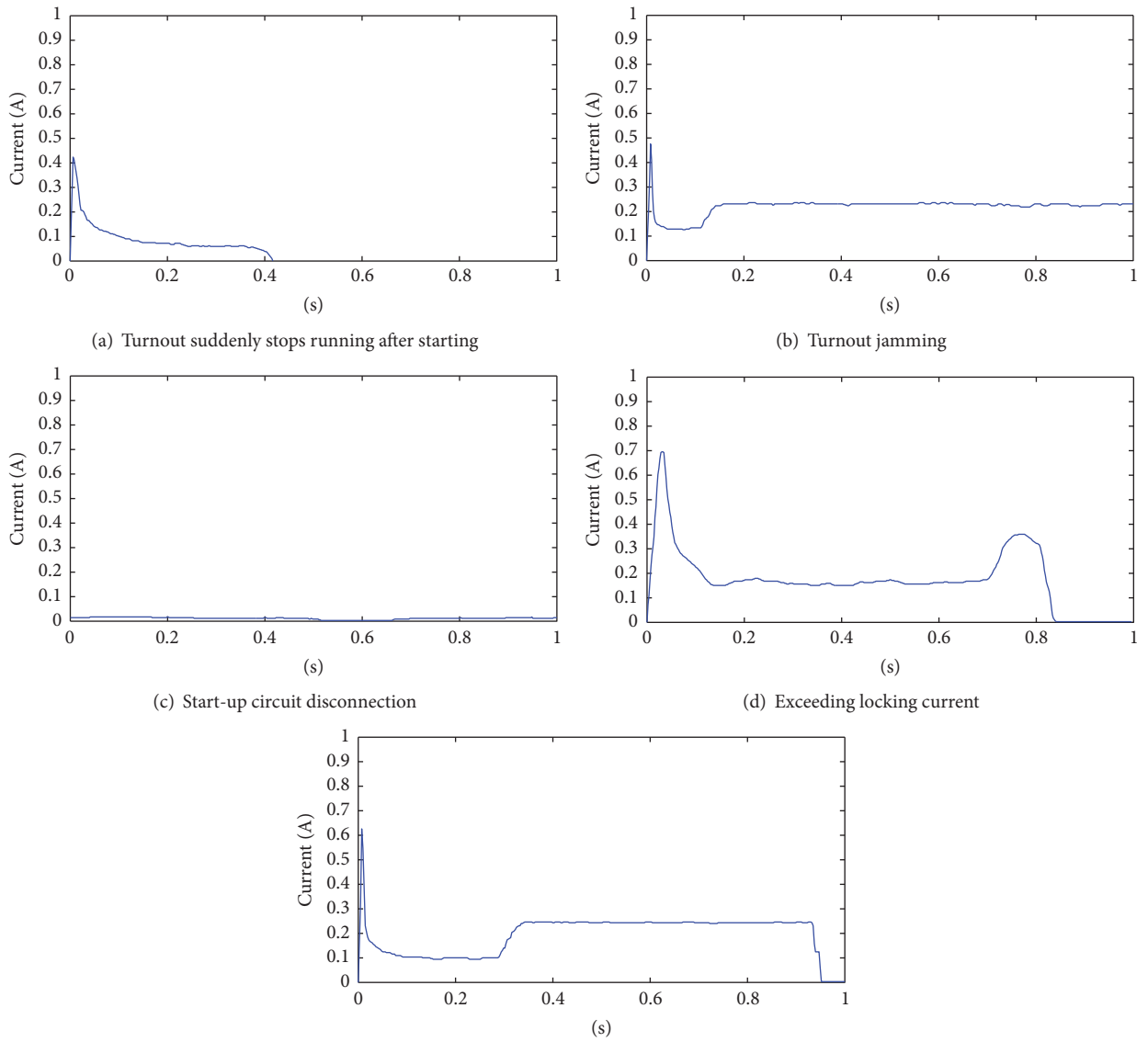

(a) Turnout suddenly stops running after starting

(b) Turnout jamming

(c) Start-up circuit disconnection

(d) Exceeding locking current

(e) Automatic actuator is not flexible

Figure 6: Turnout fault current curves.

Table 2: The number of different kinds of curves.

Type of curves	Normal	Turnout suddenly stops running after starting	Turnout jamming	Start-up circuit disconnection	Exceeding locking current	Automatic actuator is not flexible
Number of curves	0	52	52	52	52	52

Table 3: Accuracy of fault diagnosis.

Type	Turnout suddenly stops running after starting	Turnout jamming	Start-up circuit disconnection	Exceeding locking current	Automatic actuator is not flexible
Accuracy	100%	100%	100%	100%	100%

DTW scheme can greatly improve the diagnosis efficiency and accuracy without using other algorithms, rules, or a priori knowledge.

5. Discussion and Conclusions

In this study, we have developed an automatic fault diagnostic method based on DTW scheme for the railway turnouts. Firstly, all the turnout current curves captured from the MMS were normalized, and both normal and fault reference templates were identified. Then, a total of 260 turnout current curves which have never been trained were compared with 6 reference templates through DTW scheme. By seeking the minimum cumulative distance between test samples and reference templates, various fault types were identified. The analysis results indicated that the turnout faults could be diagnosed through the proposed method automatically with 100% accuracy for 5 typical fault current curves. Our scheme could avoid accidents caused by new-joined or less experienced technicians' errors and saves much manpower and material resources to improve the railway safety.

In a previous study [15], DTW was also used to analyze a similar problem; however, the analysis results showed that noises in the curves have significantly impacted the accuracy of the result, and the accuracy of system decreases as the noise level increases. This further reduces the system reliability and could even cause accidents because of fault misclassification. Unlike the previous study, in this study, a curve normalization procedure was used to eliminate the impacts of noises. In addition, Atamuradov et al. [15] used some rules to diagnose the turnout failure. However, rule-based system lacks flexibility, since the data from different MMSs may have built-in heterogeneity. In this study, the results indicate that the developed method can diagnose multiple kinds of turnout faults even if the values of current curve fluctuate much and the operation time of turnout is different. Besides, DTW does not require feature vector selection, historical data, or a priori knowledge, which is beneficial for real-time diagnosis.

Our next work would be investigating other algorithms (such as cluster algorithm or manifold learning or deep learning) to recognize the undefined type of turnout fault. Besides, big data learning issues will also be investigated since the collected current or voltage curves are extremely large in data size.

Conflicts of Interest

The authors declare that they have no conflicts of interest.

Acknowledgments

This research is supported by National Key R&D Program of China (2016YFB1200402), National Natural Science Foundation of China (61703308 and 71401127), and the State Key Laboratory of Rail Traffic Control and Safety (Contract no. RCS2017K003), Beijing Jiaotong University.

References

[1] X. Yang, X. Li, B. Ning, and T. Tang, "A survey on energy-efficient train operation for urban rail transit," *IEEE Transactions on Intelligent Transportation Systems*, vol. 17, no. 1, pp. 2–13, 2016.

[2] *Rail-way statistical bulletin in 2015*, National Railway Administration of the People's Republic of China, 2016, http://www.nra.gov.cn/fwyd/zlzx/hytj/.

[3] A. Morant, P.-O. Larsson-Kråik, and U. Kumar, "Data-driven model for maintenance decision support: A case study of railway signalling systems," *Proceedings of the Institution of Mechanical Engineers, Part F: Journal of Rail and Rapid Transit*, vol. 230, no. 1, pp. 220–234, 2016.

[4] *Selection of railway traffic accident case*, China Railway Press, Ministry of Railways of the People's Republic of China, Beijing, China, 1999, 27–87.

[5] G. Wang, T. Xu, T. Tang, T. Yuan, and H. Wang, "A Bayesian network model for prediction of weather-related failures in railway turnout systems," *Expert Systems with Applications*, vol. 69, pp. 247–256, 2017.

[6] F. Zhou, L. Xia, W. Dong, X. Sun, X. Yan, and Q. Zhao, "Fault diagnosis of high-speed railway turnout based on support vector machine," in *Proceedings of the International Conference on Industrial Technology (ICIT*, pp. 1539–1544, May 2016.

[7] L.-H. Zhao and Q. Lu, "Method of turnout fault diagnosis based on grey correlation analysis," *Journal of the China Railway Society*, vol. 36, no. 2, pp. 69–74, 2014.

[8] C. Roberts, H. P. B. Dassanayake, N. Lehrasab, and C. J. Goodman, "Distributed quantitative and qualitative fault diagnosis: Railway junction case study," *Control Engineering Practice*, vol. 10, no. 4, pp. 419–429, 2002.

[9] Y. Q. Zhai, *Research on Bayesian Networks in the Application of Rail Switch Control Circuit Fault Diagnosis*, Lanzhou Jiaotong University, 2012, 1–59.

[10] T. J. Wang and D. Yu, "Based on BP neural network turnout intelligent fault diagnosis method," *Journal of Railway Operation Technology*, vol. 17, no. 2, pp. 4–7, 2011.

[11] Y. M. Li and W. J. Wei, "Research of switch fault diagnosis system based on fuzzy neural network," *Railway Computer Application*, vol. 21, no. 1, pp. 35–39, 2012.

[12] K. Zhang, "The railway turnout fault diagnosis algorithm based on BP neural network," in *Proceedings of the IEEE International Conference on Control Science and Systems Engineering, CCSSE 2014*, pp. 135–138, chn, December 2014.

[13] M. Liu, X. Yan, X. Sun, W. Dong, and Y. Ji, "Fault diagnosis method for railway turnout control circuit based on information fusion," in *Proceedings of the 2016 IEEE Information Technology, Networking, Electronic and Automation Control Conference, ITNEC 2016*, pp. 315–320, May 2016.

[14] S. M. Wang and Y. Lei, "Fault diagnosis for railway switch control circuit based on ARPSO least squares support vector machine," *Journal of Lanzhou Jiaotong University*, vol. 29, no. 4, pp. 1–5, 2010.

[15] V. Atamuradov, F. Camci, S. Baskan, and M. Sevkli, "Failure diagnostics for railway point machines using expert systems," in *Proceedings of the 2009 IEEE International Symposium on Diagnostics for Electric Machines, Power Electronics and Drives, SDEMPED 2009*, fra, September 2009.

[16] H. D. Ardakani, C. Lucas, D. Siegel et al., "PHM for railway system—A case study on the health assessment of the point machines," in *Proceedings of the Prognostics and Health Management (PHM)*, pp. 1–5, June 2012.

[17] Q. He and Y. He, *MATLAB Extended Programming*, Tsinghua University Press, 2002, 340–349.

[18] Y. Li, D. Xue, E. Forrister, G. Lee, B. Garner, and Y. Kim, "Human Activity Classification Based on Dynamic Time Warping of an On-Body Creeping Wave Signal," *IEEE Transactions on Antennas and Propagation*, vol. 64, no. 11, pp. 4901–4905, 2016.

[19] M. Baumann, M. Ozdogan, A. D. Richardson, and V. C. Radeloff, "Phenology from Landsat when data is scarce: Using MODIS and Dynamic Time-Warping to combine multi-year Landsat imagery to derive annual phenology curves," vol. 54, pp. 72–83, 2017.

[20] S. Lu, G. Mirchevska, S. S. Phatak et al., "Dynamic time warping assessment of high-resolution melt curves provides a robust metric for fungal identification," *PLoS ONE*, vol. 12, no. 3, Article ID e0173320, pp. 1–21, 2017.

[21] J. J. Qiu, "Analysis of Action Current Curve of ZD6 Switch Machine," *Railway Signalling Communication*, vol. 4, no. 7, p. pp, 2008.

[22] Q. Guan, "High-speed Railway Switch Failure Diagnosis Based on FOA-LSSVM," *Bulletin of Science and Technology*, vol. 4, pp. 230–232, 2015.

[23] H. Yilboga, Ö. F. Eker, A. Güçlü, and F. Camci, "Failure prediction on railway turnouts using time delay neural networks," in *Proceedings of the 8th IEEE International Conference on Computational Intelligence for Measurement Systems and Applications, CIMSA 2010*, pp. 134–137, ita, September 2010.

[24] Y. M. He, *Research on Fault Diagnosis Method of High-speed Railway Turnouts*, Beijing Jiaotong University, 2014, 1–76.

[25] O. F. Eker, F. Camci, and U. Kumar, "SVM based diagnostics on railway turnouts," *International Journal of Performability Engineering*, vol. 8, no. 3, pp. 289–298, 2012.

[26] O. F. Eker, F. Camci, A. Guclu, H. Yilboga, M. Sevkli, and S. Baskan, "A simple state-based prognostic model for railway turnout systems," *IEEE Transactions on Industrial Electronics*, vol. 58, no. 5, pp. 1718–1726, 2011.

[27] C. Letot, P. Dersin, M. Pugnaioni et al., "A data driven degradation-based model for the maintenance of turnouts: A case study," *IFAC-PapersOnLine*, vol. 28, no. 21, pp. 958–963, 2015.

[28] K. K. Fu, B. L. Zheng, and X. Li, "Method of data extracting of image curve based on matlab," *Journal of Shantou University (Natural Science Edition)*, vol. 27, no. 2, pp. 52–54, 2010.

Hindawi
Journal of Advanced Transportation
Volume 2017, Article ID 7871561, 12 pages
https://doi.org/10.1155/2017/7871561

Research Article

Influences of Waiting Time on Driver Behaviors While Implementing In-Vehicle Traffic Light for Priority-Controlled Unsignalized Intersections

Bo Yang,[1] Rencheng Zheng,[1] Tsutomu Kaizuka,[1] and Kimihiko Nakano[2]

[1]*Institute of Industrial Science, The University of Tokyo, 4-6-1 Komaba, Meguro-ku, Tokyo, Japan*
[2]*Interfaculty Initiative in Information Studies, The University of Tokyo, 4-6-1 Komaba, Meguro-ku, Tokyo, Japan*

Correspondence should be addressed to Bo Yang; b-yang@iis.u-tokyo.ac.jp

Received 12 May 2017; Revised 3 September 2017; Accepted 14 September 2017; Published 17 October 2017

Academic Editor: Chunjiao Dong

In-vehicle traffic lights that assist drivers in crossing intersections are in development; however, the availability of the in-vehicle traffic light will be limited if the waiting time of a vehicle is not considered in actual traffic conditions, especially at priority-controlled unsignalized intersections that normally consist of one major and two minor roads. The present study therefore investigated the effects of the waiting time on driver behaviors to improve the in-vehicle traffic light for the priority-controlled unsignalized intersections. Gap acceptance theory that considers the waiting time was adopted in the implementation of the in-vehicle traffic light, to assist minor-road drivers in passing through the intersections by selecting appropriate major-road gaps. A driving simulator experiment involving 12 participants was performed for the minor and major roads, by applying the in-vehicle traffic light with and without the consideration of waiting time. Results demonstrate that the maximum acceleration strokes of minor-road vehicles were significantly reduced, indicating a lower possibility of aggressive driving when the in-vehicle traffic light was applied while considering the waiting time. Meanwhile, an improved steering stability was observed from the driver behaviors at the intersections, as the maximum lateral acceleration of minor-road vehicles significantly decreased when the waiting time was considered.

1. Introduction

There are thousands of accidents yearly at priority-controlled unsignalized intersections, which are one of the most common types of unsignalized intersections [1]. We previously proposed an in-vehicle traffic light based on the application of vehicular communications, displaying virtual traffic light information inside vehicles to assist drivers in safely crossing priority-controlled unsignalized intersections [2, 3]. However, the practicality of the in-vehicle traffic light at priority-controlled unsignalized intersections will be greatly limited if the waiting time of vehicles in actual traffic conditions is not considered. The present study thus aims to improve the in-vehicle traffic light by including the waiting time in the implementation of the system and performs driving simulator experiments to investigate the effects on driver behaviors when the in-vehicle traffic light considering waiting time is included.

A priority-controlled unsignalized intersection normally consists of a major road without a stop line and two minor roads that are controlled by stop lines. Vehicles on the major road are permitted to cross the intersection without stopping. In contrast, minor-road vehicles have to stop completely at the stop line first, waiting for an appropriate major-road gap to enter the intersection. Previous studies pointed out that one major problem of priority-controlled unsignalized intersections was that many drivers had difficulty in judging adequate gaps [4, 5]. Most accidents at priority-controlled unsignalized intersections were due to driver errors, especially the failures of minor-road drivers in selecting a proper

gap on the major road [6]. The American Association of State Highway and Transportation Officials therefore identified that the use of new technologies that assist drivers in judging gaps at priority-controlled unsignalized intersections is an important initiative in addressing intersection accidents [7].

Several methods have been proposed to assist drivers at priority-controlled unsignalized intersections [8–10]. Researchers from the Minnesota Department of Transportation developed an infrastructure-based system to help minor-road drivers make better decisions at rural unsignalized intersections, where multiple surveillance sensors were applied to track vehicles moving along the major road [11, 12]. Most of the technologies studied require comparatively high costs of infrastructure investment, including the installation of sensors at intersections.

V-2-X communication technologies have great potential for collecting information at priority-controlled unsignalized intersections, in that they have low deployment costs and wide operating distances. Given the application of vehicular communications, a novel concept of providing virtual traffic light information on the windshield has been presented [13, 14]. Traffic simulations have verified that traffic efficiency might be improved with virtual traffic lights [15–18].

To apply the concept of the virtual traffic light at priority-controlled unsignalized intersections, we proposed an in-vehicle traffic light system in our previous driving simulator studies according to gap acceptance theory [2, 3]. Gap acceptance theory was used to decide whether a major-road gap was appropriate for the entry of a minor-road vehicle [19]. According to the theory, the smallest major-road gap that ensures minor-road vehicles can safely cross intersections is referred to as the critical gap [20].

Previous studies considered the critical gap to be 6.5 s [21]. However, it was reported that the waiting time at intersections had a notable effect on the gap acceptance behaviors of drivers [22]. It was observed that minor-road drivers preferred to accept smaller gaps to enter intersections earlier if they had waited for a long time [23]. Other studies indicated that the longer a driver waited, the more the driver was willing to accept risks and the higher the likelihood the driver accepted a shorter gap [24, 25]. The critical gap should therefore not be considered a constant value. In fact, it would first decrease with waiting time and then converge to a constant value [26].

It remains unclear how driver behaviors are affected by the waiting time in the case of the implementation of an in-vehicle traffic light. The objective of the present study was therefore to analyze the effects on driver behaviors of the application of in-vehicle traffic lights considering the waiting time at priority-controlled unsignalized intersections.

The present paper firstly proposes the in-vehicle traffic light with consideration of the waiting time for priority-controlled unsignalized intersections and then details driving simulator experiments. Results and findings on driving operations and eye behaviors are then presented and discussed. The paper concludes with the implications of the results of the study.

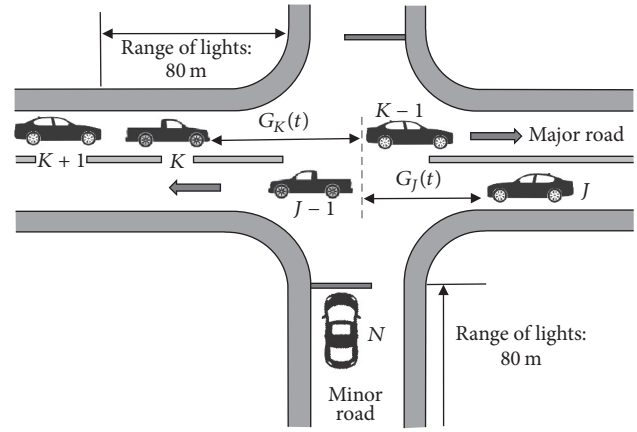

Figure 1: Gaps on the major road at a priority-controlled unsignalized intersection.

2. Methodology

To apply the waiting time in the implementation of an in-vehicle traffic light system, the modelling of priority-controlled unsignalized intersections, including the definition of the major-road gap, is firstly performed. An in-vehicle traffic light system is then proposed according to gap acceptance theory, in which the critical gap is decided considering the waiting time.

2.1. Modelling of Priority-Controlled Unsignalized Intersections. For a priority-controlled unsignalized intersection, as presented in Figure 1, when a minor-road vehicle N arrives at an intersection, the gaps on the major road can be defined as

$$G_K(t) = \frac{d_K(t)}{v_K(t)}, \qquad G_J(t) = \frac{d_J(t)}{v_J(t)}, \tag{1}$$

where $d_K(t)$ and $d_J(t)$ are the distances to the intersection and $v_K(t)$ and $v_J(t)$ are the velocities of major-road vehicles K and J at time t, respectively.

The major-road gap $G_N(t)$ for vehicle N will then be determined according to the vehicle's direction of motion, as shown in Table 1.

By comparing the major-road gap $G_N(t)$ with the critical gap G_C, the operation of a priority-controlled unsignalized intersection for vehicle N can then be expressed as

$$P_U(t) + P_V(t) = 1,$$
$$P_U(t) = \begin{cases} 1, & G_N(t) < G_C, \\ 0, & G_N(t) \geq G_C, \end{cases} \quad P_V(t) = \begin{cases} 1, & G_N(t) \geq G_C, \\ 0, & G_N(t) < G_C, \end{cases} \tag{2}$$

where $P_U(t)$ and $P_V(t)$ represent the priority statuses of major- and minor-road vehicles, respectively. $P_U(t) = 1$ means that the major-road vehicles have priority in crossing the intersection while $P_V(t) = 1$ means that the minor-road vehicle has priority in crossing.

Table 1: Major-road gap for minor-road vehicle N.

Direction of vehicle	Gap
Forward	$G_N(t) = \min(G_K(t), G_J(t))$
Left turn	$G_N(t) = G_J(t)$
Right turn	$G_N(t) = \min(G_K(t), G_J(t))$

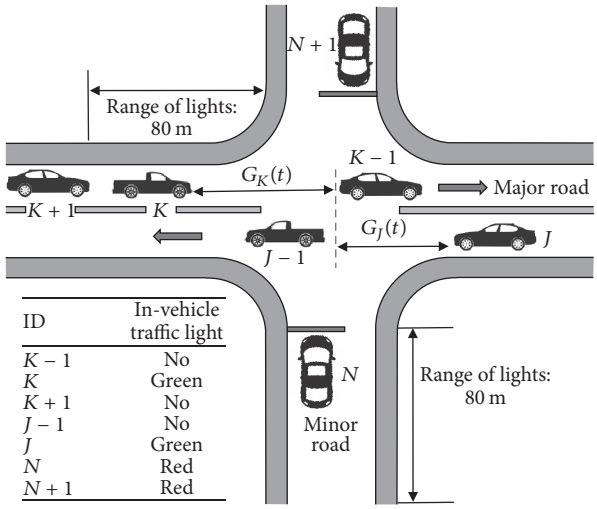

Figure 2: In-vehicle traffic lights at a priority-controlled unsignalized intersection when major-road gaps are smaller than the critical gap.

2.2. In-Vehicle Traffic Light considering the Waiting Time. As explained in the above section, the critical gap G_C will be affected by the waiting time of minor-road vehicles at intersections. According to the data from observational studies including [26], the critical gap is 6.5 s if drivers wait for less than 10 s, 5.5 s if the waiting time falls within 10 to 20 s, 5.25 s if the waiting time falls within 20 to 30 s, and 5 s if the waiting time is longer than 30 s. The relationship between the waiting time and critical gap at priority-controlled unsignalized intersections can therefore be expressed as

$$G_C(T) = 6.5 - H(T-10) - 0.25 \times H(T-20) - 0.25 \times H(T-30), \quad (3)$$

where $G_C(T)$ is the critical gap considering the waiting time and T is the waiting time of a minor-road vehicle; the value of 6.5 s is the critical gap when the waiting time is less than 10 s; $H(T-10)$, $H(T-20)$, and $H(T-30)$ are Heaviside step functions that represent the scenarios that drivers have waited for 10 to 20 s, 20 to 30 s, and longer than 30 s, respectively; and 0.25 is a parameter for adjusting the critical gap according to the changes in waiting time.

Figure 2 shows that, for a minor-road vehicle N approaching the priority-controlled unsignalized intersection, the state of the vehicle will be checked in real time to confirm whether the vehicle has arrived at the stop line. If the vehicle has arrived at the stop line, the in-vehicle traffic light system will start recording its waiting time and checking whether an oncoming minor-road vehicle exists. If an oncoming vehicle exists, the earlier minor-road vehicle will be selected as the leader, and a waiting list will be created to manage the minor-road vehicles waiting at the stop lines.

Table 2: Example of a waiting list for minor-road vehicles.

ID	Role	Direction	Rank
N	Leader	Right turn	1st
$N+1$	Follower	Forward	2nd

An example of the waiting list is shown in Table 2, according to the traffic condition presented in Figure 2. Minor-road vehicle N reaches the intersection earlier than vehicle $N+1$ and is therefore selected as the leader. If vehicle N wishes to make a right turn and turns on its right blinker while vehicle $N+1$ plans to move forward, it is possible for vehicles N and $N+1$ to collide at the intersection as their planned paths intersect. Vehicle $N+1$ is thus ranked second and will not enter the intersection together with vehicle N.

According to the above considerations of the rank and major-road gap, for minor-road vehicle N, an in-vehicle traffic light considering the waiting time $L_N(t)$ can be designed as

$$L_N(t) = -H(80 - d_N(t)) + R_N(t) \times P_N(t),$$
$$R_N(t) = \begin{cases} 2, & \text{Rank} = 1\text{st}, \\ 0, & \text{Rank} \neq 1\text{st}, \end{cases} \quad P_N(t) = \begin{cases} 0, & G_N(t) < G_C(T), \\ 1, & G_N(t) \geq G_C(T), \end{cases} \quad (4)$$

where $R_N(t)$ and $P_N(t)$ are functions for judging the rank and major-road gap of vehicle N, respectively; $L_N(t) = -1$ represents a red light, $L_N(t) = 0$ means that no light is displayed, and $L_N(t) = 1$ represents a green light; and $H(80 - d_N(t))$ is a Heaviside step function and $d_N(t)$ is the distance from vehicle N to the intersection.

For a major-road vehicle K, as shown in Figure 2, the in-vehicle traffic light considering the waiting time $L_K(t)$ can be expressed as

$$L_K(t) = H(80 - d_K(t)) + P_K(t),$$
$$P_K(t) = \begin{cases} 0, & G_N(t) < G_C(T), \\ 1, & G_N(t) \geq G_C(T), \end{cases} \quad (5)$$

where $P_K(t)$ is the function applied in judging the entry of the minor-road vehicle for vehicle K; $L_K(t) = 0$ means that no light is displayed, $L_K(t) = 1$ represents a green light, and $L_K(t) = 2$ represents a flashing yellow light that warns major-road drivers to proceed with caution; and $H(80 - d_K(t))$ is a Heaviside step function and $d_K(t)$ is the distance from vehicle K to the intersection.

An example of the in-vehicle traffic light considering the waiting time is shown in Figure 2, where major-road gaps are smaller than the critical gap. For vehicle $K+1$ that has not entered the range of the in-vehicle traffic light, or vehicles $K-1$ and $J-1$ that have crossed the intersection, no in-vehicle traffic light will be displayed. For minor-road vehicles in the range of the in-vehicle traffic light, including vehicle N, a red light will be displayed, requiring the vehicle to stop

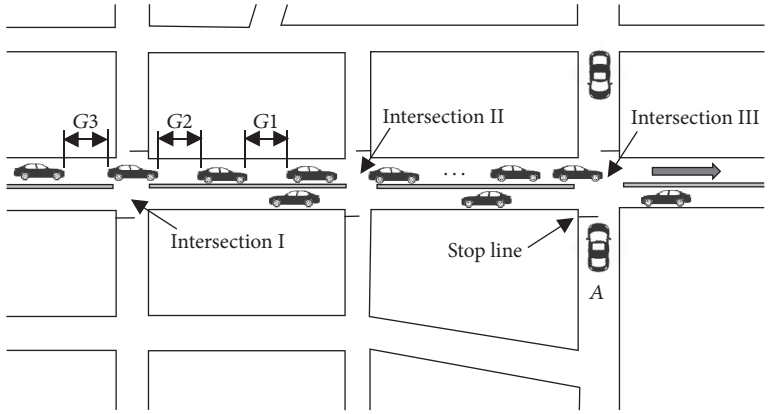

Figure 3: Driving scenario of the minor-road experiment with the participants in vehicle *A*.

at the stop line. Afterwards, the minor-road vehicles need to wait for a safe major-road gap to enter the intersection. If a safe gap appears, the light presented to the minor-road vehicle will turn green. For major-road vehicles that have entered the range of the in-vehicle traffic light, including vehicle *K*, a green light will be displayed if no minor-road vehicle is allowed to enter the intersection. If the entry of a minor-road vehicle is permitted, the in-vehicle traffic light displayed to major-road vehicles will become a flashing yellow light.

3. Experimental Study

3.1. Participants. Twelve males, ranging in age from 20 to 30 years (average of 24.5 years), participated in the study. All participants had a valid driving license and reported that their health did not adversely affect their driving performance. They had been driving for 4.7 years on average (range of 1 year to 8 years) and had a mean driving frequency of 1.2 times per week (range of once to three times per week).

3.2. Apparatus. An advanced driving simulator was used to produce realistic driving sensations for the participants. The simulator was composed of a motion platform with six degrees of freedom and a display system with a 140-degree forward field of view.

The in-vehicle traffic light system was mainly composed of a laptop computer and an iHUD head-up display (Springteq Electronics Corporation, New Taipei, Taiwan). The laptop computer was connected with the driving simulator via an Ethernet cable. During the experiments, the updated traffic information in the driving simulator, including the positions and velocities of vehicles, was transferred to the laptop computer in real time. The program of the in-vehicle traffic light, which was installed on the laptop computer, used the obtained information to judge the intersection conditions and to decide which light should be displayed. Finally, the light was presented to the participants via the head-up display, which was positioned according to guidelines for the placement of in-vehicle display systems [27].

3.3. Experimental Conditions. It was expected that the driving performances of minor-road drivers would be affected if their waiting times were considered by the in-vehicle traffic light system. Meanwhile, the driving safety of major-road drivers should also be assessed as the minor-road vehicles were allowed to enter intersections with smaller major-road gaps when considering the waiting time. Therefore, minor-road experiments and a major-road experiment were prepared for all participants to evaluate their driving behaviors.

3.3.1. Minor-Road Experiment. In the minor-road experiment, the participants were required to drive vehicle *A* to complete a right turn at intersection III. As shown in Figure 3, to analyze the effects of the waiting time, a congested major-road traffic flow was designed such that the participants waited for longer than 30 s. The congested major-road traffic flow comprised 10 vehicles and could be described with three parameters: (1) the speeds of the vehicles were set to 40 km/h, (2) the time headways between the vehicles were constant values between 2 and 4 s, which prevented the possible entry of minor-road vehicle *A* before the gaps *G*1, *G*2, and *G*3, when no in-vehicle traffic light was provided, and (3) the traffic flow rate during the experiment period was 900 vehicles/hour. Following the congested major-road traffic flow, three major-road gaps *G*1, *G*2, and *G*3 were provided as chances for the participants to cross the intersection.

To avoid learning effects, three orders of presentation of *G*1, *G*2, and *G*3 were prepared as shown in Table 3. Meanwhile, three assistance conditions were provided for each participant as presented in Table 4. The orders of *G*1, *G*2, and *G*3 and the assistance conditions were combined for the participants, considering counterbalancing.

3.3.2. Major-Road Experiment. For major-road drivers, the in-vehicle traffic light was expected to warn them of the entry of minor-road vehicles at intersections. According to the relationship between the critical gap and waiting time as shown in (3), the shortest critical gap for the minor-road vehicles was 5 s if the waiting time was longer than 30 s.

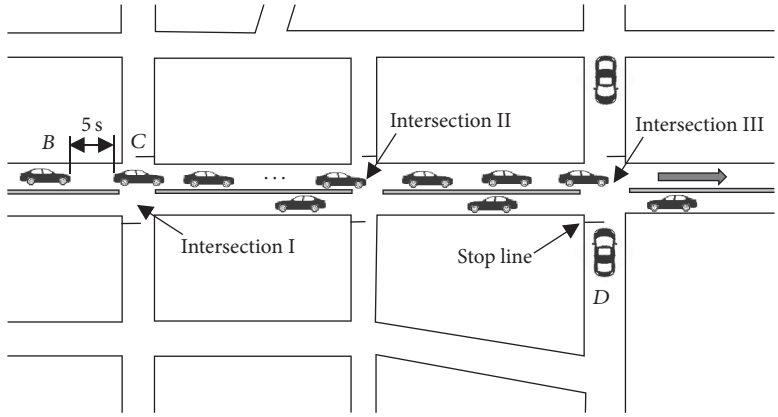

Figure 4: Driving scenario of the major-road experiment with the participants in vehicle *B*.

Table 3: Orders of major-road gaps.

Gap	Order 1	Order 2	Order 3
*G*1	5.5 s	6.0 s	6.5 s
*G*2	6.0 s	6.5 s	6.0 s
*G*3	6.5 s	5.5 s	5.5 s

Table 4: Assistance conditions of the minor-road experiment.

Number	Condition
(1)	Without in-vehicle traffic light
(2)	In-vehicle traffic light without considering waiting time
(3)	In-vehicle traffic light considering waiting time

For assessment of the driving safety of major-road drivers, the driving scenario of the major-road experiment is presented in Figure 4. Participants were in major-road vehicle *B*. Another major-road vehicle *C* was set to keep a constant gap of 5 s with vehicle *B* until vehicle *C* crossed intersection III, which was expected to offer a chance to minor-road vehicle *D* waiting at intersection III to enter. The major-road vehicles before vehicle *C* ensured that vehicle *D* waited for longer than 30 s. Similar to the case of the minor-road experiment, congested major-road traffic flow comprised 10 vehicles including vehicle *C*. The speeds of the vehicles were limited to 40 km/h and the traffic flow rate was 900 vehicles/hour. Meanwhile, constant time headways between 2 and 4 s were maintained. After vehicle *C* crossed intersection III, minor-road vehicle *D* accepted the gap between vehicles *B* and *C* and entered the intersection. The participants were required to react and avoid collisions with vehicle *D*.

The assistance conditions of the major-road experiment are presented in Table 5. As the gap of 5 s would not be accepted by the in-vehicle traffic light without considering the waiting time, the driver behaviors were analyzed under only two conditions.

3.4. Measured Variables and Evaluation Indexes. Driving data, including the positions, velocities, and acceleration of all vehicles, were recorded with the driving simulator.

Table 5: Assistance conditions in the major-road experiment.

Number	Condition
(1)	Without in-vehicle traffic light
(2)	In-vehicle traffic light considering waiting time

Meanwhile, eye-gaze data were measured with a Smart Eye Pro system (Smart Eye AB, Gothenburg, Sweden).

Four indexes were applied to evaluate driver behaviors in the minor-road experiment: the maximum acceleration stroke, blink rate, maximum lateral acceleration, and postencroachment time. The postencroachment time, maximum brake stroke, and perception response time were used for the major-road experiment.

The maximum acceleration stroke represented the maximum extent of the acceleration pedal stroke of vehicle *A*, when the participants turned right at intersection III, ranging from 0 to 1. The data were automatically recorded by the driving simulator during the experiments.

The blink rate was calculated from the waiting time of the participants at intersection III and the number of blinks during that period. The data of blink were recorded with the Smart Eye system which consisted of three cameras and two flashes. Before the experiment, adjustments and precalibrations of the eye-gaze tracking measurement were performed for every participant. The precalibration mainly comprised camera calibration, gaze calibration, and nine-point calibration. For camera calibration, the orientations, apertures, and focuses of the cameras were adjusted to keep the faces of the participants clearly positioned in the center of each image taken by the cameras. All the participants were then required to look around the three cameras and their personal profiles for eye-gaze tracking were created according to the snapshots taken by the cameras. To better recognize the eye-gaze, the profiles were optimized, especially for marking the inner and outer corners of the eyes. The gaze calibration was then performed for the three cameras to check the accuracy of the gaze calibration. Finally, a nine-point calibration was conducted to ensure the real-time detection of the visual point throughout the measuring

process. Moreover, if a deterioration in the performance of eye-gaze tracking was observed during the experiment, a recalibration could be performed to ensure a high-quality continuous measurement. Based on the accurate eye-gaze tracking data, all samples that belonged to a blink were marked with a blink id in the output data by the system. Meanwhile, the system had a filter that detected blinks by evaluating the measured eyelid opening samples over a period of approximately 700 ms, which means that blinks that lasted longer than 700 ms were not considered as blinks. Therefore, the obtained number of blinks had already been filtered automatically and could be considered reliable for evaluation.

Maximum lateral acceleration was the extreme value of lateral acceleration when vehicle A turned right at intersection III. The data of lateral acceleration were automatically recorded by the driving simulator during the experiments.

The postencroachment time was the elapsed time between the departure of a leading vehicle and the arrival of an oncoming vehicle in a conflict area. A shorter elapsed time between the departure of a leading vehicle and the arrival of an oncoming vehicle suggests greater risk of collision. The postencroachment time was chosen as a safety indicator at intersections for the following reasons that it was reported to be one of the best measures applying to the angle conflicting events, and a low value of postencroachment time indicates an encounter with high severity [28–30].

The postencroachment time T_P can be calculated as

$$T_P = \frac{S_i(t)}{v_i(t)}, \tag{6}$$

where $S_i(t)$ and $v_i(t)$ are the distance to the conflict area and the velocity of the oncoming vehicles, respectively.

In the minor-road experiment, minor-road vehicle A driven by the participants was the leading vehicle, and the arrival of the oncoming vehicle was actually controlled by the driving simulator; therefore, the values of postencroachment time were determined objectively and deemed suitable for describing the urgency of the situation. In the major-road experiment, major-road vehicle B driven by the participants acted as the oncoming vehicle. It was possible that the participants might choose to brake severely for a larger postencroachment time to satisfy their subjective safety margin. Therefore, the maximum brake stroke variable was applied for evaluating the driving safety together with the postencroachment time.

Maximum brake stroke represented the maximum extent of brake pedal stroke of the vehicle B, ranging from 0 to 1. It was automatically recorded by the driving simulator during the experiments.

The perception response time was defined as the total time, in seconds, elapsed from the entry of minor-road vehicle D to the depression of the brake pedal of major-road vehicle B, as shown in Figure 4.

3.5. Subjective Evaluations. Feelings of frustration and task difficulty were evaluated in the minor-road experiment. The feeling of safety was assessed in the major-road experiment. Evaluation scores were collected using a five-point-scale measurement questionnaire at the conclusion of each experimental session.

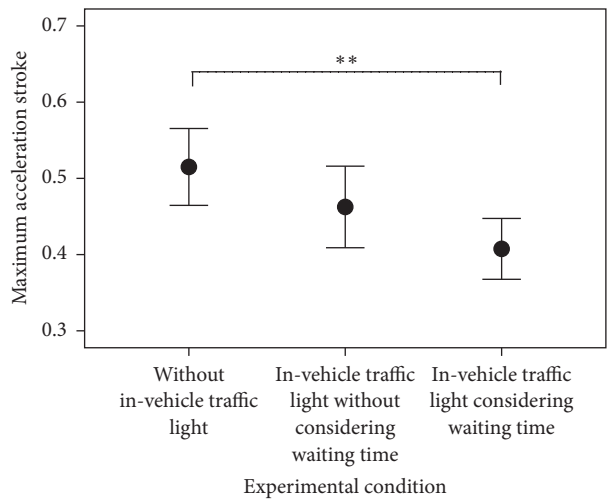

Figure 5: Results of the maximum acceleration stroke in the minor-road experiment. ** indicates a significant difference at $p < 0.01$ in statistical analysis.

3.6. Data Analysis. Statistical analysis was conducted to determine whether the consideration of waiting time significantly affected the driver behaviors and subjective evaluations for the 12 participants. The significance level was set at 0.05.

A one-way repeated measures ANOVA was conducted for the driver behaviors including the maximum acceleration stroke, blink rate, maximum lateral acceleration, postencroachment time, and perception response time.

A Wilcoxon signed-rank test was performed for the subjective evaluations.

4. Results

4.1. Driver Behaviors

4.1.1. Maximum Acceleration Stroke. The maximum acceleration stroke was used in the minor-road experiment to analyze the acceleration behaviors of the participants at intersection III. A higher maximum acceleration stroke indicates a higher possibility of aggressive driving.

Figure 5 shows that there was no significant difference in the maximum acceleration stroke between the conditions of there being no in-vehicle traffic light and there being an in-vehicle traffic light without considering the waiting time, although a decreasing trend was observed. The result for the in-vehicle traffic light considering the waiting time was significantly different from the result without an in-vehicle traffic light ($p = 0.001 < 0.05$).

4.1.2. Blink Rate. The blink rate was used to analyze the driver condition in the minor-road experiment. A higher blink rate

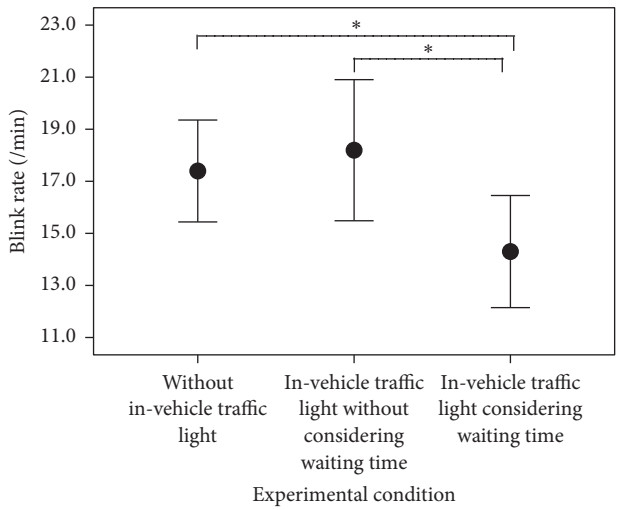

Figure 6: Results of the blink rate in the minor-road experiment. $*$ indicates a significant difference at $p < 0.05$ in statistical analysis.

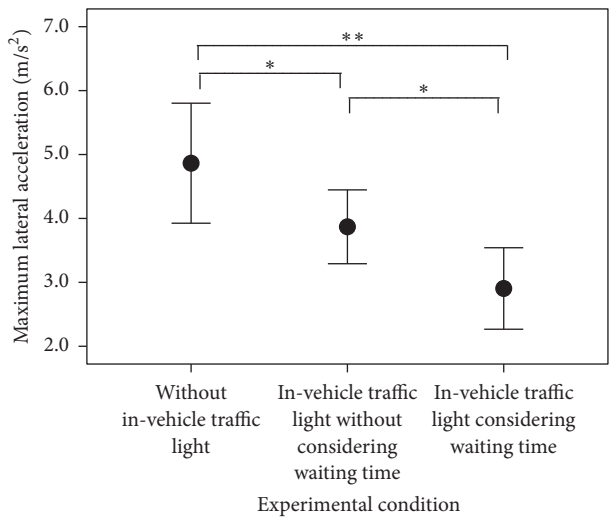

Figure 7: Results of maximum lateral acceleration in the minor-road experiment. $**$ and $*$ indicate a significant difference at $p < 0.01$ and $p < 0.05$ in statistical analysis, respectively.

might be considered the result of frustration. Figure 6 shows that when the in-vehicle traffic light considering the waiting time was applied, the blink rate was significantly lower than that for the in-vehicle traffic light without considering the waiting time ($p = 0.033 < 0.05$). Meanwhile, a significant difference in the blink rate was observed between the conditions of no in-vehicle traffic light and the provision of the in-vehicle traffic light while considering the waiting time ($p = 0.044 < 0.05$). There was no significant difference between the provision of no in-vehicle traffic light and that of the in-vehicle traffic light without considering the waiting time.

4.1.3. Maximum Lateral Acceleration. The maximum lateral acceleration was used to evaluate the steering stability in the minor-road experiment. A lower value of maximum lateral acceleration indicates better steering performance. Figure 7 shows that the maximum lateral acceleration of the minor-road vehicle was significantly lower when using the in-vehicle traffic light while considering the waiting time than when using the in-vehicle traffic light without considering the waiting time ($p = 0.049 < 0.05$). A significant difference was also observed between the conditions of no in-vehicle traffic light and the provision of the in-vehicle traffic light without considering the waiting time ($p = 0.043 < 0.05$).

4.1.4. Postencroachment Time. The postencroachment time was calculated to evaluate the driving safety in both the minor-road and major-road experiments. The results of the minor-road experiment are presented in Figure 8(a). The application of the in-vehicle traffic light while considering the waiting time significantly increased the postencroachment time, compared with the case of no in-vehicle traffic light ($p = 0.01 < 0.05$). Meanwhile, there was no significant difference in the postencroachment time between the provisions of the in-vehicle traffic light with and without the consideration of waiting time. The results of the major-road experiment are shown in Figure 8(b). When the in-vehicle traffic light with consideration of the waiting time was adopted, the postencroachment time significantly improved to have a mean value of 5.5 s, compared with the case of no in-vehicle traffic light ($p = 0.037 < 0.05$).

A longer postencroachment time indicates a lower possibility of collision at intersections. It therefore suggests that the driving safety in the minor-road experiment might not be significantly affected by consideration of the waiting time. The results of the major-road experiment imply that the driving safety of major-road drivers could be ensured when the shortest critical gap of 5 s was accepted by minor-road vehicles with the application of the in-vehicle traffic light considering the waiting time.

4.1.5. Maximum Brake Stroke. The maximum brake stroke was used to analyze the braking behaviors in the major-road experiment. Figure 9 shows that, for the maximum brake stroke in the major-road experiment, there was a significant effect of providing the in-vehicle traffic light ($p = 0.047 < 0.05$), which indicates that the maximum brake stroke could be significantly reduced by the usage of in-vehicle traffic light.

4.1.6. Perception Response Time. The perception response time was applied to evaluate the driver reactions to the entry of minor-road vehicles in the major-road experiment. A shorter perception response time indicates a faster reaction to the entry of minor-road vehicles. Figure 10 shows that the perception response time significantly reduced when the in-vehicle traffic light considering the waiting time was used ($p = 0.002 < 0.05$).

4.2. Subjective Evaluations

4.2.1. Evaluation of Frustration. Frustration was evaluated to analyze the driver condition in the minor-road experiment.

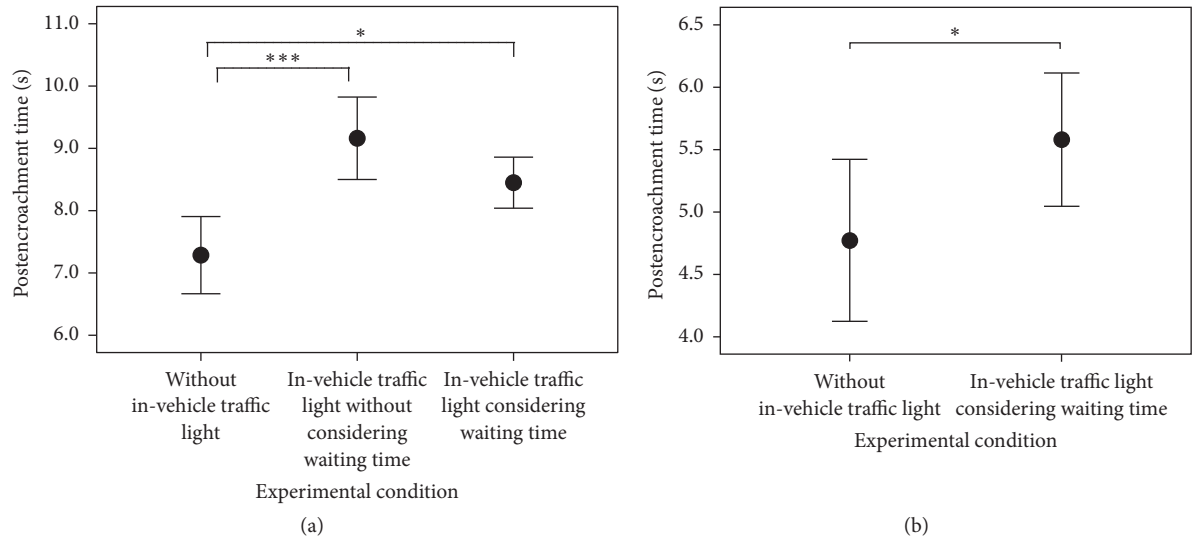

Figure 8: Results of the postencroachment time: (a) minor-road experiment; (b) major-road experiment. $***$ and $*$ indicate a significant difference at $p < 0.001$ and $p < 0.05$ in statistical analysis, respectively.

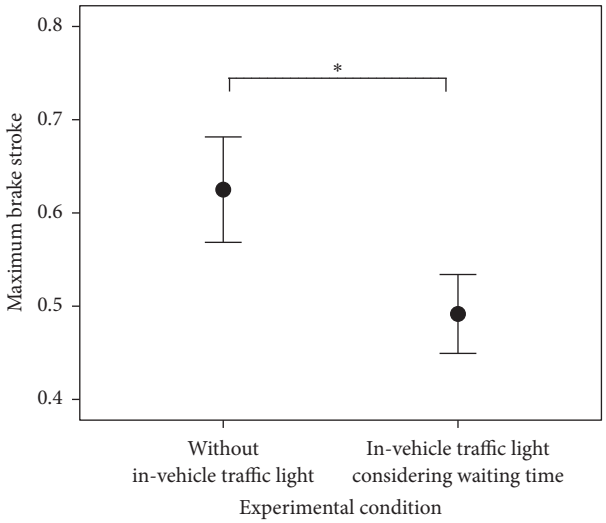

Figure 9: Results of the maximum brake stroke in the major-road experiment. $*$ indicates a significant difference at $p < 0.05$ in statistical analysis.

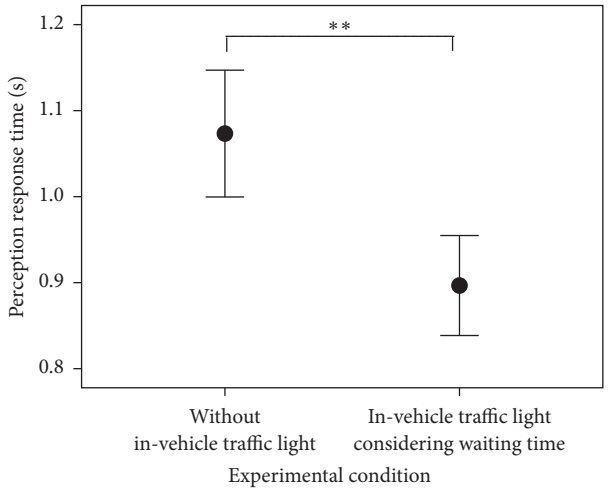

Figure 10: Results of the perception response time in the major-road experiment. $**$ indicates a significant difference at $p < 0.01$ in statistical analysis.

Figure 11 shows that the participants felt significantly more frustrated when there was no in-vehicle traffic light than when the in-vehicle traffic light without considering the waiting time was applied ($p = 0.002 < 0.05$). Moreover, the feeling of frustration was significantly less for the provision of the in-vehicle traffic light considering the waiting time than for the provision of the in-vehicle traffic light without considering the waiting time ($p < 0.001$).

4.2.2. Evaluation of Task Difficulty. The difficulties of completing the same driving task under different assistance conditions were evaluated in the minor-road experiment. Figure 12 shows that although the participants were required to turn right at the same intersection, they felt that it was significantly more difficult to complete the driving task without the in-vehicle traffic light than under the other two conditions ($p < 0.001$). No significant difference in task difficulty evaluation was observed between the cases of in-vehicle traffic lights with and without the consideration of waiting time.

4.2.3. Evaluation of Safety. Figure 13 presents the results of the driving safety evaluation of major-road drivers in the major-road experiment. A significant difference was observed between the conditions of no in-vehicle traffic light and the provision of the in-vehicle traffic light considering the waiting time ($p < 0.001$), indicating that the participants

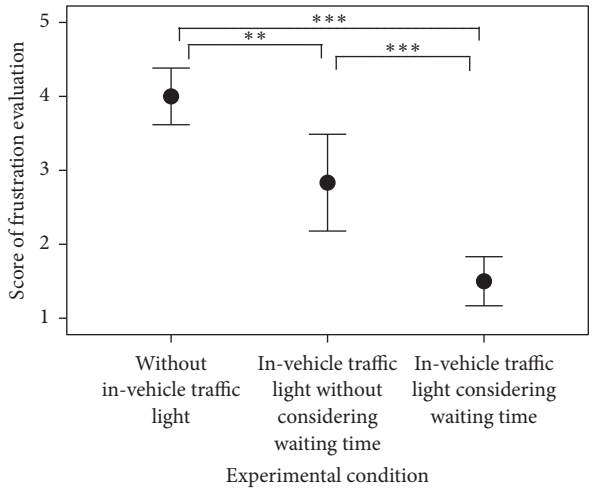

Figure 11: Scores of frustration evaluation in the minor-road experiment, ranging from 1 to 5: 1 = very low, 2 = low, 3 = average, 4 = high, and 5 = very high. $***$ and $**$ indicate a significant difference at $p < 0.001$ and $p < 0.01$ in statistical analysis, respectively.

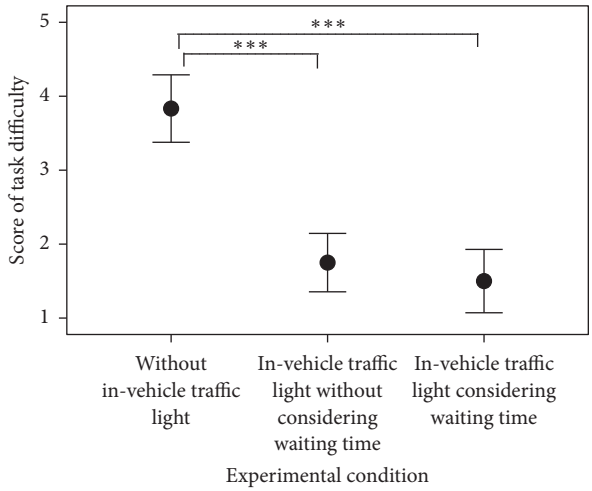

Figure 12: Scores of task difficulty evaluation in the minor-road experiment, ranging from 1 to 5: 1 = very low, 2 = low, 3 = average, 4 = high, and 5 = very high. $***$ indicates a significant difference at $p < 0.001$ in statistical analysis.

felt safer when assisted by the in-vehicle traffic light with consideration of the waiting time.

5. Discussions

It was expected that the driving experiences of minor-road vehicles would be improved through the consideration of waiting time in the implementation of an in-vehicle traffic light, without detriment to the driving safety of major-road vehicles. The experimental results were thus carefully analyzed, and several interesting results were found to deserve further discussion.

Figure 5 showed that the application of the in-vehicle traffic light considering the waiting time significantly reduced

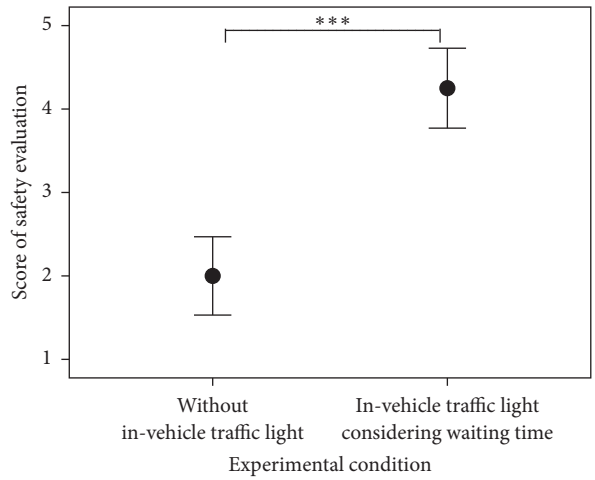

Figure 13: Scores of safety evaluation in the major-road experiment, ranging from 1 to 5: 1 = very low, 2 = low, 3 = average, 4 = high, and 5 = very high. $***$ indicates a significant difference at $p < 0.001$ in statistical analysis.

the maximum acceleration stroke of minor-road vehicles. It was revealed that the consideration of waiting time might be effective in preventing the aggressive driving of minor-road vehicles. Previous studies pointed out that acceleration-related indexes, including maximum acceleration, are suitable for evaluating aggressive or emotional driving [31, 32]. As for the cause of aggressive driving, it was reported that aggressive driving was more likely to occur in situations of dense traffic [33]. In the minor-road experiment, the continuous major-road traffic flow was considered challenging for the minor-road drivers, which might result in aggressive driving. Meanwhile, it has been demonstrated that challenging or unexpected traffic situations can induce frustration and other negative emotional states [34]. According to the frustration–aggression hypothesis, the frustration of drivers might also lead to risky and aggressive driving behaviors, including strong acceleration [35, 36].

Frustration was evaluated in the blink rate analysis and subjective evaluations. It was reported that the blink rate was highly related to the dopaminergic systems and the mental states including frustration might be effectively analyzed with the blink rate [37, 38]. The blink rate was, therefore, analyzed according to the hypothesis that the feeling of frustration can be detected by monitoring the blink rate [39]. Normally, the average blink rate is around 14 blinks per minute [40]. During the minor-road experiment, the measured blink rates ranged from 12 to 22 blinks per minute and are therefore considered reliable for evaluation. Moreover, previous studies suggested that the blink rate might increase with the level of frustration [41, 42]. According to the subjective evaluation of frustration, as shown in Figure 11, drivers felt less frustrated when provided with the in-vehicle traffic light with consideration of the waiting time than when provided with the in-vehicle traffic light without consideration of the waiting time, which coincided with the blink rate analysis. However, no significant difference in the blink rate was

observed between the conditions of no provision of the in-vehicle traffic light and the provision of the in-vehicle traffic light without considering the waiting time, although the participants reported more frustration without the in-vehicle traffic light in their subjective evaluation. This is considered due to the task difficulty. As presented in Figure 12, the participants reported that it was more difficult to complete the driving task without the in-vehicle traffic light, and it has been suggested that the blink rate tends to decrease if the task difficulty increases [43].

The maximum lateral acceleration was significantly lower when the in-vehicle traffic light was provided while considering the waiting time than when the in-vehicle traffic light was provided without considering the waiting time as shown in Figure 7. The result suggests that the steering stability of minor-road vehicles is improved by considering the waiting time when using the in-vehicle traffic light. It has been suggested that lower maximum lateral acceleration corresponds to less deviation from the idealized curved path during a turn at an intersection [44].

The major-road experiment was performed to evaluate the driving safety of major-road drivers. A critical part of driving safely is the ability to detect and respond to emergency traffic hazards. The entry of minor-road vehicles in the major-road experiment was considered an emergency hazard, and the perception response time was therefore used to analyze the detection and response ability of major-road drivers. As shown in Figure 10, when there was no in-vehicle traffic light, the perception response time ranged from 1.01 to 1.15 s. When the in-vehicle traffic light considering the waiting time was applied, the perception response time decreased and ranged from 0.84 to 0.96 s. It has been reported that the mean value of the perception response time is around 1 s [45]. Meanwhile, in analyzing the duration of a driver's perception response to intruding vehicles at intersections, another study found that the mean time from the start of motion until brake pedal application was 1.14 s, which was in accordance with the results when no in-vehicle traffic light was applied [46, 47]. It is noted that, with the provision of the in-vehicle traffic light, the major-road drivers had an advantage in detecting the entry of minor-road vehicles, as they would be immediately warned once other vehicles started entering intersections. Moreover, as presented in Figure 9, the maximum brake stroke significantly decreased with the provision of in-vehicle traffic light. It has been demonstrated that vehicle performance might deteriorate with an increase in the brake stroke [48]. The analysis of driving operations revealed that a longer postencroachment time could be achieved with a smaller maximum brake stroke by applying the in-vehicle traffic light, which suggested that the safety of major-road drivers might be ensured. Furthermore, as shown in Figure 13, the subjective evaluation of driving safety was also in accordance with the results obtained based on the driving operations.

As a limitation of the study, the practical application of the proposed in-vehicle traffic light is still needed to be studied with a large random sample, which can truly represent the driver population in reality. Actually, to represent the true driver population, a variety of factors should be taken into consideration, including gender, age, driving experience, education background, and personal characteristics [49–51]. Meanwhile, the practical application of the in-vehicle traffic light requires the deployment of vehicular communication devices for all the vehicles, and it is a difficult task to provide the same driving conditions for every participant in an actual vehicle experiment. Therefore, this study was mainly executed with a driving simulator to analyze the influences of waiting time on driver behaviors, while using the in-vehicle traffic light at priority-controlled intersections. On the other hand, considering the limited experimental conditions in this study, the acceptable sample of participants was determined to satisfy the requirement of sufficient statistical power [52]. Statistical power is the likelihood of finding statistically significant differences given that statistically significant differences actually do exist [53]. It depends on three factors: alpha level, effect size, and sample size. In this study, the alpha level and sample size were set as 0.05 and 12, respectively. Therefore, the statistical power could be estimated based on the effect size, which was related to the mean values and standard deviations. Based on the calculated results of SPSS and a widely accepted calculation method [54], the statistical power of this study was around 0.8, which was acceptable for consideration in general studies [55, 56].

6. Conclusion

Given the application of vehicular communications, the present study proposed an in-vehicle traffic light system with the consideration of waiting time to assist drivers in crossing priority-controlled unsignalized intersections. Moreover, to evaluate the effects of the waiting time on driver behaviors, two driving simulator experiments were performed with 12 participants for minor-road and major-road cases.

In the minor-road case, the application of an in-vehicle traffic light considering the waiting time significantly reduced the maximum acceleration stroke and blink rate, indicating that the aggressive driving of minor-road vehicles might be successfully avoided with such application. Meanwhile, a significant decrease was observed in the maximum lateral acceleration with the consideration of waiting time, showing that better steering stability might be achieved.

In the major-road case, it was observed that the postencroachment time significantly increased and the perception response time significantly decreased when applying the in-vehicle traffic light while considering the waiting time. The results indicate that the in-vehicle traffic light might enhance the drivers' ability to detect the entry of other vehicles, which would contribute to safe driving. According to the results of postencroachment time, it is believed that the driving safety of major-road drivers can be ensured when the in-vehicle traffic light is applied while considering the waiting time.

The present study may contribute to the development of driver assistance systems at priority-controlled unsignalized intersections and provide useful references for further applications of V-2-X communications in intelligent transportation systems. The proposed system will be implemented with a real vehicle in future work.

Conflicts of Interest

The authors declare that there are no conflicts of interest regarding the publication of this article.

Acknowledgments

This study was supported by the Next-Generation Energies for Tohoku Recovery Project.

References

[1] National Highway Traffic Safety Administration, *Fatality Analysis and Reporting System*, U. S. Department of Transportation, Washington, D. C., USA, 2014.

[2] B. Yang, R. Zheng, K. Shimono, T. Kaizuka, and K. Nakano, "Evaluation of the effects of in-vehicle traffic lights on driving performances for unsignalised intersections," *IET Intelligent Transport Systems*, vol. 11, no. 2, pp. 76–83, 2017.

[3] B. Yang, R. Zheng, and K. Nakano, "Application of in-vehicle traffic lights for improvement of driving safety at unsignalized intersections," in *Proceedings of the IEEE Intelligent Vehicles Symposium, IV 2015*, pp. 628–633, Seoul, Korea, July 2015.

[4] D. Max, S. Craig, J. W. Nicolas, and C. Janet, *Intersection Decision Support: an Overview Report #6 in the Series: Developing Intersection Decision Support Solutions*, University of Minnesota, 2007.

[5] R. David, A. Sofia, E. S. Steven, A. M. James, and Y. C. Ching, "Gap acceptance for vehicles turning left across on-coming traffic: implications for intersection decision support design," in *Proceedings of the Transportation Research Board 85th Annual Meeting*, pp. 1–25, Washington, D. C., USA, 2006.

[6] National Highway Traffic Safety Administration, *Traffic Safety Facts 2014*, U.S. Department of Transportation, Washington, D. C., USA, 2016.

[7] National Cooperative Highway Research Program, *NCHRP Report 500, Vol. 5: a Guide for Addressing Unsignalized Intersection Collisions*, Transportation Research Board, 2003.

[8] J.-A. Jang, K. Choi, and H. Cho, "A fixed sensor-based intersection collision warning system in vulnerable line-of-sight and/or traffic-violation-prone environment," *IEEE Transactions on Intelligent Transportation Systems*, vol. 13, no. 4, pp. 1880–1890, 2012.

[9] J. Fischer, A. Menon, A. Gorjestani, C. Shankwitz, and M. Donath, "Range sensor evaluation for use in cooperative intersection collision avoidance systems," in *Proceedings of the 2009 IEEE Vehicular Networking Conference, VNC 2009*, Tokyo, Japan, October 2009.

[10] M. P. Van, "Correlation of design and control characteristics with accidents at rural multi-lane highway intersections in Indiana: interim report," Tech. Rep. FHWA/IN/JHRP-77/22, Joint Highway Research Project, Indiana Department of Transportation and Purdue University, West Lafayette, Ind, USA, 1977.

[11] T. Streubel and K. H. Hoffmann, "Prediction of driver intended path at intersections," in *Proceedings of the 25th IEEE Intelligent Vehicles Symposium (IV '14)*, pp. 134–139, IEEE, Dearborn, Mich, USA, June 2014.

[12] G. Burchett and T. Maze, "Rural expressway intersections that contribute to reduced safety performance," in *Proceedings of the Mid-Continent Transportation Research Symposium*, pp. 1–14, Ames, Iowa, USA, 2005.

[13] O. K. Tonguz, "Notice of violation of IEEE publication principles biologically inspired solutions to fundamental transportation problems," *IEEE Communications Magazine*, vol. 490, no. 11, pp. 106–115, 2011.

[14] M. Ferreira, R. Fernandes, H. Conceição, W. Viriyasitavat, and O. K. Tonguz, "Self-organized traffic control," in *Proceedings of the 7th ACM International Workshop on VehiculAr InterNETworking (VANET '10)*, pp. 85–89, Chicago, Ill, USA, September 2010.

[15] B. Yang, R. Zheng, Y. Yin, S. Yamabe, and K. Nakano, "Analysis of influence on driver behaviour while using in-vehicle traffic lights with application of head-up display," *IET Intelligent Transport Systems*, vol. 10, no. 5, pp. 347–353, 2016.

[16] M. Ferreira and P. M. D'Orey, "On the impact of virtual traffic lights on carbon emissions mitigation," *IEEE Transactions on Intelligent Transportation Systems*, vol. 13, no. 1, pp. 284–295, 2012.

[17] C. O. Monreal, P. Gomes, M. K. Silvéria, and M. Ferreira, "In-vehicle virtual traffic lights, a graphical user interface," in *Proceedings of the 7th Iberian Conference on Information Systems and Technologies*, pp. 1–6, Madrid, Spain, 2012.

[18] H. Conceicao, M. Ferreira, and P. Steenkiste, "Virtual traffic lights in partial deployment scenarios," in *Proceedings of the 2013 IEEE Intelligent Vehicles Symposium, IEEE IV 2013*, pp. 988–993, Gold Coast, Australia, June 2013.

[19] Transportation Research Board, "Highway Capacity Manual," fifth edition, Washington, D. C., USA, pp. 1-1650, 2010.

[20] J. M. Bunker, "Novel methods and the maximum likelihood estimation technique for estimating traffic critical gap," *Journal of Advanced Transportation*, vol. 48, no. 6, pp. 542–555, 2014.

[21] K. Fitzpatrick, "Gaps accepted at stop-controlled intersections," *Transportation Research Record*, vol. 1303, no. 11, pp. 103–112, 1991.

[22] S. M. Tupper, M. A. Knodler, and D. S. Hurwitz, "Connecting gap acceptance behavior with crash experience," in *Proceedings of the 3rd International Conference on Road Safety and Simulation*, pp. 1–18, Indianapolis, Ind, USA, 2011.

[23] J. Thakonlaphat and S. Kazushi, "Effect of waiting time on the gap acceptance behavior of u-turning vehicles at midblock median openings," *Journal of the Eastern Asia Society for Transportation Studies*, vol. 9, pp. 1601–1613, 2011.

[24] I. A. O. Turki and S. E. Mohammad, "Gap acceptance behavior at u-turn median openings – case study in Jordan," *Jordan Journal of Civil Engineering*, vol. 7, no. 3, pp. 332–341, 2013.

[25] S. Nabaee, *An Evaluation of Gap Acceptance Behavior at Unsignalized Intersections*, Oregon State University, 2011.

[26] S. M. Tupper, *Safety and Operational Assessment of Gap Acceptance through Large-Scale Field Evaluation*, University of Massachusetts Amherst, 2014.

[27] "Japan Automobile Manufacturers Association," Guidelines for In-Vehicle Display Systems–Version 3.0, pp. 1–15, Tokyo, Japan, 2004.

[28] W. K. M. Alhajyaseen, "The development of conflict index for the safety assessment of intersections considering crash probability and severity," in *Proceedings of the 5th International Conference on Ambient Systems, Networks and Technologies, ANT 2014 and 4th International Conference on Sustainable Energy Information Technology, SEIT 2014*, pp. 364–371, bel, June 2014.

[29] *Indicators for traffic safety assessment and prediction and their application in micro-simulation modelling: a study of urban*

and suburban intersections [ph.D thesis], Royal Institute of Technology, 2005.

[30] L. Peesapati, M. Hunter, and M. Rodgers, "Evaluation of postencroachment time as surrogate for opposing left-turn crashes," *Transportation Research Record*, no. 2386, pp. 42–51, 2013.

[31] E. Roidl, B. Frehse, and R. Höger, "Emotional states of drivers and the impact on speed, acceleration and traffic violations - a simulator study," *Accident Analysis & Prevention*, vol. 70, pp. 282–292, 2014.

[32] A. N. Stephens and J. A. Groeger, "Situational specificity of trait influences on drivers' evaluations and driving behaviour," *Transportation Research Part F: Traffic Psychology and Behaviour*, vol. 12, no. 1, pp. 29–39, 2009.

[33] D. Waard, K. Brookhuis, and A. Toffetti, *Developments in Human Factors in Transportation, Design, and Evaluation*, Shaker Publishing, Maastricht, the Netherlands, 2006.

[34] Y.-C. Lee and F. K. Winston, "Stress induction techniques in a driving simulator and reactions from newly licensed drivers," *Transportation Research Part F: Traffic Psychology and Behaviour*, vol. 42, pp. 44–55, 2016.

[35] H. S. Friedman and M. W. Schustack, *Personality: classic Theories and Modern Research*, Pearson, London, UK, 5th edition, 2010.

[36] G. M. Björklund, "Driver irritation and aggressive behaviour," *Accident Analysis & Prevention*, vol. 40, no. 3, pp. 1069–1077, 2008.

[37] S. Thibaud, K. Rana, and H. Niels, "Mental state analysis using blink rate," Article ID 20140200417, US patent, US 20140200417 A1, 2014.

[38] H. Siiri, *Neural responses to observed eye blinks in normal and slow motion: an MEG study [m.s. Thesis]*, University of Helsinki, 2012.

[39] B. R. N. Ramachandran, P. S. A. Romero, J. Born, S. Winkler, and R. Ratnam, "Measuring neural, physiological and behavioral effects of frustration," in *Proceedings of the 16th International Conference on Biomedical Engineering*, pp. 43–46, Singapore, 2016.

[40] M. J. Doughty and T. Naase, "Further analysis of the human spontaneous eye blink rate by a cluster analysis-based approach to categorize individuals with 'normal' versus 'frequent' eye blink activity," *Fırat Sağlık Hizmetleri Dergisi*, vol. 32, no. 6, pp. 294–299, 2006.

[41] K. Fukuda, "Eye blinks: New indices for the detection of deception," *International Journal of Psychophysiology*, vol. 40, no. 3, pp. 239–245, 2001.

[42] M. Al-Abdulmunem and S. T. Briggs, "Spontaneous blink rate of a normal population sample," *International Contact Lens Clinic*, vol. 26, no. 2, pp. 29–32, 1999.

[43] J. Oh, S.-Y. Jeong, and J. Jeong, "The timing and temporal patterns of eye blinking are dynamically modulated by attention," *Human Movement Science*, vol. 31, no. 6, pp. 1353–1365, 2012.

[44] S. Classen, O. Shechtman, B. Stephens et al., "The impact of roadway intersection design on driving performance of young and senior adults," *Traffic Injury Prevention*, vol. 8, no. 1, pp. 69–77, 2007.

[45] J. K. Caird, S. L. Chisholm, C. J. Edwards, and J. I. Creaser, "The effect of yellow light onset time on older and younger drivers' perception response time (PRT) and intersection behavior," *Transportation Research Part F: Traffic Psychology and Behaviour*, vol. 10, no. 5, pp. 383–396, 2007.

[46] D. V. McGehee, E. N. Mazzae, G. H. S. Baldwin et al., "Examination of drivers' collision avoidance behavior using conventional and antilock brake systems on the Iowa driving simulator," *National Highway Traffic Safety Administration*, pp. 1–102, 1999, Washington, D. C., USA.

[47] E. N. Mazzae, F. S. Barickman, G. Forkenbrock, G. H. Baldwin, and S., "NHTSA light vehicle antilock brake system research program task 5.2/5.3: test track examination of drivers' collision avoidance behavior using conventional and antilock brakes," *National Highway Traffic Safety Administration*, pp. 1–161, 2003.

[48] S. G. Roberts and T. D. Day, "Integrating design and virtual test environments for brake component design and material selection," *SAE Technical Papers*, 2000.

[49] A. N. Stephens and M. Fitzharris, "Validation of the driver behaviour questionnaire in a representative sample of drivers in Australia," *Accident Analysis & Prevention*, vol. 86, pp. 186–198, 2016.

[50] F. Sagberg, "Road accidents caused by drivers falling asleep," *Accident Analysis & Prevention*, vol. 31, no. 6, pp. 639–649, 1999.

[51] B. Woodrow and A. D. Thomas, *Human Factors in Intelligent Transportation Systems*, Psychology Press, 1st edition, 1997.

[52] M. Kumar and G. S. Rao, *Statistical Techniques for Transportation Engineering*, Butterworth-Heinemann, 1st edition, 2017.

[53] E. Bradley, *Research and Evaluation in Counseling (Research, Statistics, &Amp; Program Evaluation)*, Wadsworth Publishing, 1st edition, 2007.

[54] S. Chow, J. Shao, and H. Wang, *Sample Size Calculations in Clinical Research*, Chapman & Hall/CRC Biostatistics Series, 2nd edition, 2007.

[55] J. Cohen, "A power primer," *Psychological Bulletin*, vol. 112, no. 1, pp. 155–159, 1992.

[56] B. M. Scott, "Sample size required for adverse impact analysis," *Applied HRM Research*, vol. 6, no. 1, pp. 13–32, 2001.

Hindawi
Journal of Advanced Transportation
Volume 2017, Article ID 6458495, 21 pages
https://doi.org/10.1155/2017/6458495

Research Article

Road Surface State Recognition Based on SVM Optimization and Image Segmentation Processing

Jiandong Zhao,[1] Hongqiang Wu,[1] and Liangliang Chen[2]

[1]*School of Mechanical and Electronic Control Engineering, Beijing Jiaotong University, Beijing 100044, China*
[2]*National Engineering Laboratory for Surface Transportation Weather Impacts Prevention, Broadvision Engineering Consultants, Kunming 650041, China*

Correspondence should be addressed to Jiandong Zhao; zhaojd@bjtu.edu.cn

Received 3 April 2017; Accepted 1 June 2017; Published 6 July 2017

Academic Editor: Xiaoming Chen

Adverse road condition is the main cause of traffic accidents. Road surface condition recognition based on video image has become a central issue. However, hybrid road surface and road surface under different lighting environments are two crucial problems. In this paper, the road surface states are categorized into 5 types including dry, wet, snow, ice, and water. Then, according to the original image size, images are segmented; 9-dimensional color eigenvectors and 4 texture eigenvectors are extracted to construct road surface state characteristics database. Next, a recognition method of road surface state based on SVM (Support Vector Machine) is proposed. In order to improve the recognition accuracy and the universality, a grid searching algorithm and PSO (Particle Swarm Optimization) algorithm are used to optimize the kernel function factor and penalty factor of SVM. Finally, a large number of actual road surface images in different environments are tested. The results show that the method based on SVM and image segmentation is feasible. The accuracy of PSO algorithm is more than 90%, which effectively solves the problem of road surface state recognition under the condition of hybrid or different video scenes.

1. Introduction

According to statistics, 16.12% of traffic accidents on the highway are ascribed to slippery road conditions [1] since 2007 in China. By analysis of accidents' characteristics, it can be concluded that the traffic accident rate increases under the water, snow, ice, and freezing road surface conditions and that road surface conditions greatly affect the highway traffic safety and transport efficiency. Therefore, it is urgent to carry out research on the road surface state recognition and provide reference and theoretical basis for traffic control and meteorological management to ensure traffic safety [2].

In the field of traffic meteorology, the road surface state can be categorized in dry, wet, water, snow, and ice types according to different forms of liquid on road surface. At present, the road surface detection sensor is the main entrance to obtain the information of road surface slippery conditions. Cai et al. [3] used underground embedded road surface condition detector to realize the recognition. Gailius and Jacenas [4] collected the frictional noise between the tire and the road surface and obtained the road surface characteristics based on the noise spectrum analysis method. Qi et al. [5] extracted road surface characteristics and anti-hold-process parameters, according to the principle of maximum proximity to identify the state of the road surface. Alonso et al. [6] proposed a real-time acoustics road surface state recognition system based on tire-road noise and used the noise measurement system and the signal processing algorithm for road surface state classification, and finally, precise classification of dry and wet road state was realized. Wang et al. [7] proposed D-S evidence theory and artificial neural network method for recognition and prediction of traffic state level under adverse weather conditions. However, the road surface sensor can only obtain the information of the section and the maintenance is extremely inconvenient; hence the actual effect is not ideal.

With the widespread application of road surveillance cameras, more and more scholars pay attention to the image processing technology of road surface slippery condition recognition. Andreas and Wilco [8] extracted the gray scale

feature of road surface image and designed the neural network classifier for road surface state recognition. Anis et al. [9] analyzed the set and spectrum of road surface reflection image and described the correlation between the surface texture and the friction coefficient, by which the reflection image of designated location can be monitored and identified. Chen [10] extracted low-order statistical features of road surface images including gray level cooccurrence matrix texture feature parameters and used linear discriminant function to determine the road surface state. Ueda et al. [11] and Yoda et al. [12] measured and analyzed the road surface roughness, the proportion of low-frequency reflection signal components and high-frequency components, and the average reflection intensity to determine the state of the road surface based on CCD camera technology. Yamamoto et al. [13] applied the human-computer interaction method to extract the gray scale value and temperature characteristics parameters of the road surface for the road surface state prediction, and measurement accuracy was tested to be more than 80%. Muneo et al. [14] used vehicle camera to collect traffic information; the parameters of road surface image polarization characteristics were utilized to establish the road slippery condition evaluation model. Becchi et al. [15] obtained the water condition video of the road surface; the rain density judge values and image analysis results were combined to evaluate the depth of water film on the road surface, by which the road condition evolution pattern can be forecasted. Fukui et al. [16] analyzed the slippery condition of the road by calculating the brightness and spatial spectrum of road surface images. Li et al. [17] extracted RGB, HIS, and YUV of road surface images and established the road surface state recognition model based on improved BP neural network. The recognition accuracy rate of this model could reach more than 85%. However, it was still on the theoretical research stage with the small size of training sample. Liu and Huang [18] collected wet road images and then designed a SVM classifier of road slippery state classification. Among them, the misjudgment rate of the dry state is slightly high, while the recognition accuracy of snow state is slightly high. Besides, the identification of hybrid road surface state was still to be studied. Wan et al. [19] used the RBF neural network model to discriminate the slippery conditions of different roads, and the recognition accuracy was 78.4%. Among them, the recognition accuracy of dry and silt state is low, and the recognition accuracy of snow and ice state is high.

Image feature extraction is a key step in image recognition. Zhang et al. [20] extracted the eigenvector of RGB color moment and the Munsell color moment from the images. The results show that the color moment feature can describe the color characteristic of the image well. Shinde et al. [21] extracted a variety of color features of images to form a preprocessing database of color eigenvector and then used machine learning to perform image classification experiments. The experimental results show that the classification accuracy can be achieved based on multiple color feature databases. Bhave et al. [22] extracted the color feature by calculating the average value of each color component and then used gray level cooccurrence matrix to extract texture eigenvectors. Based on the feature values above, image state can be classified. Haralick et al. [23] proposed some easy-to-calculate texture eigenvectors based on the gray level cooccurrence matrix. The texture feature is used to identify the aerial images. Experimental results show that the texture feature is the applicability of image classification. Mohanaiah et al. [24] extracted the four image texture eigenvectors based on the gray level cooccurrence matrix, including the second moment, correlation, inverse moment, and entropy. The recognition experiments show that calculation time can be saved and the recognition accuracy is high via these texture features.

Reviewing the above literatures, it is found that the existing problems and development trends of image recognition technology are as follows:

(1) Image recognition technology is the main technology of road surface recognition. However, due to the complexity of the road scene and the weak adaptability of the vision system to the illumination change, the road condition detection method based on machine vision has the problem of weak adaptability, the poor robustness of illumination, and low recognition accuracy at present.

(2) The identification of the hybrid road surface state is one of the main problems in this study.

(3) Using SVM, neural network, and other machine learning methods to identify the road surface state is the development trend.

(4) Extracting appropriate multidimensional color and texture eigenvectors can help to improve the accuracy of road surface state recognition.

Therefore, this paper presents a new method based on SVM classifier and image segmentation processing to solve the problem of the small size of the sample and nonlinear and high-dimension pattern recognition. First of all, the comprehensive sample database of road surface state is established by collecting road surface images in different scenes through a variety of ways. Then, 13-dimensional color and texture eigenvectors are extracted to build the training database of road surface state. Next, the optimal parameters of the SVM classifier are trained by the grid searching optimization algorithm and the PSO algorithm, respectively. Thus two kinds of road surface state classification models are built and the performances of the two optimization classification models are compared. For the hybrid road surface state recognition, the road surface state image is segmented into blocks and the overall state of road surface state is presented. Finally, the algorithm proposed is tested and the ideal recognition results are obtained based on the large-scale samples.

2. Eigenvectors Extraction of Road Surface State from Images

The road surface image information mainly includes color, texture, shape, and other characteristics. In this paper, representatively typical road surface state image samples are

selected and color and texture eigenvectors are extracted, and the road surface state image feature database can be formed by researching color and the texture characteristics of road state.

2.1. Extraction of Color Eigenvectors. Color eigenvectors of road surface image are usually stable and not sensitive to size or direction. Among them, the color moment feature has the characteristics of translation invariance, rotation invariance, and scale invariance, which can ensure the integrity of image color information [20, 21, 25]. Therefore, this paper adopts the third-order color moment method to extract the road surface image color feature. The definitions are as follows:

$$\mu_i = \frac{1}{N}\sum_{j=1}^{N} p_{i,j},$$

$$\sigma_i = \left\{\frac{1}{N}\sum_{j=1}^{N}\left(p_{i,j}-\mu_i\right)^2\right\}^{1/2}, \quad (1)$$

$$s_i = \left\{\frac{1}{N}\sum_{j=1}^{N}\left(p_{i,j}-\mu_i\right)^3\right\}^{1/3},$$

where i is the color channel and j is the gray value of image. μ_i is the first-order color moment of image i. σ_i is the second-order color moment. s_i is the third-order color moment. p is the probability of the pixels with gray scale j occurrences in the ith color channel of image. N is the total number of pixels in the image. Equation (2) is a 9-dimensional color moment vector, indicating the color feature of images, based on the HSV (hue, saturation, and brightness) color model:

$$F_{\text{color}} = \left[\mu_H, \sigma_H, s_H, \mu_S, \sigma_S, s_S, \mu_V, \sigma_V, s_V\right]. \quad (2)$$

2.2. Extraction of Texture Eigenvectors. Gray level cooccurrence matrix can better represent the texture information [23, 26, 27]. In this paper, we choose the gray level cooccurrence matrix method to extract four commonly used texture features of road surface images.

(1) Energy

$$\text{ASM} = \sum_i\sum_j q\left(i, j \mid d, \theta\right)^2. \quad (3)$$

Energy reflects the texture thickness of image. When the texture is coarse relatively, ASM is larger; on the contrary, ASM is smaller, where i, j are gray scale values of pixels. d is the spatial relationship between the two pixels. θ is the generated direction of the gray level cooccurrence matrix. q is the number of occurrences of i and j pixels with the spatial relationship d.

(2) Entropy

$$\text{ENT} = -\sum_i\sum_j q\left(i, j \mid d, \theta\right)\log_2 q\left(i, j \mid d, \theta\right). \quad (4)$$

Entropy reflects the amount of the image information. When the image has more textures, the entropy value is larger. If the image contains fewer textures, the entropy value is smaller. If the image has no textures, the entropy value is close to zero.

(3) Contrast

$$\text{CON} = \sum_i\sum_j \left(i-j\right)^2 q\left(i, j \mid d, \theta\right). \quad (5)$$

The contrast reflects the clarity of the image texture. In images, the deeper the texture groove, the greater the contrast, and the clearer the image texture visual effect.

(4) Correlation

$$\text{COR} = \sum_i\sum_j \frac{(ij)\, q\left(i, j\right) - \lambda_1\lambda_2}{\varepsilon_1\varepsilon_2}, \quad (6)$$

where $\lambda_1 = \sum_i\sum_j i \cdot q(i, j)$, $\lambda_2 = \sum_i\sum_j j \cdot q(i, j)$, ${\varepsilon_1}^2 = \sum_i\sum_j q(i, j)(i-\lambda_1)^2$, and ${\varepsilon_2}^2 = \sum_i\sum_j q(i, j)(i-\lambda_2)^2$.

Correlation value reflects the correlation of local gray scale in images. When the values of the matrix elements are evenly equal, the correlation value is large. On the contrary, when the values of the matrix elements are very different, the correlation value is small.

Based on the research above, a set of 13-dimensional road surface state eigenvectors is determined as

$$\text{feature} = \left[\mu_H, \sigma_H, s_H, \mu_S, \sigma_S, s_S, \mu_V, \sigma_V, s_V, \text{ASM}, \text{ENT}, \text{CON}, \text{COR}\right]. \quad (7)$$

3. Database Construction of Road Surface State Feature

3.1. Image Samples Collection of Road Surface State. As shown in Figure 1, we set up a road surface image acquisition experimental system including the road surface image acquisition camera, the hard disk video recorder, and the computer. This system can cover the entire road and achieve all-weather road image acquisition.

The basis of road surface state recognition is to establish the road surface state feature database, which needs to collect a large number of road surface state image samples through various ways. Because of the simplicity of the road surface images collected by the experimental system, we also use the highway video surveillance resources, network resources, and other video resources to collect road images to expand the sample database.

3.2. Image Samples Database Construction of Road Surface State. The road surface state is divided into five types including dry, wet, water, ice, and snow. According to the influence of original images to samples database under the condition of different images size and lighting scenes, the original image segmentation principle is proposed as shown in Table 1. According to Table 1, original images are divided into blocks,

Figure 1: Road surface images acquisition system.

Table 1: Image segmentation principle.

Size of images (px)	Size of blocks (px)
100000 ≤ image < 1000000	80 × 80
1000000 ≤ image < 2000000	100 × 100
2000000 ≤ image < 3000000	200 × 200
3000000 ≤ image < 5000000	300 × 300
5000000 ≤ image < 8500000	500 × 500

and then the single state blocks are selected to construct the road surface state samples, which effectively guarantee the quality and purity of the road surface image database.

In this paper, 500 dry images, 500 wet images, 500 water images, 500 snow images, and 500 ice images totaling 2500 images were collected to construct the sample database. Some of the image samples are shown in Figure 2.

3.3. Database Construction of Road Surface State Feature. Based on the road surface state image sample database, 500 samples were collected for each state, and the color and texture eigenvectors were extracted to build the road surface state feature database. Figures 3–6 show part of the color and texture feature curves of 200 samples for each state.

As shown in Figure 3, the range of V first-order moment of dry samples is $[0.31, 0.93]$, the range of V first-order moment of the wet samples is $[0.48, 0.73]$, the range of V first-order moment of water samples is $[0.47, 0.88]$, the range of V first-order moment of snow samples is $[0.71, 0.94]$, and the range of V first-order moment of ice samples is $[0.41, 0.93]$. It can be seen that there is a large difference in first-order moment values between dry samples and snow samples, while the first-order moment curves of the wet, water, and ice samples show characteristics of overlapping.

As shown in Figure 4, the range of V second-order moment of dry samples is $[0.03, 0.21]$, the range of V second-order moment of wet samples is $[0.04, 0.20]$, the range of V second-order moment of water samples is $[0.01, 0.25]$, the range of V second-order moment of snow samples is $[0.01, 0.07]$, and the range of second moment of ice samples is $[0.04, 0.16]$. It can be seen that the V second moment values of snow samples are small, and there is a big difference with the other four samples. The V second moment curves of dry, wet, water, and ice samples are hard to distinguish because of obvious overlapping.

As shown in Figure 5, the range of energy values of the dry samples is $[1.52, 4.74]$, the range of energy values of the wet samples is $[1.71, 4.92]$, the range of energy values of the water samples is $[0.18, 2.48]$, the range of energy values of the snow samples is $[0.01, 2.13]$, and the range of energy values of ice samples is $[1.86, 4.94]$. It can be seen that the energy value curves of water and snow samples are overlapped, while the curves of energy values for dry, wet, and ice samples show characteristics of overlap.

As shown in Figure 6, the range of entropy of dry samples is $[0.01, 0.35]$, the entropy of wet samples is $[0.01, 0.36]$, the range of entropy of water samples is $[0.04, 0.98]$, the range of entropy of snow samples is $[0.14, 0.99]$, and the range of entropy of the ice samples is $[0.03, 0.25]$. It can be seen that the entropy curves of wet and ice samples are overlapped, and the entropy curves of dry, water, and snow samples are overlapped.

It can be concluded that the single feature curves of the five states have an overlapping area, but there are obvious differences in the feature vectors between at least two kinds of states. The 13-dimensional feature mentioned in this paper can help to accurately identify the road surface state.

4. Design of SVM Classification Optimization

4.1. Design of Classifier Based on SVM. The principle of SVM [28, 29] is to find the optimal hyperplane, which ensures the accuracy of the hyperplane classification, while the distance on both sides of the hyperplane can be maximized. A nonlinear multiclass SVM classifier is designed for the recognition of hybrid road surface states. The nonlinear-to-linear

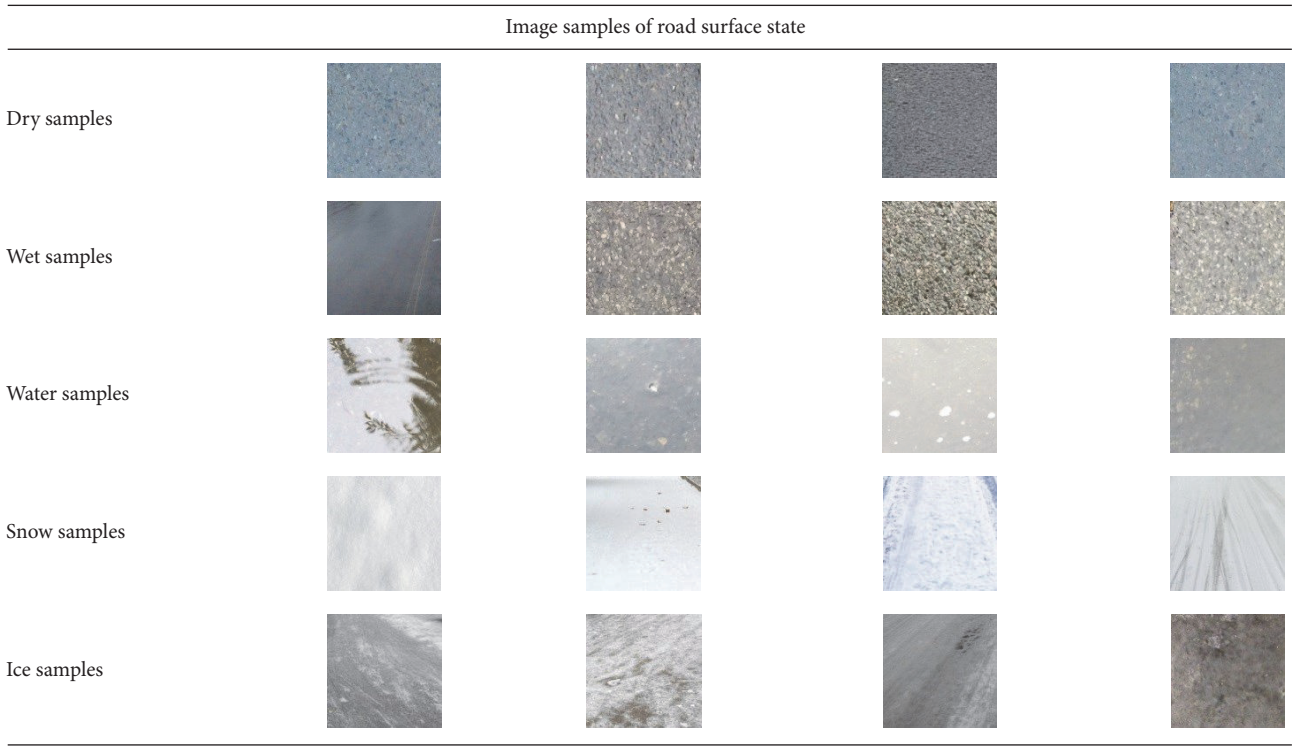

Figure 2: Road surface image sample library.

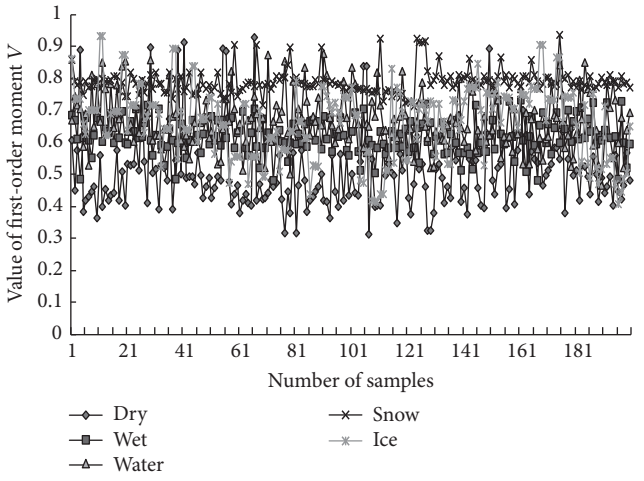

Figure 3: Color eigenvector: V first-order moment.

transformation depends on the nonlinear transformation from the kernel function to input space. Classifier design algorithm is as follows.

Linear SVM classification function is as follows:

$$f(x) = \operatorname{sgn}\{(w^* \cdot x) + b^*\} = \operatorname{sgn}\left\{\left(\sum_{\alpha=1}^{t} a_\alpha y_\alpha (x_\alpha \cdot x_\tau)\right) + b^*\right\} \quad (8)$$

$$\tau = 1, 2, \ldots, l,$$

where x is the input vector. y is the vector type. l is the number of input vectors. w^* is the optimal weight vector. b^* is the optimal bias. $a > 0$ is the multiplier for the Lagrangian function. x_α is the support vector. t is the number of support vectors.

For the nonlinear classification function, the existence of misclassified samples is allowed by introducing nonnegative slack variable ξ_τ ($\tau = 1, 2, \ldots, l$), and the classification hyperplane is

$$y_\tau \left[(w \cdot x_\tau) + b\right] + \xi_\tau \geq 1, \quad \tau = 1, 2, \ldots, l. \quad (9)$$

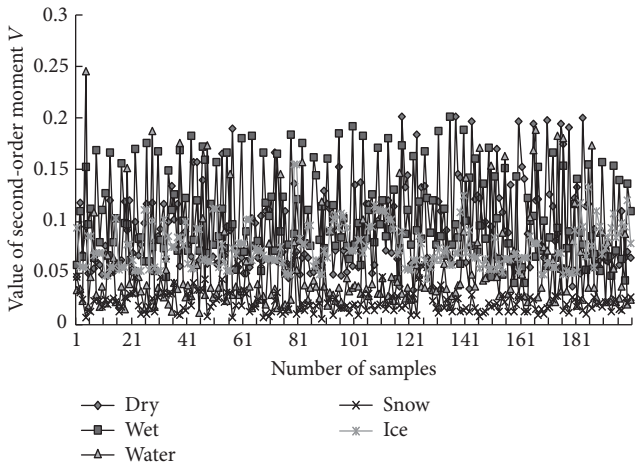

Figure 4: Color eigenvector: V second-order moment.

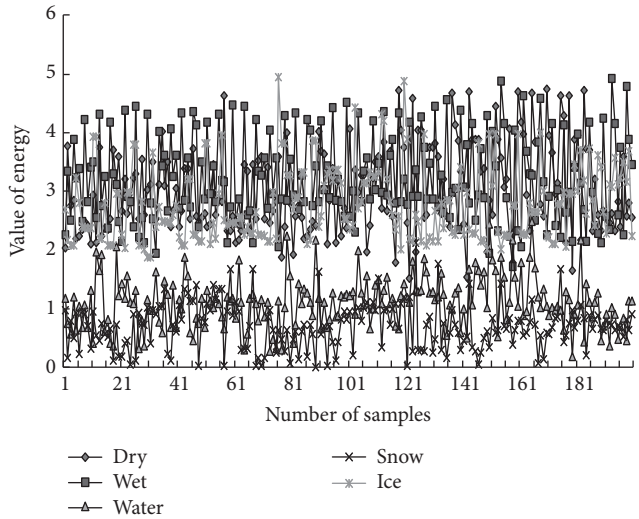

Figure 5: Texture eigenvectors: energy.

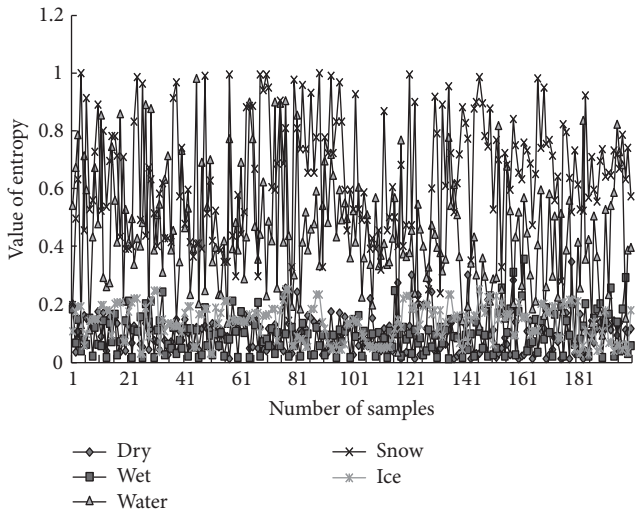

Figure 6: Texture eigenvectors: entropy.

In this case, the reciprocal of the maximum classification interval is $\min \Phi(w) = (1/2)\|w\|^2 + C(\sum_{i=1}^{l} \xi_\tau)$, where $C > 0$ is the penalty factor for SVM.

After constructing the optimal hyperplane, the most widely used Gaussian kernel function $K(x) = \exp[-g|x - x_\tau|^2]$ is used [28, 29], and the input vector x is transformed from the input space R^n to the high-dimensional feature space H with K transformation,

$$x \to K(x) = \left(K(x_1), K(x_2), \ldots, K(x_l)\right)^T. \quad (10)$$

Then the input vector x is replaced by the eigenvector $K(x)$, and the nonlinear optimal classification function is obtained as

$$\begin{aligned} f(x) &= \operatorname{sgn}(w \cdot K(x) + b) \\ &= \operatorname{sgn}\left(\sum_{\alpha=1}^{t} a_\alpha y_\alpha K(x_\alpha) \cdot K(x_\tau) + b\right). \end{aligned} \quad (11)$$

Based on the nonlinear optimal classification function, the main idea of multiclassification can be explained as follows: Assuming that a SVM classifier is designed between every two types of samples, $k(k-l)/2$ SVM classifiers need to be designed for k samples [28]. Therefore, ten SVM classifiers are designed for the five road states. When classifying an unknown sample, each classifier evaluates and counts its type, and the most statistical result can be regarded as the type of the test sample.

4.2. Parameter Optimization of SVM. In the process of SVM classification and identification, the penalty factor C and Gaussian kernel function factor g have a great impact on the accuracy of training [30, 31]. The higher C can result in overlearning state, which means training set classification accuracy is high while test set classification accuracy is too low. The higher g can lead to excessive support vectors and interfere with the efficiency of training and learning [31]. In order to solve the problems above, the grid searching algorithm and Particle Swarm Optimization algorithm are used to obtain the optimal parameters of C and g and improve the recognition efficiency and accuracy of SVM.

4.2.1. Parameters Optimization Based on Grid Searching Algorithm. Based on the grid searching algorithm, the principle of parameter optimization [30] is to make the SVM penalty factor C and Gaussian kernel function factor g divide the image into grids in a certain range and then traverse all the points in the grids to obtain the values. For the defined C and g, the K-CV (cross-validation) method is used to get the training set of this group to verify the classification accuracy. Finally, the best combination of C and g with the highest classification accuracy of verified raining set is obtained. Where the range of C is set to $[2^{-8}, 2^8]$, the range of g is set to $[2^{-8}, 2^8]$.

Among them, there will be many combinations corresponding to the highest verification classification accuracy. The combination of the smallest C is selected as the best one, and if the corresponding g are more than one, the firstly searched combination can be selected as the best one.

4.2.2. Parameters Optimization Based on Particle Swarm Algorithm. The basic principle of Particle Swarm Optimization (PSO) [31–33] is as follows: suppose that an ethnic group $X = (x_1, x_2, \ldots, x_n)$ consists of n particles in a m-dimensional search space, where the position of the ith particle (the optimal solution) is $x_i = (x_{i1}, x_{i2}, \ldots, x_{im})^T$, the velocity is $V_i = (v_1, v_2, \ldots, v_m)^T$, and the optimal position $P_i = (p_{i1}, p_{i2}, \ldots, p_{im})^T$ of the particle is denoted as *pbest*. The globally optimal solution $P_g = (p_{g1}, p_{g2}, \ldots, p_{gm})^T$ of the ethnic group is denoted as *gbest*. After finding the two optimal solutions, the particle velocity and position vector are updated based on

$$\begin{aligned} v_{id}(t+1) &= w \cdot v_{id}(t) + c_1 r_1 \cdot \left(pbest(t) - x_{id}(t)\right) \\ &\quad + c_2 r_2 \cdot \left(gbest(t) - x_{id}(t)\right), \\ x_{id}(t+1) &= x_{id}(t) + v_{id}(t+1), \end{aligned} \quad (12)$$

where $1 \le i \le n$ and $1 \le d \le m$. w is the inertia weight. c_1, c_2 are acceleration constants, generally set as 2. r_1, r_2 are random numbers ranging between 0 and 1. t is the number of iterations.

Parameters optimization based on the particle swarm algorithm is as follows.

Step 1. Initialize the size and initial velocity of the particle (C, g), and initialize the parameters c_1, c_2 and the maximum number of iterations t.

Step 2. The fitness value of each particle (C, g) is calculated, and the classification accuracy, R = number of samples correctly classified/total number of samples, trained by cross-validation of SVM is used to evaluate the fitness value of each particle.

Step 3. The fitness value of each particle (C, g) and its optimal position are compared, respectively, and the optimal value *pbest* is obtained. If the current value is better than *pbest*, *pbest* is set as the current value, which means the *pbest* location is set as the current location.

Step 4. Comparing the fitness value of each particle (C, g) and the optimal value *gbest* of the ethnic group, if the current value is better than *gbest*, the subscript and fitness value of the current particle are set as the subscript and the fitness value of *gbest*.

Step 5. According to (12), the particle velocity and position are updated.

Step 6. When the end condition is reached, the t times of iterations are completed, and the optimal value *gbest* is output and the best parameter (C, g) can be obtained.

5. Image Blocks Validation of Road Surface State

Firstly, two SVM parameters optimization algorithms are used to obtain two groups of optimal training parameters

Table 2: The road surface condition classification model.

Number of training samples	Parameters optimization time consuming (s)	Optimal (C, g)	Training accuracy
2000	Grid algorithm 2.6482	Grid algorithm (16, 0.5)	Grid optimization model 90.97%
	PSO algorithm 0.6848	PSO algorithm (12, 0.46)	PSO optimization model 99.12%

Table 3: Classification model performance test.

Number of test samples	Test accuracy
500	Grid optimization model 88.63%
	PSO optimization model 97.02%

(C, g). Then 80% of the samples in the road surface state feature database are trained based on the best training parameters (C, g), and two road surface state classification models are obtained. After that, the remaining 20% of the data samples are tested to examine the performance of the two classification models. Finally, the road surface state samples in an actual environment are selected for experimental validation.

5.1. Establishment of Training Model. (1) Mark the surface state conditions: dry as D, wet as Wt, water as Wr, snow as S, and ice as I. The eigenvectors of 400 samples of each road state were extracted to form the training database.

(2) The training data is inputted into SVM classifier; the best training parameters (C, g) are gotten. And then, two kinds of classification models are established.

From Table 2, it can be seen that the training accuracies of the two classification models are almost the same. However, the PSO algorithm is significantly less time-consuming and with better applicability than the grid searching algorithm.

(3) 20% of the sample data were tested by the classification model to verify the recognition performance of the two classification models. The test results are shown in Table 3.

From Table 3, it can be seen that the accuracy of the PSO model is higher than that of the grid searching algorithm, and the performance of the PSO model is better.

5.2. Image Segmentation Recognition of Actual Road Surface. Firstly, the actual road surface image is divided into blocks according to the segmentation principle. Next, the 13-dimensional feature of each block is extracted. Then the road surface block feature vectors are input into two classification models mentioned above. And the state of each block will be recognized. When all the blocks are recognized, the proportion of each state will be counted.

5.2.1. Image Validation of Dry State. The recognition results of the dry road surface state under good illumination condition (from the experimental system) are shown in Figure 7 and Tables 4 and 5.

Table 6 shows the statistic results of each road surface state.

From Table 6, it can be seen that the test ratio of dry state is 93.33% after the grid searching optimization. After the optimization by PSO, the ratio of dry state is 100% and increases by 6.67%.

Table 4: Recognition results of grid.

Column	Row								
	1	2	3	4	5	6	7	8	9
1	D	D	D	D	D	D	D	D	D
2	D	D	D	D	D	D	D	D	D
3	D	D	D	D	D	D	D	D	D
4	D	D	D	D	D	D	D	D	D
5	D	D	D	D	D	D	D	D	D

Table 5: Recognition results of PSO.

Column	Row								
	1	2	3	4	5	6	7	8	9
1	D	D	D	D	D	D	D	D	D
2	Wt	D	D	D	D	D	D	D	D
3	D	D	D	D	Wt	D	D	D	D
4	D	D	D	D	D	D	D	D	D
5	D	D	D	D	D	D	Wt	D	D

The recognition results of dry road surface state under adverse lighting conditions (from the experimental system) are shown in Figure 8 and Tables 7 and 8.

Table 9 shows the statistic results of each road surface state.

From Table 9, it can be seen that the proportion of the test images identified as dry is 77.78% after optimization by the grid search algorithm. After the PSO optimization, the test image recognition rate is 95.56% and increases by 17.78%.

5.2.2. Image Validation of Wet State. The recognition results of the wet road surface state under good illumination condition (from the surveillance system) are shown in Figure 9 and Tables 10 and 11.

Table 12 shows the statistic recognition results of each road surface state.

From Table 12, it can be seen that the proportion of the test images identified as wet is 81.25% after optimization by the grid search algorithm. After the PSO optimization, the test image recognition rate is 93.75% and increases by 12.50%.

The recognition results of the wet road surface state under adverse illumination condition (from the experimental system) are shown in Figure 10 and Tables 13 and 14.

Table 15 shows the recognition results of each road surface state.

From Table 15, it can be seen that the proportion of the test images identified as wet is 80.00% after optimization by the

Table 6: The dry road surface image identification results statistics.

State	State symbol	Number of blocks	Grid search	PSO	Grid search/%	PSO/%
Dry	D	45	42	45	93.33%	100%
Wet	Wt		3	0	6.67%	0
Water	Wr		0	0	0	0
Snow	S		0	0	0	0
Ice	I		0	0	0	0

(a) (b)

Figure 7: Image test results of dry road surface state under good lighting condition (from the experimental system). (a) Image of dry road surface. (b) Image blocks.

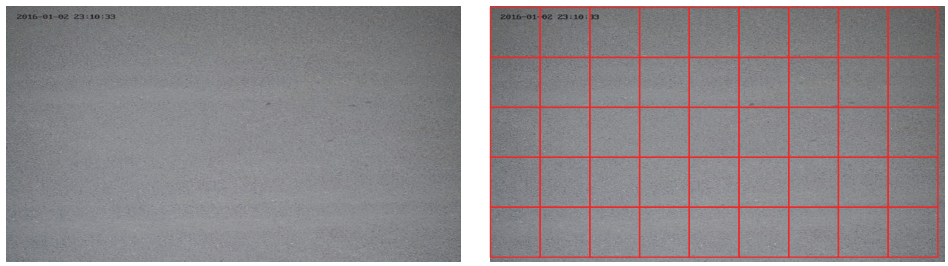

(a) (b)

Figure 8: Image test results of dry road surface state under adverse lighting condition (from the experimental system). (a) Image of dry road surface state. (b) Image blocks.

Table 7: Recognition results of grid.

Column	Row								
	1	2	3	4	5	6	7	8	9
1	D	D	D	D	Wt	D	D	D	D
2	Wt	D	D	D	D	D	D	Wt	D
3	D	Wt	D	D	Wt	D	D	D	Wt
4	D	D	D	Wt	D	D	D	D	Wt
5	Wt	D	D	D	D	D	Wt	D	D

Table 8: Recognition results of PSO.

Column	Row								
	1	2	3	4	5	6	7	8	9
1	D	D	D	D	D	D	D	D	D
2	D	D	D	D	D	D	D	D	D
3	D	D	D	D	D	D	D	D	D
4	D	D	D	D	Wt	D	D	D	D
5	D	D	D	D	D	D	D	Wt	D

grid search algorithm. After the PSO optimization, the test image recognition rate is 93.33% and increases by 13.33%.

5.2.3. Image Validation of Water State. The recognition results of the water road surface state under good illumination condition (from the mobile camera) are shown in Figure 11 and Tables 16 and 17.

Table 18 shows the recognition results of each road surface state.

From Table 18, it can be seen that the proportion of the test images identified as water is 78.57% after optimization by the grid search algorithm. After the PSO optimization, the test image recognition rate is 96.42% and increases by 17.85%.

The recognition results of the water road surface state with reflection (from the Internet images) are shown in Figure 12 and Tables 19 and 20.

Table 21 shows the recognition results of each road surface state.

Table 9: The dry road surface image identification results statistics.

State	State symbol	Number of blocks	Grid search	PSO	Grid search/%	PSO/%
Dry	D	45	35	43	77.78%	95.56%
Wet	Wt		10	2	22.22%	4.44%
Water	Wr		0	0	0	0
Snow	S		0	0	0	0
Ice	I		0	0	0	0

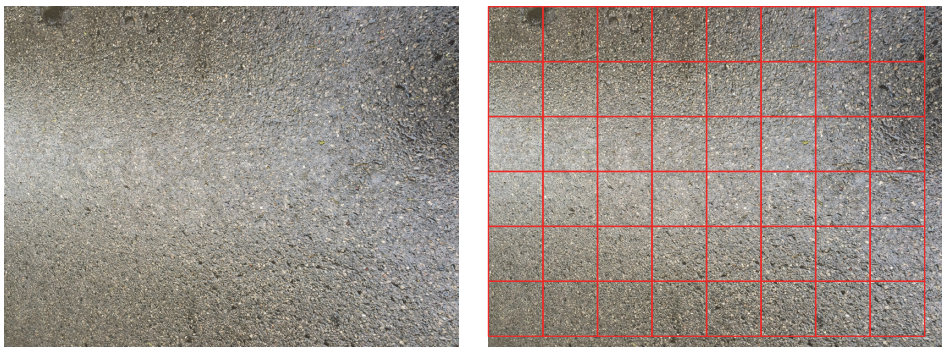

(a) (b)

Figure 9: Image test results of wet road surface state under good lighting condition (from the surveillance system). (a) Image of wet road surface state. (b) Image blocks.

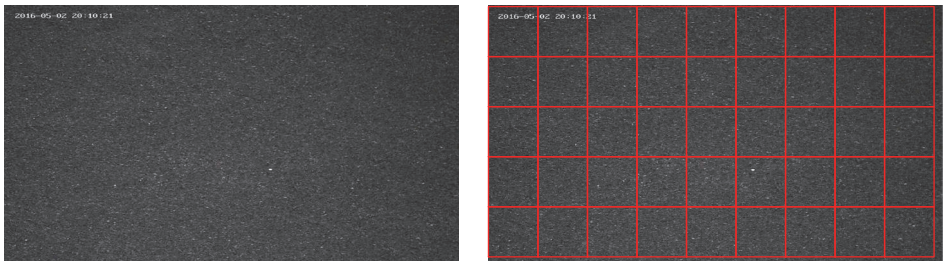

(a) (b)

Figure 10: Image test results of wet road surface state under good lighting condition (from the experimental system). (a) Image of wet road surface state. (b) Image blocks.

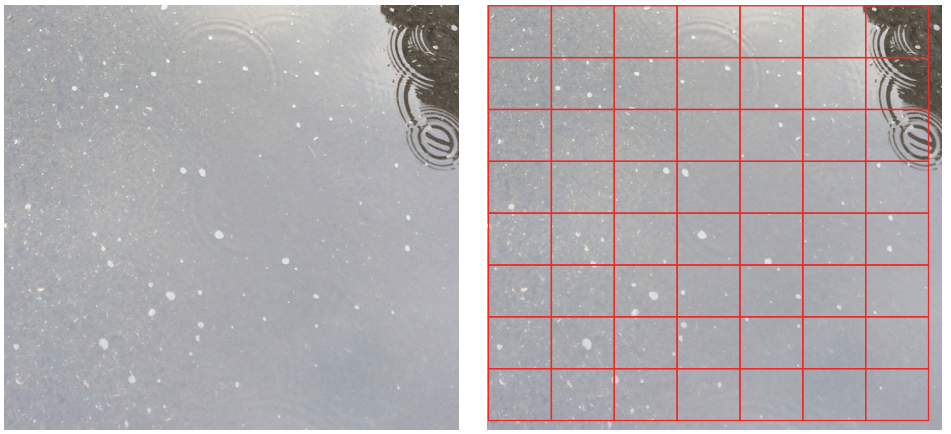

(a) (b)

Figure 11: Image test results of water road surface state under good lighting condition (from the mobile camera). (a) Image of water road surface state. (b) Image blocks.

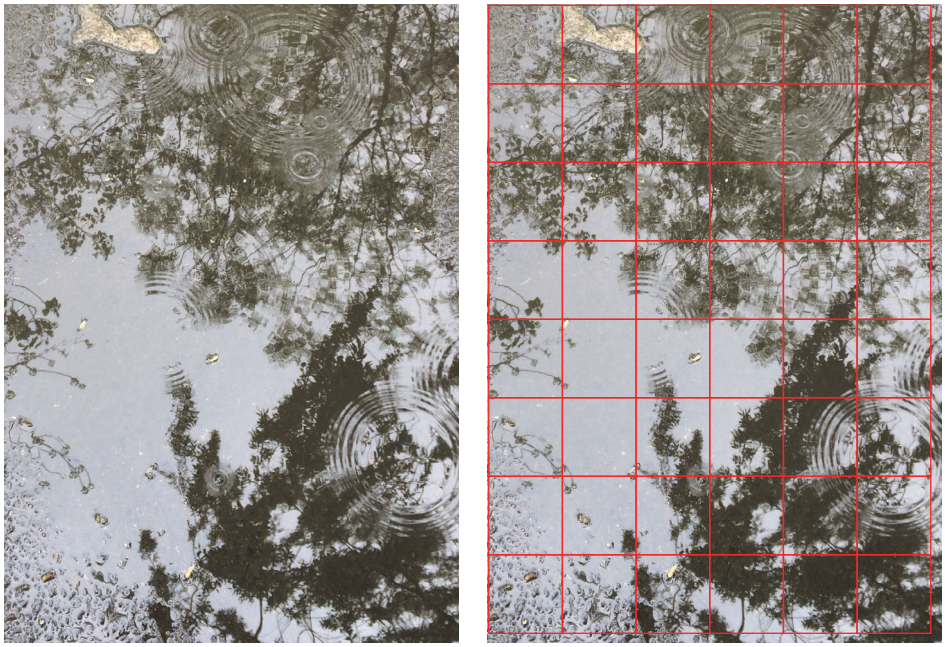

(a) (b)

Figure 12: Image test results of water road surface state with reflection (from the Internet images). (a) Image of water road surface state. (b) Image blocks.

(a) (b)

Figure 13: Image test results of snow road surface (from the Internet images). (a) Image of snow road surface state. (b) Image blocks.

From Table 21, it can be seen that the proportion of the test images identified as water is 75.00% after optimization by the grid search algorithm. After the PSO is optimized, the test image recognition rate is 89.59% and increases by 14.59%.

5.2.4. Image Validation of Snow State. The recognition results of the snow road surface state (from the Internet images) are shown in Figure 13 and Tables 22 and 23.

Table 24 shows the recognition results of each road surface state.

From Table 24, it can be seen that the proportion of the test images identified as water is 67.35% after optimization by the grid search algorithm. After the PSO optimization, the test image recognition rate is 85.71% and increases by 18.36%.

Table 10: Recognition results of grid.

Column	Row							
	1	2	3	4	5	6	7	8
1	Wt	Wt	Wt	Wt	Wt	D	Wt	Wt
2	Wt	Wt	Wt	Wt	Wt	D	Wt	D
3	Wt	Wt	Wt	Wt	Wt	Wt	D	D
4	Wt	Wt	Wt	Wt	Wt	Wt	Wt	D
5	D	Wt	Wt	Wt	Wt	Wt	Wt	Wt
6	D	Wt	Wt	Wt	Wt	Wt	Wt	D

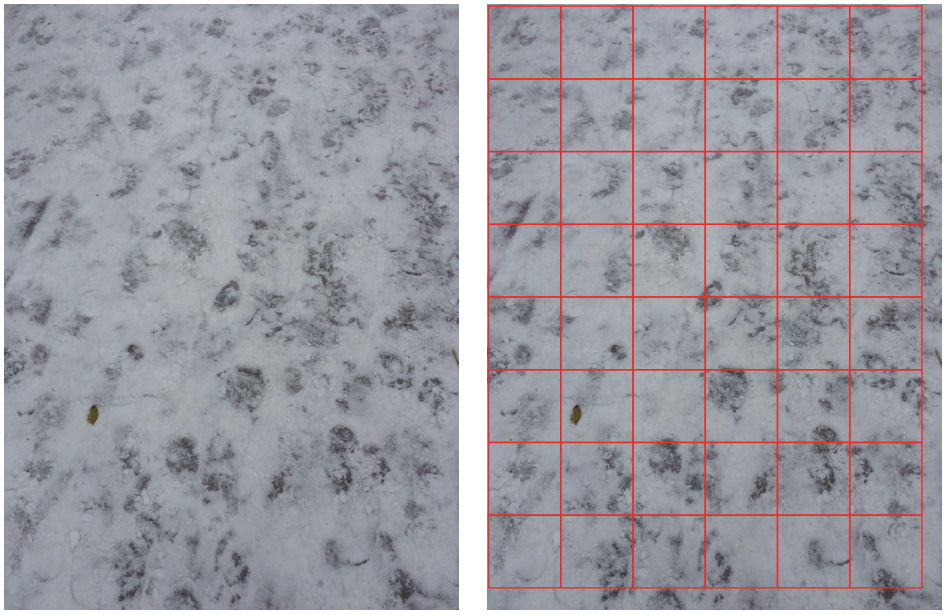

(a) (b)

Figure 14: Image test results of snow road surface (from the surveillance system). (a) Image of snow road surface state. (b) Image blocks.

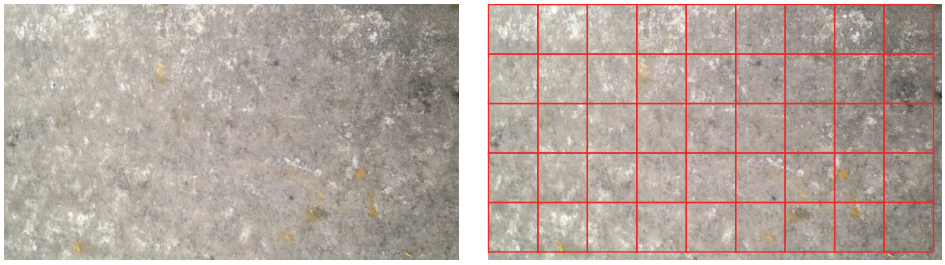

(a) (b)

Figure 15: Image test results of ice road surface under good illumination condition (from the experimental system). (a) Image of ice road surface state. (b) Image blocks.

Table 11: Recognition results of PSO.

Column	Row							
	1	2	3	4	5	6	7	8
1	Wr	Wt	Wt	Wt	Wt	Wt	Wt	Wt
2	Wt	Wt	Wt	Wt	Wt	Wt	Wt	Wt
3	Wt	Wt	Wt	Wt	Wt	Wr	Wt	Wt
4	Wt	Wt	Wt	Wt	Wt	Wt	Wt	Wt
5	Wt	Wt	Wt	Wr	Wt	Wt	Wt	Wt
6	Wt	Wt	Wt	Wt	Wt	Wt	Wt	Wt

The recognition results of the snow road surface state (from the surveillance system) are shown in Figure 14 and Tables 25 and 26.

Table 27 shows the recognition results of each road surface state.

From Table 27, it can be seen that the proportion of the test images identified as water is 77.55% after optimization by the grid search algorithm. After the PSO optimization, the test image recognition rate is 91.84% and increases by 14.29%.

5.2.5. Image Validation of Ice State. The recognition results of the ice road surface state under good illumination condition (from the experimental system) are shown in Figure 15 and Tables 28 and 29.

Table 30 shows the recognition results of each road surface state.

From Table 30, it can be seen that the proportion of the test images identified as ice is 93.33% after optimization by the grid search algorithm. After the PSO optimization, the test image recognition rate is 97.78% and increases by 4.45%.

The recognition results of the ice road surface state with snow (from the Internet image) are shown in Figure 16 and Tables 31 and 32.

Table 12: The wet road surface image identification results statistics.

State	State symbol	Number of blocks	Grid search	PSO	Grid search/%	PSO/%
Dry	D		9	0	18.75%	0
Wet	Wt		39	45	81.25%	93.75%
Water	Wr	48	0	3	0	6.25%
Snow	S		0	0	0	0
Ice	I		0	0	0	0

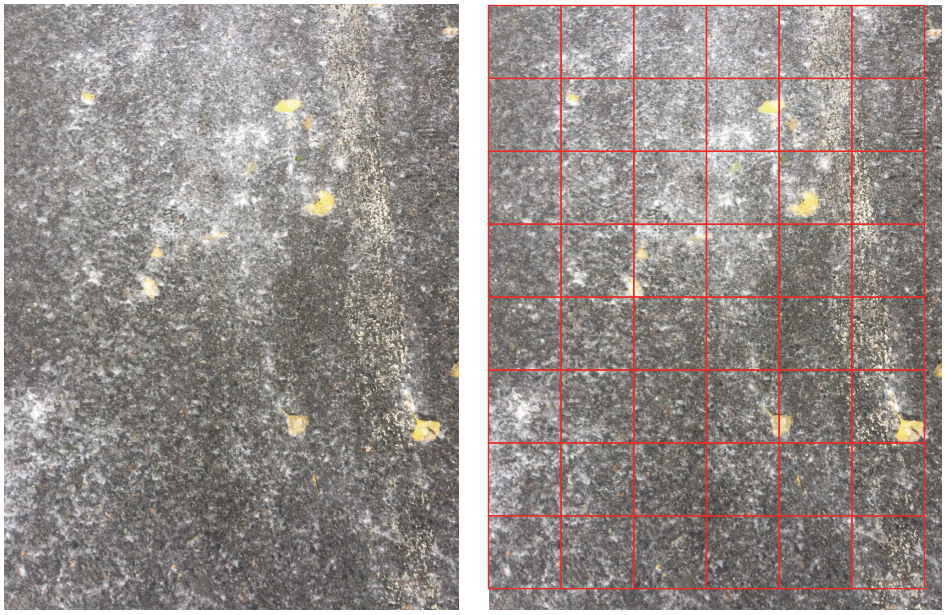

(a) (b)

Figure 16: Image test results of ice road surface with snow (from the Internet image). (a) Image of ice road surface state. (b) Image blocks.

(a) (b)

Figure 17: Image test results of hybrid road surface (from the mobile image). (a) Image of hybrid road surface state. (b) Image blocks.

Table 33 shows the recognition results of each road surface state.

From Table 33, it can be seen that the proportion of the test images identified as ice is 71.11% after optimization by the grid search algorithm. After the PSO optimization, the test image recognition rate is 77.78% and increases by 6.67%.

5.2.6. Image Validation of Hybrid State. The recognition results of the ice, wet, and water hybrid state (from the mobile image) are shown in Figure 17 and Tables 34 and 35.

Table 36 shows the recognition results of each road surface state.

From Table 36, it can be seen that the error rate of each image block is relatively high on hybrid road condition after

Table 13: Recognition results of grid.

Column	Row								
	1	2	3	4	5	6	7	8	9
1	Wt	Wt	Wt	Wt	Wt	D	Wt	Wt	D
2	Wt	Wt	Wt	Wt	Wt	Wr	Wt	D	Wt
3	Wt	Wt	D	Wt	Wt	D	Wt	Wt	Wt
4	Wt	Wt	Wt	Wt	Wt	D	Wt	I	Wt
5	Wt	Wt	Wt	Wt	Wt	D	Wt	Wt	Wt

Table 14: Recognition results of PSO.

Column	Row								
	1	2	3	4	5	6	7	8	9
1	Wt	Wt	Wt	Wt	Wt	Wt	Wt	Wr	Wt
2	Wt	Wt	Wt	Wt	Wt	Wt	Wt	Wt	Wt
3	Wt	Wt	Wt	I	Wt	Wt	Wt	Wt	Wt
4	Wt	Wt	Wt	Wt	I	Wt	Wt	Wt	Wt
5	Wt	Wt	Wt	Wt	Wt	Wt	Wt	Wt	Wt

Table 15: The wet road surface image identification results statistics.

State	State symbol	Number of blocks	Grid search	PSO	Grid search/%	PSO/%
Dry	D	45	7	0	15.56%	0
Wet	Wt		36	42	80.00%	93.33%
Water	Wr		1	1	2.22%	2.22%
Snow	S		0	0	0	0
Ice	I		1	2	2.22%	4.44%

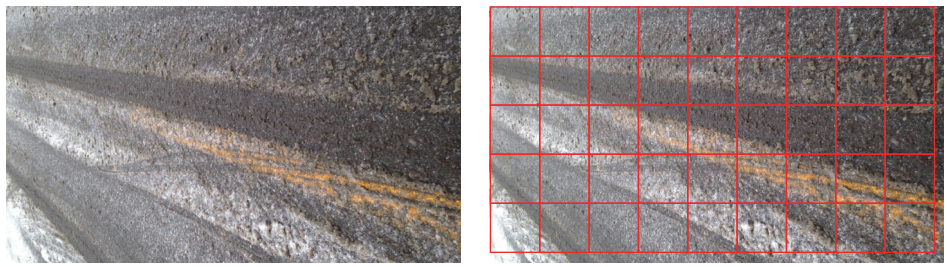

(a) (b)

Figure 18: Image test results of hybrid road surface (from the surveillance system). (a) Image of hybrid road surface state. (b) Image blocks.

the grid searching optimization. After PSO optimization, the recognition accuracy of each block of the test image is improved, and the distribution of road conditions can be given accurately.

The recognition results of the ice, wet, and water hybrid state (from the surveillance system) are shown in Figure 18 and Tables 37 and 38.

Table 39 shows the recognition results of each road surface state.

From Table 39, it can be seen that the error rate of each image block is relatively high on hybrid road condition after

the grid searching optimization. After PSO optimization, the recognition accuracy of each block of the test image is improved, and the distribution of road conditions can be given accurately.

6. Conclusions

There are a large number of traffic accidents caused by bad weather condition or slippery road condition. Therefore, road states greatly affect the traffic safety and transport efficiency on highway. It is of great social significance to study the

Table 16: Recognition results of grid.

Column	Row						
	1	2	3	4	5	6	7
1	Wr	S	Wr	Wr	Wr	Wr	I
2	Wr	Wr	Wr	Wt	Wt	Wr	Wr
3	Wr	Wr	Wt	Wr	Wr	I	Wr
4	I	Wr	Wr	Wr	Wr	Wr	Wr
5	Wr	Wr	Wr	Wr	Wr	Wr	Wr
6	Wr	Wr	Wr	Wr	Wr	Wr	D
7	Wr	S	Wr	Wr	Wr	Wr	I
8	I	Wr	Wr	Wr	Wr	Wr	I

Table 17: Recognition results of PSO.

Column	Row						
	1	2	3	4	5	6	7
1	Wr	Wr	Wr	Wr	Wr	Wr	Wr
2	Wr	Wr	Wr	Wr	Wr	Wr	Wr
3	Wr	Wr	Wr	Wr	Wr	Wr	Wr
4	Wr	Wr	Wr	Wr	Wr	Wr	Wt
5	Wr	Wr	Wr	Wr	Wr	Wr	Wr
6	Wr	Wr	Wr	Wr	Wr	Wr	Wr
7	Wr	Wr	Wr	Wr	Wr	D	Wr
8	Wr	Wr	Wr	Wr	Wr	Wr	Wr

Table 18: The water road surface image identification results statistics.

State	State symbol	Number of blocks	Grid search	PSO	Grid search/%	PSO/%
Dry	D	56	1	1	1.79%	1.79%
Wet	Wt		3	1	5.36%	1.79%
Water	Wr		44	54	78.57%	96.42%
Snow	S		2	0	3.57%	0
Ice	I		6	0	10.71%	0

Table 19: Recognition results of grid.

Column	Row					
	1	2	3	4	5	6
1	Wr	S	Wr	Wr	Wr	I
2	Wr	Wr	Wr	Wt	Wr	Wr
3	Wr	Wt	Wr	Wr	I	Wr
4	I	Wr	Wr	D	Wr	Wr
5	Wr	Wr	Wr	Wr	Wr	Wr
6	Wr	Wr	Wr	Wr	Wr	Wr
7	Wr	S	Wr	Wr	Wr	I
8	I	Wr	Wr	Wr	Wr	I

Table 20: Recognition results of PSO.

Column	Row					
	1	2	3	4	5	6
1	Wt	Wr	Wr	Wr	Wt	Wr
2	Wr	Wr	Wr	Wr	Wt	Wr
3	Wr	Wr	Wr	Wr	Wr	Wr
4	Wr	Wr	Wr	Wr	Wt	Wr
5	Wr	Wr	Wr	Wr	Wr	Wr
6	Wr	Wr	Wr	Wr	Wr	Wr
7	Wr	Wr	Wr	Wr	Wr	Wr
8	I	Wr	Wr	Wr	Wr	Wt

Table 21: The water road surface image identification results statistics.

State	State symbol	Number of blocks	Grid search	PSO	Grid search/%	PSO/%
Dry	D	48	2	0	4.17%	0
Wet	Wt		2	4	4.16%	8.33%
Water	Wr		36	43	75%	89.59%
Snow	S		2	0	4.17%	0
Ice	I		6	1	12.5%	2.08%

Table 22: Recognition results of grid.

Column	Row						
	1	2	3	4	5	6	7
1	Wr	S	S	S	S	S	I
2	S	I	S	S	S	S	S
3	S	I	S	I	S	S	S
4	S	I	S	S	I	S	S
5	I	S	S	S	S	S	I
6	I	I	S	S	S	I	Wr
7	I	I	S	S	S	I	S

Table 23: Recognition results of PSO.

Column	Row						
	1	2	3	4	5	6	7
1	Wr	S	S	S	S	S	S
2	S	S	S	S	S	S	S
3	S	S	S	S	S	S	S
4	S	S	S	S	I	S	S
5	I	S	S	S	S	S	S
6	S	I	S	S	S	I	Wr
7	S	S	S	S	S	I	S

classification of wet and slippery road condition, which can provide reference and theoretical basis for traffic control and meteorological management and ensure traffic safety.

There are many limitations in using instrument to recognize road surface conditions, and image recognition is becoming the main technology for recognizing road surface state. However, recognition under hybrid road conditions and different lighting conditions are two problems that need to be solved.

Based on SVM algorithm and image segmentation processing technology, we propose a method of video image processing technology for road surface state recognition. First

Table 24: The snow road surface image identification results statistics.

State	State symbol	Number of blocks	Grid search	PSO	Grid search/%	PSO/%
Dry	D	49	0	0	0	0
Wet	Wt		0	0	0	0
Water	Wr		2	2	4.08%	4.08%
Snow	S		33	42	67.35%	85.71%
Ice	I		14	5	28.57%	10.20%

Table 25: Recognition results of grid.

Column	Row					
	1	2	3	4	5	6
1	S	S	S	S	S	I
2	D	D	S	S	S	S
3	S	S	S	S	D	D
4	S	S	S	Wr	D	S
5	S	S	S	S	S	S
6	S	S	S	S	S	S
7	S	S	S	D	Wt	S
8	S	S	S	D	Wt	S

Table 26: Recognition results of PSO.

Column	Row					
	1	2	3	4	5	6
1	S	S	S	S	S	I
2	S	S	S	S	S	S
3	S	S	S	S	S	I
4	S	S	S	S	S	S
5	S	S	S	S	S	S
6	S	S	S	S	S	S
7	S	S	S	S	Wt	S
8	S	S	S	S	S	I

Table 27: The snow road surface image identification results statistics.

State	State symbol	Number of blocks	Grid search	PSO	Grid search/%	PSO/%
Dry	D	49	7	0	14.29%	0
Wet	Wt		2	1	4.08%	2.04%
Water	Wr		1	0	2.04%	0%
Snow	S		38	45	77.55%	91.84%
Ice	I		1	3	2.04%	6.12%

Table 28: Recognition results of grid.

Column	Row								
	1	2	3	4	5	6	7	8	9
1	I	I	I	I	I	I	I	Wt	I
2	I	I	I	I	I	I	I	Wt	I
3	I	I	I	I	I	I	I	I	I
4	I	I	I	I	I	I	I	I	I
5	I	I	I	I	I	Wt	I	I	I

Table 29: Recognition results of PSO.

Column	Row								
	1	2	3	4	5	6	7	8	9
1	I	I	I	I	I	I	I	I	I
2	I	I	I	I	I	I	I	I	I
3	I	I	I	I	I	I	I	Wt	I
4	I	I	I	I	I	I	I	I	I
5	I	I	I	I	I	I	I	I	I

Table 30: The ice road surface image identification results statistics.

State	State symbol	Number of blocks	Grid search	PSO	Grid search/%	PSO/%
Dry	D	45	0	0	0	0
Wet	Wt		3	1	6.67%	2.22%
Water	Wr		0	0	0	0
Snow	S		0	0	0	0
Ice	I		42	44	93.33%	97.78%

Table 31: Recognition results of grid.

Column	Row					
	1	2	3	4	5	6
1	D	I	Wt	I	I	I
2	I	I	I	I	I	D
3	D	I	I	I	I	I
4	Wt	I	I	I	I	Wt
5	I	Wr	I	I	I	I
6	D	Wt	D	I	I	I
7	I	I	I	I	I	I
8	I	I	I	D	D	Wt

Table 32: Recognition results of PSO.

Column	Row					
	1	2	3	4	5	6
1	I	I	I	I	S	I
2	I	I	I	S	I	I
3	I	I	I	S	S	I
4	I	I	I	I	I	I
5	I	I	I	I	I	Wt
6	I	Wt	Wt	I	I	I
7	I	I	I	I	Wt	Wt
8	I	I	I	I	I	Wt

Table 33: The ice road surface image identification results statistics.

State	State symbol	Number of blocks	Grid search	PSO	Grid search/%	PSO/%
Dry	D	45	42	45	93.33%	100%
Wet	Wt		3	0	6.67%	0
Water	Wr		0	0	0	0
Snow	S		0	0	0	0
Ice	I		0	0	0	0

Table 34: Recognition results of grid.

Column	Row							
	1	2	3	4	5	6	7	8
1	Wt	D	Wr	Wr	Wr	Wr	D	D
2	Wt	Wt	D	Wr	Wr	Wr	D	Wt
3	Wt	Wt	D	Wr	Wr	Wr	D	Wt
4	Wt	Wt	Wr	Wt	Wr	Wt	D	Wt
5	S	S	Wt	Wt	Wt	Wt	D	Wt
6	D	Wt	Wr	Wt	D	D	D	D

Table 35: Recognition results of PSO.

Column	Row							
	1	2	3	4	5	6	7	8
1	Wt	D	D	Wt	Wr	Wt	Wr	Wr
2	D	D	D	Wt	Wr	Wt	Wr	Wt
3	D	D	Wr	Wr	Wr	Wt	Wt	Wr
4	D	D	Wr	Wr	Wr	Wt	D	Wt
5	D	Wt	Wr	Wr	Wr	Wr	Wt	Wt
6	D	D	Wr	Wr	Wr	Wr	Wr	Wt

Table 36: The hybrid road surface image identification results statistics.

State	State symbol	Number of blocks	Grid search	PSO	Grid search/%	PSO/%
Dry	D	48	14	13	29.17%	27.08%
Wet	Wt		19	14	39.58%	29.17%
Water	Wr		13	21	27.08%	43.75%
Snow	S		2	0	0.42%	0
Ice	I		0	0	0	0

Table 37: Recognition results of grid.

Column	Row								
	1	2	3	4	5	6	7	8	9
1	Wt	Wr	I	Wr	Wt	I	I	I	S
2	Wt	I	I	I	Wt	I	I	Wt	S
3	Wt	Wr	S	Wr	Wt	I	Wt	Wt	S
4	Wt	Wr	I	Wr	Wt	Wt	I	Wr	Wr
5	Wt	Wr	I	Wr	Wt	I	Wr	Wr	S

Table 38: Recognition results of PSO.

Column	Row								
	1	2	3	4	5	6	7	8	9
1	I	I	I	I	I	I	Wt	Wt	I
2	I	Wt	Wt	I	I	I	I	I	I
3	S	S	S	I	I	I	I	I	I
4	S	I	S	I	I	I	Wt	I	I
5	S	I	I	I	I	I	S	I	Wt

of all, according to the segmentation principle, the road surface samples are divided into blocks and the road surface state sample database is constructed. Then, 9-dimensional color eigenvectors and 4-dimensional texture eigenvectors are extracted to form a 13-dimensional eigenvectors database which can describe the road surface state. After that, the SVM classifier is trained by using grid searching optimization and PSO optimization to obtain the road surface state classification model. And then, the performances of two classification models are tested. Finally, a road surface state recognition program was developed to test the actual road surface state images in a variety of environments.

The test results show that (1) the establishment of a perfect sample database is the basis for accurate recognition of road surface state. The quality and purity of the sample database can be ensured by dealing with single state image blocks. (2) Each feature value of the five states has overlapping parts, while 13-dimensional eigenvectors can satisfy the need of state recognition accurately. (3) After the SVM parameter optimization, the performance of road state classification model is superior, in which the performance of the PSO algorithm is better than that of the grid searching optimization algorithm, and the accuracy of state recognition is improved. (4) Image segmentation method can be used to obtain the distribution of road surface state, which solves the problem of hybrid road surface state and road surface under different

Table 39: The hybrid road surface image identification results statistics.

State	State symbol	Number of blocks	Grid search	PSO	Grid search/%	PSO/%
Dry	D	45	0	0	0	0
Wet	Wt		14	6	31.11%	13.33%
Water	Wr		12	0	26.67%	0
Snow	S		5	7	11.11%	15.56%
Ice	I		14	32	31.11%	71.11%

light conditions. The recognition accuracy of single state is above 90%, and the recognition accuracy of hybrid state is more than 85%.

Conflicts of Interest

The authors declare that there are no conflicts of interest regarding the publication of this article.

Authors' Contributions

Jiandong Zhao and Hongqiang Wu presented the algorithms, analyzed the data, and cowrote the paper; Liangliang Chen installed the experimental system and performed the experiments.

Acknowledgments

This work is supported by the Fundamental Research Funds for the Central Universities (2016JBM053).

References

[1] X. Sun, *Research on Risk Coupling of Highway Traffic Safety Based on Catastrophe Theory*, Beijing Jiaotong University, Beijing, 2015.

[2] Z. J. Bao, Y. Y. Tang, and C. C. Li, *Highway Traffic Safety and Weather Effects*, China Communications Press, Beijing, China, 2008.

[3] L. Cai, D. C. Zhang, B. Li, L. D. Gao, and L. Wang, "Traffic meteorological embedded road conditions detector test method research," *Road Traffic and Safety*, vol. 14, no. 6, pp. 55–59, 2014.

[4] D. Gailius and S. Jacenas, "Ice detection on a road by analyzing tire to road friction ultrasonic noise," *Ultragarsas*, vol. 62, no. 2, pp. 17–20, 2007.

[5] Z. Qi, B. Wang, X. Pei, and G. Ma, "A method of road surface identification based on road characteristics and the features of antilock braking adjustment," *Automotive Engineering*, vol. 36, no. 3, pp. 310–315, 2014.

[6] J. Alonso, J. M. López, I. Pavón et al., "On-board wet road surface identification using tyre/road noise and support vector machines," *Applied Acoustics*, vol. 76, no. 1, pp. 407–415, 2014.

[7] W. Wang, Q. Wu, X. Chu, and Y. Wu, "Discussion to information acquisition technology and safety identification method of traffic environment," in *Proceedings of the 2008 Pacific-Asia Workshop on Computational Intelligence and Industrial Application, PACIIA '08*, pp. 874–878, December 2008.

[8] K. Andreas and B. Wilco, "Winter road condition recognition using video image classification," *Journal of the Transportation Research Record*, vol. 1627, no. 1, pp. 29–33, 1998.

[9] S. Anis, K. Majdi, and B. Jacques, "Characterization of road micro texture by means of image analysis," *Laboratoire Signal, Image at Communications*, vol. 264, no. 5, pp. 464–468, 2008.

[10] Y. Chen, "Image analysis applied to black ice detection," in *Applications of Artificial Intelligence IX*, Proceedings of SPIE, pp. 551–562, April 1991.

[11] K. Ueda, I. Horiba, and K. ledaga, "A detecting method of wet condition on road using image processing," *Information Processing Society of Japan*, vol. 35, no. 6, pp. 1072–1080, 1994.

[12] S. Yoda, H. Okabe, J. Takagi, and T. Yamashita, "Road surface recognition sensor using an optical spatial filter," in *Proceedings of the IEEE Conference on Intelligent Transportation System*, pp. 253–257, 1997.

[13] I. Yamamoto, M. Kawana, and I. Yamazaki, "The application of visible image road surface sensors to winter road management," in *Proceedings of the IEEE Conference on Society of Automotive Engineers of Japan*, pp. 1–11, 2005.

[14] Y. Muneo, U. Koji, H. Isao, Y. Shin, and T. Sadayuk, "Detection of wet-road conditions from images captured by a vehicle-mounted camera," *Journal of Robotics and Mechatronics*, vol. 17, no. 3, pp. 269–276, 2005.

[15] I. Becchi, E. Caporali, F. Castelli, and C. Lorenzini, "Field analysis of the water film dynamics on a road pavement," *Physics and Chemistry of the Earth, Part C: Solar, Terrestrial and Planetary Science*, vol. 26, no. 10-12, pp. 717–722, 2001.

[16] H. Fukui, J. Takagi, Y. Murata, and M. Takeuchi, "Image processing method to detect road surface condition using optical spatial frequency," in *Proceedings of the 1997 IEEE Conference on Intelligent Transportation Systems, ITSC*, pp. 1005–1009, November 1997.

[17] H. Li, Y. H. Feng, and J. Lin, "Study on road surface condition identification based on BP network improved," *Microcomputer Information*, vol. 26, no. 2, pp. 3-4, 2010.

[18] X. Y. Liu and Q. D. Huang, "Study on classifier of wet-road images based on SVM," *Journal of Wuhan University of Technology (Transportation Science and Engineering)*, vol. 35, no. 4, pp. 784–787, 2011.

[19] J. Wan, K. Zhao, and W. F. Wang, "Classification of slippery road images based on high-dimensional features and RBF Neural Network," *Journal of Transportation Information and Safety*, vol. 31, no. 2, pp. 32–35, 2013.

[20] S. B. Zhang, S. H. Quan, and Y. Shi, "Study on image retrieval algorithm based on color moment," *Computer Engineering*, vol. 40, no. 6, pp. 252–255, 2014.

[21] S. R. Shinde, S. Sabale, and S. Kulkarni, "Experiments on content based image classification using Color feature extraction," in *Proceedings of the 2015 International Conference on Communication, Information and Computing Technology, ICCICT '15*, January 2015.

[22] A. M. Bhave, M. Wanjari, and G. Sawarkar, "IRetrieval: image retrieval based on color feature and texture feature," *International Journal of Advanced Research in Computer Science*, 2014.

[23] R. M. Haralick, K. Shanmugam, and I. Dinstein, "Textural features for image classification," *IEEE Transactions on Systems, Man and Cybernetics*, vol. 3, no. 6, pp. 610–621, 1973.

[24] P. Mohanaiah, P. Sathyanarayana, and L. Gurukumar, "Image texture feature extraction using GLCM approach," *International Journal of Scientific and Research Publications*, 2013.

[25] E. G. Karakasis, G. A. Papakostas, D. E. Koulouriotis, and V. D. Tourassis, "A unified methodology for computing accurate quaternion color moments and moment invariants," *IEEE Transactions on Image Processing*, vol. 23, no. 2, pp. 596–611, 2014.

[26] M. Benco, R. Hudec, and P. Kamencay, "An advanced approach to extraction of colour texture features based on GLCM," *International Journal of Advanced Robotic Systems*, vol. 11, no. 1, pp. 129–163, 2014.

[27] R. Quevedo, E. Valencia, J. M. Bastías, and S. Cárdenas, "Description of the enzymatic browning in avocado slice using GLCM image texture," *Lecture Notes in Computer Science*, vol. 8334, pp. 93–101, 2014.

[28] A. Gain and D. Roy, "A novel algorithm for object detection in low contrast image and recognition by SVM," *International Journal of Science and Research*, vol. 4, no. 10, 2015.

[29] P. Lameski, E. Zdravevski, and R. Mingov, "SVM parameter tuning with grid search and its impact on reduction of model over-fitting," *International Joint Conference on Rough Sets*, vol. 9437, pp. 464–474, 2015.

[30] O. Devos, C. Ruckebusch, A. Durand, L. Duponchel, and J.-P. Huvenne, "Support vector machines (SVM) in near infrared (NIR) spectroscopy: focus on parameters optimization and model interpretation," *Chemometrics and Intelligent Laboratory Systems*, vol. 96, no. 1, pp. 27–33, 2009.

[31] J. Caliaperumal, S. Wowk, and S. Jones, "Simultaneous feature selection and LS-SVM parameters optimization algorithm based on PSO," in *Proceedings of the 2009 WRI World Congress on Computer Science and Information Engineering, CSIE '09*, vol. 5, pp. 723–727, April 2009.

[32] A. Ozbeyaz, M. I. Gursoy, and R. Coban, "Regularization and kernel parameters optimization based on PSO algorithm in EEG signals classification with SVM," in *Proceedings of the 2011 IEEE 19th Signal Processing and Communications Applications Conference (SIU)*, pp. 399–402, Antalya, Turkey, April 2011.

[33] C. López-Franco, L. Villavicencio, N. Arana-Daniel, and A. Y. Alanis, "Image classification using PSO-SVM and an RGB-D sensor," *Mathematical Problems in Engineering*, vol. 2014, Article ID 695910, 17 pages, 2014.